The Reduction of Carboxylic Acids to Alcohols over Palladium-Promoted Rhenium and Tungsten Oxides

---

A Dissertation
presented to
the Faculty of the School of Engineering & Applied Science
University of Virginia

---

in partial fulfillment
of the requirements for the degree
Doctor of Philosophy
in the subject of
Chemical Engineering

by

James D. Kammert

Charlottesville, Virginia
January 2019

The Reduction of Carboxylic Acids to Alcohols over Palladium-Promoted Rhenium and Tungsten Oxides

Abstract

The direct catalytic reduction of carboxylic acids is an important reaction in the conversion of biomass-derived chemicals to useful products. The combination of metal function and a supported metal oxide can produce a catalyst that is capable of performing this reaction. The performance of the resulting catalyst depends strongly on the selection of both the metal and the metal oxide. Recent studies using metal-promoted rhenium oxide catalysts to reduce carboxylic acids to alcohols demonstrated activity at significantly lower H_2 pressures than would be required using traditional copper-based catalysts. The active state of metal-promoted rhenium catalysts used for the direct reduction of carboxylic acids remains elusive, which has hindered the development of a mechanistic understanding of these types of catalysts.

In this dissertation, palladium-promoted rhenium oxide (Pd-promoted Re) catalysts supported on SiO_2 were synthesized using a stepwise incipient wetness impregnation method. The SiO_2-supported, Pd-promoted Re catalysts (Pd/SiO_2, Re/SiO_2, and $PdRe/SiO_2$) were characterized using electron microscopy, X-ray absorption spectroscopy (XAS), and probe molecule adsorption (H_2, CO, and N_2). Palladium supported on SiO_2 was not active for the reduction of propionic acid to oxygenates, while supported Re/SiO_2 was minimally active for the production of a small amount of a mixture of propanal and 1-propanol after pre-reduction of the Re/SiO_2 in H_2 at elevated temperature. Promotion of Re/SiO_2 with Pd formed an active catalyst for propionic acid reduction without pretreatment, and resulted in the reduction of the Re component of the catalyst to an average oxidation state of 4+ as determined by XAS. Transient kinetic analysis was used to determine the turnover frequency and coverage of reactive intermediates leading to propionic acid reduction products over $PdRe/SiO_2$, and results suggested that rapid turnover of

intermediates leading to aldehydes was followed by very slow turnover of intermediates leading to alcohols on the catalyst surface.

Palladium-promoted Re/TiO_2 catalysts were also synthesized using a stepwise incipient wetness impregnation method. Reaction kinetics studies of the reduction of propionic acid over PdRe supported on SiO_2 and TiO_2 found a 0.6 order in H_2 and a 0.1-0.2 order in propionic acid pressure. The reduction of propionic acid in D_2 resulted in an inverse kinetic isotope effect of 0.79, and cofeeding water had no effect on the steady-state reduction of propionic acid. On the other hand, cofeeding water did result in a transient change in the rate of 1-propanol formation over $PdRe/SiO_2$, which was studied using diffuse reflectance infrared Fourier transform spectroscopy (DRIFTS). Results from DRIFTS revealed significant coverage of the SiO_2 support with alkoxy species, which could be removed from the SiO_2 surface by water or propionic acid. These propoxy species could not be detected on $PdRe/TiO_2$ under similar conditions. Transient kinetic analysis revealed similar turnover of intermediates leading to propanal and 1-propanol on the $PdRe/TiO_2$ surface. These results were consistent with a 2-step cascade reaction, whereby reduction of propionic acid led to the formation of propanal, which was subsequently hydrogenated to form 1-propanol.

Finally, Pd-promoted tungsten oxide (PdW) and phosphotungstic acid (PdPTA) were supported on SiO_2, TiO_2, and ZrO_2 using wetness impregnation techniques. These catalysts demonstrated higher rates of propionic acid reduction than the previously studied Pd-promoted Re catalysts under similar conditions, and gave similar product distributions. Catalytic activity and product selectivity depended on the support, the active tungsten phase, and the pretreatment conditions. The reason for enhanced activity over Re-based catalysts and the role of acid site type and density in these catalysts warrants further study.

Acknowledgments

The work presented here would not have been possible without the support of many wonderful people. First and foremost, I would like to thank Professor Robert J. Davis, my advisor, who has taken so much time to help me become a better public speaker, writer, and international researcher. I will be forever grateful for the wisdom and opportunities you provided during my time at UVA. To the members of my committee, Dr. William Epling, Dr. Brent Gunnoe, Dr. Gaurav Giri, and Dr. Christopher Paolucci, thank you for all of your helpful conversations and insights.

Dr. Matthew Neurock and Ashwin Chemburkar at the University of Minnesota, Dr. Gopinathan Sankar, Dr. Ian Godfrey, and Dr. Adam Clark at University College London, and Dr. Eli Stavitski and Dr. Klaus Attenkoffer at Brookhaven National Lab are acknowledged for their helpful input, enlightening conversations, and senses of humor during late nights at ESRF, Diamond, and NSLS-II. Richard White, Helge Heinrich, and Cathy Dukes are acknowledged for their assistance running various pieces of research equipment at UVA. Ricky Buchanan is acknowledged for his help machining parts for various projects, and Teresa Morris and Jennifer Davis are thanked for their assistance with procurement and handling difficult suppliers.

The members of the Davis lab during my time at UVA are acknowledged, including Dr. Juan Lopez-Ruiz, Dr. Derek Falcone, Dr. Sabra Hanspal, Dr. Kehua Yin, Dr. Benjamin Huang, Dr. Zachary Young, Gordon Brezicki, Tyler Prillaman, Zhongwen Luo, Naomi Miyake, and Lu Yang. I have learned so much through my time working with you all. Dr. Nicholas "Caveman" Kaylor and Dr. Jiahan "The One" Xie are acknowledged for being supportive peers, teachers, and great friends. I will not forget the many times when, in the dead of night, we all happened to arrive at the same time to collect our time points.

To my parents, Lisa and Mark Kammert, my sister Allison, my grandparents Eugenie,

Drayton, Marlyna, and Jim, and all of my friends at UVA and scattered around the world, thank you for your encouragement and kind words, which made it much easier to stay positive even when things got difficult. Thank you for understanding over the last 5 years when I have been too busy to talk or visit as much as I would have liked. Finally, thank you to Stephanie Guthrie, your support has meant so much to me over the last several years. You have been patient, kind, and motivating through every challenge we have faced together.

This material is based upon work supported by the National Science Foundation (NSF) under Award No. EEC-0813570. Any opinions, findings, and conclusions or recommendations expressed in this material are those of the author(s) and do not necessarily reflect the views of the NSF.

Contents

List of figures

List of tables

I should certainly not have undertaken these tedious calculations if an extraordinary interest had not been connected with them.[1]

Svante Arrhenius

1

Introduction

1.1 Importance of biologically-derived chemicals

Atmospheric CO_2 concentrations on our planet remained fairly constant on geological timescales until the end of the 18th century.[2] Around that time, the Industrial Revolution initiated a significant increase in the consumption of fossil resources, leading to a rapid production of atmospheric CO_2 that is expected to impact global climate and international policy well into the next century.[3] Dependence on fossil resources for our energy and chemical products is not only to a threat to the global environment, but also creates the potential for global economic turmoil when oil prices become volatile. Recent periods of oil price uncertainty, such as the

energy crisis of the 1970s or the Iraq war in the mid-2000s, caused research interests to shift towards the production of chemicals and fuels from renewable, domestic feedstocks to mitigate this uncertainty.[4]

Biomass has the potential to be a carbon neutral feedstock for fuels, and a cost-competitive alternative to petroleum as a feedstock for value-added chemicals.[5–7] While current oil and natural gas costs preclude the use of a large amount of biomass as liquid fuels, their potential as feedstocks for the chemicals industry is much greater. Even though only a small fraction of oil (<2%) refined in the United States is currently used to produce chemical products,[8] the value of this small fraction is approximately equal to the total value of gasoline, jet fuel, and fuel oils produced from ~85% of the barrel after it is processed to value-added chemicals.[9] The effective hydrogen to carbon ratio of biomass is similar to many value-added chemicals, meaning that inefficient oxidation processes might be partially avoided by using biomass as a chemical feedstock.[10] Furthermore, demand for chemical products, including plastics, textiles, and construction materials, is expected to increase by nearly 60% by 2050.[11] Increasing demand and advancing technology have produced a market where biologically-derived chemicals are beginning to compete as value added products.[12]

Biomass-to-chemicals conversions struggle with cost competitiveness due to a lack of aggregate research compared to the conversion of petroleum products to chemicals.[14] In the current petrochemical industry, feedstocks are composed of hydrocarbons that need to be functionalized to produce value-added products. In contrast, biomass contains an abundance of functionalized compounds that must be either selectively defunctionalized to produce value-added products via drop-in processes (i.e., utilizing existing processes to produce products from a different feedstock)

or converted to chemical products via more efficient emerging processes (utilizing new technology and processes).[10] Before chemicals can be produced cost-effectively from biomass, the chemistry of converting oxygenated compounds needs to be more thoroughly researched. The most economical route to chemicals is to produce a small number of versatile molecules with a wide range of applications. These versatile molecules are called platform molecules in the chemicals industry, and they consist of single molecules or families of molecules, such as carboxylic acids, that can be produced in bulk and converted into a wide range of functional products, as illustrated in Figure 1.1. The platform molecule approach offers economies of scale for the production of commodity and specialty chemicals and therefore has an advantage over chemicals produced from start to finish for a single end-use. However, many biologically-derived molecules contain multiple functional groups, so conversion must be selective to produce the desired products.

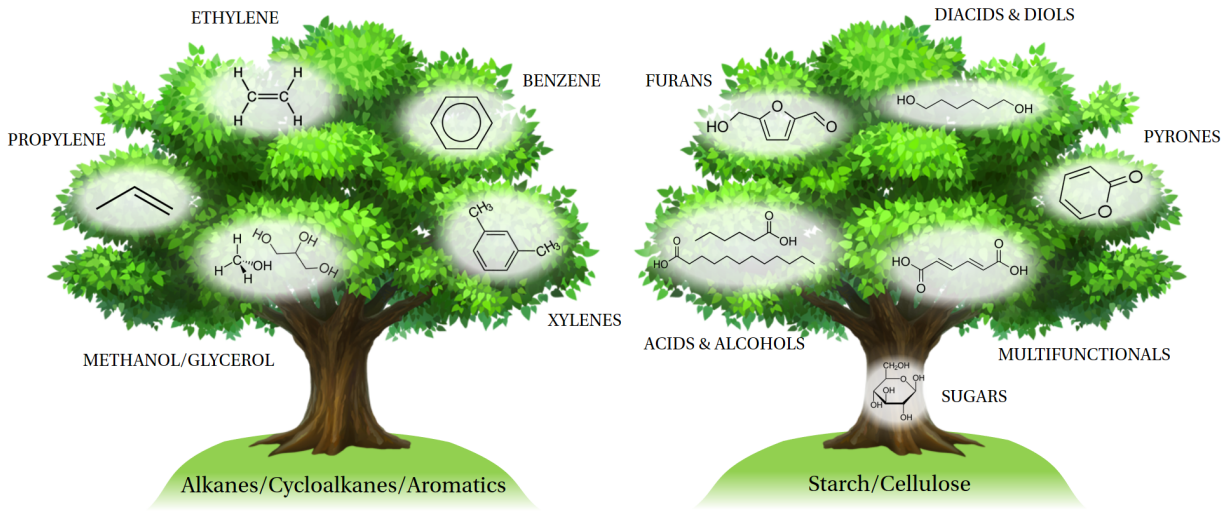

Figure 1.1: Left: Petrochemical platform molecule "tree" derived from crude oil refining, where each platform molecule has a large number of end uses. **Right:** An analogous biologically-derived platform chemical "tree", incorporating molecules that could be obtained in bulk from the fermentation of sugars. Adapted from the Center for Biorenewable Chemicals website.[13]

1.2 Carboxylic acids as platform molecules: feedstocks and applications

Carboxylic acids can be obtained from plant, animal, and microorganism sources as oils, emulsions, and aqueous solutions. One major source of biologically-derived carboxylic acids and esters at the time of this writing is lauric oils, which are oils derived from coconut and palm kernel fruit. These oils are comprised primarily of short- and medium-chain fatty acids and triglycerides, with carbon chain lengths ranging from C_6 to C_{18}.[15] Of these carbon chain lengths, the short chain C_6 to C_{10} fraction can be esterified and converted to alcohols for use as plasticizers and high-performance lubricants. This fraction, however, only accounts for about 15% of the oils that can be derived from coconut and palm. The other 85% consists of the longer chain acids C_{12} to C_{18}, mostly C_{12} and C_{14}, which can be converted to alcohols via the same process for use as detergent feedstocks.

While there are many uses for coconut and palm kernel oil, the long turnover for feedstock growth and limited control over their chain length make responding to market demand difficult. A desire for continuous processes with chain length control led to the development of technology to produce fatty acids from genetically engineered organisms such as *E. coli*.[16] Unlike coconut and palm oils that consist mainly of triglycerides, these carboxylic acids are produced as free fatty acids. Accordingly, technology for the direct conversion of these free acids without the need for an intermediate esterification step has the potential to increase the commercial viability of such processes.

A 2004 study performed by the US Department of Energy (DOE) identified building block chemicals that could be produced biologically and converted to a variety of high-value chemicals.[17] The 12 so-called "top" building blocks that warranted investigation are shown in

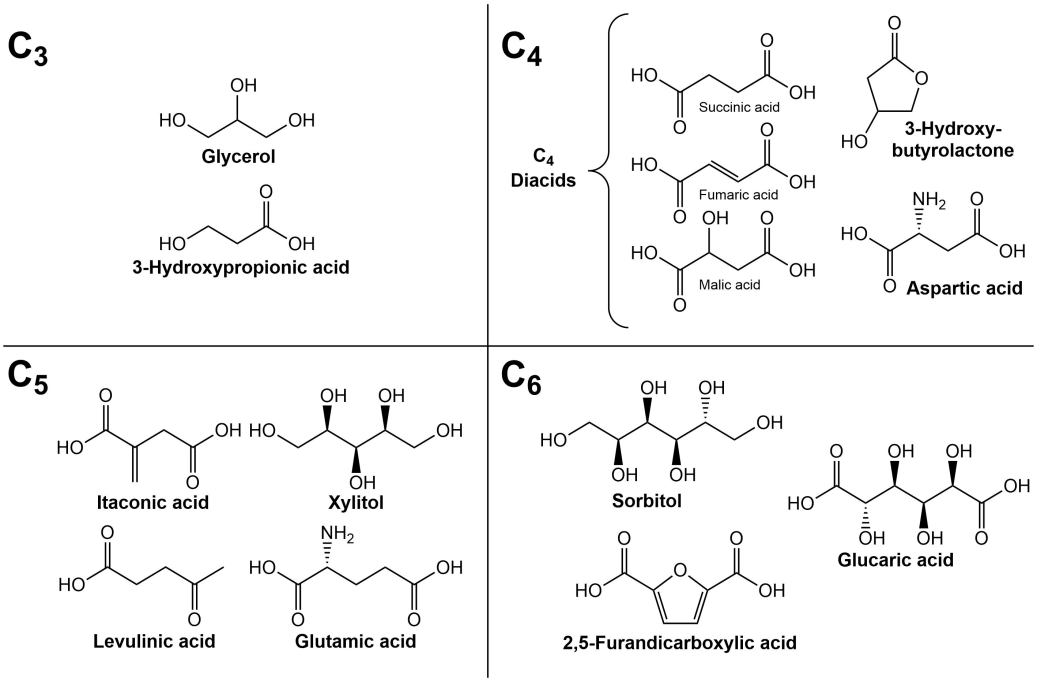

Figure 1.2: "Top" 12 biologically-derived building block molecules identified by Werpy and Peterson.[17] Reproduced with permission from Nikolau et al.[19]

Figure 1.2. Nine out of the 12 building blocks identified were carboxylic acids or cyclic esters (lactones). Evidently, carboxylic acids made up a large fraction of molecules that could be produced in bulk from fermentable biomass. Several years later, this list was revisited based on the research activity that each of these molecules had received and the commercial viability of each molecule was considered .[18] Out of the original 9 carboxylates identified, 5 demonstrated short-term promise for commercial production. These acids were furandicarboxylic acid (FDCA), lactic acid, succinic acid, 3-hydroxypropionic acid (HPA), and levulinic acid.

Out of the 5 acids demonstrating commercial viability, FDCA, lactic acid, succinic acid, and HPA can potentially be reduced to produce value-added molecules. Reduction of FDCA could be used to produce 2,5-dihydroxymethyl-furan or -tetrahydrofuran, which could be used for the manufacture of polyesters.[17] Reduction of lactic acid could be used to produce propylene glycol, and subsequent dehydration of propylene glycol would yield propylene oxide, which each

have a wide variety of uses.[18] Reduction of succinic acid could produce 1,4-butanediol, tetrahydrofuran, and γ-butyrolactone. The projected market for succinic acid and its derivatives is estimated to be as much as 2.45×10^5 tons per year.[18] Reduction of HPA could be used to produce 1,3-propanediol, which is expected to reach a market value of $620 million by 2021[12] and is used primarily for the production of polytrimethylene terephthalate.[6]

Carboxylic acids can also be found in bio-oils produced from fast pyrolysis processes.[20] Fast pyrolysis bio-oils range in pH from around 2-3, as a result of their short-chain (C_1-C_3) carboxylic acid content. These acids can be removed by distillation, but this process results in the removal of volatile aldehydes and esters as well. The remediation of bio-oil using an acid-reduction treatment could mitigate the acidity of the oil and simultaneously upgrade its energy density by converting acids to their corresponding alcohols. However, water as a product of this upgrading reaction would have to be removed from the upgraded oil product.

1.3 Reduction of carboxylic esters and acids over bifunctional heterogeneous catalysts

Early work on the heterogeneously catalyzed reduction of acids and esters focused primarily on the conversion of esters to alcohols using H_2. In the 1930s, Adkins et al. demonstrated that copper chromite ($CuCr_2O_4$) catalysts, now called Adkins-type catalysts, were capable of performing the catalytic reduction of ethyl esters to their corresponding alcohols under 22 MPa H_2 at 523 K.[21] Over the last century, this catalyst has become the industrial standard for the selective reduction of esters.[22,23] Significant study of this catalyst has taken place since its discovery, leading to an enhanced understanding of the mechanism behind its activity. Studies performed by Yan et al. and Rieke et al. analyzed the reduction of fluorinated and long-chain esters.[24,25]

In their work, the proposed mechanism of ester reduction is via a hemiacetal intermediate which may be formed by adjacent metal-metal oxide sites such as those found in $CuCr_2O_4$. While this catalyst has been a powerful tool for the hydrogenation of carboxylic acids and esters, recent research in the area focuses reducing the H_2 pressure requirement for the reduction reaction, and eliminating Cr from the catalyst to reduce pollution caused by Cr leaching.[26] More information on the state of this field at the end of the 20th century can be found in a summary written by Turek et al.[27]

As copper is believed to be the active metal for reaction, many studies focused on the role of Cu in the reduction of esters and acids independent of a promoter. Evans et al. found that the reduction of alkyl esters over Raney Cu proceeded through a dissociative adsorption step, whereby esters would split into acyl and alkoxy species as they were adsorbed on the catalyst surface.[28] Work by Santiago et al. investigated the reduction of acetic acid and esters to alcohols using a Cu supported on SiO_2 catalyst.[29] Their study also concluded that the rate of reduction on the copper surface was limited by the dissociative adsorption of esters on the Cu surface and hydrogenation of the resulting surface acyl species, resulting in a reactive surface highly covered by acetate intermediates. When Cortright et al. studied the reduction of lactic acid to 1,2-propanediol under atmospheric H_2 pressures over a similar catalyst, they observed the formation of an intermediate 2-hydroxypropanal, consistent with the previously proposed model.[30] The participation of dehydration sites in the reaction was also suggested after observing the reduction of lactic acid to propionic acid as a side product.

Around the same time, interest began to develop around the use of metal oxides for the selective reduction of short-chain carboxylic acids such as acetic and propionic acid to their corre-

sponding aldehydes and alcohols.[31] Investigation of the reduction of acetic acid revealed reducible metal oxides such as those of Fe and Sn produced more acetaldehyde than metal oxides that were more difficult to reduce.[32,33] Mixtures of Pt with reducible metal oxide powders resulted in enhanced catalytic reduction of carboxylic acids, suggesting that both metal and metal oxide active sites played a role in carboxylic acid reduction chemistry. Subsequent work led to the proposal that a metallic phase was needed to activate hydrogen, while the purpose of the oxide phase was to perform the carboxylic acid reduction assisted by activated H provided by spillover from the metallic phase to the oxide phase.[34] Several studies by Rachmady and Vannice supported this assessment, demonstrating catalytic activity for the reduction of acetic acid using Pt/TiO_2, a metal supported on a reducible metal oxide support, and $Pt\text{-}Fe/TiO_2$, a metal and reducible metal oxide supported on a reducible metal oxide support.[35,36] Using diffuse reflectance infrared Fourier transform spectroscopy (DRIFTS), Rachmady and Vannice correlated an IR band near 1680 cm^{-1} with the temperature-programmed desorption of ketene, suggesting the presence of acetyl species on the catalyst surface under near-reaction conditions.[37]

Supported Ru-Sn borides also received significant attention as catalysts for the selective reduction of esters to alcohols.[38,39] These catalysts resulted in the formation of a majority of primary alcohols rather than aldehydes in contrast to high-temperature work studying Sn oxides without a promoter. Furthermore, the boride materials were not only active for the reduction of esters to alcohols, but also capable of selectively breaking C-O bonds, resulting in the formation of unsaturated alcohols from unsaturated esters at H_2 pressures of over 20 MPa. Characterization of the Ru-Sn borides revealed the role of Sn in dispersing Ru, and also revealed the formation of both alloyed RuSn metal particles and Ru-O-Sn bonds which suggested neighboring metallic Ru

and oxidized Sn could interact.[40] The level of interaction between Ru and Sn in the active catalyst was evidently quite important. Subsequent work by Cheah and Tang found that Ru/Al_2O_3 in the absence of the Sn promoter was more active for the reduction of 9-octadecenoic acid but resulted in the formation of saturated alcohols and other side products.[41] A 2:1 mixture of Sn to Ru resulted in a 95% yield of alcohol products, and was 79% selective to the unsaturated alcohol product. Further study suggested that the synthesis method of this catalyst was important to its performance, and the partial covering of Ru active sites by Sn was deemed critical to maintain the high selectivity of the catalyst to unsaturated products.[42] The hemiacetal mechanism for ester reduction proposed by Rieke et al. was also proposed to be the mechanism of ester reduction over Ru-Sn catalysts.[43] Further details on Ru-Sn and other catalysts for the reduction of esters and carboxylic acids can be found in a review by Pritchard et al.[44]

The rationale for an effective catalyst design is not immediately apparent from the results presented in this section. In the Pt/TiO_2 system, it was evident that the metal oxide (TiO_2) catalyzed acid reduction, while the metal was responsible for activating H_2. In other systems such as monometallic Cu or Ru catalysts, the need for bifunctionality involving a metal and an oxide was not so clearly demonstrated as the catalyst was active in the absence of an oxide promoter (such as Cr or Sn oxide). This dissonance has made it difficult to guide the rational design of effective catalysts for the reduction of acids and esters.

1.4 Rhenium oxide as a catalyst for the reduction of carboxylic acids to alcohols

Many of the catalysts discussed in the previous section share a similar drawback. The selective conversion of carboxylic acids and esters to alcohols for these catalysts required H_2 pressures

that were extreme, typically over 20 MPa. Indeed, early work by Broadbent et al. studying bulk Re oxides as hydrogenation catalysts utilized H_2 pressures of 10-30 MPa.[45–48] However, Trivedi et al. found that adding a promoter such as Ru, Pd, Rh, or Pt to supported Re/SiO_2 catalysts allowed the reaction to proceed at significantly lower pressures of 3.5 MPa.[49] Several industrial patents followed over the next decade, indicating that the technology had strong commercial viability.[50–54] In 2012, Trivedi et al.'s study was reproduced by Takeda et al. who found that Pd-promoted Re/SiO_2 demonstrated the highest activity and selectivity when compared to the other Pt-group-metal-promoted Re on a variety of supports.[55]

Several studies have probed the nature of the interaction between the Pt group metal promoter and the active Re phase. Minh et al. found that Pd promoted Re/TiO_2 reduced aqueous succinic acid to 1,4-butanediol (BDO).[56] The extent of interaction between the Pd and Re in the catalyst was probed by Ly et al. who varied the amount of Re added to a Pd/TiO_2 catalyst using a wetness impregnation method and a catalytic reduction method.[57] In the wetness impregnation method, Re was deposited in an uncontrolled manner, and required a >3.5 wt.% loading to reach maximum BDO production. In the catalytic reduction method, The Pd/TiO_2 catalyst was pretreated in an aqueous solution of the Re metal precursor and H_2, which resulted in deposition of the Re either directly upon the Pd surface or adjacent to Pd on the TiO_2 support. This method required only 0.6-0.8 wt.% loading of Re to reach maximum BDO productivity, suggesting the importance of adjacent Pd and Re particles. Poorer overall performance of catalysts synthesized by catalytic reduction were explained by further characterization, which revealed that wetness impregnation led to significantly more dispersed Re than the catalytic reduction method.[58] However, no electronic interaction of the Pd and Re in the catalyst was observed

using X-ray photoelectron spectroscopy.

The oxidation state of Re in the active catalyst is also believed to have significant effect on the rate of carboxylic acid conversion. Manyar er al. found that Pt-promoted Re/TiO_2 was a much more active catalyst for the reduction of stearic acid in dodecane than Pt-promoted Re/Al_2O_3.[59] The oxidation state of these catalysts was determined using a liquid-phase, *in situ* X-ray absorption cell to follow the X-ray absorption near edge structure (XANES) of the Pt and Re during a typical reaction.[60] On the active TiO_2-supported catalyst, 93% of the Pt in the Pt-promoted Re was found in the metallic state after reduction in tetrahydrofuran (THF), while the Re was only 78% reduced to Re^0. On the inactive Al_2O_3-supported catalyst, only 73% of the Pt was found in the metallic state, while Re was 95% metallic after reduction in THF. Earlier work by Ly et al.[58] and the reduction of stearic acid studied by Takeda et al.[61] also found that Re in their active Pd-promoted Re catalysts was in an oxidation state somewhere between Re^{4+} and Re^0 even after high-temperature reduction, but proposed that activity was a result of a mixture of metallic and oxidized Re. Rosmysłowicz et al. studied Re/TiO_2 using XPS and found that pretreatment of a Re/TiO_2 catalyst at 673 K in H_2 led to reduction of the Re^{7+} in the catalyst to Re^{4+}, producing and active catalyst for stearic acid reduction in the absence of a promoter.[62] Evidently, the active states of Re and its oxides have not been very well defined.

The surface reaction path and mechanism of carboxylic acid reduction on metal-promoted Re catalysts has received significant speculation in the last several years. Manyar et al.[59] proposed that the interaction of the carbonyl group in the carboxylic acid interacted with oxygen vacancies in TiO_2 created by H spillover from Pt to the TiO_2 support. The addition of Re was proposed to increase the activity of stearic acid reduction by increasing the interaction of stearic acid with

the catalyst surface through the carbonyl oxygen. Takeda et al. observed a 1.3 order and 1.2 order in H_2 over Pd-promoted Re/SiO_2 and Re/SiO_2, respectively, and proposed that hydrogen availability on the catalyst surface played a key role in the rate of reduction of stearic acid.[61] They also observed an order in stearic acid of 0.1 over the Pd-promoted Re/SiO_2 and 0.8 over the Re/SiO_2, which they attributed to an increase in the strength of the interaction between stearic acid and the Re component of the catalyst caused by Pd. Finally, Rosmysłowicz et al. reported a first-order dependence on the rate of stearic acid reduction in H_2.[62] They attributed this order to the generation of a reactive intermediate on the catalyst surface consisting of the stearic acid adsorbed on a Re-O-Ti^{n+} surface site and molecular H_2, reacting in an Eley-Rideal-type mechanism. In contrast to these proposed paths, a DFT study by Pallassana and Neurock on Pd(111), Re(0001), and Pd overlayers on Re found that the reduction of acetic acid could pass through an acetyl intermediate which would be hydrogenated to form an aldehyde on the Re(0001) surface.[63] The C-OH bond breaking step and acetyl hydrogenation step were predicted to have very similar barriers on the metal surface while the aldehyde could go on to be easily hydrogenated on either Re or Pd metal surfaces with a lower barrier. However, Pallassana and Neurock focused their study on the energetics of acetic acid reduction over metallic Pd and compared those results to metallic Re, while experiments suggest that Re is oxidized under reaction conditions.

1.5 Goals of this work

The rational design of catalysts for reduction of carboxylic acids over heterogeneous catalysts is still not completely understood, and the mechanism of reduction of carboxylic acids using supported Re catalysts remains a mystery. The review of the literature presented here illustrates

that the interaction of support, metal promoter, and active metal are complex and often convoluted, as in promoted metal oxide catalysts materials supported on TiO_2. These systems often suffer from a lack of *in situ* characterization. This dissertation attempts to clarify the picture of carboxylic acid reduction using Pd-promoted Re catalysts by investigating some of the more fundamental aspects of these catalysts. The catalytic conversion of carboxylic acids was carried out in a gas-phase system to remove solvent effects. *In situ* characterization was used when possible. In Chapter 2 of this dissertation, a Pd-promoted Re/SiO_2 catalyst for the gas-phase reduction of propionic acid to 1-propanol was extensively characterized using electron microscopy, X-ray absorption spectroscopy, and transient kinetic analysis. In Chapter 3, the steady state kinetics of propionic acid reduction were investigated over Pd-promoted Re supported on SiO_2 and TiO_2, and transient kinetic analysis was used to estimate the coverage of reactive intermediates and catalyst turnover frequencies over the TiO_2-supported catalyst. In Chapter 4, oxide-supported tungsten oxide and phosphotungstic acid were investigated for the reduction of propionic acid. The objectives of this work are as follows:

1. To determine the structure and oxidation state of the Pd-promoted Re/SiO_2 catalyst under reaction conditions,

2. To propose a surface reaction path and develop insights into the mechanism for the reduction of carboxylic acids to primary alcohols over Pd-promoted Re catalysts,

3. To apply an understanding of the bifunctional catalyst system to rationally design an improved catalyst for the reduction of carboxylic acids.

References

1. Arrhenius, S. On the influence of carbonic acid in the air upon the temperature of the ground. *Philosophical Magazine and Journal of Science* **41,** 239–276 (1896).

2. Neftel, A., Moor, E., Oeschger, H. and Stauffer, B. Evidence from polar ice cores for the increase in atmospheric CO_2 in the past two centuries. *Nature* **315,** 45–47 (1985).

3. Intergovernmental Panel on Climate Change. *Special Report: Global Warming of 1.5°C* tech. rep. (2018).

4. Ragauskas, A. J., Williams, C. K., Davidson, B. H., Britovsek, G., Cairney, J., Eckert, C. A., Frederick, W. J., Hallett, J. P., Leak, D. J., Liotta, C., Mielenz, J. R., Murphy, R., Templer, R. and Tschaplinski, T. The Path Forward for Biofuels and Biomaterials. *Science* **311,** 484–489 (2006).

5. Huber, G. W. and Corma, A. Synergies between bio- and oil refineries for the production of fuels from biomass. *Angewandte Chemie - International Edition* **46,** 7184–7201 (2007).

6. Corma, A., Iborra, S. and Velty, A. Chemical routes for the transformation of biomass into chemicals. *Chemical reviews* **107,** 2411–502 (2007).

7. Besson, M., Gallezot, P. and Pinel, C. Conversion of biomass into chemicals over metal catalysts. *Chemical reviews* **114,** 1827–70 (2014).

8. *EIA Refinery Yields* https://www.eia.gov/petroleum/data.cfm (2017).

9. Christensen, C. H., Rass-Hansen, J., Marsden, C. C., Taarning, E. and Egeblad, K. The renewable chemicals industry. *ChemSusChem* **1,** 283–289 (2008).

10. Vennestrøm, P. N. R., Osmundsen, C. M., Christensen, C. H. and Taarning, E. Beyond petrochemicals: The renewable chemicals industry. *Angewandte Chemie - International Edition* **50,** 10502–10509 (2011).

11. International Energy Agency. *The Future of Petrochemicals* tech. rep. (International Energy Agency, 2018).

12. Vivek, N., Pandey, A. and Binod, P. in *Current Developments in Biotechnology and Bioengineering* 719–738 (Elsevier, 2017).

13. *Center for BioRenewable Chemicals Webpage* https://www.cbirc.iastate.edu/overview/mission/ (2016).

14. Schlaf, M. Selective deoxygenation of sugar polyols to α,ω-diols and other oxygen content reduced materials–a new challenge to homogeneous ionic hydrogenation and hydrogenolysis catalysis. *Dalton transactions,* 4645–53 (2006).

15. Gervajio, G. C. in *Kirk-Othmer Encyclopedia of Chemical Technology* 1–38 (2012).

16. San, K.-Y. and Han, S. *US Patent* 9388434 (2013).

17. Werpy, T. and Peterson, G. *Top Value Added Chemicals from Biomass Volume 1 – Results of Screening for Potential Candidates from Sugars and Synthesis Gas* tech. rep. (2004).

18. Bozell, J. J. and Petersen, G. R. Technology development for the production of biobased products from biorefinery carbohydrates – the US Department of Energy's "Top 10" revisited. *Green Chemistry* **12,** 539–554 (2010).

19. Nikolau, B. J., Perera, M. A. D. N., Brachova, L. and Shanks, B. Platform biochemicals for a biorenewable chemical industry. *Plant Journal* **54,** 536–545 (2008).

20. Czernik, S. and Bridgwater, A. V. Overview of applications of biomass fast pyrolysis oil. *Energy and Fuels* **18,** 590–598 (2004).

21. Adkins, H. and Folkers, K. THE CATALYTIC HYDROGENATION OF ESTERS TO ALCOHOLS. *Journal of the American Chemical Society* **53,** 1095–1097 (1931).

22. Nebesh, E., Kelly, D. G. and Novak, L. T. *US Patent* 5124295 (1992).

23. Thakur, D. S. and Carrick, W. J. *US Patent* 9120086 (2015).

24. Yan, T. Y., Albright, L. F. and Case, L. C. Hydrogenolysis of esters, particularly perfluorinated esters. *Industrial and Engineering Chemistry Product Research and Development* **4,** 101–107 (1965).

25. Rieke, R. D., Thakur, D. S., Roberts, B. D. and White, G. T. Fatty methyl ester hydrogenation to fatty alcohol part I: correlation between catalyst properties and activity/selectivity. *Journal of the American Oil Chemists' Society* **74,** 333–339 (1997).

26. Chen, Y. and Chang, C. Cu-B_2O_3/SiO_2, an effective catalyst for synthesis of fatty alcohol from hydrogenolysis of fatty acid esters. *Catalysis Letters* **48,** 2–5 (1997).

27. Turek, T., Trimm, D. L. and Cant, N. W. The Catalytic Hydrogenolysis of Esters to Alcohols. *Catalysis Reviews* **36,** 645–683 (1994).

28. Evans, J. W., Wainwright, M. S., Cant, N. W. and Trimm, D. L. Structural and Reactivity Effects in the Copper-Catalyzed Hydrogenolysis of Aliphatic Esters. *Journal of Catalysis* **88,** 203–213 (1984).

29. Santiago, M., Sánchez-Castillo, M., Cortright, R. and Dumesic, J. Catalytic Reduction of Acetic Acid, Methyl Acetate, and Ethyl Acetate over Silica-Supported Copper. *Journal of Catalysis* **193,** 16–28 (2000).

30. Cortright, R., Sanchez-Castillo, M. and Dumesic, J. Conversion of biomass to 1,2-propanediol by selective catalytic hydrogenation of lactic acid over silica-supported copper. *Applied Catalysis B: Environmental* **39,** 353–359 (2002).

31. Pestman, R., van Duijne, a., Pieterse, J. and Ponec, V. The formation of ketones and aldehydes from carboxylic acids, structure-activity relationship for two competitive reactions. *Journal of Molecular Catalysis A: Chemical* **103,** 175–180 (1995).

32. Pestman, R., Koster, R., van Duijne, A., Pieterse, J. and Ponec, V. Reactions of carboxylic acids on oxides: 2. Bimolecular reaction of aliphatic acids to ketones. *Journal of Catalysis* **168,** 265–272 (1997).

33. Rachmady, W. and Vannice, M. Acetic Acid Reduction to Acetaldehyde over Iron Catalysts I. Kinetic Behavior. *Journal of Catalysis* **208,** 158–169 (2002).

34. Pestman, R., Koster, R., Boellaard, E., van der Kraan, A. and Ponec, V. Identification of the active sites in the selective hydrogenation of acetic acid to acetaldehyde on iron oxide catalysts. *Journal of Catalysis* **174,** 142–152 (1998).

35. Rachmady, W. and Vannice, M. Acetic acid hydrogenation over supported platinum catalysts. *Journal of Catalysis* **192,** 322–334 (2000).

36. Rachmady, W. and Vannice, M. Acetic Acid Reduction by H_2 on Bimetallic Pt-Fe Catalysts. *Journal of Catalysis* **209,** 87–98 (2002).

37. Rachmady, W. and Vannice, M. Acetic Acid Reduction by H_2 over Supported Pt Catalysts: A DRIFTS and TPD/TPR Study. *Journal of Catalysis* **207,** 317–330 (2002).

38. Narasimhan, C. S., Deshpande, V. M. and Ramnarayan, K. Selective hydrogenation of methyl oleate to oleyl alcohol on mixed ruthenium-tin boride catalysts. *Applied Catalysis* **48** (1989).

39. Narasimhan, C. S., Deshpande, V. M. and Ramnarayan, K. Mixed Ruthenium-Tin Boride Catalysts for Selective Hydrogenation of Fatty Acid Esters to Fatty Alcohols. *Industrial and Engineering Chemistry Research* **28,** 1110–1112 (1989).

40. Deshpande, V. M., Patterson, W. R. and Narasimhan, C. S. Studies on ruthenium-tin boride catalysts I. Characterization. *Journal of Catalysis* **121,** 165–173 (1990).

41. Cheah, K. Y., Tang, T. S., Mizukami, F., Niwa, S.-i., Toba, M. and Choo, Y. M. Selective hydrogenation of oleic acid to 9-octadecen-1-ol: Catalyst preparation and optimum reaction conditions. *Journal of the American Oil Chemists' Society* **69,** 410–416 (1992).

42. Tang, T.-S., Cheah, K.-Y., Mizukami, F., Niwa, S.-i. and Toba, M. Hydrogenation of 9-octadecenoic acid by Ru–Sn–Al_2O_3 catalysts: Effects of catalyst preparation method. *Journal of the American Oil Chemists' Society* **71,** 501–506 (1994).

43. Pouilloux, Y., Autin, F., Guimon, C. and Barrault, J. Hydrogenation of fatty esters over ruthenium–tin catalysts; characterization and identification of active centers. *Journal of Catalysis* **176,** 215–224 (1998).

44. Pritchard, J., Filonenko, G. A., van Putten, R., Hensen, E. J. M. and Pidko, E. A. Heterogeneous and homogeneous catalysis for the hydrogenation of carboxylic acid derivatives: history, advances and future directions. *Chem. Soc. Rev.* **44,** 3808–3833 (2015).

45. Broadbent, H. S. and Bartley, W. J. Rhenium Catalysts. VII. Rhenium(VI) Oxide. *The Journal of Organic Chemistry* **28,** 2345–2347 (1963).

46. Broadbent, H. S. and Seegmiller, D. W. Rhenium Catalysts. VIII. Rhenium(II) Oxide Dihydrate from Perrhenate via Alkali Metal-Amine Reductions. *The Journal of Organic Chemistry* **28,** 2347–2350 (1963).

47. Broadbent, H. S. and Selin, T. G. Rhenium Catalysts. VI. Rhenium(IV) Oxide Hydrate. *The Journal of Organic Chemistry* **28,** 2343–2345 (1963).

48. Broadbent, H. S., Campbell, G. C., Bartley, W. J. and Johnson, J. H. Rhenium and Its Compounds as Hydrogenation Catalysts. III. Rhenium Heptoxide. *The Journal of Organic Chemistry* **24,** 1847–1854 (1959).

49. Trivedi, B., Grote, D. and Mason, T. Hydrogenation of Carboxylic Acids and Synergistic Catalysts. *Journal of the American Oil Chemists' Society* **58,** 17–20 (1981).

50. Trivedi, B. C. *US Patent* 4104478 (1978).

51. Snappe, R. and Bouronville, J.-P. *French pat.* 2505819 (1981).

52. Mabry, M., Prichard, W. and Ziemecki, S. *US Patent* 4550185 (1985).

53. Rao, V. *US Patent* 4782167 (1988).

54. Kitson, M. and Williams, P. S. *US Patent* 4985572 (1991).

55. Takeda, Y., Nakagawa, Y. and Tomishige, K. Selective hydrogenation of higher saturated carboxylic acids to alcohols using a ReO_x–Pd/SiO_2 catalyst. *Catalysis Science & Technology* **2,** 2221 (2012).

56. Minh, D. P., Besson, M., Pinel, C., Fuertes, P. and Petitjean, C. Aqueous-Phase Hydrogenation of Biomass-Based Succinic Acid to 1,4-Butanediol Over Supported Bimetallic Catalysts. *Topics in Catalysis* **53,** 1270–1273 (2010).

57. Ly, B. K., Minh, D. P., Pinel, C., Besson, M., Tapin, B., Epron, F. and Especel, C. Effect of Addition Mode of Re in Bimetallic Pd–Re/TiO_2 Catalysts Upon the Selective Aqueous-Phase Hydrogenation of Succinic Acid to 1,4-Butanediol. *Topics in Catalysis* **55,** 466–473 (2012).

58. Ly, B. K., Tapin, B., Aouine, M., Delichere, P., Epron, F., Pinel, C., Especel, C. and Besson, M. Insights into the Oxidation State and Location of Rhenium in Re-Pd/TiO_2 Catalysts for Aqueous-Phase Selective Hydrogenation of Succinic Acid to 1,4-Butanediol as a Function of Palladium and Rhenium Deposition Methods. *ChemCatChem* **7,** 2161–2178 (2015).

59. Manyar, H. G., Paun, C., Pilus, R., Rooney, D. W., Thompson, J. M. and Hardacre, C. Highly selective and efficient hydrogenation of carboxylic acids to alcohols using titania supported Pt catalysts. *Chemical communications (Cambridge, England)* **46,** 6279–81 (2010).

60. Sá, J., Kartusch, C., Makosch, M., Paun, C., van Bokhoven, J. a., Kleymenov, E., Szlachetko, J., Nachtegaal, M., Manyar, H. G. and Hardacre, C. Evaluation of Pt and Re oxidation state in a pressurized reactor: difference in reduction between gas and liquid phase. *Chemical communications (Cambridge, England)* **47,** 6590–2 (2011).

61. Takeda, Y., Shoji, T., Watanabe, H., Tamura, M., Nakagawa, Y., Okumura, K. and Tomishige, K. Selective hydrogenation of lactic acid to 1,2-propanediol over highly active ruthenium-molybdenum oxide catalysts. *ChemSusChem* **8,** 1170–1178 (2015).

62. Rozmysłowicz, B., Kirilin, A., Aho, A., Manyar, H., Hardacre, C., Wärnå, J., Salmi, T. and Murzin, D. Y. Selective hydrogenation of fatty acids to alcohols over highly dispersed ReO_x/TiO_2 catalyst. *Journal of Catalysis* **328,** 197–207 (2015).

63. Pallassana, V. and Neurock, M. Reaction Paths in the Hydrogenolysis of Acetic Acid to Ethanol over Pd(111), Re(0001), and PdRe Alloys. *Journal of Catalysis* **209,** 289–305 (2002).

2

Reduction of Propionic Acid over a Pd-Promoted ReO_x/SiO_2 Catalyst Probed by X-Ray Absorption Spectroscopy and Transient Kinetic Analysis

This chapter is adapted from "Kammert, J. D.; Xie, J.; Godfrey, I. J.; Unocic, R. R.; Stavitski, E.; Attenkofer, K.; Sankar, G.; Davis, R. J. Reduction of Propionic Acid over a Pd-Promoted ReO_x/SiO_2 Catalyst Probed by X-Ray Absorption Spectroscopy and Transient Kinetic Analysis. ACS Sustain. Chem. Eng. 2018, 6 (9), 12353–12366." Copyright 2018 American Chemical Society

Abstract

A Pd-promoted Re/SiO_2 catalyst was prepared by sequential impregnation and compared to monometallic Pd/SiO_2 and Re/SiO_2. All samples were characterized by electron microscopy, H_2 and CO chemisorption, H_2 temperature-programmed reduction, and *in situ* X-ray absorption spectroscopy at the Re L_{III} and Pd K-edges. The samples were also tested in the reduction of propionic acid to 1-propanol and propionaldehyde at 433 K in 0.1-0.2 MPa H_2. Whereas monometallic Pd was inactive for carboxylic acid reduction, monometallic Re catalyzed aldehyde formation, but only after high-temperature pre-reduction that produced metallic Re. When Pd was present with Re in a bimetallic catalyst, Pd facilitated the reduction of Re in H_2 to $\sim$4+ oxidation state at modest temperatures, producing an active catalyst for the conversion of propionic acid to 1-propanol. Under the conditions of this study, the orders of reaction in propionic acid and H_2 were approximately zero and one, respectively. Transient kinetic analysis of the carboxylic acid reduction to alcohols suggested that at least 50% of the Re in the bimetallic catalyst participated in the catalytic reaction. The Pd is proposed to enhance the catalytic activity of the bimetallic catalyst by spilling over hydrogen that can partially reduce Re and react with surface intermediates.

2.1 Introduction

The recent increase in demand for renewable chemical feedstocks and carbon-neutral sources of energy has placed the spotlight on the utilization of biomass and bio-oil for the production of chemicals and fuels.[1–4] Specialty chemicals are still produced mostly by the transformation of fossil fuels[5] as they offer better returns on investment due to decades of research and

development. In contrast to the functionalization chemistry required to convert oil derivatives into consumer products, biomass conversion will require the development of defunctionalization processes.[6]

One area of focus in biomass conversion research is the utilization of lauric oils, e.g. coconut and palm kernel oils, containing significant amounts of short- and medium-chain fatty acids.[7] The free fatty acids and triglycerides in these feedstocks have carbon chain lengths between C_6 and C_{22}, which can be refined to fatty alcohols for use as detergents, lubricants, plasticizers, and high-performance oils for jet engines[4,7] via reduction of the acid functional group. The development of low-cost processes for the production of these types of specialty chemicals has the potential to increase the sustainability and CO_2-neutrality of the chemicals and fuels industries.[2,8]

The current industrial process to produce renewable fatty alcohols involves the reduction of fatty acid esters over a copper-based catalyst.[4,7,9–11] Traditionally, the catalyst used in the process is copper chromite ($CuCr_2O_4$), also known as an Adkins-type catalyst, which consists of a mixed oxide of copper and chromium. It can be extruded with clay or other supports, and is mixed with alkali or alkaline earth metals to improve its activity.[10,11] While copper chromite has been known to be an effective catalyst for many years, recent concerns about the leaching of toxic Cr^{6+} ions[9,12,13] have prompted research on non-chromium-containing catalysts. Additionally, the conditions used to carry out this process commercially are known to be rather extreme, utilizing H_2 pressures upwards of 25 MPa.[9] Therefore, the design of a catalyst that can operate under lower pressure conditions is highly desirable.

The bulk fermentation of sugars by engineered micro-organisms has the potential to se-

lectively produce a variety of carboxylic acids on a large scale.[14,15] Short-chain carboxylic acids can also be produced by the fast pyrolysis of biomass, where potential applications of this bio-oil will require remediation of the resulting acidity.[16] Direct reduction of carboxylic acids (instead of esters) to alcohols is thus a motivation of research on new catalysts, in order to take advantage of this large-scale production of free acids. Recent work has shown the reduction of carboxylic acids can be catalyzed by a variety of metal and metal oxide surfaces, generally consisting of a mixture of reducible precious metal and oxophilic metal components. Examples include studies by Primo et al.[17] and Rachmady and Vannice[18] who demonstrated the activity of Ru and Pt supported on TiO_2. Catalysts such as $RuSn/Al_2O_3$[19] and $RuMo/ZrO_2$[20] have also been studied for reduction of carboxylic acids in polar solvents. More detailed information about the reduction of carboxylic acids and their derivatives can be found in the review by Pritchard et al.[21]

Rhenium in particular has demonstrated an ability to catalyze the selective reduction of carboxylic acids to alcohols. More than a half century ago, solid rhenium oxide surfaces having Re in several different oxidation states were active in the reduction of a number of carboxylic acids at 423-443 K and dihydrogen pressures between 13.5 and 27.0 MPa.[22–25] In most cases, the major product was the corresponding monoalcohol, with yields reported up to 100%. The patent literature reports on several inventions describing the use of supported rhenium catalysts promoted by palladium, silver, and copper.[26–29] A recent study by Takeda et al. involving Ru, Rh, Ir, Pt, and Pd added to a Re/SiO_2 catalyst reported that the Pd-promoted Re/SiO_2 system is the most active and selective of these materials for the reduction of stearic acid in a 1,4-dioxane solvent,[30] and that the metal-promoted Re catalysts are capable of operating at significantly lower H_2 pressures and temperatures than those required by Re alone.

The support of the Pd-promoted Re-based (PdRe) catalysts has a significant influence on their activity in the liquid-phase reduction of fatty acids to fatty alcohols. Takeda et al. demonstrated that PdRe was significantly more active on a SiO_2 support than on a variety of other supports including Al_2O_3, TiO_2, and C, and that Re was the main active material in the catalyst.[30] Corbel-Demailly et al. reported that PdRe/TiO_2 catalyzed the aqueous-phase reduction of succinic and levulinic acids to their corresponding α,ω-diols.[31] Interestingly, Rozmyslowicz et al. demonstrated that a monometallic Re/TiO_2 catalyst could still facilitate the reduction of stearic acid in decane solvent without Pd promotion after pretreatment with H_2 at 673 K.[32] The underlying reasons for the observed influence of the support and promoter remain unclear. Besson et al. used X-ray photoelectron spectroscopy (XPS) to conclude that active catalysts for reduction of succinic and levulinic acids to their corresponding diols in the aqueous phase appeared to consist mostly of Re oxide in a 3+ oxidation state.[31,33–36] Both Re/SiO_2 and PdRe/SiO_2 catalysts were characterized after catalytic reduction of stearic acid in dioxane using *ex situ* X-ray absorption spectroscopy (XAS).[37] White line analysis of the Re L_{III} edge data suggested that Re in these materials resides in an average oxidation state near 2+ after reaction, which has also been reported to be among the active oxidation states of Re as a bulk oxide.[23]

To remove the complicating influence of solvents and liquid phase acids, we have studied the catalyst structure and transient reaction kinetics of carboxylic acid reduction in the gas phase. The investigation of a Pd-promoted Re/SiO_2 catalyst under gas phase reduction conditions should eliminate the dissolution of metals that can also cause particle growth. In particular, *in situ* X-ray absorption spectroscopy and *ex situ* electron microscopy were used to examine the chemical state and distribution of the metal components on the catalyst support and the transient

kinetic analysis provided important information on the utilization of Re in the active material, which is currently unknown.

2.2 Experimental Methods

2.2.1 Catalyst synthesis

Catalysts used in this study were synthesized by an incipient wetness impregnation method, with each component of the catalyst being added stepwise as outlined by Takeda et al.[30] For example, the desired loading of the metal salt (aqueous tetraaminepalladium(II) nitrate, 10 wt%, Aldrich; ammonium perrhenate, Aldrich, 99%) was added to a quantity of distilled, deionized water (16.8 MΩ) to form a solution equal in volume to the pore volume of the SiO_2 support (Fuji Silysia Chemical Ltd, 0.72 $cm^3\ g^{-1}$, 511 $m^2\ g^{-1}$). This solution was mixed with the support until a homogeneously-distributed sample was formed. The impregnated sample was dried at 368 K in air for 12 h, and then treated in air at 773 K for 3 h after ramping for 3 h. In the bimetallic catalyst, the Re was added first, prior to heating in air to 773 K, after which the Pd solution was added to the supported Re catalyst, dried in air at 368 K, and heated in air to 773 K for a second time. The weight loading of supported metals after synthesis was determined by inductively coupled plasma optical emission spectroscopy (ICP-OES) performed by Galbraith Laboratories, Knoxville, TN.

2.2.2 Adsorption of H_2, CO, and N_2

The chemisorption of H_2 (Praxair, 5.0) and CO (Praxair, 3.0) and physisorption of N_2 (Praxair, 5.0) were carried out using a Micromeritics ASAP 2020 instrument. Prior to chemisorp-

tion measurements, samples were heated to 473 K (Pd/SiO_2, $PdRe/SiO_2$) or 673 K (Re/SiO_2) under flowing H_2 at 4 K min^{-1}, then held at 473 K (or 673 K) for 1 hour under flowing H_2. The samples were then evacuated at 473 K and degassed for 2 h before cooling to 373 K or 308 K for H_2 chemisorption or 308 K for CO chemisorption. Either H_2 or CO was dosed from 0.001-0.06 MPa, and the total monolayer chemisorption values are reported after extrapolation of the higher pressure linear region of the isotherm to zero pressure. Prior to N_2 physisorption measurements, catalysts were degassed by heating to 723 K under vacuum for 4 h before cooling to liquid N_2 temperature for analysis. Physisorption results were analyzed using the BET analysis of the N_2 (Praxair, 5.0) adsorption isotherm.

2.2.3 Temperature-Programmed Reduction

Temperature-programmed reduction (TPR) was carried out using a Micromeritics AutoChem II 2920 instrument equipped with a thermal conductivity detector. All catalysts were heated to 308 K under Ar (Praxair, 5.0) before switching to a reducing gas mixture. The reducing gas mixture of 5% H_2 in Ar (Praxair, certified mixture) passed through the catalyst bed at a flow rate of 50 cm^3 min^{-1} while the bed temperature was ramped at 10 K min^{-1} to 573 K.

2.2.4 Transmission Electron Microscopy

Transmission electron microscopy (TEM), scanning transmission electron microscopy with a high-angle annular dark-field detector (STEM-HAADF) and energy-dispersive X-ray spectroscopy (EDS) were performed on an FEI Titan 80-300 operating at 300 kV that is equipped with a Gatan 794 Multi-scan Camera (EFTEM) and an energy-dispersive spectrometer for elemental X-ray analysis at the University of Virginia. High-resolution STEM-HAADF imaging

with EDS mapping was carried out using a Hitachi HF-3300 operating at 300 kV and equipped with a Bruker SDD-EDS detector at Oak Ridge National Lab. Samples were prepared by sonicating 50 mg of each sample in cyclohexane or hexanes for 30 min, followed by dropwise impregnation onto a Ni or Au grid coated with lacey carbon (400 mesh, Ted Pella).

2.2.5 X-ray Absorption Spectroscopy

In situ X-ray absorption spectroscopy (XAS) was carried out on beamline B18 of the Diamond Light Source (DLS) at the Harwell Science & Innovation Campus, Didcot, United Kingdom, operated at 3.0 GeV and with a typical current of *ca.* 300 mA. The setup of this beamline has been described previously.[38] All XAS measurements associated with Re were performed in transmission at the Re L_{III}-edge (10.535 keV). The XAS measurements associated with Pd were performed in fluorescence using a 9 element Ge solid state detector at the Pd K-edge (24.353 keV). Both edges were collected with a spot size of 0.2 x 0.25 mm. The Re L_{III}-edge experiments performed at DLS used a Si(111) double crystal monochromator and Cr-coated harmonic rejection mirrors. Experiments performed at the Pd K-edge used a Si(311) double crystal monochromator with Pt-coated harmonic rejection mirrors. The XAS experiment relevant to the high-temperature reduction of Re/SiO_2 was carried out on beamline 8-ID of the National Synchrotron Light Source II (NSLS-II) at Brookhaven National Laboratory in Brookhaven, New York, operated at 3.0 GeV and with a typical current of *ca.* 325 mA. The capabilities of this beamline have previously been summarized.[39] The Re L_{III}-edge experiments performed at NSLS-II used a Si(111) double crystal monochromator with uncoated Si higher harmonic rejection mirrors and a spot size of 0.25 mm.

To secure samples in the beam path, pellets of catalyst were pressed gently to form flat cylinders, and the amount of catalyst for transmission experiments was adjusted to give an edge jump ($\Delta\mu x$) of around 1. At DLS, these pellets were placed inside an *in situ* reaction chamber made of bored-through poly-ether ether ketone (PEEK). Kapton windows were secured in place with poly(trifluoroethylene) washers on either side of the chamber to ensure a gas-tight seal. The PEEK reaction chamber was held in place by a bronze sample holder with a heating element so that the temperature of the reaction chamber could be controlled. A Re foil (Goodfellow, 12.5 μm, 99.99%) was used as a reference at the Re L_{III}-edge, and a Pd metal foil (Goodfellow, 12.5 μm, 99.95%) was used as a reference at the Pd K-edge. For the high-temperature pretreatment, a brass sample holder was used in place of the PEEK chamber.

Before each treatment, the fresh catalyst pellet was first purged of O_2 by flushing the reaction chamber for 15 min with N_2. To perform the *in situ* experiments, two different methods were used. In the first method, designated as "no pretreatment" or NP, 4% H_2 in N_2 was passed through a room-temperature saturator containing propionic acid and then over the catalyst at 30 $cm^3\ min^{-1}$ for 15 min before ramping the temperature at 3 K min^{-1} to 413 K. The temperature was held at 413 K for 1 h before ramping again at 3 K min^{-1} to 433 K. The temperature was then held at 433 K for 1 h after which the sample was cooled to room temperature and purged with pure N_2. In the second method, designated as "low-temperature pretreatment" or LTP, 4% H_2 in N_2 was passed over the catalyst for 15 min at 30 $cm^3\ min^{-1}$ before ramping the temperature at 3 K min^{-1} to 453 K. The temperature was held at 453 K for 30 min before cooling at 10 K min^{-1} to 433 K when the flow was passed through a saturator containing propionic acid and then over the catalyst bed. The temperature was then held at 433 K for 1 h then cooled at 10 K min^{-1}

to 413 K and held for 1 h after which the sample was cooled to room temperature and purged with pure N_2. The "high-temperature pretreatment", abbreviated HTP, was performed by first purging the sample chamber with N_2 at 100 cm^3 min^{-1}. The gas flow was then switched to 4% H_2 in N_2 and the catalyst bed was then heated to 673 K at 6 K min^{-1}. The catalyst bed was held at 673 K for 1 h, and then cooled to 433 K. The catalyst bed was held at 433 K for 20 minutes while spectra were collected and then cooled to room temperature.

All XAS results were processed using Demeter XAS analysis freeware created by Bruce Ravel.[40] Results from X-ray absorption near-edge spectroscopy (XANES) were background-corrected and normalized uniformly at each edge using Athena, an XAS background correction application that is part of the Demeter software package. The oxidation state of each sample was determined by the shift in the maximum of the derivative in the edge energy compared to known standards.[41,42] The standards used for Re were Re metal foil, (Goodfellow, 12.5 μm, 99.99%), ReO_2 powder (Aldrich, 99.7%), ReO_3 powder (Pfaltz & Bauer, 99.9%) and Re_2O_7 powder (Aldrich 99.9%) for oxidation states of 0, +4, +6, and +7, respectively. The standards used for Pd were Pd foil (Goodfellow, 12.5 μm, 99.95%), and PdO powder (Aldrich, 99.999%), for oxidation states of 0 and +2, respectively. The EXAFS results were also background corrected and normalized in Athena, then k^3-weighted and Fourier transformed to change from k-space to R-space. The R-space data for standards were then fitted to multi-shell models over k-ranges from approximately 3 to 13 for Pd and 3 to 16 for Re at nodes in the fine structure. Fitting was performed in Artemis with FEFF6, yielding an S_0^2 value of 0.830 for all metallic Re shells, 0.748 for all oxidized Re shells, 0.829 for all metallic Pd shells, and 0.641 for all oxidized Pd shells.

2.2.6 Reduction Reactions

The reduction of propionic acid (Sigma Aldrich, 99.5%) to 1-propanol and propionaldehyde or butyric acid (Sigma-Aldrich, 99.0%) to 1-butanol and butyraldehyde was carried out in a stainless steel downward flow reactor with inner diameter 0.46 cm contained within the reactor system depicted in Figure 2.1. The catalyst bed consisted of the supported metal catalyst powder (0.060-0.140 g) resting on a plug of glass wool. Temperature measurements were made using a thermocouple inserted from the top of the reactor tube into the middle of the catalyst bed. Prior to reaction, the system (including the liquid saturators) was purged with flowing N_2 at 30 cm^3 min^{-1} for at least 10 min. After purging with N_2, the reactor was purged with H_2 at 15 cm^3 min^{-1} for 10 min before ramping the temperature to 433 K. Once the temperature was stable the flow was passed through a stainless-steel saturator to form a mixture of 1 vol.% carboxylic acid in H_2 (0.1-0.22 MPa) that was fed to the catalyst bed. The effluent gases were separated and quantified using an SRI 8610C gas chromatograph (GC-FID) equipped with an MXT-WAX column (0.53 mm i.d., 30 m) and a flame-ionization detector (FID). To obtain order of reaction in H_2, the H_2 partial pressure was varied by partially replacing H_2 with N_2 at the appropriate flowrate while maintaining a constant pressure of acid. To obtain the order of reaction in acid, the partial pressure of the acid was varied while maintaining a constant pressure of H_2. The total flowrate was kept constant for all variations in reactant partial pressures.

The conversion of the acid to its corresponding aldehyde and alcohol was evaluated from the integrated product peak areas. Methane was used as the internal standard, which prevented the quantification of any C_2 through C_4 hydrocarbons that might have been formed during the kinetic experiments. Hydrocarbon products were typically produced in very low amounts (be-

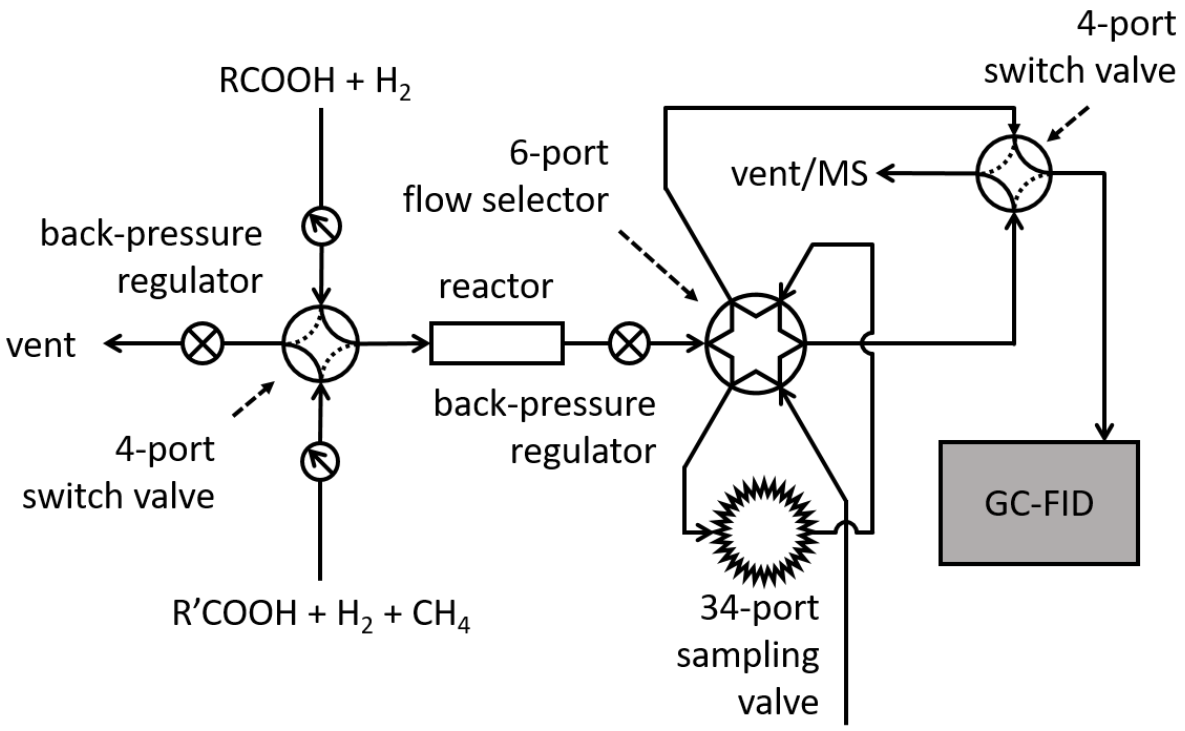

Figure 2.1: Schematic representation of the reactor system used to collect steady-state and transient reaction kinetics.

tween 5-10% selectivity) under the conditions studied here. The fractional conversion (f_i) of acid i to its corresponding alcohol and aldehyde products j was calculated using the expression

$$f_i = \frac{\sum M_j}{M_i + \sum M_j} \tag{2.1}$$

where M_j is the molar flow rate of the component j. Similarly, the selectivity of the reaction towards each product j was calculated using the expression

$$S = \frac{M_j}{\sum M_j} \tag{2.2}$$

2.2.7 Transient Kinetic Analysis

The transient kinetic analysis carried out in this work was performed in a manner analogous to steady-state isotopic transient kinetic analysis (SSITKA).[43] This technique can be used to approximate the turnover frequency and number of reactive intermediates leading to products on the active sites of a catalyst. The SSITKA technique is a well-established method that has been used by our group to investigate ammonia synthesis,[44,45] CO oxidation,[46,47] CO hydrogenation[48], and the Guerbet coupling of ethanol.[49,50] All transient kinetic experiments performed in the current study were carried out using the reactor that is illustrated in Figure 2.1.

The transient kinetic experiment proceeds by first allowing a reaction to reach steady-state, and then abruptly switching from the reactant to a different (but structurally similar) reactant that is converted at a similar rate (in this case modified only by the insertion of a CH_2 group into the carbon chain) and observing the transient response of the system. In the experiments reported here, the transient response of the catalyst after switching between butyric and propionic acid was studied. In a typical switching experiment, an inert tracer is fed with one of the reactant streams to correct for the gas-phase holdup in the reactor system. Figure 2.2 presents an ideal normalized transient kinetic response curve after replacing butyric acid with propionic acid. The decay of the tracer is indicative of the characteristic gas-phase holdup of the reactor system, representative of the non-ideal nature of the step switch assuming there is no interaction between the inert tracer and the catalyst surface. After the switch in reactant acid from C_4 to C_3, the products of these acids will decrease (C_4) or increase (C_3), crossing near 0.5, as shown in Figure 2.2.

As is commonly done in the SSITKA experiment, kinetic parameters can be derived from the individual normalized transient response curves (F_i). The area below each normalized tran-

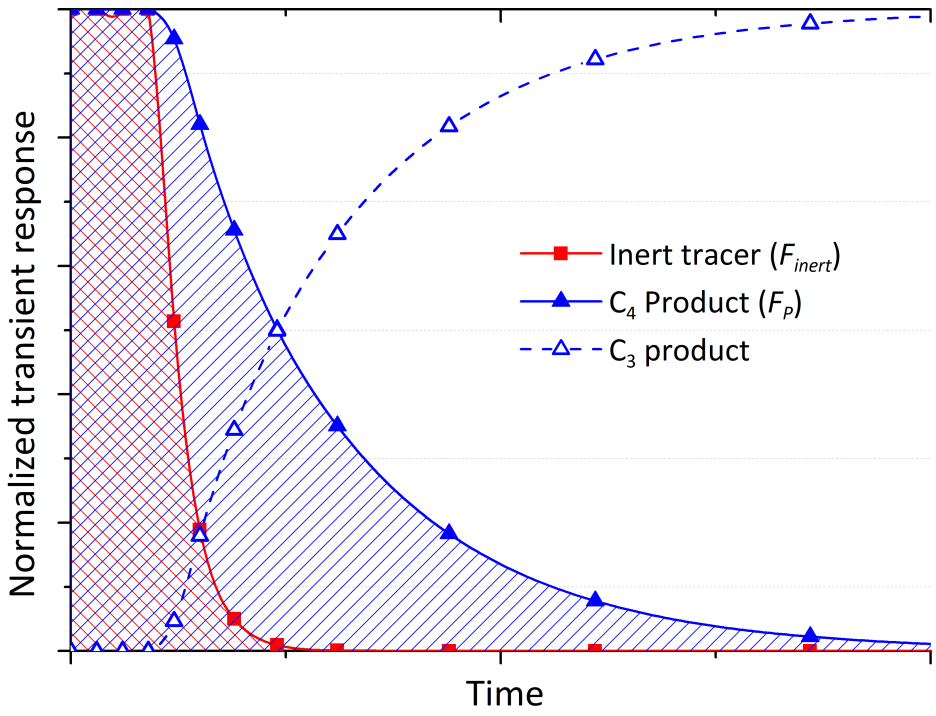

Figure 2.2: Theoretical transient response curves for products undergoing a reactant switch from C_4 reactant to C_3 reactant. Decay of the inert tracer (red squares) is used to correct for the gas-phase holdup of the reactor system when calculating the mean surface residence time from the integral of the C_4 product decay (filled blue triangles) and C_3 product replacement (open blue triangles).

sient response curve is representative of the mean surface residence time (τ_i) after correction by the response of the inert tracer, given by

$$\tau_i = \int_{t_0}^{\infty} (F_i - F_{inert})\, dt \tag{2.3}$$

Here the inverse of the mean surface residence time is equivalent the turnover frequency of the catalyst for the given product, or simply

$$TOF_i = (\tau_i)^{-1} \tag{2.4}$$

From the mean surface residence time τ_i and the rate of formation of a product by the catalyst (R_i), it is also possible to calculate the surface coverage of reactive intermediates (N_i) leading to a given product, given by

$$N_i = R_i \cdot \tau_i \tag{2.5}$$

Further discussion of the SSITKA technique and considerations can be found in the review by Shannon and Goodwin.[43]

The SSITKA method works well because there is almost no perturbation in the steady state rate during the switch between different isotopes of the reactant. In the transient method used in this work, we switched between C_4 and C_3 acids to acquire the transient kinetics. There was a small difference in the steady state rate of conversion of these two acids, but the difference did not appear to significantly affect the expected transient behavior as summarized in Figure 2.2.

The transient kinetic experiments performed in this work were carried out using the reaction procedure described earlier. The reaction was allowed to come to steady-state during conversion of the original reactant, at which point flow was started through the modified reactant saturator. Once the flow had stabilized, the reactant flow path was switched from the original reactant saturator to the modified reactant saturator using a 4-way valve. The transient behavior of the product alcohols was monitored with time on stream using the GC-FID described earlier, while the transient behavior associated with the aldehyde was monitored by collecting samples of the reactor effluent in the 34-port sampling valve with 16 samples loops depicted in Figure 2.1 and subsequently injecting the samples into the GC-FID. The influence of flow rate was explored by adjusting the gas flows and repeating the experiment.

2.3 Results

2.3.1 Elemental Analysis and Adsorption of H_2, CO, and N_2

Results from ICP-OES, H_2 and CO chemisorption, and N_2 physisorption for the catalysts studied in this work are shown in Table 2.1. Each of the catalysts had a high surface area, greater than 400 $m^2\ g^{-1}$, which is similar to the support. The elemental analysis for the Re loading revealed about 1.0-1.5 wt% less Re than the nominal loading, which may be the result of partial volatilization of Re_2O_7 during the 773 K thermal treatments.

The chemisorption of H_2 on the monometallic Pd catalyst at 373 K indicates approximately 39% of Pd atoms were exposed, assuming a stoichiometry of H to surface Pd equal to 1. When the temperature of the H_2 chemisorption was decreased to 308 K, chemisorption increased by 50%, consistent with the formation of a β-PdH phase. During chemisorption of CO,

a stoichiometry of between 0.5 and 1 for CO/Pd is appropriate.[51] Assuming a CO to surface Pd ratio of 0.75,[52] the fraction of Pd exposed is equal to 43%, which is consistent with the results from H_2 chemisorption.

In contrast, the monometallic Re catalyst and the PdRe bimetallic catalyst chemisorbed a smaller fraction of H_2 at 373 K, with a H/metal ratio of 0.11 for both samples. This low uptake was likely a result of the high barrier to H_2 chemisorption on Re.[53] The total uptake of H_2 on the PdRe catalyst at 373 K was below the additive total of 37.1 μmol g_{cat}^{-1} that would be expected if each metal (Pd, Re) adsorbed independently and was of the same dispersion as their monometallic counterparts. The higher total uptake of H_2 on the PdRe catalyst at 308 K compared to that at 373 K is consistent with the formation of a β-PdH phase, as observed with the monometallic Pd catalyst. This result can be compared to previously reported H_2 uptake results on a Pd-promoted Re/Al_2O_3 catalyst[54] that showed strong interaction of Pd with Re, which inhibited the formation of bulk β-PdH. Even in the presence of excess Re, apparently minimal interaction between the Re and Pd left the surface Pd on our $PdRe/SiO_2$ catalyst available for reaction with H_2 leading to formation of bulk β-PdH. Results from CO chemisorption on the Re-containing catalysts also revealed relatively low uptake, with a CO/Re ratio of 0.16 for the monometallic catalyst and a CO/metal ratio of 0.13 for the bimetallic catalyst. Similar to the case with H_2, the uptake of CO was below the additive total of 88.2 μmol g_{cat}^{-1} that would be expected from independent adsorption onto a mixture the two metals that was equally as dispersed as their monometallic counterparts. These chemisorption results indicate a change in dispersion or metal availability in at least one of the supported metal components when the two metals are combined on one support.

Table 2.1: Results from elemental analysis and gas adsorption.

Sample	Metal loading (wt %)		Surface Area ($m^2\ g^{-1}$)	Chemisorption (μmol g_{cat}^{-1})		
				H_2 (373 K)	H_2 (308 K)	CO (308 K)
Pd/SiO_2	1.03% Pd	–	484	18.9	30.9	31.7
Re/SiO_2	–	6.52% Re	433	19.8	17.6	57.7
$PdRe/SiO_2$	0.88% Pd	6.91% Re	460	24.9	32.4	60.0

For the PdRe catalyst, surface Pd still accounts for some of the observed H_2 chemisorption, resulting in the increase in H_2 uptake relative to either of the monometallic catalysts. In the case of CO chemisorption, a different trend is observed. The CO chemisorption uptake on the $PdRe/SiO_2$ is nearly identical to that measured on the Re/SiO_2. Previous work has shown that Re^{7+} and Re^{4+} interact weakly with CO leading to minimal chemisorption,[55] while completely reduced Re demonstrates higher CO chemisorption uptake.[56] The observation that CO chemisorption on the PdRe catalyst was not a simple combination of adsorption on Pd/SiO_2 and Re/SiO_2 is attributed to a larger fraction of partially-oxidized Re species present in the bimetallic system, which had undergone a lower temperature H_2 pretreatment than the more highly reduced Re/SiO_2 after high temperature reduction.

2.3.2 Temperature Programmed Reduction

As illustrated in Figure 2.3, the monometallic Pd catalyst began to reduce immediately upon heating H_2, with maximum hydrogen consumption rate at 354 K. The monometallic Re catalyst did not consume any H_2 until 525 K and reached a maximum consumption rate at 536 K. The bimetallic catalyst exhibited two H_2 consumption peaks at low temperature, with maxima at 353 K and 368 K, and no H_2 consumption peaks at higher temperatures. These results agree with those from H_2 TPR reported previously using a number of reducible, noble-metal-

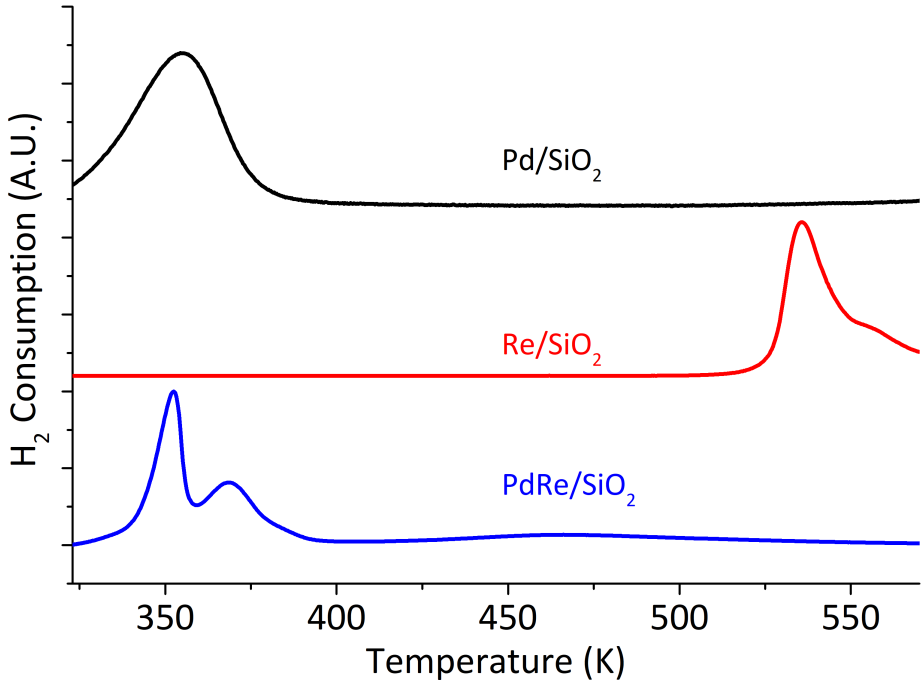

Figure 2.3: Temperature programmed reduction of the synthesized catalysts at a ramp rate of 10 K min^{-1}.

promoted, oxophilic metal oxides supported on SiO_2,[30] and on Pd-promoted Re supported on Al_2O_3 systems.[57] The TPR results in Figure 2.3 suggest that the addition of Pd to a Re catalyst lowers the temperature at which the Re is reduced, presumably by spillover of atomic H from Pd to the Re. In addition, low-melting-temperature metal oxides, such as Re_2O_7 with a melting point of 630 K, are capable of spreading across oxide supports and reacting during thermal treatments due to their low Tammann temperatures.[58] The mobility of Re^{7+} oxides could have resulted in the migration of Re toward Pd during heating, leading to lower temperature reduction via spillover of surface H from Pd to Re.

2.3.3 Transmission Electron Microscopy

Image analysis of the fresh $PdRe/SiO_2$ catalyst acquired by STEM-HAADF shown in Figure 2.4 gave an average metal particle size of 3.2±1.5 nm. Elemental analysis by EDS (shown in Figure A.1) showed the fresh catalyst particles had many smaller particles that contained only Re and fewer larger particles containing Pd. The average metal particle size of $PdRe/SiO_2$ after use in propionic acid reduction increased slightly to 3.9±1.5 nm. The mapping of the metallic components of the $PdRe/SiO_2$ catalyst after use in propionic acid reduction is shown in Figure 2.5. The mapping results revealed that Pd and Re were not co-located. Whereas Pd EDS mapping correlates well with the visible nanoparticles in Figure 2.5(a), the Re EDS mapping suggests Re is highly dispersed across the surface of the material.

Image analysis of the fresh and used Pd/SiO_2 catalysts by STEM HAADF gave an average particle size of 3.1±0.8 nm and 3.0±1.0 nm, respectively. Image analysis of the fresh Re/SiO_2 was consistent with a very wide range of particles. Some Re particles were >100 nm whereas Re was also detected by EDS on SiO_2 regions in which no particles could be imaged. Evidently much of the Re is highly dispersed across much of the support. After use for 24 h in the reduction of 1 kPa propionic acid in 0.1 MPa H_2 at 433 K, the Re was observed to transform into to a mixture of larger particles ∼20-50 nm across and highly dispersed particles of an average size <1 nm. Images of the monometallic catalysts can be found in the supporting information in Figures A.2 and A.3.

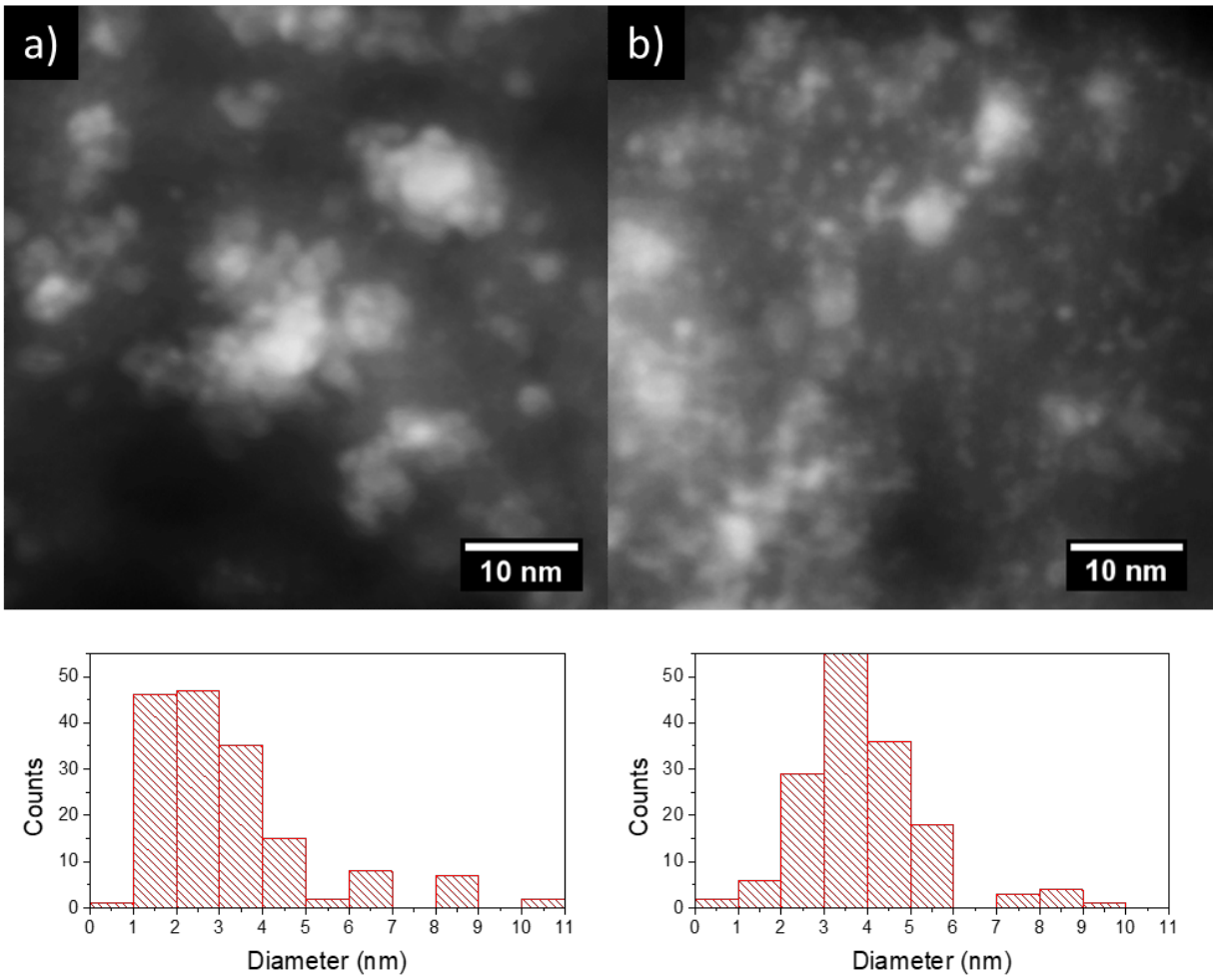

Figure 2.4: STEM-HAADF images of $PdRe/SiO_2$ catalyst (a) before and (b) after use for the reduction of propionic acid for 24 h with associated particle size distributions. Reactions were carried out at 433 K, in 0.1 MPa H_2 and 1 kPa propionic acid.

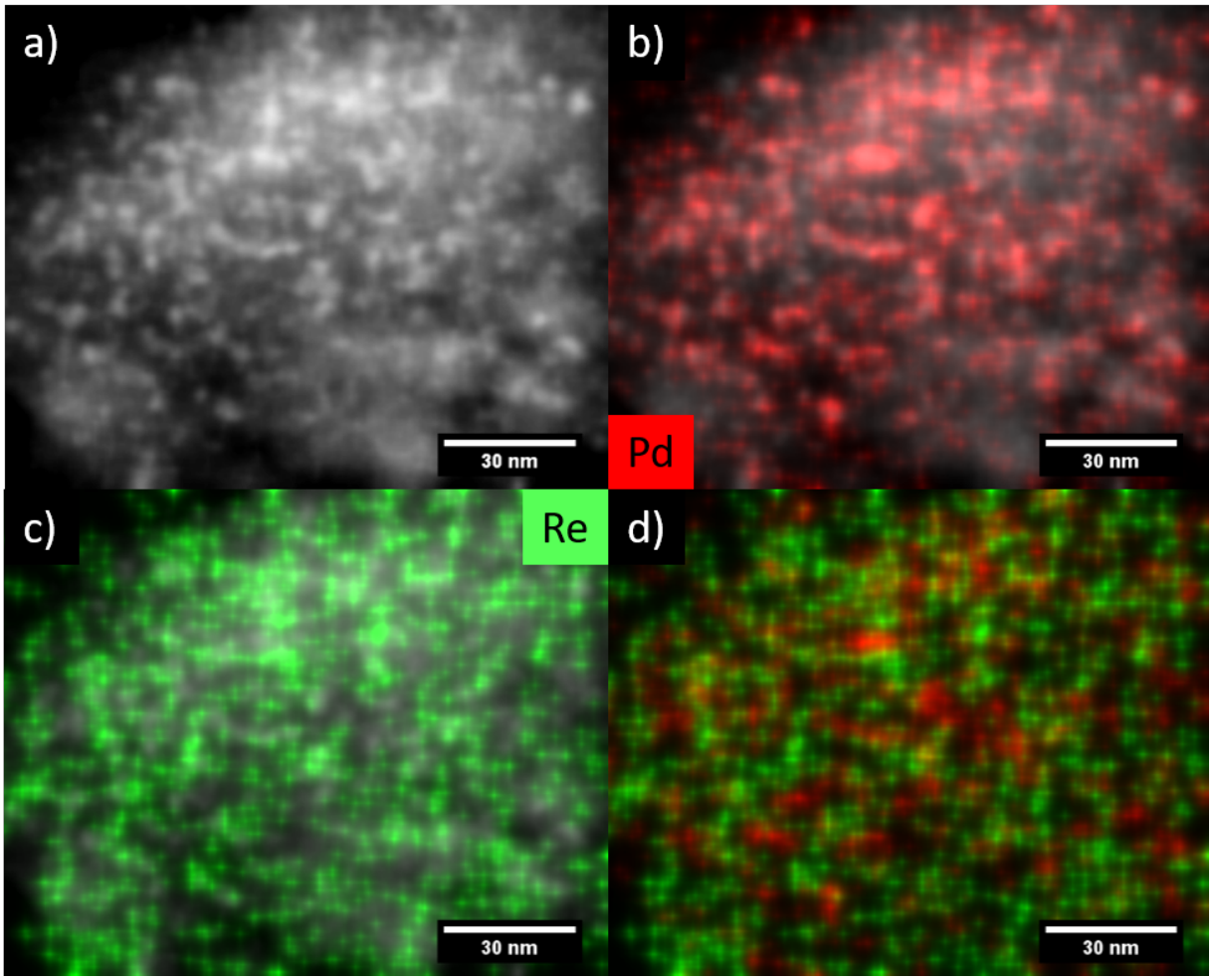

Figure 2.5: STEM-EDS mapping of $PdRe/SiO_2$ catalyst after reduction of 1 kPa propionic acid in 0.1 MPa H_2 for 24 h at 433 K, showing (a) STEM image, (b) EDS signal corresponding to Pd overlaid on STEM image, (c) EDS signal corresponding to Re overlaid on STEM image, and (d) composite EDS signals corresponding to Pd and Re.

2.3.4 X-ray Absorption Spectroscopy

The Re L_{III}-edge XANES associated with the catalyst samples are shown in Figure 2.6. The highest whiteline intensity (maximum absorbance at the absorption edge) was associated with the as-synthesized catalysts at room temperature prior to exposure to H_2 or H_2/acid mixtures. The whiteline intensity and the edge position, defined as the first maximum of the first derivative of the absorption edge, were both consistent with Re in the air-exposed catalysts residing in a 7+ oxidation state, typical of Re_2O_7.

A correlation between the Re L_{III}-edge energy and the formal oxidation state of each Re standard was used to approximate the oxidation state of the catalysts in the presence of reactant gases. Previous studies have shown that the oxidation state and edge position of Re oxides at the L_{III}-edge appear fairly linear between Re^0 and Re^{6+}, while Re^{7+} does not follow the same linear trend.[41,42] To minimize the error of this correlation at higher oxidation states, a linear interpolation was used between each of the data points. The results of this correlation can be seen in Figure 2.6(b) and (d). When the monometallic Re/SiO_2 catalyst was treated at low temperature (433-453 K) in flowing 4% H_2 in N_2, with or without co-fed propionic acid, the Re appeared to reduce slightly to an average oxidation state between Re^{6+} and Re^{7+} as can be seen in Figure 2.6(d). At the higher pretreatment temperature of 673 K (HTP), the monometallic Re/SiO_2 was reduced in H_2 very nearly to metal, which is consistent with the TPR results showing this elevated temperature is required to substantially reduce the supported Re species.

The as-synthesized $PdRe/SiO_2$ catalyst at room temperature had spectral features associated with Re^{7+}, similar to the as-synthesized monometallic Re/SiO_2 catalyst. When the $PdRe/SiO_2$ was directly exposed to propionic acid vapor in the 4% H_2/N_2 mixture at 433 K (NP) to simulate

reaction conditions, the Re L_{III} edge whiteline intensity and the edge energy decreased, corresponding to an average oxidation state of +5.0. When the as-synthesized $PdRe/SiO_2$ catalyst was pretreated at 453 K (LTP) in flowing 4% H_2 in N_2, the Re L_{III} edge whiteline intensity decreased more significantly and the edge position moved to even lower energy, associated with reduction to an average oxidation state of +3.6. Evidently, the slightly higher pretreatment temperature in H_2 was able to more extensively reduce Re than the reaction conditions. Most importantly, the presence of Pd facilitated the low-temperature partial reduction of Re, consistent with results from H_2 TPR (Figure 2.3).

The EXAFS fitting results from the *in situ* experiments are summarized in Table 2.2, and the fitting results for the standards are summarized in the appendix in Table A.1. As the ratio of tetrahedrally coordinated to octahedrally coordinated Re in Re_2O_7 may vary depending on the ratio of bulk to molecularly dispersed material,[59] the first shell Re-O coordination number could not be used to make conclusions about the Re species present. Instead, analysis of the EXAFS corresponding to the Re oxide standards revealed that as the oxidation state of Re decreased, the Re-O interatomic distance increased, as shown in Figure A.4. When the first shell Re-O scattering paths of the oxide standards were fitted, the average Re-O distance was observed to increase with decreasing oxidation state from 1.74 Å for Re-O in Re_2O_7 to 2.00 Å for Re-O in ReO_2. The EXAFS in Figure 2.7(a) did not reveal significant changes in the first-shell Re-O interatomic distance for Re/SiO_2 samples treated up to 453 K in H_2, with or without propionic acid. The EXAFS in Figure 2.7(b) associated with $PdRe/SiO_2$ showed a clear increase in the first-shell Re-O interatomic distance, indicating that the Re in the $PdRe/SiO_2$ catalysts was reduced significantly. The fitted Re-O bond distances of 2.033 (NP) and 2.072 Å (LTP) for the

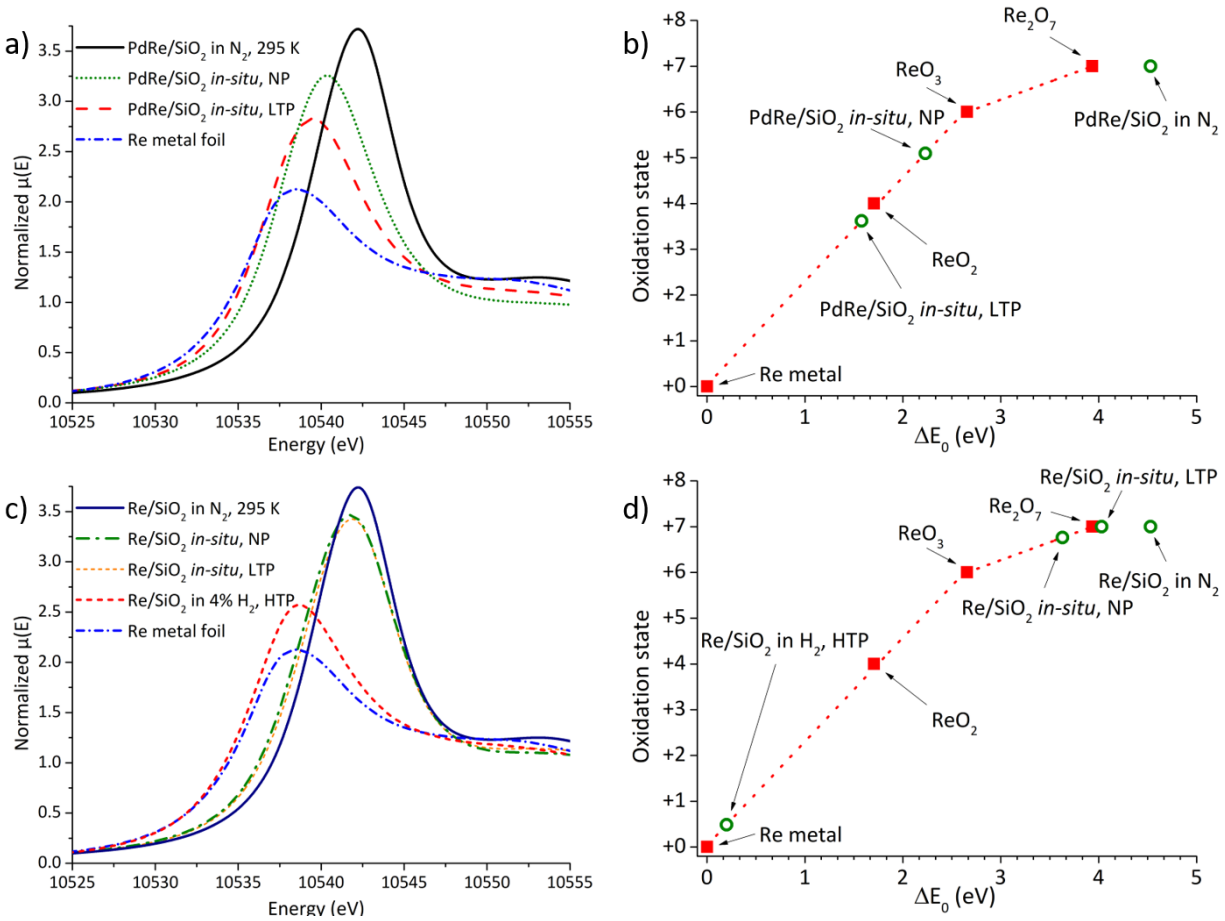

Figure 2.6: Re L_{III} edge XANES and correlated average oxidation states. Spectra were collected at 433 K unless specified, and spectra denoted "*in-situ*" were collected in flowing 4% H_2/N_2 passing through a room temperature propionic acid saturator. (a) $PdRe/SiO_2$ XANES before treatment, and after NP or LTP. (b) Correlation between edge energy and oxidation state for $PdRe/SiO_2$. (c) Re/SiO_2 XANES before treatment, and after NP, LTP, or without propionic acid after HTP. (d) Correlation between edge energy and oxidation state for Re/SiO_2.

$PdRe/SiO_2$ catalysts under 4% H_2/N_2 and acid are slightly elongated from the ReO_2 standard. These elongated Re-O distances suggest that Re has an oxidation state between 3+ and 4+ in the $PdRe/SiO_2$ under reaction conditions. Representative EXAFS fitting results are shown in Figure A.5.

The Pd K-edge XANES shown in Figure 2.8 and Figure A.6 confirmed that Pd in both the bimetallic PdRe and monometallic Pd samples was oxidic after synthesis but was reduced to metal under reaction conditions. The Pd K-edge EXAFS were consistent with a first shell

Pd-Pd coordination number of between 8.1 and 8.5 (depending on pretreatment) for Pd/SiO_2 under reaction conditions, correlating to about 70% dispersion assuming spherical metal particles,[60] which is consistent with an average particle size of 1.5 nm. Although the Pd particle size estimated from EXAFS is slightly below that estimated from H_2 chemisorption and electron microscopy, all of the techniques suggest that Pd is highly dispersed on the catalyst surface. No Pd-Re interactions were evident based on the Pd K-edge EXAFS of either of the studied $PdRe/SiO_2$ samples (without pretreatment or pretreated at 453 K) under reaction conditions. Representative radial distribution functions of the Pd samples can be found in Figure A.4 in the appendix.

2.3.5 Catalytic Reduction of Propionic Acid

The rates of conversion of propionic acid to 1-propanol and propionaldehyde over Re/SiO_2 and $PdRe/SiO_2$ catalysts at steady state are summarized in Table 2.3. The Pd/SiO_2 sample is not shown in Table 2.3 as it only produced a small amount of light hydrocarbons. Over $PdRe/SiO_2$, 1-propanol was the major product of the reaction, but the selectivity shifted towards propionaldehyde at the highest flowrate (lowest conversion). Small amounts (5-10%) of light hydrocarbons were also observed in the product stream, but are not included in Table 2.3 because of overlap with the methane internal standard. Hydrocarbon products have previously been attributed to the decarbonylation or decarboxylation of the C_N acid to form C_{N-1} hydrocarbons or the secondary reduction of the C_N alcohol to form C_N hydrocarbons.32 The increase in 1-propanol selectivity with increasing acid conversion suggests that most of the propionaldehyde was subsequently hydrogenated to 1-propanol on the catalyst. A physical mixture of the monometallic Re/SiO_2 and

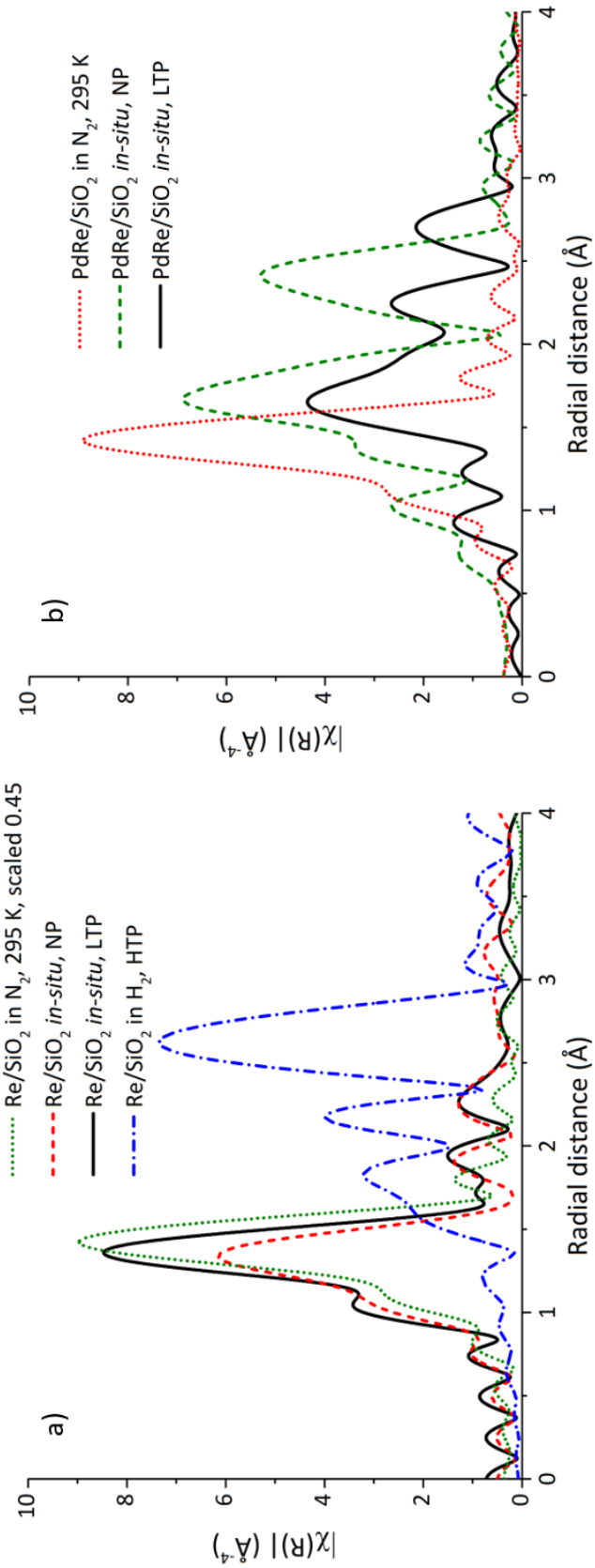

Figure 2.7: Magnitude of the Fourier transform (not corrected for phase shift) of the Re L_{III}-edge EXAFS associated with (a) Re/SiO_2 and (b) $PdRe/SiO_2$ after various pretreatments. Spectra were collected at 433 K unless specified, and spectra denoted as "*in-situ*" were collected in flowing 4% H_2/N_2 passing through a room temperature propionic acid saturator.

Table 2.2: EXAFS fitting results for SiO_2-supported PdRe, Re, and Pd catalysts.

Sample	Pretreatment	*In situ*	Temp. (K)	Edge	Shell	R (Å)	N	σ^2 (Å^2)	ΔE_0 (eV)	R-factor
$PdRe/SiO_2$	none	N_2	Ambient	Re L_{III}	Re-O	1.737 ±0.002	4.5 ±0.2	0.0010 ±0.0003	6.9 ±0.6	0.02
				Pd K	Pd-O	2.021 ±0.007	4.1 ±0.3	0.0006 ±0.0010	-1.7 ±0.9	0.01
				Pd K	Pd-Pd	3.059 ±0.013	4.7 ±2.0	0.0041 ±0.0030		
				Pd K	Pd-Pd	3.451 ±0.009	5.4 ±2.7	0.0039 ±0.0036		
	NP	4% H_2/N_2,	433	Re L_{III}	Re-O	2.033 ±0.014	4.5 ±0.6	0.0051 ±0.0015	8.9 ±2.1	0.02
		propionic acid		Pd K	Pd-Pd	2.738 ±0.002	8.1 ±0.3	0.0078 ±0.0003	-5.5 ±0.3	0.01
	LTP	4% H_2/N_2,	433	Re L_{III}	Re-O	2.079 ±0.021	2.6 ±0.5	0.0044 ±0.0027	9.7 ±2.3	0.03
		propionic acid		Pd K	Pd-Pd	2.739 ±0.003	8.2 ±0.4	0.0077 ±0.0004	-5.4 ±0.4	0.01
Re/SiO_2	none		Ambient	Re L_{III}	Re-O	1.737 ±0.007	4.5 ±0.5	0.0010 ±0.0007	7.0 ±1.7	0.01
	NP	4% H_2/N_2,	433	Re L_{III}	Re-O	1.683 ±0.016	2.0 ±0.4	0.0023 ±0.0014	-10. ±4.7	0.03
	LTP	propionic acid	433	Re L_{III}	Re-O	1.691 ±0.010	2.0 ±0.3	0.0011 ±0.0010	-0.8 ±2.7	0.02
	HTP	4% H_2/N_2	433	Re L_{III}	Re-O	2.023 ±0.021	2.0 ±0.6	0.0098 ±0.0044	6.3 ±1.7	0.03
				Re L_{III}	Re-Re	2.759 ±0.008	5.7 ±0.6	0.0073 ±0.0007		
Pd/SiO_2	none	N_2	Ambient	Pd K	Pd-O	2.029 ±0.009	4.0 ±0.5	0.0011 ±0.0014	-0.6 ±1.2	0.03
				Pd K	Pd-Pd	3.061 ±0.021	4.1 ±2.8	0.0058 ±0.0051		
				Pd K	Pd-Pd	3.456 ±0.015	4.8 ±3.8	0.0055 ±0.0058		
	NP	4% H_2/N_2,	433	Pd K	Pd-Pd	2.739 ±0.003	8.5 ±0.4	0.0088 ±0.0004	-5.3 ±0.3	0.01
	LTP	propionic acid	433	Pd K	Pd-Pd	2.750 ±0.004	8.2 ±0.4	0.0094 ±0.0005	-5.9 ±0.4	0.01

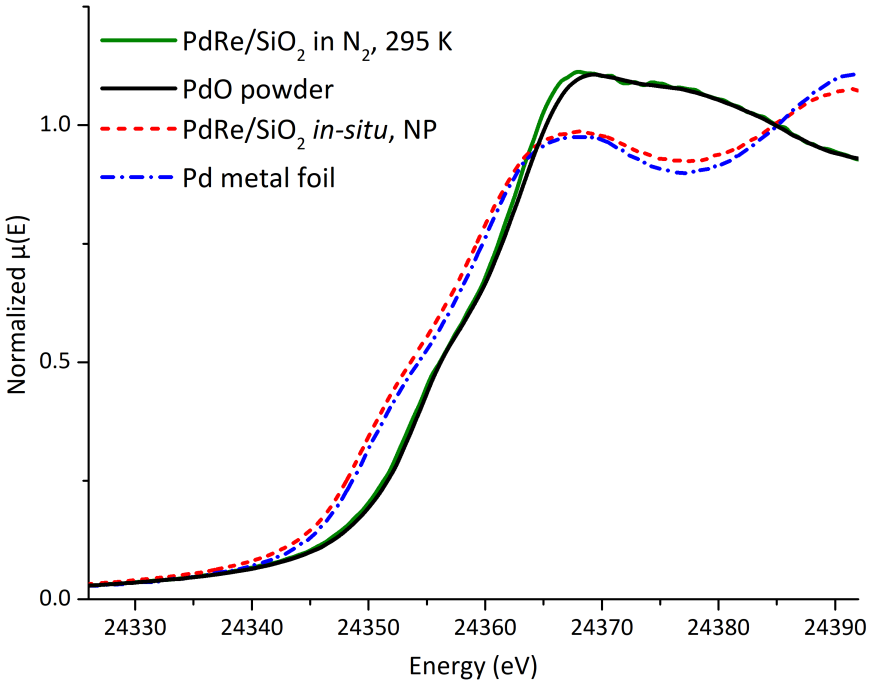

Figure 2.8: Pd K-edge near-edge spectra. Solid lines are for as-synthesized $PdRe/SiO_2$ compared to PdO standard. Dashed lines are for the $PdRe/SiO_2$ sample under reaction conditions (433 K, in 4% H_2/N_2 passed through a room temperature propionic acid saturator) compared to Pd metal foil.

Pd/SiO_2 catalysts with the same ratio of metals was also tested for reduction of propionic acid. The relative rate over the physical mixture was only 30% of that of the bimetallic catalyst under the same conditions, but both systems produced a majority of alcohol product. When the H_2 pressure and propionic acid concentration were varied over $PdRe/SiO_2$, the alcohol formation reaction was observed to be first order and nearly zero order, respectively, as shown in Figure 2.9. These orders of reaction are similar to those that have been reported previously for stearic acid reduction in 1,4-dioxane[37] and for the reduction of octanoic acid in a decane solvent (see Figure A.8), suggesting the reaction mechanism is unchanged by the presence of solvent.

The rate of propionic acid conversion over Re/SiO_2 pretreated at 673 K in H_2 was substantially lower than that measured over $PdRe/SiO_2$ (Table 2.3). The high temperature pretreatment of Re/SiO_2 was needed to reduce the supported Re oxide and generate catalytic activity, which

Table 2.3: Steady state reduction of propionic acid over at 433 K, 1 kPa propionic acid in 0.1 MPa H_2.

Catalyst	Gas flow rate (cm^3 min^{-1})	Conversion (%)	Rate of acid conversion (mol g_{cat}^{-1} h^{-1})	Selectivity of oxygenates[a] 1-propanol	propionaldehyde
$PdRe/SiO_2$	15	7.1	1.6×10^{-4}	80	20
	30	4.0	2.0×10^{-4}	74	26
	60	2.5	2.4×10^{-4}	64	36
Re/SiO_2[b]	18	4.3	6.3×10^{-5}	22	78
	28	2.2	4.2×10^{-5}	13	87
	51	1.4	4.8×10^{-5}	11	89

(a) Does not account for the small amount of light hydrocarbons
(b) Re/SiO_2 was pretreated at 673 K under flowing H_2 for 1 h

is consistent with the TPR results in Figure 2.3. Over Re/SiO_2, the major product of propionic acid reduction was propionaldehyde. Extrapolation of the results in Table 2.3 for Re/SiO_2 to infinite flowrate indicates an initial selectivity to propionaldehyde of 97%, suggesting that the primary reaction during propionic acid reduction over Re/SiO_2 is aldehyde formation. In all of the cases reported here, the linear dependence of propionic acid conversion on inverse flowrate indicates the reaction was differential as is illustrated in Figure A.9.

2.3.6 Transient Kinetic Analysis of Carboxylic Acid Reduction

The mean surface residence times of species leading to alcohol and aldehyde products and the numbers of the reactive intermediates on the catalyst surface leading to those products were quantified using transient kinetic analysis. The transient experiments were performed at various flowrates to evaluate the importance of product readsorption on the kinetic parameters. Transient kinetic analysis associated with $PdRe/SiO_2$ was performed over alcohol selectivity ranges from 64-80%.

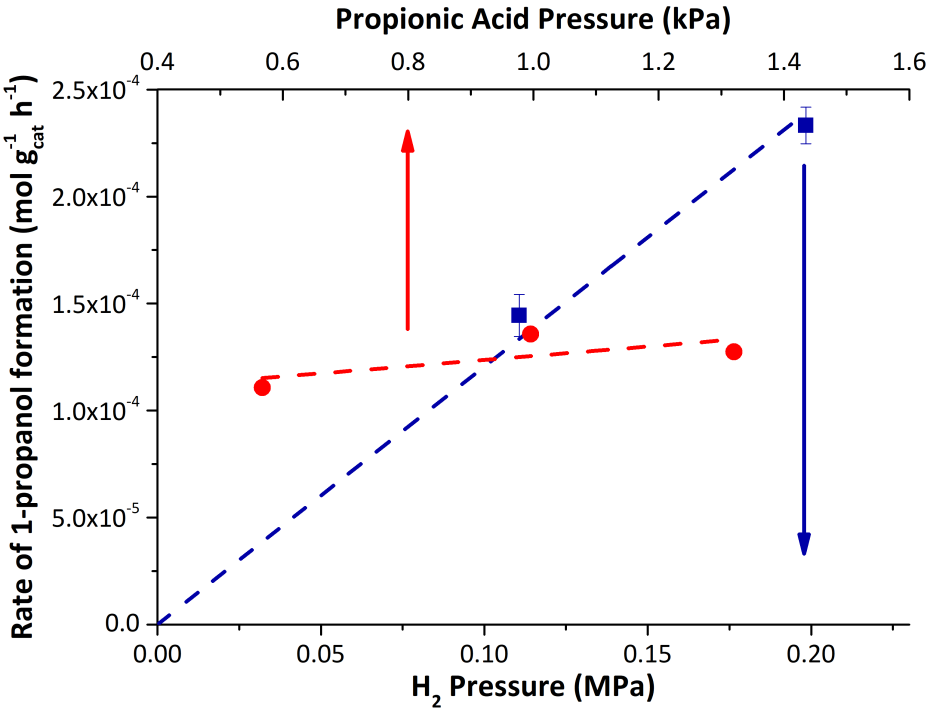

Figure 2.9: Influence of reactant partial pressures on observed rate of 1-propanol formation over $PdRe/SiO_2$ at 433 K. When H_2 pressure was varied, propionic acid pressure was held at 1 kPa, and when propionic acid pressure was varied, H_2 pressure was held at 0.1 MPa.

The time constant of the gas-phase holdup in the reactor system was measured as the total flow rate was varied over the range of 15 cm^3 min^{-1} to 60 cm^3 min^{-1}. The gas-phase holdup could not be measured directly during the alcohol transient because the decay of the methane tracer was faster than the sampling rate. The very short time constant of the gas-phase holdup (measured during aldehyde experiments) was negligible in comparison to the alcohol transient times and was not included in the calculation of the mean surface residence times for species leading to alcohols. In contrast, the mean surface residence times of species leading to aldehyde products was much shorter than those leading to alcohols, so the gas phase holdup was properly accounted for in the aldehyde transient results.

Examples of normalized transient curves during carboxylic acid reduction are shown in Figure 2.10. Since the reaction is zero order in acid, a slight difference in the gas phase concentrations of C_3 and C_4 acids will not affect their measured reaction rates. By integrating the response after the switch in reactant, the mean surface residence time of the species leading to a specified product was calculated. The mean surface residence times for reactants leading to alcohol products during the reduction of propionic and butyric acid are shown in Figure 2.11 as a function of inverse flowrate. An estimate of the intrinsic mean surface residence time in the absence of readsorption effects (τ_0) can be derived from extrapolating the lines in Figure 2.11 to infinite flowrate (1/F = 0). The intrinsic mean surface residence time is then used to determine an intrinsic turnover frequency and the number of reactive intermediates on the catalyst, N_i in the absence of readsorption effects. These results are summarized in Table 2.4.

The intrinsic TOF for 1-propanol formation over $PdRe/SiO_2$ is 1.6 times that of 1-butanol formation, which is very similar to the ratio of the global rates of formation of 1-propanol to 1-

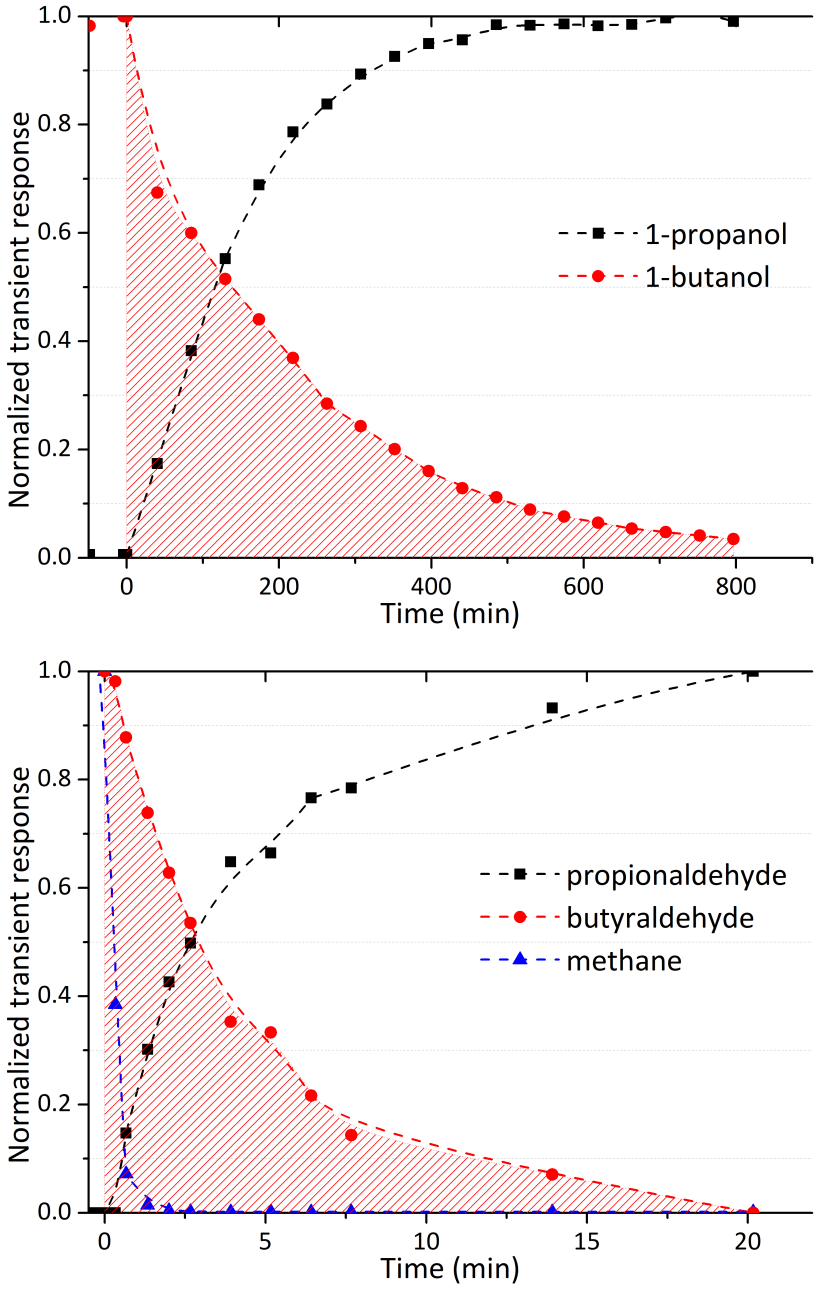

Figure 2.10: Example of transient product responses during carboxylic acid reduction obtained after a reactant switch from butyric acid to propionic acid.

Table 2.4: Kinetic parameters derived from transient kinetic analysis of 1 kPa propionic and butyric acid reduction in 0.1 MPa H_2 at 433 K, including the ratio of reactive intermediates to Re atoms N_i/Re.

Catalyst	Product	Rate of formation[a] (mol g_{cat}^{-1} h^{-1})	τ_0 (min)	TOF[b] (s^{-1})	N_i/Re[c]
$PdRe/SiO_2$	1-propanol	1.6×10^{-4}	81	2.1×10^{-4}	0.59
	propionaldehyde	6.3×10^{-5}	2.0	8.3×10^{-3}	0.006
	1-butanol	6.9×10^{-5}	130	1.3×10^{-4}	0.40
	butyraldehyde	3.1×10^{-5}	2.0	8.4×10^{-3}	0.003
Re/SiO_2	propionaldehyde	3.7×10^{-5}	1.4	1.1×10^{-2}	0.003
	butyraldehyde	2.1×10^{-5}	1.7	1.0×10^{-2}	0.002

(a) Calculated by extrapolation to infinite flowrate
(b) TOF is calculated as τ_0^{-1}
(c) Ratio of intermediates leading to specified product divided by total Re in sample

butanol of 2.3. Therefore, the same fraction of the active surface is involved in both reactions. The number of reactive surface intermediates leading to 1-propanol or 1-butanol is calculated to be 59% or 40% of the total Re in the $PdRe/SiO_2$ catalyst respectively, (see Table 2.4). Variation of the H_2 pressure during the transient experiment revealed a nearly first-order dependence on H_2 of the intrinsic TOF of alcohol formation from both butyric and propionic acids, as shown in Figure A.10. The intrinsic kinetic parameters determined at 0.2 MPa (as summarized in Table A.4 and Figure A.11) are also consistent with approximately 50% of the Re participating in the reaction. A mean surface residence time of 450 min (corresponding to a 0.1 N_i/Re ratio) was observed for 1-propanol formation on Re/SiO_2 at 0.1 MPa H_2 pressure and 1 kPa propionic acid, but the effects of flowrate could not be eliminated due to limits on the detection of the very minor alcohol products. The intrinsic TOF for production of aldehydes on the $PdRe/SiO_2$ and Re/SiO_2 catalysts was about 2 orders of magnitude greater than that of alcohols formed over $PdRe/SiO_2$. All associated transient response results can be found in Tables A.2 and A.3 in the appendix.

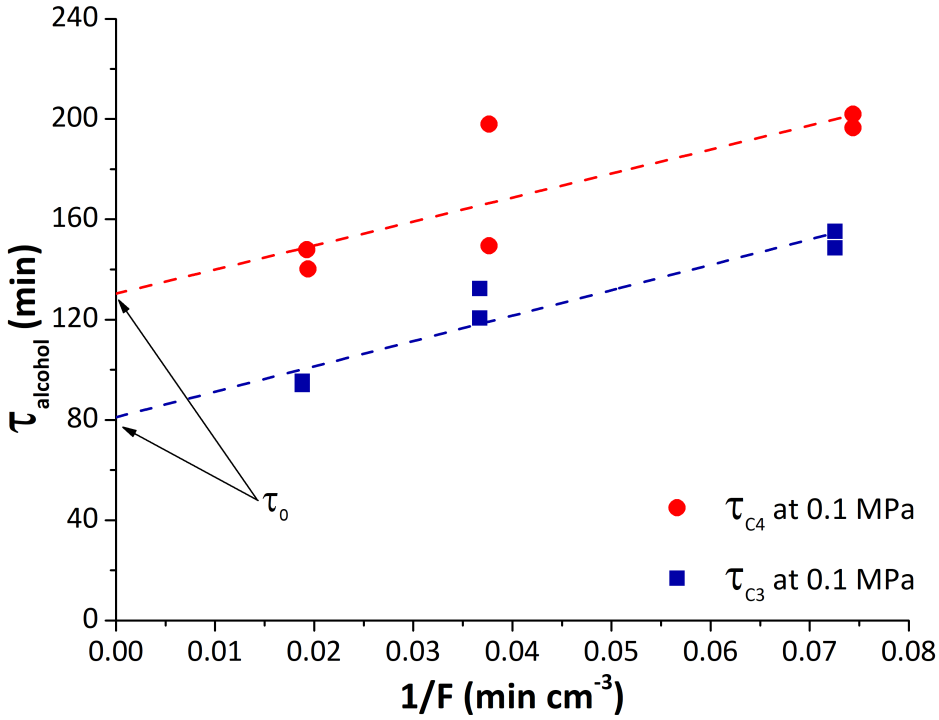

Figure 2.11: Mean surface residence times of species leading to alcohols at 433 K over $PdRe/SiO_2$ extrapolated to infinite flowrate to remove artifacts from product readsorption. Red circles represent results from butyric acid conversion at 0.1 MPa H_2 pressure while blue squares represent results from propionic acid conversion at 0.1 MPa H_2 pressure. The conversion ranged from 2.5-7% over the range of flowrates used.

2.4 Discussion

2.4.1 Reducibility of $PdRe/SiO_2$

The results from H_2 TPR and *in situ* XAS confirm that Pd facilitates the reduction of Re^{7+} on the air-exposed, as-synthesized Pd-promoted Re/SiO_2 catalyst at lower temperatures than required for the reduction of the un-promoted Re/SiO_2. This phenomenon is well-established for Pt-promoted Re catalysts on Al_2O_3[41,61,62] and has been suggested previously using TPR in other supported Re systems promoted by Rh[63], Pd, Ru, and Ir.[30] The additional low-temperature reduction peak observed in H_2 TPR of the $PdRe/SiO_2$ catalyst compared to the Pd/SiO_2 catalyst (Figure 2.3) corresponds to the low-temperature partial reduction of Re^{7+} oxide likely by H_2 spillover. Results from H_2 chemisorption, which show that Re did not suppress formation of β-phase Pd hydride, suggest that some surface Pd in the PdRe sample is available for H_2 adsorption and therefore for spillover to the Re. High-resolution STEM with EDS mapping also suggests that the metals on the PdRe catalyst remain highly dispersed during reaction, and that Re and Pd do not appear to form significant amounts of bimetallic nanoparticles. The Re appeared to be highly dispersed and Pd existed almost exclusively in larger well-dispersed metal particles, which is also consistent with extensive spillover of H from Pd as the main reason for enhanced Re reduction in the presence of Pd. The XAS performed in this work suggests that under reaction conditions, Pd in the $PdRe/SiO_2$ remains entirely metallic, while the Re resides in an average oxidation state of around 4+. Partially-reduced Re oxides have demonstrated carboxylic acid reduction activity in the past, and Re^{4+} in particular has been observed to have remarkable selectivity to alcohols in the catalytic reduction of carboxylic acids to alcohols.[64] Analysis of the Re-O interatomic dis-

tances in the EXAFS is consistent with XANES, indicating the Re is partially reduced to around Re^{4+} from its initial Re^{7+} state. The Re-O first shell interatomic distance in the bimetallic PdRe sample is slightly longer than the interatomic distance of Re-O in the Re^{4+} standard, whether or not the sample was pretreated prior to reaction. Evidently, there was little contribution to the EXAFS from higher oxidation states and we conclude that nearly all of the Re in the bimetallic catalyst was partially reduced in the presence of Pd and H_2. Likewise, very little evidence from Re-Re scattering associated with zero-valent Re was observed on the $PdRe/SiO_2$ catalyst. For the monometallic Re catalyst, the as-synthesized sample revealed a short Re-O interatomic distance and XANES features consistent with Re^{7+} oxide species. High-temperature pretreatment in H_2 resulted in nearly complete reduction of Re to the metal. It should be emphasized that a high temperature pretreatment was required for an active Re/SiO_2 catalyst. Consistent with H_2 TPR, results from XANES and EXAFS showed negligible reduction of Re/SiO_2 at 453 K. Evidently the predominant Re^{7+} species that is present after low temperature reduction is the least active Re species for carboxylic acid reduction in H_2 at 433 K.

Based on the interpretation of the XAS results, H_2 and CO chemisorption, H_2 TPR, and STEM-EDS, a schematic for the evolution of the catalyst structure is summarized in Figure 2.12. The metals in both the Re and PdRe catalysts are expected to be completely oxidized after catalyst synthesis. However, the chemical state of each catalyst under reaction conditions is related strongly to its treatment before reaction. Monometallic Re/SiO_2 was observed to remain in a highly oxidized state under reaction conditions, both without pretreatment and with pretreatment at 453 K under 4% H_2. When exposed to high-temperature pretreatment in H_2 at 673 K, the monometallic catalyst appeared to be nearly completely reduced. The Re in the $PdRe/SiO_2$

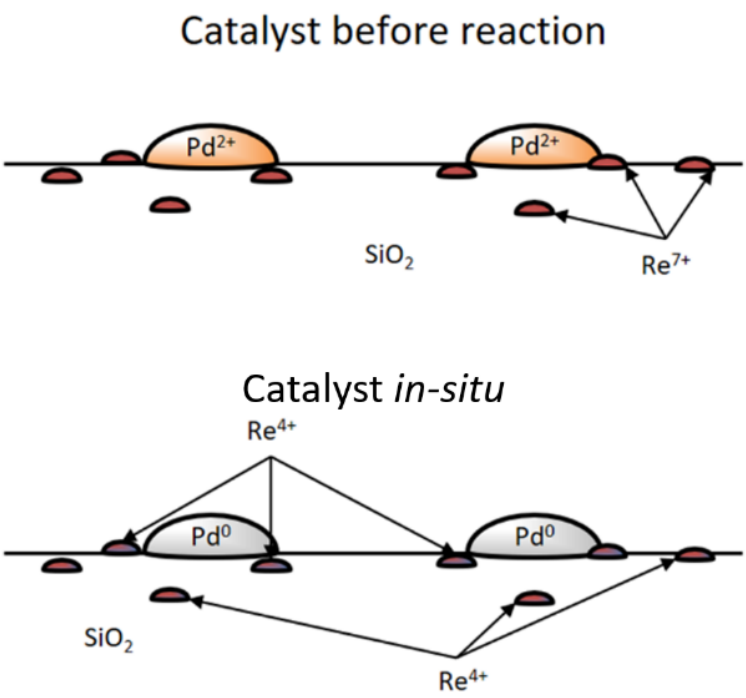

Figure 2.12: Representation of $PdRe/SiO_2$ catalyst surface before and after pretreatments leading to an active catalyst.

catalyst on the other hand was only partially reduced both with and without low-temperature pretreatments in H_2. Under gas phase conditions, controlled reduction of the Re to an intermediate oxidation state for reaction occurs mainly when the catalyst is promoted by Pd. Our results contrast those in which a $PdRe/SiO_2$ catalyst was reported to contain a significant fraction of Re metal after liquid-phase reduction of stearic acid to stearyl alcohol[37], but are consistent with other works that propose partially reduced Re oxide with Re in about a 4+ oxidation state as the average oxidation state of Re species on the catalyst.

2.4.2 Surface Reactions

The transient kinetics experiments reveal the number of intermediates that ultimately form products, but there can be species that are equilibrated on the surface and actually convert in the

reverse direction during the transient. Therefore, the number of reactive intermediates determined by this method is actually a lower bound on the number of active sites on the catalyst surface. Using transient kinetic analysis, the reported ratio of reactive intermediates that produce alcohols and aldehydes to Re atoms on the catalyst operating at steady state is about 50% in the $PdRe/SiO_2$ catalyst (Table 2.4). We have based our analysis on the ratio of intermediates to total Re atoms present. It is quite possible that some of the intermediates leading to product are located on surfaces other than Re, such as the Pd surface. The reported uptake of H_2 in the $PdRe/SiO_2$ catalyst would correspond to a maximum dispersion of Pd of 60%, with the real value likely closer to that observed in the monometallic Pd/SiO_2 of 39%. Using a Pd dispersion of 60% as an upper bound, the ratio of surface Pd atoms to total Re on the catalyst is 1:7.5. Since the number of surface intermediates leading to alcohols and aldehydes far outnumbers the amount of potentially available Pd by about 3 to 1, we conclude that a majority of reactive intermediates leading to alcohols cannot be on the Pd surface. Instead, the reactive intermediates must be located on the Re or the support surface.

Takeda et al.[37] reported a turnover frequency of 4.0 h^{-1} (or $1.1x10^{-3}$ s^{-1}) at 413 K under 8 MPa H_2 for stearic acid reduction in liquid dioxane solvent using an analogous $PdRe/SiO_2$ catalyst. Extrapolating the intrinsic TOF at 433 K for vapor phase propionic acid reduction to 1-propanol to 8 MPa H_2 (assuming first order in H_2) gives an estimated TOF of $1.7x10^{-2}$ s^{-1} on our $PdRe/SiO_2$, which is about an order of magnitude greater than that reported by Takeda et al. Our higher estimated TOF can be explained by several factors. First, Takeda et al. normalize their observed rate by the total amount of Re in their catalyst, whereas our TOF from transient kinetic studies suggests the number of reactive intermediates on the catalyst surface is equal to

half of the total Re in the catalyst. Second, the reaction in the current work was studied at a temperature 20 K higher than that used by Takeda et al. Finally, influences of chain length and solvent might affect the reaction rate between the two systems.

The number of reactive intermediates on $PdRe/SiO_2$ associated with aldehyde formation was two orders of magnitude smaller than that associated with alcohol formation but turned over much more rapidly. A slightly smaller number of intermediates leading to aldehydes having the same turnover frequency was also observed on the monometallic Re/SiO_2. Based on the observed trends in reactivity, the Re oxidation state appears to play a role in the selectivity of carboxylic acid reduction to alcohol or aldehyde products. Promotion of the Re with Pd appears to be responsible for the enhanced reduction of Re to a more active, partially reduced form. The presence of Pd may also increase the hydrogen availability to the active intermediate Re oxides, thereby hydrogenating aldehydes to alcohols. The importance of the distance between Re and Pd for spillover to take place is evidenced by the results from the physical mixture of Pd/SiO_2 and Re/SiO_2. When the two metals were separated on different support particles, the mixed catalyst bed was still able to reduce propionic acid to a majority of 1-propanol, albeit at 30% the rate of the two metals on the same support particles. This result demonstrates that Pd is capable of promoting the Re for selective reduction of carboxylic acids to alcohols, even when not in direct physical contact with the Re. The first order dependence of the turnover frequency on the dihydrogen pressure indicates that hydrogen availability is critical to the activity of the Re-based catalysts studied here. Transient kinetic analysis suggests that changing the dihydrogen pressure from 0.1 to 0.2 MPa did not increase the number of reactive intermediates on the surface. The higher H_2 pressure may instead facilitate a more rapid hydrogenation of adsorbed intermediates

leading to alcohols.

2.5 Conclusions

Results from extensive characterization of the monometallic Pd and Re catalysts as well as the bimetallic PdRe catalyst revealed the structural evolution of the active $PdRe/SiO_2$ catalyst for the reduction of propionic acid to 1-propanol. During reducing pretreatment or reaction, the highly dispersed Re (7+) oxide is partially reduced to a Re ($\sim$4+) oxide, through a process that is facilitated by the presence of metallic Pd, presumably via hydrogen spillover. This intermediate oxide of Re is a catalytically active phase of Re since metallic Pd does not convert carboxylic acids under the conditions of study. Transient kinetic experiments revealed the number of reactive intermediates involved in the catalytic turnover was equal to at least 50% of the number of atoms of Re in the catalyst.

Acknowledgements

This material is based upon work supported by the National Science Foundation (NSF) under Award No. EEC-0813570. Any opinions, findings, and conclusions or recommendations expressed in this material are those of the author(s) and do not necessarily reflect the views of the NSF. Electron microscopy was performed in the University of Virginia's Nanomaterials Characterization Facility, and at Oak Ridge National Laboratory's Center for Nanophase Materials Science. This work was carried out with the support of the Diamond Light Source on proposal number SP13561-1. We thank Diamond Light Source for access to beamline B18 that contributed to the results presented here. Dr. Giannantonio Cibin is also acknowledged for his assistance in the setup of the in situ reactor at Diamond Light Source. This research also

used beamline 8-ID of the National Synchrotron Light Source II, a U.S. Department of Energy (DOE) Office of Science User Facility operated for the DOE Office of Science by Brookhaven National Laboratory under Contract No. DE-SC0012704.

References

1. Corma, A., Iborra, S. and Velty, A. Chemical routes for the transformation of biomass into chemicals. *Chemical reviews* **107,** 2411–502 (2007).

2. Bozell, J. J. and Petersen, G. R. Technology development for the production of biobased products from biorefinery carbohydrates – the US Department of Energy's "Top 10" revisited. *Green Chemistry* **12,** 539–554 (2010).

3. Chheda, J. N., Huber, G. W. and Dumesic, J. A. Liquid-phase catalytic processing of biomass-derived oxygenated hydrocarbons to fuels and chemicals. *Angewandte Chemie (International ed. in English)* **46,** 7164–83 (2007).

4. Besson, M., Gallezot, P. and Pinel, C. Conversion of biomass into chemicals over metal catalysts. *Chemical reviews* **114,** 1827–70 (2014).

5. Vennestrøm, P. N. R., Osmundsen, C. M., Christensen, C. H. and Taarning, E. Beyond petrochemicals: The renewable chemicals industry. *Angewandte Chemie - International Edition* **50,** 10502–10509 (2011).

6. Schlaf, M. Selective deoxygenation of sugar polyols to α,ω-diols and other oxygen content reduced materials–a new challenge to homogeneous ionic hydrogenation and hydrogenolysis catalysis. *Dalton transactions,* 4645–53 (2006).

7. Gervajio, G. C. in *Kirk-Othmer Encyclopedia of Chemical Technology* 1–38 (2012).

8. Gallezot, P. Conversion of biomass to selected chemical products. *Chemical Society reviews* **41,** 1538–58 (2012).

9. Chen, Y. and Chang, C. Cu-B_2O_3/SiO_2, an effective catalyst for synthesis of fatty alcohol from hydrogenolysis of fatty acid esters. *Catalysis Letters* **48,** 2–5 (1997).

10. Nebesh, E., Kelly, D. G. and Novak, L. T. *US Patent* 5124295 (1992).

11. Thakur, D. S. and Carrick, W. J. *US Patent* 9120086 (2015).

12. Huang, H., Wang, S., Wang, S. and Cao, G. Deactivation Mechanism of Cu/Zn Catalyst Poisoned by Organic Chlorides in Hydrogenation of Fatty Methyl Ester to Fatty Alcohol. *Catalysis Letters* **134,** 351–357 (2009).

13. Brands, D., UA-Sai, G., Poels, E. and Bliek, A. Sulfur deactivation of fatty ester hydrogenolysis catalysts. *Journal of Catalysis* **186,** 169–180 (1999).

14. Wu, H., Karanjikar, M. and San, K.-Y. Metabolic engineering of Escherichia coli for efficient free fatty acid production from glycerol. *Metabolic Engineering* **25,** 82–91 (2014).

15. Jansen, M. L. A. and van Gulik, W. M. Towards large scale fermentative production of succinic acid. *Current Opinion in Biotechnology* **30,** 190–197 (2014).

16. Czernik, S. and Bridgwater, A. V. Overview of applications of biomass fast pyrolysis oil. *Energy and Fuels* **18,** 590–598 (2004).

17. Primo, A., Concepción, P. and Corma, A. Synergy between the metal nanoparticles and the support for the hydrogenation of functionalized carboxylic acids to diols on Ru/TiO_2. *Chemical Communications* **47,** 3613 (2011).

18. Rachmady, W. and Vannice, M. Acetic acid hydrogenation over supported platinum catalysts. *Journal of Catalysis* **192,** 322–334 (2000).

19. Toba, M., Tanaka, S.-i., Niwa, S.-i., Mizukami, F., Koppány, Z., Guczi, L., Cheah, K.-Y. and Tang, T.-S. Synthesis of alcohols and diols by hydrogenation of carboxylic acids and esters over Ru–Sn–Al_2O_3 catalysts. *Applied Catalysis A: General* **189,** 243–250 (1999).

20. Chen, L., Li, Y., Zhang, X., Zhang, Q., Wang, T. and Ma, L. Mechanistic insights into the effects of support on the reaction pathway for aqueous-phase hydrogenation of carboxylic acid over the supported Ru catalysts. *Applied Catalysis A: General* **478,** 117–128 (2014).

21. Pritchard, J., Filonenko, G. A., van Putten, R., Hensen, E. J. M. and Pidko, E. A. Heterogeneous and homogeneous catalysis for the hydrogenation of carboxylic acid derivatives: history, advances and future directions. *Chem. Soc. Rev.* **44,** 3808–3833 (2015).

22. Broadbent, H. S. and Bartley, W. J. Rhenium Catalysts. VII. Rhenium(VI) Oxide. *The Journal of Organic Chemistry* **28,** 2345–2347 (1963).

23. Broadbent, H. S. and Seegmiller, D. W. Rhenium Catalysts. VIII. Rhenium(II) Oxide Dihydrate from Perrhenate via Alkali Metal-Amine Reductions. *The Journal of Organic Chemistry* **28,** 2347–2350 (1963).

24. Broadbent, H. S. and Whittle, C. W. Rhenium and Its Compounds as Hydrogenation Catalysts. II. Rhenium Heptaselenide. *Journal of the American Chemical Society* **81,** 3587–3589 (1959).

25. Broadbent, H. S. and Johnson, J. H. Rhenium Catalysts. IV. Rhenium(III) Oxide from Perrhenate via Borohydride Reduction. *The Journal of Organic Chemistry* **27,** 4400–4402 (1962).

26. Snappe, R. and Bouronville, J.-P. *French pat.* 2505819 (1981).

27. Mabry, M., Prichard, W. and Ziemecki, S. *US Patent* 4550185 (1985).

28. Rao, V. *US Patent* 4782167 (1988).

29. Kitson, M. and Williams, P. S. *US Patent* 4985572 (1991).

30. Takeda, Y., Nakagawa, Y. and Tomishige, K. Selective hydrogenation of higher saturated carboxylic acids to alcohols using a ReO_x–Pd/SiO_2 catalyst. *Catalysis Science & Technology* **2,** 2221 (2012).

31. Corbel-Demailly, L., Ly, B.-K., Minh, D.-P., Tapin, B., Especel, C., Epron, F., Cabiac, A., Guillon, E., Besson, M. and Pinel, C. Heterogeneous catalytic hydrogenation of biobased levulinic and succinic acids in aqueous solutions. *ChemSusChem* **6,** 2388–95 (2013).

32. Rozmysłowicz, B., Kirilin, A., Aho, A., Manyar, H., Hardacre, C., Wärnå, J., Salmi, T. and Murzin, D. Y. Selective hydrogenation of fatty acids to alcohols over highly dispersed ReO_x/TiO_2 catalyst. *Journal of Catalysis* **328,** 197–207 (2015).

33. Minh, D. P., Besson, M., Pinel, C., Fuertes, P. and Petitjean, C. Aqueous-Phase Hydrogenation of Biomass-Based Succinic Acid to 1,4-Butanediol Over Supported Bimetallic Catalysts. *Topics in Catalysis* **53,** 1270–1273 (2010).

34. Tapin, B., Epron, F., Especel, C., Ly, B. K., Pinel, C. and Besson, M. Influence of the Re introduction method onto Pd/TiO_2 catalysts for the selective hydrogenation of succinic acid in aqueous-phase. *Catalysis Today* **235,** 127–133 (2014).

35. Ly, B. K., Minh, D. P., Pinel, C., Besson, M., Tapin, B., Epron, F. and Especel, C. Effect of Addition Mode of Re in Bimetallic Pd–Re/TiO_2 Catalysts Upon the Selective Aqueous-Phase Hydrogenation of Succinic Acid to 1,4-Butanediol. *Topics in Catalysis* **55,** 466–473 (2012).

36. Ly, B. K., Tapin, B., Aouine, M., Delichere, P., Epron, F., Pinel, C., Especel, C. and Besson, M. Insights into the Oxidation State and Location of Rhenium in Re-Pd/TiO_2 Catalysts for Aqueous-Phase Selective Hydrogenation of Succinic Acid to 1,4-Butanediol as a Function of Palladium and Rhenium Deposition Methods. *ChemCatChem* **7,** 2161–2178 (2015).

37. Takeda, Y., Tamura, M., Nakagawa, Y., Okumura, K. and Tomishige, K. Characterization of Re-Pd/SiO_2 Catalysts for Hydrogenation of Stearic Acid. *ACS Catalysis* **5,** 7034–7047 (2015).

38. Dent, A. J., Cibin, G., Ramos, S., Smith, A. D., Scott, S. M., Varandas, L., Pearson, M. R., Krumpa, N. A., Jones, C. P. and Robbins, P. E. B18: A core XAS spectroscopy beamline for Diamond. *Journal of Physics: Conference Series* **190** (2009).

39. Palomino, R. M., Stavitski, E., Waluyo, I., Chen-Wiegart, Y. c. K., Abeykoon, M., Sadowski, J. T., Rodriguez, J. A., Frenkel, A. I. and Senanayake, S. D. New In-Situ and Operando Facilities for Catalysis Science at NSLS-II: The Deployment of Real-Time,

Chemical, and Structure-Sensitive X-ray Probes. *Synchrotron Radiation News* **30,** 30–37 (2017).

40. Ravel, B. and Newville, M. ATHENA, ARTEMIS, HEPHAESTUS: Data analysis for X-ray absorption spectroscopy using IFEFFIT. *Journal of Synchrotron Radiation* **12,** 537–541 (2005).

41. Hilbrig, F., Michel, C. and Haller, G. L. A XANES-TPR study of $PtRe/Al_2O_3$ catalysts. *The Journal of Physical Chemistry* **96,** 9893–9899 (1992).

42. Tougerti, A., Cristol, S., Berrier, E., Briois, V., La Fontaine, C., Villain, F. and Joly, Y. XANES study of rhenium oxide compounds at the L_1 and L_3 absorption edges. *Physical Review B - Condensed Matter and Materials Physics* **85,** 1–8 (2012).

43. Shannon, S. and Goodwin, J. Characterization of Catalytic Surfaces by Isotopic-Transient Kinetics during Steady-State Reaction. *Chemical Society reviews,* 677–695 (1995).

44. McClaine, B. C. and Davis, R. J. Isotopic Transient Kinetic Analysis of Cs-Promoted Ru/MgO during Ammonia Synthesis. *Journal of Catalysis* **210,** 387–396 (2002).

45. McClaine, B. C. and Davis, R. J. Importance of product readsorption during isotopic transient analysis of ammonia synthesis on Ba-promoted Ru/BaX catalyst. *Journal of Catalysis* **211,** 379–386 (2002).

46. Calla, J. T., Bore, M. T., Datye, A. K. and Davis, R. J. Effect of alumina and titania on the oxidation of CO over Au nanoparticles evaluated by ^{13}CC isotopic transient analysis. *Journal of Catalysis* **238,** 458–467 (2006).

47. Calla, J. T. and Davis, R. J. Oxygen-exchange reactions during CO oxidation over titania- and alumina-supported Au nanoparticles. *Journal of Catalysis* **241,** 407–416 (2006).

48. Shou, H. and Davis, R. J. Multi-product steady-state isotopic transient kinetic analysis of CO hydrogenation over supported molybdenum carbide. *Journal of Catalysis* **306,** 91–99 (2013).

49. Birky, T. W., Kozlowski, J. T. and Davis, R. J. Isotopic transient analysis of the ethanol coupling reaction over magnesia. *Journal of Catalysis* **298,** 130–137 (2013).

50. Hanspal, S., Young, Z. D., Shou, H. and Davis, R. J. Multiproduct steady-state isotopic transient kinetic analysis of the ethanol coupling reaction over hydroxyapatite and magnesia. *ACS Catalysis* **5,** 1737–1746 (2015).

51. Pinna, F., Signoretto, M., Strukul, G., Polizzi, S. and Pernicone, N. Pd-SiO_2 catalysts. Stability of β-PdH_x as a function of Pd dispersion. *Reaction Kinetics and Catalysis Letters* **60,** 9–13 (1997).

52. Joyal, C. L. M. and Butt, J. B. Chemisorption and disproportionation of carbon monoxide on palladium/silica catalysts of differing percentage metal exposed. *Journal of the Chemical Society, Faraday Transactions 1* **83,** 2757–2764 (1987).

53. Chadzyński, G. W. and Kubicka, H. Chemisorption of hydrogen and oxygen on γ-alumina-supported rhenium. Part 1. Chemisorption of hydrogen. *Thermochimica Acta* **158,** 369–383 (1990).

54. Thompson, S. T. and Lamb, H. H. Palladium-Rhenium Catalysts for Selective Hydrogenation of Furfural: Evidence for an Optimum Surface Composition. *ACS Catalysis* **6,** 7438–7447 (2016).

55. Nacheff, M. S., Kraus, L. S., Ichikawa, M., Huffman, B. M., Butt, J. B. and Sachtler, W. M. Characterization and catalytic function of Re^{0} and Re^{4+} in $ReAl_2O_3$ and PtRe Al_2O_3 catalysts. *Journal of Catalysis* **106,** 263–272 (1987).

56. Kunkes, E. L., Simonetti, D. A., West, R. M., Serrano-Ruiz, J. C., Gärtner, C. A. and Dumesic, J. A. Catalytic Conversion of Biomass to Monofunctional Hydrocarbons and Targeted Liquid-Fuel Classes. *Science* **322,** 417–421 (2008).

57. Ziemecki, S. B., Jones, G. A. and Michel, J. B. Surface mobility of Re_2O_7 in the system $Re^{7+}Pd^{0}$ γ-Al_2O_3. *Journal of Catalysis* **99,** 207–217 (1986).

58. Wang, C.-b., Cai, Y. and Wachs, I. E. Reaction-Induced Spreading of Metal Oxides onto Surfaces of Oxide Supports during Alcohol Oxidation : Phenomenon , Nature , and Mechanisms. *Langmuir* **15,** 1223–1235 (1999).

59. Krebs, B., Müller, A. and Beyer, H. H. The crystal structure of rhenium(VII) oxide. *Inorganic Chemistry* **8,** 436–443 (1969).

60. Jentys, A. Estimation of mean size and shape of small metal particles by EXAFS. *Physical Chemistry Chemical Physics* **1,** 4059–4063 (1999).

61. Bolivar, C., Charcosset, H., Frety, R., Primet, M., Tournayan, L., Betizeau, C., Leclercq, G. and Maurel, R. Platinum-rhenium/alumina catalysts I. Investigation of reduction by hydrogen. *Journal of Catalysis* **39,** 249–259 (1975).

62. Mieville, R. L. Platinum-rhenium interaction: A temperature-programmed reduction study. *Journal of Catalysis* **87,** 437–442 (1984).

63. Chia, M., Pagán-Torres, Y. J., Hibbitts, D., Tan, Q., Pham, H. N., Datye, A. K., Neurock, M., Davis, R. J. and Dumesic, J. A. Selective hydrogenolysis of polyols and cyclic ethers over bifunctional surface sites on rhodium-rhenium catalysts. *Journal of the American Chemical Society* **133,** 12675–12689 (2011).

64. Broadbent, H. S. and Selin, T. G. Rhenium Catalysts. VI. Rhenium(IV) Oxide Hydrate. *The Journal of Organic Chemistry* **28,** 2343–2345 (1963).

3

Reaction Kinetics and Mechanism for the Catalytic Reduction of Propionic Acid over Supported ReO_x Promoted by Pd

Abstract

Titania-supported Pd, Re, and Pd-promoted Re catalysts were prepared by incipient wetness impregnation. Samples were characterized using X-ray diffraction and H_2 chemisorption. Reaction kinetics measurements revealed that the rate of reduction of propionic acid using H_2 over the Re-containing catalysts was insensitive to propionic acid pressure and 0.6 order in H_2 pressure. The apparent barriers of propionic acid reduction over $PdRe/SiO_2$ and $PdRe/TiO_2$ were 60 and 75 kJ mol^{-1}, respectively. An inverse kinetic isotope effect of 0.79 was observed for the reduction of propionic acid over Pd-promoted Re, while a normal kinetic isotope effect of 1.6 was observed for hydrogenation of propanal under similar conditions. Cofeeding of water and infrared spectroscopy were used to probe the identity of reactive intermediates on the catalyst surface. A large reservoir of propoxy species was found on the SiO_2-supported PdRe catalyst under reaction conditions, which contributed to a transient response in alcohol production lasting over 10 hours when reaction conditions were changed. These species could not be detected on the $PdRe/TiO_2$ surface. Turnover frequencies and coverages of reactive intermediates over Pd-promoted Re/TiO_2 catalysts were determined using transient kinetic analysis, which revealed less than 2% of the Re takes part in the reaction. Propionic acid reduction by Pd-promoted Re is proposed to take place through a 2-step cascade reaction through a propanal intermediate.

3.1 Introduction

Consumption of oil resources as chemical feedstocks is predicted to grow nearly 60% from 2018 to 2050 in response to increases in global population and wealth. These changes are expected to increase demand for high-value chemical products such as packaging and construction

materials.[1] However, mounting concerns about the environmental impact of both obtaining and using fossil resources have increased demand for renewable resources and have driven interest in biomass-derived chemical feedstocks. The majority of harvested biomass resources in the United States today are used for energy production (i.e., burned), but their valorization offers a less carbon-intensive alternative to fossil resources for chemicals production.[2] Specifically, fermentation of harvested biomass to produce biological platform molecules has been proposed as a way to meet the growing demand for chemicals with renewable resources.[3] In their 2004 study, Werpy and Peterson reported that a variety of potential building block molecules could be derived from fermentation of biomass. The majority of the most promising molecules identified are carboxylic acids that may subsequently require reduction to produce value-added products. As an example, 3-hydroxypropionic acid (3-HPA), which can be produced biologically, can be used as a platform to produce a number of value-added molecules including 1,3-propanediol (1,3-PDO). As an emerging commodity chemical, 1,3-PDO has a wide range of uses including as a monomer to produce polytrimethylene terephthalate.[4] The market for 1,3-PDO is expected to grow rapidly from its 2014 value of $310 million to a value of around $620 million by 2021.[5]

The cost-effective conversion of carboxylic acids obtained from biomass will require an improved understanding of the direct reduction reaction. Current methods of reduction of carboxylic acids include the use of metal hydrides, which present safety issues and produce large amounts of waste, or copper-based (including Adkins-type, $CuO/CuCr_2O_4$) catalysts, which despite their high H_2 pressure requirements are still used industrially for the reduction of esters to alcohols.[6,7] Therefore, processes that operate at lower pressures without Cr are desirable. Heterogeneous bimetallic catalysts containing a reducible platinum group metal together with

an oxophilic metal are capable of performing the reduction of carboxylic acids under the desired conditions. The oxophilic metal (such as Re[8–11]) is often present in its oxidized form, or supported on a reducible oxide such as TiO_2.[11,12] More information about the heterogeneous and homogeneous reduction of carboxylic acids and esters can be found in the review by Pritchard et al.[13]

Investigation of the reduction of carboxylic acids over bifunctional catalysts has resulted in a variety of mechanistic proposals. Previous work by Rachmady and Vannice found that Pt/TiO_2 was an active catalyst for the reduction of acetic acid using H_2, and predicted that TiO_2 was the active species for reduction of acetic acid to acetaldehyde.[14] After investigating a Ru/TiO_2 catalyst for the reduction of oleic acid, Mendes et al.[12] proposed reaction pathway involving interaction of partially reduced Ti^{n+} species in the TiO_2 support adjacent to supported metallic particles. When Ly et al. prepared a Pd-promoted Re/TiO_2 catalyst via a reductive deposition of Re onto Pd/TiO_2, the amount of Re required to reach maximum activity for the reduction of succinic acid to 1,4-butanediol was reduced by about 75%, suggesting that Re proximity to Pd is important, presumably involving spillover of H_2 from Pd to activate the catalyst for reaction.[10,15] As Pd is excellent at activating H_2, excess coverage of Pd by added Re could eventually inhibit catalyst activity because of the very low availability of surface Pd. Recent work by Rozmyslowicz et al. demonstrated that Pd or other promoters were not necessary to produce an active Re catalyst on TiO_2, and that simply pretreating Re/TiO_2 at 673 K in H_2 (resulting in the reduction of Re) was sufficient to generate a catalyst with significant carboxylic acid reduction activity.[16]

Rozmyslowicz et al. reported evidence for an aldehyde intermediate during carboxylic acid reduction to alcohol, indicating a two-step cascade reaction was at play. They modeled

the reaction assuming an Eley-Rideal type mechanism involving the reaction of fluid-phase H_2 with the adsorbed carboxylic acid. In contrast, Takeda et al. proposed the hydrogenation of stearic acid on bifunctional adjacent Pd and Re metal surfaces supported on SiO_2 occurs via heterolytic dissociation of H_2 followed by hydride attack on the carboxylate carbon.[17] Palladium was proposed to enhance the activity of the catalyst by increasing the binding energy of the carboxylic acid to the reactive surface. Further study of this catalyst using transient kinetic analysis found that aldehyde turnover on the catalyst surface occurred more rapidly than turnover of the catalyst surface to produce alcohols.[18] Prior computational work by Pallassana et al. investigating the adsorption and reaction of acetic acid on Re(0001), Pd(111), and overlayers of Pd on Re suggested that activation of the C-OH bond on metallic Re(0001) had approximately the same barrier (90 kJ mol^{-1}) as hydrogenation of the resulting acetyl (88 kJ mol^{-1}).[19] As previous work suggests Re is the active phase for reduction of the carboxylic acid, mechanistic information is still lacking. Moreover, the state of the Re in the calculations mentioned above was metallic, which may not be representative of the supported Re catalysts discussed above.

In this work, we investigated the effects of reactant concentrations, conversion, support, and temperature on the reduction of propionic acid by SiO_2- and TiO_2-supported Re, with and without the presence of a Pd promoter. The reduction of propionic acid using D_2 instead of H_2 was performed to provide insight into the mechanism of the surface reaction. The identity of surface reactive intermediates leading to 1-propanol was investigated using diffuse reflectance infrared Fourier transform spectroscopy (DRIFTS). Transient kinetic analysis of propionic acid reduction over TiO_2-supported Pd-promoted Re was used to determine the coverage of reactive intermediates leading to alcohols. All experiments were performed in the gas-phase to eliminate

solvent effects, and reduction of propionic acid was used as a model reaction over SiO_2- and TiO_2-supported Re and Pd-promoted Re catalysts at mild conditions. The results of the work confirm the bifunctional role of Pd in a Pd-promoted Re catalyst is to facilitate H_2 spillover to a Re active site for carboxylic reduction, and to promote aldehyde hydrogenation to alcohol.

3.2 Experimental Methods

3.2.1 Catalyst Synthesis

All catalysts were synthesized using a stepwise incipient wetness impregnation method. The desired metal loading of Re (ammonium perrhenate, Aldrich, 99% or perrhenic acid, 99.99%, 76.5% solution in water, Acros Organics) or Pd (aqueous tetraaminepalladium(II) nitrate, 10 wt%, Aldrich) metal salt was added to a quantity of distilled, deionized water (16.8 MΩ) to form a solution equal in volume to the pore volume of the SiO_2 support (Fuji Silysia Chemical Ltd, 511 $m^2\ g^{-1}$ 75-150 μm particle size) or TiO_2 support (Degussa P25, 47 $m^2\ g^{-1}$, 55-180 μm particle size). This solution was added to the support until the point of incipient wetness. For SiO_2-supported catalysts, the impregnated sample was dried at 368 K in air for 12 h, ramped in air to 773 K over 3 h, and held for an additional 3 h in air at 773 K. For a bimetallic SiO_2-supported catalyst, Re was added first as ammonium perrhenate and dried at 368 K prior to heating in air to 773 K, after which the Pd solution was added to the supported Re catalyst, dried in air at 368 K, and heated in air to 773 K for a second time. For all Re-containing TiO_2-supported catalysts, Pd was added first to the TiO_2 support, dried, and treated in air at 773 K. Subsequently, Re was added as perrhenic acid in the last metal addition step and dried at 343 K for 2 hours prior to use.

3.2.2 X-Ray Diffraction

Powder X-ray diffraction (XRD) was carried out under ambient conditions using a Malvern Panalytical Empyrean X-ray Diffractometer using Cu Kα radiation with a wavelength of 1.541 Å. Scans were taken from 20 to 80° (2θ) at a step size of 0.014° at 88 s per step, and high-resolution scans used for particle size analysis were taken from 30 to 40° (2θ) at a step size of 0.014° at 188 s per step. The average PdO crystallite size was estimated using the Scherrer equation from the full width at half-height of the PdO 101 reflection peak in high resolution scans.

3.2.3 Adsorption of H_2

The number of available H_2 adsorption sites was counted by the chemisorption of H_2 (Praxair, 5.0) using a Micromeritics ASAP 2020 instrument. Prior to analysis, each sample was heated to 473 K in flowing H_2 at 10 K min^{-1}, then held at 473 K for 1 h under flowing H_2. The monometallic Re/TiO_2 was heated to 673 K in flowing H_2 at 10 K min^{-1}, to mimic the conditions required to activate it for reaction. All samples were then evacuated at 473 K for 3 h, then cooled to 373 K to perform the H_2 uptake experiment. Dihydrogen was dosed at pressures ranging from 0.13 to 67 kPa. The chemisorption values reported here were obtained by extrapolating the total H_2 uptake in the linear high pressure portion of the isotherm to its y-intercept, which was taken to be the theoretical monolayer coverage. The H_2 and CO uptake of the SiO_2-supported catalysts have been reported previously.[18]

3.2.4 Catalytic Reactions

The reduction of propionic acid (Sigma Aldrich, 99.5%), propanal (Sigma Aldrich, 99%), and 1-propanol (Sigma Aldrich, 99%) was carried out in a stainless-steel flow reactor tube with an inner diameter of 0.46 cm. A typical reactor bed was packed with 0.100 g of the catalyst supported between two plugs of glass wool. Temperature measurements were made using a thermocouple inserted from the top of the reactor tube into the middle of the catalyst bed. Prior to reaction, the system (including the liquid saturators) was purged with flowing N_2 at 30 cm^3 min^{-1} for at least 10 min. After purging with N_2, the catalyst bed was heated under flowing H_2 at 30 cm^3 min^{-1} to 433 K at which point the flow was passed through the stainless-steel saturators to form a saturated vapor of reactant(s) in H_2, D_2 (Praxair, 2.7), or N_2 that was fed to the catalyst bed. The effluent gases were separated using an on-line SRI 8610C gas chromatograph (GC) equipped with either an MXT-WAX or MXT-Q-PLOT (0.53 mm i.d., 30 m) column and quantified using a flame-ionization detector (FID).

The conversion of the acid, alcohol, or aldehyde to its corresponding products was evaluated from the integrated product peak areas. Light hydrocarbon products propane and ethane could not be separated using the MXT-WAX column during analysis of products from of propanoic acid reduction. Therefore, the overlapping peak corresponding to hydrocarbons was evaluated in moles of carbon and denoted as light hydrocarbons, or "LHC". The fractional conversion (f_i) of each reactant i to its corresponding products j was calculated using the expression

$$f_i = \frac{\sum M_j}{M_i + \sum M_j} \tag{3.1}$$

where M_j is the carbon molar flow rate of the component j. Similarly, the selectivity of the reaction towards each product j was calculated using the expression

$$S = \frac{M_j}{\sum M_j} \tag{3.2}$$

3.2.5 Diffuse Reflectance Infrared Fourier Transform Spectroscopy

The diffuse reflectance infrared Fourier transform spectra of beds of SiO_2- and TiO_2-supported catalysts exposed to propionic acid, propanal, and 1-propanol in H_2 and N_2 were recorded using a Bruker Vertex 70 FTIR spectrometer equipped with a liquid-nitrogen-cooled MCT detector. Samples were supported in the beam path using a Harrick Praying Mantis *in situ* reactor cell with 5 mm ZnSe windows. Spectra were collected as the average of 800 scans at a resolution of 2 cm^{-1}. Silica-supported catalysts were ground to a fine powder before analysis to improve the reflectance signal. Gas lines to the *in situ* cell were further purified using an OMI purifier (Supelco) upstream of two vapor saturators with bypass lines. Prior to analysis, all SiO_2-supported catalyst powders were purged in N_2 (Praxair, 5.0) then heated to 673 K in 15 cm^3 min^{-1} flowing H_2 at 10 K min^{-1}, held at 673 K for 1 h, and cooled to reaction temperature before obtaining a spectral background. Titania-supported catalysts were heated at 10 K min^{-1} to 473 K in 15 cm^3 min^{-1} flowing H_2 and held at that temperature for 1 h, then cooled to reaction temperature. Repeated scans were then taken every 20 minutes until the end of each experiment. Two temperature-controlled stainless-steel saturators with separate inlets and outlets were used to feed or co-feed reactants to the *in situ* cell during experiments. The resulting spectra were normalized to a reference spectrum taken after the catalyst pretreatment, background corrected,

and converted to Kubelka-Munk units using the Kubelka-Munk equation.[20]

3.2.6 Transient Kinetic Analysis

The reactor setup and theory of the transient kinetic analysis technique have been described in the previous chapter and will not be described in detail here. In summary, the down-flow reactor used to perform the transient kinetic analysis consisted of a vertically oriented 3 cm long segment of 0.64 cm O.D. 316 stainless steel tubing with a 10 μm stainless steel frit supporting the catalyst bed. The transient analysis experiment was performed by switching between 0.5 kPa of either propionic acid or butyric acid (Sigma Aldrich, 99.0%) in H_2 and analyzing the resulting transient response as described previously.[18] Further details about transient kinetic analysis can be found in the review by Shannon and Goodwin.[21]

3.3 Results

3.3.1 Adsorption of H_2 and X-Ray Diffraction

The dispersion of Pd and total H_2 adsorption of Re and PdRe catalysts was determined by H_2 chemisorption and X-ray diffraction. The H_2 chemisorption results are summarized in Table 3.1, and the XRD results are summarized in Figure B.1 in the appendix. The H_2 uptake by a 1 wt % Pd/TiO_2 catalyst indicated that the synthesis method produced Pd particles that were 34% dispersed. The dispersion of Re was not calculated using the H_2 chemisorption results, as Re has been observed to remain oxidized even after pretreatment at elevated temperatures in the presence of reducible metals.[22,23] The three bimetallic catalysts studied adsorbed amounts of H atoms equal to 46%, 32%, and 48% of the total metals loading on $1Pd8Re/TiO_2$, $1Pd13Re/TiO_2$,

Table 3.1: Weight loading and H_2 chemisorption results of TiO_2-supported catalysts.

Catalyst	Metal Loading[a] (wt %) Pd	Re	Chemisorption H_2 (μmol g_{cat}^{-1})	H/M[c]
1Pd/TiO_2	1.0[b]	—	15.8	0.34
8Re/TiO_2	—	7.87	69.4[d]	0.33
1Pd8Re/TiO_2 (PdRe/TiO_2)	0.84	7.74	115.	0.46
1Pd13Re/TiO_2	0.71	12.7	118.	0.32
0.5Pd8Re/TiO_2	0.37	7.64	107.	0.48

(a) Measured by inductively coupled plasma optical emission spectroscopy at Galbraith Laboratories.

(b) Calculated weight loading based on synthesis procedure.

(c) Ratio of H adatoms to total metal atoms.

(d) Re/TiO_2 was pretreated at 673 K.

and 0.5Pd8Re/TiO_2, respectively. The total uptake was more than the sum of the Pd and Re uptake on monometallic samples, suggesting that H_2 spillover had increased the amount of H_2 chemisorption on the Re. Increasing the weight loading of Re did not have a significant effect on H_2 uptake compared to the 1Pd8Re/TiO_2. It should be noted that TiO_2 is partially reducible and may affect the chemisorption uptake.

3.3.2 Influence of Reactant Concentrations

The reduction of propionic acid was investigated over 1 wt % Pd, 8 wt % Re supported on SiO_2 (PdRe/SiO_2), 1 wt % Pd, 8 wt % Re supported on TiO_2, (PdRe/TiO_2), 8 wt % Re supported on SiO_2 (Re/SiO_2), 8 wt % Re supported on TiO_2 (Re/TiO_2), and 1 wt % Pd supported on TiO_2 (Pd/TiO_2) under 0-0.3 MPa H_2 pressure and 0-0.5 kPa propionic acid. Oxygenated C_3 products (1-propanol and propanal) were not produced over Pd/SiO_2 under the conditions studied. After about 10 h of reaction during which slight deactivation was observed, the rate of propionic acid

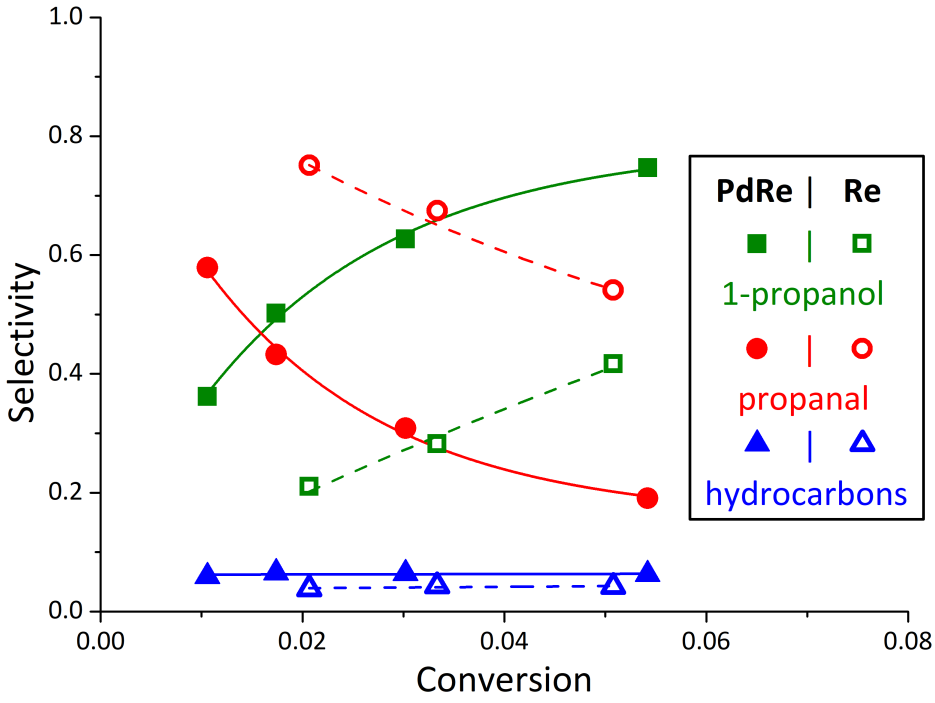

Figure 3.1: Effect of conversion (measured by varying flowrate) on selectivity during the reduction of propionic acid to alcohols, aldehydes, and hydrocarbons over $PdRe/SiO_2$ (0.1 MPa H_2 and 0.5 kPa propionic acid) and Re/SiO_2 at 433 K (0.3 MPa H_2 and 1.0 kPa propionic acid). The $PdRe/SiO_2$ catalyst was not reduced prior to reaction, whereas the Re/SiO_2 catalyst was pretreated at 673 K in H_2 *in situ* for 1 hour prior to reaction. Dashed and solid lines indicate trends.

reduction reached a steady state. The effect of conversion on the selectivity of the products of propionic acid reduction at steady state over Re/SiO_2 and $PdRe/SiO_2$ is shown in Figure 3.1. At very low conversions of propionic acid, the product selectivity shifts towards mostly aldehydes over both $PdRe/SiO_2$ and Re/SiO_2. While this trend is much more obvious for Re/SiO_2, even when Pd was present on the catalyst, the aldehyde became the majority product at the lowest conversion.

Interestingly, when the flow of H_2 was replaced with N_2 during steady state reaction over the $PdRe/SiO_2$ catalyst, a transient decay in the rate of alcohol production was observed, and only traces of other products were observed. This phenomenon is illustrated in Figure 3.2, and was investigated further using *in situ* DRIFTS. In contrast, when the flow of acid was stopped while

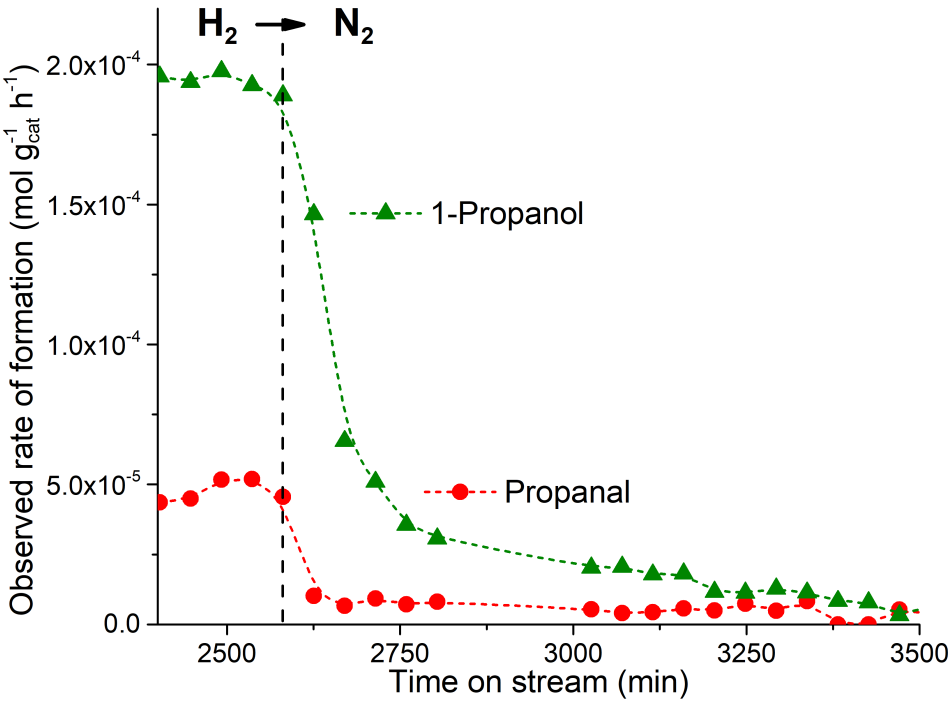

Figure 3.2: Transient response of 1-propanol formation over $PdRe/SiO_2$ at 433 K observed after changing conditions from 1.1 kPa propionic acid in 0.08 MPa H_2/0.22 MPa N_2 to 1.1 kPa propionic acid in 0.3 MPa N_2. Dashed lines indicate trends.

the reaction was at steady state, and the catalyst bed was purged with only H_2, the production of alcohols immediately ceased.

The product selectivities during reduction of propionic acid over $PdRe/TiO_2$ in H_2 were very similar to that over $PdRe/SiO_2$, but the observed rates were 30% higher over $PdRe/TiO_2$. In contrast to the Pd/SiO_2 (which produced no C_3 oxygenates), the Pd/TiO_2 catalyst produced a small amount of 1-propanol, which has been previously attributed to the formation of reduced Ti^{n+} species formed by H spillover.[11] The rate over Pd/TiO_2 was 26% of that observed over the $PdRe/TiO_2$. The Re/TiO_2 catalyst displayed similar initial activity to that of $PdRe/TiO_2$ after pretreatment at 673 K for 1 h in H_2, but rapidly deactivated to a steady state rate that was 64% of that achieved with $PdRe/TiO_2$. Under the same conditions, $PdRe/TiO_2$ was 69% selective

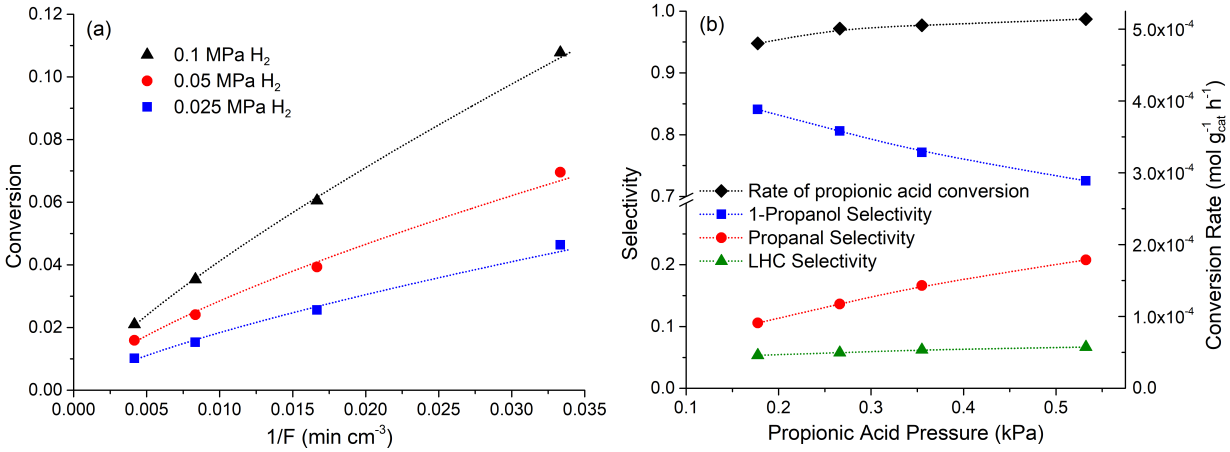

Figure 3.3: Influence of (a) flowrate and H_2 pressure on the reduction of 0.5 kPa propionic acid at 433 K, and (b) propionic acid pressure (at constant mass of catalyst and flowrate) on rate and selectivity of propionic acid (0.5 kPa) reduction over $PdRe/TiO_2$ at 433 K. Dashed lines indicate trends.

to 1-propanol (at 6.1% conversion), while Re/TiO_2 was only 52% selective to 1-propanol (at 8.5% conversion). Apparently, the role of the Pd promoter was somewhat diminished on the titania support relative to the silica support. The total rate of propionic acid consumption over the Pd-promoted Re catalysts (primarily to 1-propanol and propanal) varied with a 0.6 order dependence on the H_2 pressure. The relationship between inverse flowrate and conversion at various H_2 pressures is plotted in Figure 3.3(a). In contrast, the rate of propionic acid conversion was nearly independent of the total propionic acid pressure (0.1 order), and is shown in Figure 3.3(b). The product distribution was observed to shift away from aldehydes towards alcohols as the propionic acid pressure was decreased. As the conversion of propionic acid is in a zero-order regime, product selectivity should not be dependent on conversion. Therefore, this behavior is consistent with Langmuirian competitive adsorption of propionic acid and propanal on active sites for aldehyde hydrogenation.

The hydrogenation of 1 kPa propanal to 1-propanol in 0.1 MPa H_2 at 353 K using $PdRe/SiO_2$ (reduced under reaction conditions) and Re/SiO_2 (pretreated in flowing H_2 at 673 K for 1 h) was

also investigated. The monometallic Pd/SiO_2 catalyst was also tested but deactivated significantly with time on stream. Although steady state rates could not be reported, a high initial rate of aldehyde reduction lead to 1-propanol under the conditions studied. For the Re-based catalysts, the propanal reduction rate was nearly zero order in propanal concentration and nearly half order in H_2 pressure under the conditions studied. These reaction kinetics are consistent with a Langmuir-Hinshelwood reaction mechanism in which the surface is saturated with propanal and a single C-H bond formation step is the rate determining step. The reaction of 0.05 kPa 1-propanol in H_2 was also investigated over $PdRe/SiO_2$ at 403 K. A nearly half order in H_2 pressure and -0.3 order in alcohol pressure were observed for the formation of products, which were dominated by propane and propanal. The reduction of primary alcohols to alkanes may proceed by either S_N2-like hydride attack on the C atom in the C-O bond, or via the well-known E_2 acid-catalyzed dehydration mechanism, either of which could explain the nearly half order dependence of alcohol hydrogenolysis on H_2 pressure.[24]

3.3.3 Influence of Temperature

The effect of temperature on the rate of reduction of propionic acid over supported Re and Pd-promoted Re was investigated. The apparent barrier for propionic acid (0.5 kPa) conversion over $PdRe/SiO_2$ (in 0.1 MPa H_2) or Re/SiO_2 (in 0.3 MPa H_2) at 423-443 K was 60 kJ mol^{-1}. The apparent barriers for propionic acid conversion over $PdRe/TiO_2$ and Re/TiO_2 in propionic acid (0.5 kPa) and H_2 (0.1 MPa) were 75 and 71 kJ mol^{-1}, respectively. The effect of temperature on the conversion of propionic acid by PdRe supported on SiO_2 and TiO_2 is shown in Figure 3.4. As the temperature was increased from 423 K to 443 K, the selectivity of propionic acid

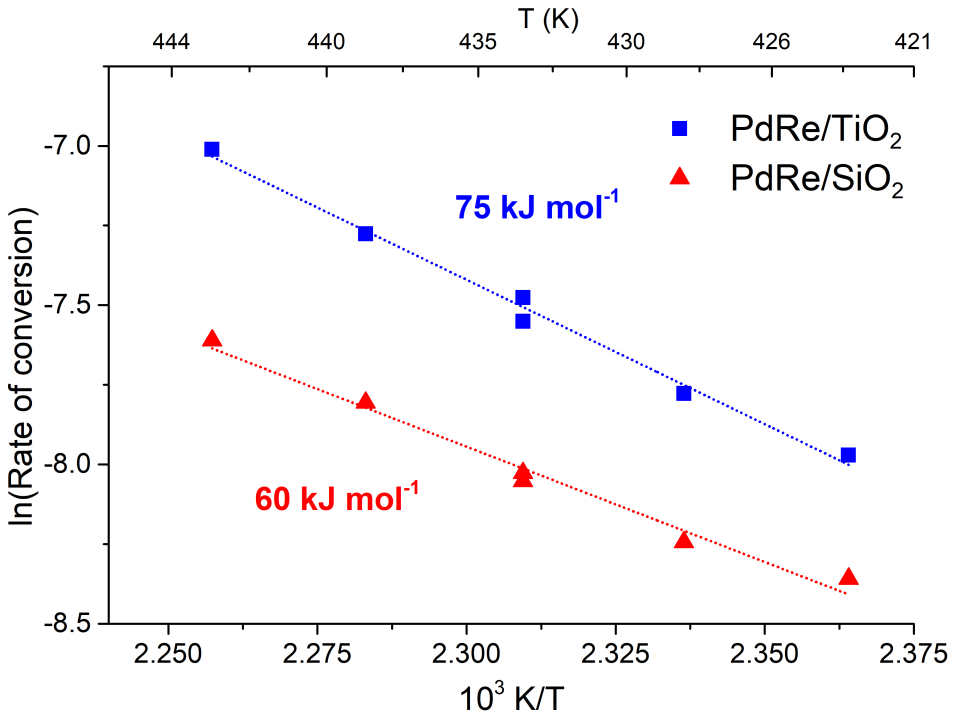

Figure 3.4: Influence of temperature on propionic acid (0.5 kPa) reduction in 0.1 MPa H_2 over $PdRe/SiO_2$ and $PdRe/TiO_2$. Conversion ranged between 4.5 and 18%.

conversion increased slightly towards 1-propanol (from 78% to 81%) and LHC (from 6% to 8%), while propanal selectivity decreased (from 16% to 11%) over $PdRe/TiO_2$, presumably as a result of increased conversion at higher temperature. Similar behavior was observed over Re/TiO_2, $PdRe/SiO_2$, and Re/SiO_2.

As propanal and 1-propanol were also potentially converted during propionic acid reduction, the effect of temperature on their reduction was studied as well. The apparent barriers to 1-propanol formation from propanal using $PdRe/SiO_2$ and Re/SiO_2 was 24 and 29 kJ mol^{-1}, respectively, indicating that the reduction of propanal to form 1-propanol occurs readily over Re surfaces, albeit at a lower rate than over PdRe. The observed low barrier to hydrogenation of the aldehyde intermediate is not surprising, as hydrogenation reactions of unsaturated C=O bonds often have low barriers (see, for example, reduction of aldehydes over Ni catalysts supported on

kieselguhr).[25] When the reduction of 1-propanol was studied over $PdRe/SiO_2$ at lower temperature, the majority product (>80% selectivity) was propane in all cases, and the apparent barrier to 1-propanol conversion was 70 kJ mol^{-1}.

3.3.4 Influence of Cofeeding Intermediates and Products

As water is a co-product of propionic acid reduction, the cofeeding of water to $PdRe/SiO_2$ and Re/SiO_2 catalysts after reaching steady state was investigated. While Re/SiO_2 was not significantly affected by the cofeeding of water vapor, the $PdRe/SiO_2$ demonstrated an unexpected response as illustrated in Figure 3.5. When the co-fed water was introduced, a significant increase in 1-propanol formation occurred, followed by a return to the prior steady state rate before water addition over approximately 10 h on stream. Conversely, when the co-fed water was removed from the reactant stream, a significant drop in 1-propanol formation rate was observed, followed again by a return to the same steady state, over approximately 10 h on stream. The amount of propanal observed in the reactor effluent was also found to be 21% lower in the presence of water in the reactant stream. The integrated amounts of missing or excess 1-propanol observed during the transient responses to water addition or removal were 3.7×10^{-4} or 3.4×10^{-4} mol 1-propanol g_{cat}^{-1}, respectively. These transient amounts of 1-propanol were quite similar to surface coverages of intermediates leading to 1-propanol reported previously over $PdRe/SiO_2$ during a transient switching between propionic acid and butyric acid under similar conditions,[18] suggesting water may be promoting the desorption of a pool of reactive intermediates leading to alcohols that covers a large fraction of the catalyst surface. The nature of the adsorbed species was investigated further using *in situ* DRIFTS, as will be discussed later.

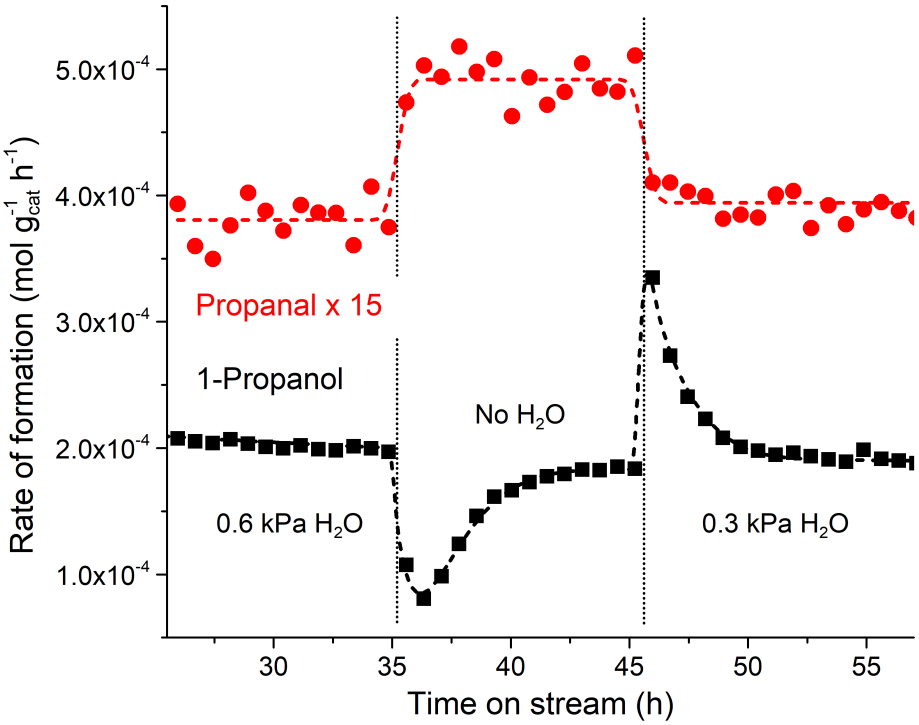

Figure 3.5: Effect of cofeeding water on the rate of formation of 1-propanol and propanal during the reduction of 0.3 kPa propionic acid in 0.1 MPa H_2.

As aldehydes are considered to be intermediate products to alcohol formation, butanal was cofed in the reactant stream after reaching steady state in the conversion of propionic acid. When butanal was introduced to the reactant stream, the steady state rate of 1-propanol formation decreased slightly, and 1-butanol was observed as a product. No butanal or additional other products were observed in the reactor effluent, indicating the complete conversion of butanal to 1-butanol. When butanal was removed from the reactant stream, 1-butanol continued to leave the reactor bed for over 10 h. These results suggested that alcohol products may be retained in the catalyst bed for over 10 h before leaving the bed as measurable product, despite the fact that they are readily formed from aldehydes.

3.3.5 Mixed Beds and Ordered Beds

To probe the role of each metal in the PdRe catalyst, the conversion of propionic acid at 433 K in single beds and mixed beds of Pd/SiO_2 and Re/SiO_2 was studied at 433 K using a reactant stream consisting of 30 cm^3 min^{-1} containing 0.3 MPa H_2 and 1 kPa propionic acid. The results from these experiments are summarized in Figure 3.6. As discussed earlier, the Pd/SiO_2 catalyst produced entirely hydrocarbon products, expected to be mostly ethane, and was less active than all other catalysts except for Re/SiO_2 without any pretreatment.[26] Without pretreatment in H_2 at 673 K, the Re/SiO_2 catalyst was minimally active, producing 81% propanal, 15% hydrocarbons, and 4% 1-propanol. When the Re/SiO_2 catalyst was pretreated in H_2 at 673 K, the activity of the catalyst more than doubled, and the selectivity to 1-propanol increased to 26%. Total selectivity to oxygenates increased to 96%, and selectivity to light hydrocarbon products fell to 4%. On the other hand, $PdRe/SiO_2$ under the same conditions was more than 3 times as active for the reduction of propionic acid, and produced 65% 1-propanol, 29% propanal, and only 6% light hydrocarbons.

When monometallic Pd/SiO_2 and Re/SiO_2 were placed in series under the same conditions, an effect of the bed co-location and bed order was observed. The beds in series were not pretreated at high temperature in H_2, but the observed activity of the beds in series was higher than the sum of the Pd/SiO_2 and Re/SiO_2 exposed to the same startup conditions, and larger amounts of 1-propanol than expected were observed. Apparently, the presence of the Pd bed either before or after the bed of Re/SiO_2 is capable of activating the Re/SiO_2 for reaction, likely as a result hydrogen spillover between beds, leading to an effective high-temperature H_2 pretreatment and increasing H_2 availability to the Re active site. When the order of the beds is considered,

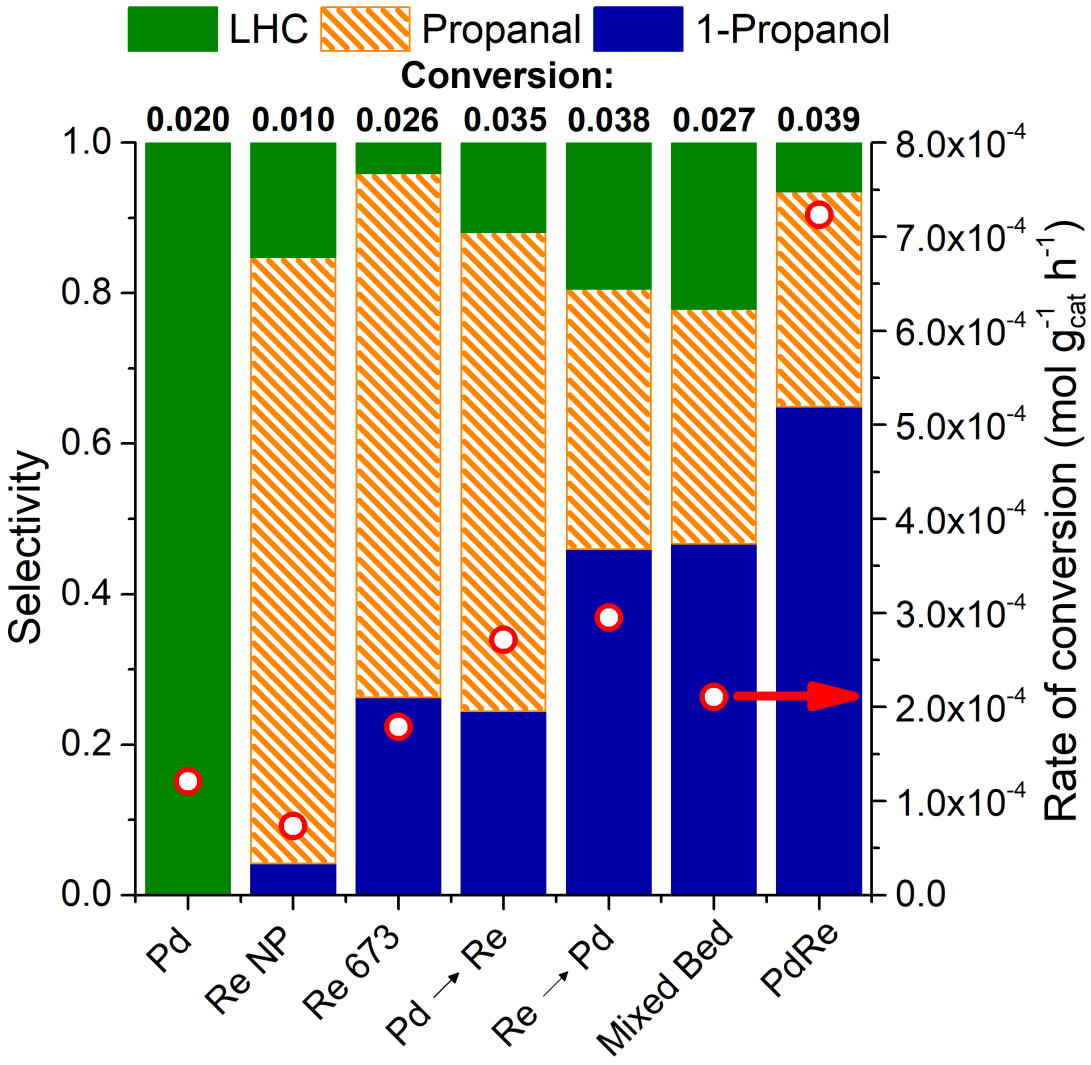

Figure 3.6: Product selectivity (represented by bars) and rate of reaction (represented by red points) for Pd/SiO_2, Re/SiO_2, and $PdRe/SiO_2$ between 1-4% conversion. All reactions took place using a reactant feed of 30 cm^3 min^{-1} of 1 kPa propionic acid in 0.3 MPa H_2 at 433 K.

the Re bed followed by the Pd bed demonstrated a higher selectivity of 46% to 1-propanol than the Pd bed followed by Re which was only 24% selective to 1-propanol. On the other hand, the Pd bed followed by Re demonstrated a lower selectivity to hydrocarbons of 12% than the Re bed followed by Pd that produced 20% hydrocarbons. The increase in light hydrocarbon products can be attributed to the decarbonylation of products 1-propanol or propanal over the Pd bed to form ethane.[26] When a physically mixed bed of the same metal loadings of Pd and Re was tested for activity, the observed rate and selectivity pattern were more similar to the bed of Re followed by the bed of Pd. The activity was not very different from the separated beds, which may have been a result of similar behavior to that observed by Ly et al., where mobile Re_2O_7 was reduced onto the active Pd surface under reactor startup conditions resulting in decreased catalytic activity.[10] Nevertheless, the performance of the bimetallic catalyst was superior in terms of activity and alcohol selectivity compared to any combination of the monometallic catalyst beds. Thus, proximity of the Pd and Re are critical for performance.

3.3.6 Kinetic Isotope Effects

The steady-state rates obtained during reduction of propionic acid using either H_2 or D_2 are summarized in Table 3.2. When D_2 was substituted for H_2 while using either a Re/SiO_2, $PdRe/SiO_2$, or $PdRe/TiO_2$ catalyst to reduce propionic acid, the rate of propionic acid conversion increased, demonstrating an inverse kinetic isotope effect. Inverse kinetic isotope effects, sometimes called equilibrium isotope effects, occur when the equilibrium of a reaction is shifted by D in a direction that enhances the rate of product formation.[27] In this case, the observed rate of conversion of propionic acid is observed to have an isotope effect ($rate_H/rate_D$) of 0.79

over $PdRe/SiO_2$ and $PdRe/TiO_2$, and 0.84 over Re/SiO_2. Inverse isotope effects have also been observed for the reduction of ethyl butyrate and butyric acid over $Co/\gamma\text{-}Al_2O_3$ catalysts.[28] The selectivity of propionic acid conversion to 1-propanol increased as a result of the switch from H_2 to D_2, likely as a result of an increase in conversion. An inverse isotope effect ($rate_H/rate_D = 0.59$) was observed for the rate of reduction of 1-propanol to propane, which was similar to the isotope effect observed by Falcone et al. during the hydrogenolysis of glycerol using Pt-promoted Re catalysts.[29] The hydrogenation of propanal to form 1-propanol over both $PdRe/SiO_2$ and Re/SiO_2 results in a normal kinetic isotope effect of 1.6 and 1.5, respectively (Table 3.3), and is similar to behavior observed by Meemken et al. during the hydrogenation or deuteration of the carbonyl group in 2,2,2-trifluoroacetophenone over 5 wt % Pt/Al_2O_3.[30]

3.3.7 Diffuse Reflectance Infrared Fourier Transform Spectroscopy

The SiO_2- and TiO_2-supported Pd, Re, and PdRe catalysts were investigated using *in situ* DRIFTS to explore the identity of species leading to alcohols, which were previously reported to cover a large fraction of the surface of $PdRe/SiO_2$.[18] When the SiO_2 support and Pd/SiO_2 were exposed to 15 cm^3 min^{-1} of 0.3 kPa propionic acid in 0.1 MPa H_2 at 413 K, IR features corresponding to adsorbed propionic acid appeared immediately. Features on SiO_2 arising from exposure to propionic acid are listed in Table B.1, and are shown in Figure B.2. These features were followed shortly (after exposure to acid) by a shoulder peak at 1755 cm^{-1} attributed to the formation of the silyl ester of propionic acid on the SiO_2 surface. Apparently, silyl ester formation was somewhat suppressed in the Pd/SiO_2 catalyst based on the relative ratio of the ester shoulder to the main carbonyl vibrational mode.

Table 3.2: Comparison of the rate of reduction of 0.5 kPa propionic acid, in 0.1 MPa H_2 or D_2, at 433 K, flowed at 30 cm^3 min^{-1} to form 1-propanol, propanal, and light hydrocarbons (LHC) over $PdRe/SiO_2$, $PdRe/TiO_2$, and Re/SiO_2 catalysts.

H_2/D_2	Catalyst	Conversion	Rate of reduction (mol g_{cat}^{-1} h^{-1})	Product selectivity			Overall isotope effect ($rate_H/rate_D$)
				1-Propanol	Propanal	LHC	
H_2	$1Pd8Re/SiO_2$	6.9%	2.6×10^{-4}	0.81	0.10	0.08	**0.79**
D_2	$1Pd8Re/SiO_2$	8.7%	3.4×10^{-4}	0.84	0.08	0.08	
H_2	$1Pd8Re/TiO_2$	7.9%	2.8×10^{-4}	0.84	0.09	0.07	**0.79**
D_2	$1Pd8Re/TiO_2$	10.%	3.5×10^{-4}	0.87	0.06	0.07	
H_2	$8Re/SiO_2$	2.6%	9.1×10^{-5}	0.29	0.66	0.05	**0.84**
D_2	$8Re/SiO_2$	3.0%	1.1×10^{-4}	0.35	0.59	0.07	

Table 3.3: Comparison of the rate of reduction of 1 kPa propanal using $PdRe/SiO_2$ or Re/SiO_2 in 0.1 MPa H_2 or D_2, at 363 K, flowed at 30 cm^3 min^{-1} to form 1-propanol.

H_2/D_2	Catalyst	Conversion	Rate of reduction (mol g_{cat}^{-1} h^{-1})	Product selectivity to 1-propanol	Overall isotope effect ($rate_H/rate_D$)
H_2	$1Pd8Re/SiO_2$	3.0%	4.4×10^{-3}	>0.99	**1.6**
D_2	$1Pd8Re/SiO_2$	1.9%	2.8×10^{-3}	>0.99	
H_2	$8Re/SiO_2$	1.4%	1.3×10^{-3}	>0.99	**1.5**
D_2	$8Re/SiO_2$	0.95%	8.7×10^{-4}	>0.99	

Weak vibrations near 1915 cm^{-1} and 2051 cm^{-1} assigned to C≡O formation were also observed over Pd/SiO_2, having frequencies corresponding to both linear and bridge-bonding C≡O. Interestingly, these adsorbed CO features were much weaker in the spectra of both $PdRe/SiO_2$ and $PdRe/TiO_2$, indicating that the presence of Re may play a secondary role in preventing significant C≡O uptake on the Pd surface. The spectra of these materials in the C≡O stretching region are shown in appendix Figure B.6.

When the Re/SiO_2 and $PdRe/SiO_2$ catalysts were exposed to propionic acid and H_2 under the same conditions, an unknown reactive surface species was observed with vibrational modes in the C-H stretching and backbone deformation regions. The intensity of these features relative to carbonyl stretching was correlated to catalyst activity, suggesting that they were related to product formation. This species could not be removed from $PdRe/SiO_2$ by treatment of the catalyst at 673 K in H_2. When the reaction conditions were changed from 0.3 kPa propionic acid in 0.1 MPa H_2 to 0.3 kPa propionic acid in 0.1 MPa N_2, the C-H vibrational modes associated with the unknown species decreased over time. Performing this experiment in a packed-bed reactor resulted in a transient decay of 1-propanol formation after switching from H_2 to N_2 as shown in Figure 3.2. When H_2 was reintroduced to the DRIFTS cell along with the acid, the unknown C-H stretching modes returned. Similarly, when 0.4 kPa water was cofed with 0.3 kPa of propionic acid in 0.1 MPa H_2 through a catalyst bed already at steady state, the same C-H vibrational modes decreased with time. This phenomenon is illustrated in detail in Figure 3.7.

In Figure 3.7(a), the C-H stretching modes corresponding to the unknown species at 2969, 2945, 2928, and 2887 cm^{-1} decreased over time during water cofeeding. In Figure 3.7(b), the disappearance of the silyl ester shoulder peak during water cofeeding is shown. In the region

shown in Figure 3.7(c), the intensity of weak shoulder peaks corresponding to C-H deformation modes at 1480 and 1458 cm^{-1} decrease during water cofeeding. Figure 3.7(d) compares the intensity of the silyl ester shoulder mode (measured at 1760 cm^{-1}) to the intensity of the unknown C-H stretching modes (measured at 2970 cm^{-1}) over time, indicating that water removes the silyl esters rapidly, but then takes over 10 hours to remove the unknown surface species. When the water was removed from the reactant stream, the modes of the unknown species returned over time, also shown in Figure 3.7(a-d). As discussed earlier, changing the amount of co-fed water resulted in a transient increase or decrease (Figure 3.5) in the observed rate of formation of 1-propanol, followed by a return to the previous steady state. In the context of the DRIFTS results, this result indicates that an increase or decrease in the intensity of these C-H vibrational modes is a result of the formation or removal, respectively, of reactive intermediates leading to 1-propanol on the catalyst surface. Comparison of the unknown surface species to the SiO_2 support exposed to 0.1 kPa 1-propanol and subsequently purged with pure H_2 (shown in Figure 3.7(e)) suggests that the unknown surface species is a propoxy species bound to the SiO_2 support. The assignments of features arising from SiO_2 exposure to 1-propanol are reported in Table B.1.

When H_2 was replaced with D_2 as the reductant, the formation of features that have been previously associated with a dideuteromethylene moiety (shown in Figure 3.8) were observed in the C-D vibration region, indicating that this surface intermediate contains a similar dideuteromethylene moiety and is similar in structure to the hydrogenated product 1-propanol.[37] The assignments of the observed features discussed here over $PdRe/SiO_2$ and $PdRe/TiO_2$ can be found in Table 3.4. Complete spectra corresponding to these catalysts under the listed conditions are shown in Figure B.3 and Figure B.4.

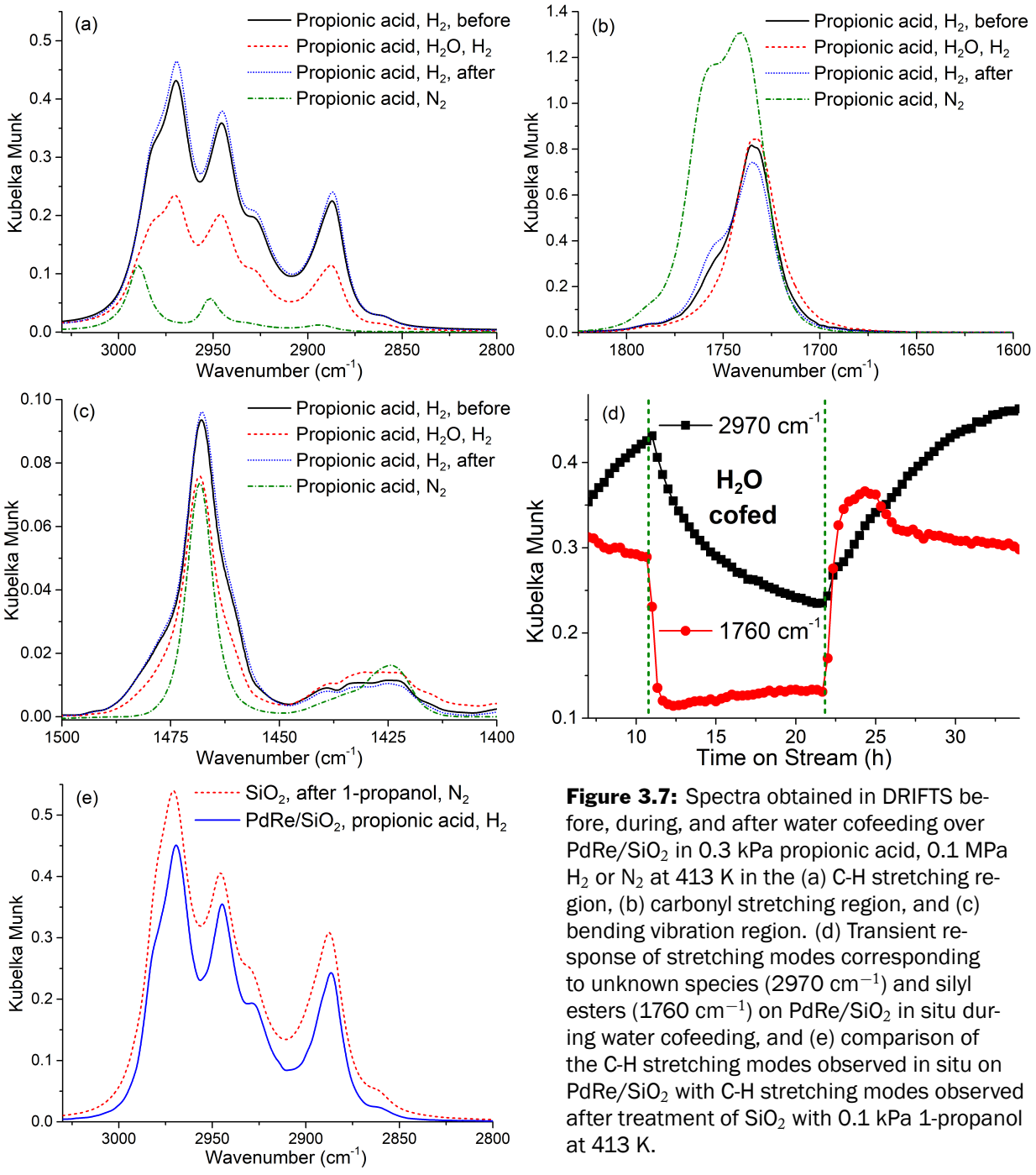

Figure 3.7: Spectra obtained in DRIFTS before, during, and after water cofeeding over $PdRe/SiO_2$ in 0.3 kPa propionic acid, 0.1 MPa H_2 or N_2 at 413 K in the (a) C-H stretching region, (b) carbonyl stretching region, and (c) bending vibration region. (d) Transient response of stretching modes corresponding to unknown species (2970 cm^{-1}) and silyl esters (1760 cm^{-1}) on $PdRe/SiO_2$ in situ during water cofeeding, and (e) comparison of the C-H stretching modes observed in situ on $PdRe/SiO_2$ with C-H stretching modes observed after treatment of SiO_2 with 0.1 kPa 1-propanol at 413 K.

Table 3.4: Vibrational modes observed by DRIFTS during *in situ* reduction of propionic acid over $PdRe/SiO_2$ and $PdRe/TiO_2$.

Adsorbent	Conditions	Vibrational mode	Frequency (cm^{-1})	Assignment
$PdRe/SiO_2$	0.3 kPa propionic acid, 0.1 MPa H_2, 413 K	ν(OH)	3530-3130 broad	Propionic acid, water (physisorbed)
		$\nu_a(CH_3)$	2990	Propionic acid (physisorbed, silyl ester)[31]
			2969	Propoxy
		$\nu_a(CH_2)$	2951	Propionic acid (physisorbed, silyl ester)
			2945	Propoxy
		$\nu_s(CH_3)$	2931 sh	Propionic acid (physisorbed, silyl ester)
			2928 sh	Propoxy
		$\nu_s(CH_2)$	2893	Propionic acid (physisorbed, silyl ester)
			2887	Propoxy
		ν(C≡O)	1929	CO (bridging)[32]
		ν(C=O)	1755	Propionic acid, silyl ester[31]
			1740-1730	Propionic acid, physisorbed/dimer
		δ(C–H)	1480	Propoxy[33]
			1467	Propionic acid[31]
			1458	Propoxy[33]
		ν(C–O)/δ(C–H)	1440, 1428	Propionic acid[31]
		δ/ω(C–H)	1399	Propoxy[33]
			1386	Propionic acid[31]
			1370	Propionic acid
$PdRe/TiO_2$	0.3 kPa propionic acid, 0.1 MPa H_2, 413 K	ν(OH)	3500-3100 broad	Propionic acid, water (physisorbed)
		$\nu_a(CH_3)$	2994	Propionic acid (vapor)
			2978	Propionic acid, bidentate[34,35]
		$\nu_a(CH_2)$	2944	Propionic acid, bidentate
		$\nu_s(CH_3)$	2930-2900 w	Propionic acid, bidentate
		$\nu_s(CH_2)$	2884	Propionic acid, bidentate
		ν(C≡O)	2021	CO (linear, very low coverage)[32]
			1925	CO (bridging)
		ν(C=O)	1791,1772,1732	Propionic acid, (vapor, monomer and dimer)
		ν_a(O–C=O)	1520	Propionic acid, bidentate[34,36]
		δ(C–H)	1470	Propionic acid
		ν_s(O–C=O)	1436	Propionic acid, bidentate[36]
		δ(C–H)	1418	Propionic acid (vapor)
		δ(C–H)	1377	Propionic acid

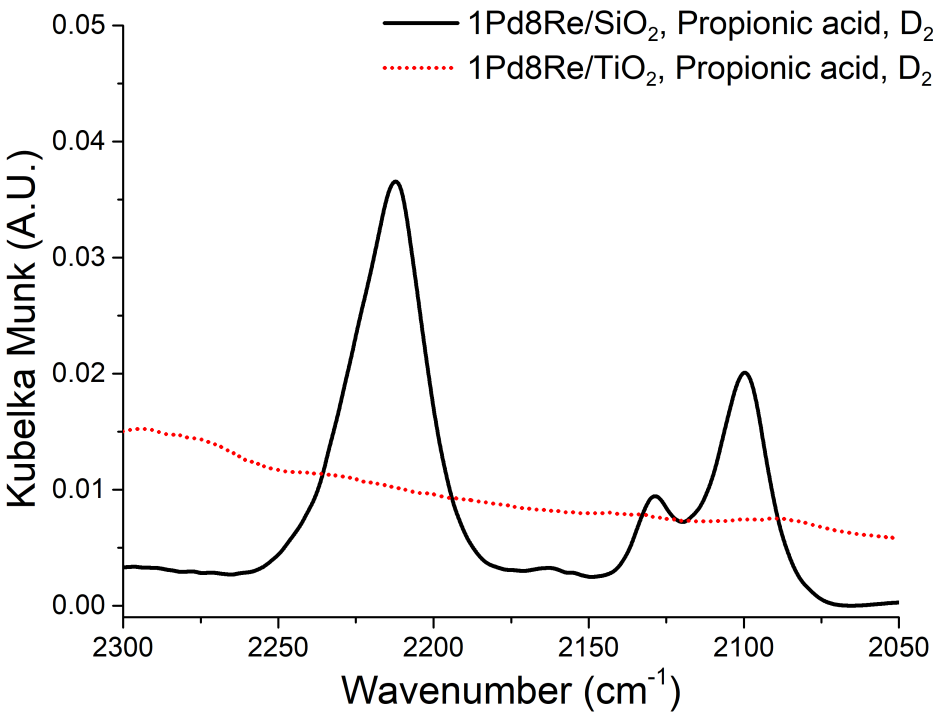

Figure 3.8: Comparison of vibrational modes observed using DRIFTS in the C-D stretching region after feeding 0.1 MPa D_2 and 0.3 kPa propionic acid to $PdRe/SiO_2$ (solid line) and $PdRe/TiO_2$ (dotted line).

When $PdRe/TiO_2$ was exposed to 15 cm^3 min^{-1} of 0.3 kPa propionic acid in 0.1 MPa H_2, no propoxy species were observed in the resulting spectra. Instead, the majority species on the surface of the catalyst appeared to be a strongly bound bidentate propionate species. These species were identified by slightly red-shifted C-H stretching modes from the gas-phase propanoic acid, and COO stretching modes around 1520 cm^{-1} and 1420 cm^{-1} corresponding to bidentate propionate species.[34] Diffuse reflectance spectra of $PdRe/TiO_2$ and TiO_2 exposed to 0.3 kPa propionic acid in 0.1 MPa H_2 at 413 K are shown in Figure B.5 in the appendix. When the H_2 was exchanged for D_2 during reaction over $PdRe/TiO_2$, vibrational modes corresponding to the dideuteromethylene in a propoxy species were not observable in the C-D stretching region as shown in Figure 3.8, indicating that a negligible fraction of the catalyst surface is covered by these types of species under reaction conditions.

3.3.8 Transient Kinetic Analysis

The number of reactive intermediates on the surface of Pd-promoted Re/TiO_2 (N_i) and mean surface residence time of reactive intermediates leading to products (τ_i) were quantified using transient kinetic analysis. The formation of alkoxy species on the SiO_2 surface was undesirable for studying the behavior of reactive intermediates on the active metal surface, as it led to holdup times of many hours for the alcohol as the SiO_2-supported alkoxy species desorbed from the SiO_2 surface. The TiO_2-supported PdRe catalyst did not form a reservoir of propoxy species on the support surface that could be detected by DRIFTS, so transient kinetic analysis was performed using 1 wt % Pd, 8 wt % Re/TiO_2 (1Pd8Re/TiO_2), 1 wt % Pd, 13 wt % Re/TiO_2 (1Pd13Re/TiO_2), and 0.5 wt % Pd, 8 wt % Re/TiO_2 (0.5Pd8Re/TiO_2). The coverage of the catalyst surface by reactive intermediates leading to each product at the time of the switch was measured over a flowrate range of 30-90 cm^3 min^{-1}. Results from DRIFTS suggest the catalyst surface is highly covered with strongly bound propionic acid species. Additionally, the reduction of carboxylic acids to primary alcohols is expected to proceed through an aldehyde intermediate. Taking these assumptions into consideration, quantitative results from the transient kinetic analysis were obtained from the highest flowrate (90 cm^3 min^{-1}) to minimize the amount of product readsorption contributing to the mean surface residence time while still producing a secondary reaction product. This type of analysis has been performed previously while investigating the Guerbet coupling of ethanol.[38] All results (Table 3.5) are corrected for gas-phase holdup in any dead volume of the reactor using the transient response of a methane tracer, which did not have any effect on the observed rates of formation of oxygenated products.

In Figure 3.9, the transient response of propanal and 1-propanol over 1 wt % Pd, 8 wt %

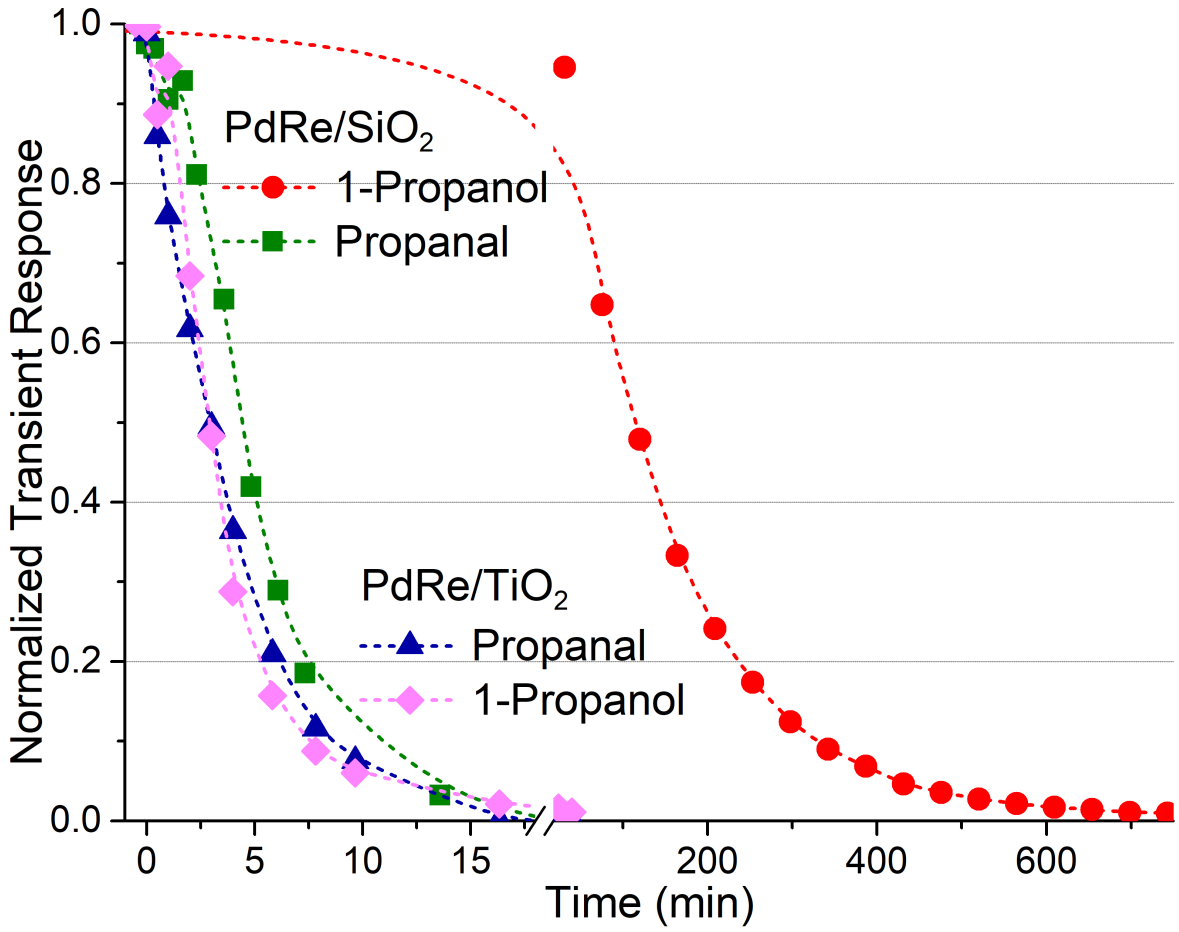

Figure 3.9: Normalized transient response to a reactant switch from 0.5 kPa propionic acid to 0.5 kPa butyric acid at 30 cm^3 min^{-1} in 0.1 MPa H_2 at 433 K over 1Pd8Re/TiO_2, and normalized transient response to a reactant switch from 1 kPa propionic acid to 1 kPa butyric acid under the same conditions over 1Pd8Re/SiO_2. The x-axis is broken at 18 min, after which the timescale has been compressed to display the complete 1-propanol transient.

Table 3.5: Parameters derived from transient kinetic analysis of 0.5 kPa propionic and butyric acid reduction in 0.1 MPa H_2 at 433 K, including the ratio of reactive intermediates to Re atoms N_i/Re.

Catalyst	Product	Rate of formation[a] (mol g_{cat}^{-1} h^{-1})	τ (min)	TOF[b] (s^{-1})	Surface coverage (mol g_{cat}^{-1})	N_i/Re[c]
1Pd8Re/TiO_2	1-propanol	2.1×10^{-4}	1.4	1.2×10^{-2}	5.2×10^{-6}	0.012
	propanal	7.5×10^{-5}	1.2	1.4×10^{-2}	1.5×10^{-6}	0.004
	1-butanol	1.8×10^{-4}	2.3	7.3×10^{-3}	6.9×10^{-6}	0.017
	butanal	3.5×10^{-5}	0.9	1.9×10^{-2}	5.1×10^{-7}	0.001
1Pd13Re/TiO_2	1-propanol	3.6×10^{-4}	1.1	1.5×10^{-2}	6.9×10^{-6}	0.010
	propanal	2.1×10^{-4}	0.5	3.0×10^{-2}	1.8×10^{-6}	0.003
	1-butanol	1.6×10^{-4}	1.7	9.6×10^{-3}	4.7×10^{-6}	0.007
	butanal	8.4×10^{-5}	0.5	3.5×10^{-2}	6.7×10^{-7}	0.001
0.5Pd8Re/TiO_2	1-propanol	2.5×10^{-4}	2.0	8.4×10^{-3}	8.2×10^{-6}	0.021
	propanal	8.8×10^{-5}	2.0	8.5×10^{-3}	2.9×10^{-6}	0.007
	1-butanol	1.1×10^{-4}	3.8	4.4×10^{-3}	7.2×10^{-6}	0.018
	butanal	5.4×10^{-5}	1.2	1.4×10^{-2}	1.1×10^{-6}	0.003

(a) Obtained from results at a flowrate of 90 cm^3 min^{-1}
(b) TOF is calculated as τ^{-1}
(c) Ratio of intermediates leading to specified product divided by total Re in sample

Re/TiO_2 following a switch in reactant from propionic acid to butyric acid is compared to the transient response of product formation over PdRe/SiO_2, which was reported previously.[18] In the absence of high coverage of the support surface by propoxy species (demonstrated by DRIFTS), the coverage of reactive intermediates on 1Pd8Re/TiO_2 leading to 1-propanol was 0.012 N_i/Re.

3.4 Discussion

When the contact time of the reactant stream with the catalyst bed was reduced by increasing the flowrate, the selectivity of propionic acid conversion towards 1-propanol began to decrease, and the selectivity towards propanal increased accordingly. This behavior is consistent with a two-step reaction path, where propionic acid is first converted into propanal, which is then rapidly hydrogenated to form 1-propanol. This result also indicates that the formation of

the aldehyde intermediate is typically followed by desorption and readsorption steps, wherein the aldehyde leaves the acid reduction site (which is enhanced by H_2 spillover from nearby Pd in the bimetallic catalyst) and is subsequently hydrogenated on another site. The resulting increase in selectivity towards 1-propanol when a bed of monometallic Pd is placed downstream of Re supports this hypothesis, and also indicates that one key function of Pd in the bimetallic catalyst is to facilitate the hydrogenation of the resulting aldehydes to form alcohols, resulting in a more selective catalyst. The overlapping transient response of propanal and 1-propanol produced over $PdRe/TiO_2$ catalysts indicates rapid hydrogenation as well, as alcohol formation is observed as soon as aldehyde formation is observed. Finally, the higher rate of propanal hydrogenation observed at lower temperature in the absence of propionic acid suggests that 1-propanol formation may also occur rapidly during propionic acid reduction. Indeed, all observed behavior supports a 2-step cascade reaction where reduction of the acid to form an aldehyde is followed by rapid hydrogenation of the aldehyde to an alcohol.

Hydrogenation of propanal had a lower apparent barrier (24-29 kJ mol^{-1}) than the formation of oxygenates over the Re-containing active site (60-75 kJ mol^{-1}). Similar results were found by Rozmyslowicz et al.,[16] who reported an aldehyde intermediate during stearic acid reduction in 2-4 MPa H_2 in decane over 4 wt % Re/TiO_2. Rozmyslowicz et al. used kinetic modeling to derive a barrier of 106 $\pm$ 3 kJ mol^{-1} for stearic acid reduction to octadecanal, while the subsequent aldehyde hydrogenation barrier was 39 $\pm$ 22 kJ mol^{-1}. These calculated values were somewhat higher than those observed here, but the relative heights of the barriers are consistent.

In situ DRIFTS highlights the unusual behavior of SiO_2 as a catalyst support in the presence of alcohols. Apparently, the surface reaction path of propionic acid reduction over PdRe

on a SiO_2 support involves two extra steps, the first involving the trapping of the *n*-alcohol product as an alkoxy species on SiO_2, and the second being the release of the alkoxy species by either carboxylic acids (fed as reactant), water (formed by reduction of carboxylic acid to produce an aldehyde) or by subsequently produced alcohols. Strongly bound alkoxy species (as alkoxysilanes) can be formed by contact of alcohols with SiO_2,[39] which may occur by esterification of *n*-alcohols with silanol species on silica,[40] as well as by direct alcoholysis of Si-O-Si bonds in a non-defected SiO_2 surface.[41] In light of this observation, future investigation of the transient kinetics of metal-catalyzed reactions on SiO_2 supports should be undertaken cautiously. Silylation of the silica support is one potential way to mitigate alkoxysilane formation during transient studies.[42] However, depending on the exposure time and temperature, even non-defected SiO_2 surfaces may react with alcohols to generate alkoxysilane species as mentioned earlier.

When the transient kinetics of propionic acid reduction over 1Pd8Re/SiO_2 (previously studied[18]) and 1Pd8Re/TiO_2 are compared, similar coverages of reactive intermediates leading to propanal (0.006 N_i/Re on 1Pd8Re/SiO_2 versus 0.004 N_i/Re on 1Pd8Re/TiO_2) were measured. In contrast, the coverage of reactive intermediates leading to 1-propanol was 0.59 N_i/Re on the SiO_2-supported catalyst versus 0.012 N_i/Re on the TiO_2-supported catalyst. The lower coverage of intermediates leading to alcohols on 1Pd8Re/TiO_2 can be attributed to the lack of a large reservoir of propoxy species on the support surface, which was not observed by DRIFTS on the TiO_2 surface. A comparison of the transient response observed over 1Pd8Re/SiO_2 and 1Pd8Re/TiO_2 is shown in Figure 3.9. Furthermore, the previously observed transient behavior can now be explained by the removal of alkoxysilane species from the SiO_2 surface as 1-propanol (as shown in Figure 3.10). This removal occurred on the same timescale as the replacement of

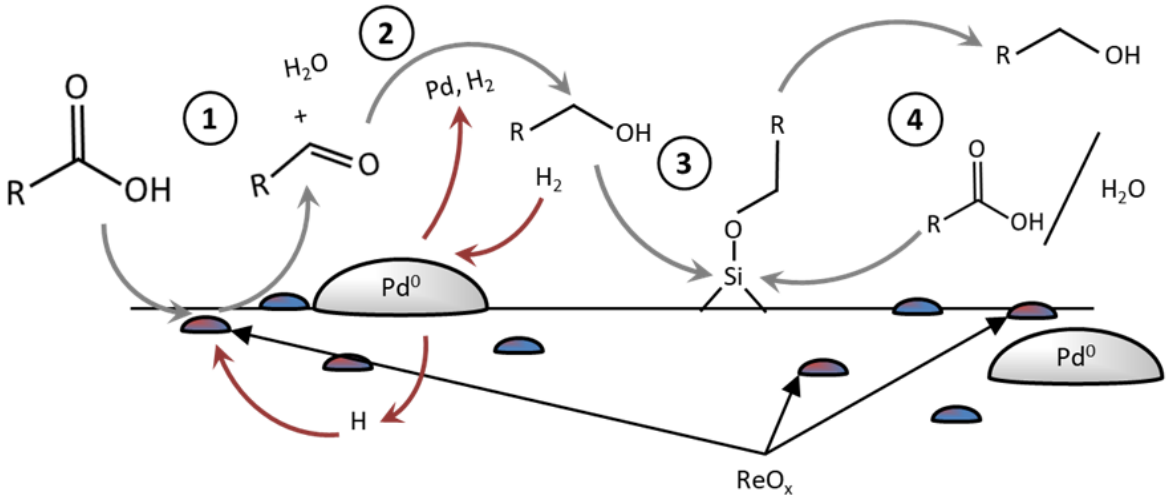

Figure 3.10: Representation of the reduction of carboxylic acids over Pd and Re followed by interaction with the SiO_2 support. (1): Reduction of acid to aldehyde, beginning the cascade reaction. (2): Hydrogenation of the aldehyde to form the *n*-alcohol. (3): Esterification/alcoholysis of SiO_2 with alcohol to form alkoxysilane. (4): Liberation of alkoxysilane from support surface.

products in the reactor outlet, suggesting that a majority of the product alcohol molecules were readsorbed as propoxy species prior to leaving the reactor bed. Moreover, catalytic turnover occurring on the active metal components of the SiO_2-supported catalyst was masked by the slower turnover of the large pool of alkoxides on the SiO_2 support. When TiO_2 was used as the support instead of SiO_2, bidentate-adsorbed carboxylic acids covered the TiO_2 surface, and coverage of product alcohol on the support surface was not observed. This suggested the catalytic turnover of reactants on the active metals was probed directly, and revealed production of the aldehyde and alcohol products on similar time scales. The N_i/Re of 0.012 over the 1Pd8Re/TiO_2 indicates that a majority of the Re atoms do not have adsorbed reactive intermediates leading to products.

The observed 0.6 order dependence of propionic acid reduction on H_2 pressure suggests that the rate-determining step in acid reduction depends strongly on the availability of H at the active site. On the other hand, propionic acid is expected to interact strongly with metal surfaces,[19,43] which would explain why the rate of conversion demonstrated a near-zero order

dependence on propionic acid pressure reaction as propionic acid likely saturates the surface at very low concentrations. Prior investigation of the reduction of acetic acid by Pt/TiO_2 by Rachmady and Vannice found that order in H_2 varied from 0.4 to 0.6, while order in acetic acid varied from 0.2 to 0.4 under similar conditions.[14] The slightly higher order in acid over Pt/TiO_2 could be attributed to weaker interaction of the acetic acid with the TiO_2 active sites, as discussed by Rachmady et al. and demonstrated by Kim et al.[44] Despite the high order of H_2 on the alcohol formation rate, an inverse kinetic isotope effect of 0.79 was observed for the reduction of propionic acid over the Re-containing catalysts.

An inverse kinetic isotope effect suggests that a H-addition step is less likely to be rate limiting.[27] Therefore, potential explanations for the observed inverse isotope effect include the formation of a partially hydrogenated reactive intermediate (such as dioxyethylidene or weakly adsorbed propionic acid species), or enhanced coverage of dissociated D on the catalyst surface leading to an increase in the rate of reduction of the carboxylic acid. Work by Bender et al. demonstrated that inverse isotope effects of similar magnitude could be observed during the oxidative addition of D_2 to transition metal complexes, suggesting that H_2/D_2 dissociative adsorption could also be a rate-determining step.[45] However, the rate of propanal hydrogenation was higher than the rate of propionic acid reduction observed over Re/SiO_2, despite the fact that hydrogenation was carried out at a lower temperature, which suggests that dissociation of hydrogen is not a limiting step in this system.

An isotope effect of 0.59 was observed for the reduction of 1-propanol to propane over $PdRe/SiO_2$. Acid-catalyzed dehydration of primary alcohols is well-known to undergo E_2-type bimolecular elimination to produce alkenes. Therefore, an inverse isotope effect for 1-propanol

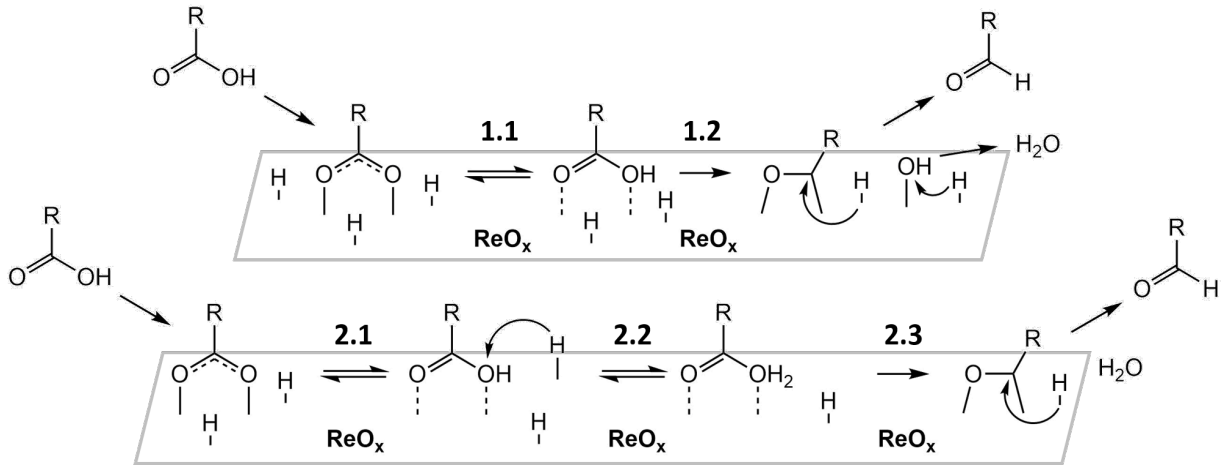

Figure 3.11: Proposed mechanism for the reduction of carboxylic acids resulting from a rate-determining C-OH bond breaking step (1.2, top) or C-OH_2 bond breaking step (2.3, bottom).

reduction could also be explained by the equilibration of surface $H^{\delta+}/D^{\delta+}$ (on ReO_x) and adsorbed 1-propanol species with a protonated or deuterated alkyloxonium ion. Subsequent E_2 elimination of water and a proton would produce propene, which would be rapidly hydrogenated.

Here we propose a similar C-O(H/D) or C-O(H_2/D_2) bond breaking step is rate-limiting, as discussed by Pallassana and Neurock.[19] The potential mechanisms proposed are shown in Figure 3.11. These mechanisms are expected to require either a strong Lewis acid (Route 1, top) or a mixture of Lewis and Brønsted acid sites (Route 2, bottom). In both cases, propionic acid adsorbs dissociatively to form strongly bound propionate at the active site. The concentration of surface propionic acid is determined by the equilibrium of H addition back onto the propionate species (1.1, 2.1). The surface propionic acid either undergoes rate determining C-OH bond breaking (1.2) or further addition of a hydrogen (2.2) followed by rate determining C-OH_2 bond breaking (2.3). In both cases, an equilibrium deuterium effect of similar magnitude to that seen in 1-propanol reduction resulting from deuteration of the propionate or propionic acid would occur. Furthermore, an order in H_2 of between 0.5 and 1 would be observed, which is consistent

with the observed orders of propionic acid reduction over Pd-promoted Re observed here and elsewhere.[16] Derivation of the corresponding rate law is provided in Appendix B.

3.5 Conclusions

Palladium-promoted Re catalysts supported on SiO_2 and TiO_2 were synthesized by a stepwise incipient wetness impregnation method. The Re-based catalysts were active for the conversion of propionic acid to a mixture of 1-propanol, propionaldehyde, and light hydrocarbons, as well as the reduction of propanal and 1-propanol. Decreasing the conversion of the reactant over the active catalysts resulted in a shift in product selectivity that favored propanal over 1-propanol. The conversion of propionic acid had a 0.6 order dependence on H_2 pressure over all Re-based catalysts. Apparent barriers to propionic acid conversion were in the range of 60-75 kJ mol^{-1} over the SiO_2 and TiO_2 supported Re-based catalysts. Inverse kinetic isotope effects of 0.79, 0.59, and a normal kinetic isotope effect of 1.6 were observed for the catalytic reduction of propionic acid, 1-propanol, and propanal, respectively, when D_2 was substituted for H_2 in the reactant stream over $PdRe/SiO_2$. Cofeeding water or switching H_2 to N_2 during steady-state conversion of propionic acid in H_2 over $PdRe/SiO_2$ resulted in transient 1-propanol formation lasting approximately 10 hours after the change in reactant concentration. The transient response caused by water was investigated using DRIFTS, and attributed to the liberation of propoxy species from the SiO_2 support surface by propionic acid or water. Transient kinetic analysis of propionic acid reduction on $PdRe/TiO_2$ revealed that the coverage of reactive intermediates leading to products on the active Re metal surface for propionic acid conversion was less than 2% of the number of Re atoms in the catalyst. Turnover frequencies on the order of

10^{-2} s^{-1} were calculated, which were much greater than previously reported turnover frequencies. These results highlight the reactive behavior of SiO_2 in the presence of alcohols. The behavior of propionic acid reduction over Pd-promoted Re catalysts is consistent with a two-step cascade reaction where the carboxylic acid is reduced to an aldehyde, which is rapidly hydrogenated to form an alcohol. Moreover, the observed kinetic behavior is consistent with a rate-determining C-OH or C-OH_2 bond-breaking step.

Acknowledgements

Helpful discussions with Dr. Matthew Neurock and Ashwin Chemburkar are acknowledged. Naomi Miyake is acknowledged for collection of X-ray diffraction patterns presented here. This material is based upon work supported by the National Science Foundation (NSF) under Award No. EEC-0813570. Any opinions, findings, and conclusions or recommendations expressed in this material are those of the author(s) and do not necessarily reflect the views of the NSF.

References

1. International Energy Agency. *The Future of Petrochemicals* tech. rep. (International Energy Agency, 2018).

2. Vennestrøm, P. N. R., Osmundsen, C. M., Christensen, C. H. and Taarning, E. Beyond petrochemicals: The renewable chemicals industry. *Angewandte Chemie - International Edition* **50,** 10502–10509 (2011).

3. Werpy, T. and Peterson, G. *Top Value Added Chemicals from Biomass Volume 1 – Results of Screening for Potential Candidates from Sugars and Synthesis Gas* tech. rep. (2004).

4. Corma, A., Iborra, S. and Velty, A. Chemical routes for the transformation of biomass into chemicals. *Chemical reviews* **107,** 2411–502 (2007).

5. Vivek, N., Pandey, A. and Binod, P. in *Current Developments in Biotechnology and Bioengineering* 719–738 (Elsevier, 2017).

6. Ullrich, J. and Breit, B. Selective Hydrogenation of Carboxylic Acids to Alcohols or Alkanes Employing a Heterogeneous Catalyst. *ACS Catalysis* **8,** 785–789 (2018).

7. Thakur, D. S. and Carrick, W. J. *US Patent* 9120086 (2015).

8. He, D.-h., Wakasa, N. and Fuchikami, T. Hydrogenation of Carboxylic Acids Using Bimetallic Catalysts consisting of group 8 to 10, and group 6 or 7 metals. *Tetrahedron Letters* **36,** 1059–1062 (1995).

9. Takeda, Y., Nakagawa, Y. and Tomishige, K. Selective hydrogenation of higher saturated carboxylic acids to alcohols using a ReO_x–Pd/SiO_2 catalyst. *Catalysis Science & Technology* **2,** 2221 (2012).

10. Ly, B. K., Minh, D. P., Pinel, C., Besson, M., Tapin, B., Epron, F. and Especel, C. Effect of Addition Mode of Re in Bimetallic Pd–Re/TiO_2 Catalysts Upon the Selective Aqueous-Phase Hydrogenation of Succinic Acid to 1,4-Butanediol. *Topics in Catalysis* **55,** 466–473 (2012).

11. Manyar, H. G., Paun, C., Pilus, R., Rooney, D. W., Thompson, J. M. and Hardacre, C. Highly selective and efficient hydrogenation of carboxylic acids to alcohols using titania supported Pt catalysts. *Chemical communications (Cambridge, England)* **46,** 6279–81 (2010).

12. Mendes, M., Santos, O., Jordão, E. and a.M Silva. Hydrogenation of oleic acid over ruthenium catalysts. *Applied Catalysis A: General* **217,** 253–262 (2001).

13. Pritchard, J., Filonenko, G. A., van Putten, R., Hensen, E. J. M. and Pidko, E. A. Heterogeneous and homogeneous catalysis for the hydrogenation of carboxylic acid derivatives: history, advances and future directions. *Chem. Soc. Rev.* **44,** 3808–3833 (2015).

14. Rachmady, W. and Vannice, M. Acetic acid hydrogenation over supported platinum catalysts. *Journal of Catalysis* **192,** 322–334 (2000).

15. Ly, B. K., Tapin, B., Aouine, M., Delichere, P., Epron, F., Pinel, C., Especel, C. and Besson, M. Insights into the Oxidation State and Location of Rhenium in Re-Pd/TiO_2 Catalysts for Aqueous-Phase Selective Hydrogenation of Succinic Acid to 1,4-Butanediol as a Function of Palladium and Rhenium Deposition Methods. *ChemCatChem* **7,** 2161–2178 (2015).

16. Rozmysłowicz, B., Kirilin, A., Aho, A., Manyar, H., Hardacre, C., Wärnå, J., Salmi, T. and Murzin, D. Y. Selective hydrogenation of fatty acids to alcohols over highly dispersed ReO_x/TiO_2 catalyst. *Journal of Catalysis* **328,** 197–207 (2015).

17. Takeda, Y., Tamura, M., Nakagawa, Y., Okumura, K. and Tomishige, K. Characterization of Re-Pd/SiO_2 Catalysts for Hydrogenation of Stearic Acid. *ACS Catalysis* **5,** 7034–7047 (2015).

18. Kammert, J. D., Xie, J., Godfrey, I. J., Unocic, R. R., Stavitski, E., Attenkofer, K., Sankar, G. and Davis, R. J. Reduction of Propionic Acid over a Pd-Promoted ReO_x/SiO_2 Catalyst Probed by X-ray Absorption Spectroscopy and Transient Kinetic Analysis. *ACS Sustainable Chemistry & Engineering* **6,** 12353–12366 (2018).

19. Pallassana, V. and Neurock, M. Reaction Paths in the Hydrogenolysis of Acetic Acid to Ethanol over Pd(111), Re(0001), and PdRe Alloys. *Journal of Catalysis* **209,** 289–305 (2002).

20. Nobbs, J. H. Kubelka—Munk Theory and the Prediction of Reflectance. *Review of Progress in Coloration and Related Topics* **15,** 66–75 (1985).

21. Shannon, S. and Goodwin, J. Characterization of Catalytic Surfaces by Isotopic-Transient Kinetics during Steady-State Reaction. *Chemical Society reviews,* 677–695 (1995).

22. Chia, M., Pagán-Torres, Y. J., Hibbitts, D., Tan, Q., Pham, H. N., Datye, A. K., Neurock, M., Davis, R. J. and Dumesic, J. A. Selective hydrogenolysis of polyols and cyclic ethers over bifunctional surface sites on rhodium-rhenium catalysts. *Journal of the American Chemical Society* **133,** 12675–12689 (2011).

23. Daniel, O. M., Delariva, A., Kunkes, E. L., Datye, A. K., Dumesic, J. a. and Davis, R. J. X-ray Absorption Spectroscopy of Bimetallic Pt-Re Catalysts for Hydrogenolysis of Glycerol to Propanediols. *ChemCatChem* **2,** 1107–1114 (2010).

24. Sheldon, R. A. and van Bekkum, H. *Fine Chemicals through Heterogeneous Catalysis* 415 (Wiley, Weinheim, Germany, 2000).

25. Oldenburg, C. C. and Rase, H. F. Kinetics of aldehyde hydrogenation: Vapor-phase flow system and supported nickel catalyst. *AIChE Journal* **3,** 462–466 (1957).

26. Lugo-José, Y. K., Monnier, J. R. and Williams, C. T. Gas-phase, catalytic hydrodeoxygenation of propanoic acid, over supported group VIII noble metals: Metal and support effects. *Applied Catalysis A: General* **469,** 410–418 (2014).

27. Jones, W. D. Isotope Effects in C-H Bond Activation Reactions by Transition Metals. *Accounts of Chemical Research* **36,** 140–146 (2003).

28. Gnanamani, M. K., Jacobs, G., Keogh, R. a. and Davis, B. H. Deuterium kinetic isotopic study for hydrogenolysis of ethyl butyrate. *Journal of Catalysis* **277,** 27–35 (2011).

29. Falcone, D. D., Hack, J. H., Klyushin, A. Y., Knop-Gericke, A., Schlogl, R. and Davis, R. J. Evidence for the Bifunctional Nature of Pt-Re Catalysts for Selective Glycerol Hydrogenolysis. *ACS Catalysis* **5,** 5679–5695 (2015).

30. Meemken, F., Baiker, A., Dupré, J. and Hungerbühler, K. Asymmetric catalysis on cinchonidine-modified Pt/Al_2O_3: Kinetics and isotope effect in the hydrogenation of trifluoroacetophenone. *ACS Catalysis* **4,** 344–354 (2014).

31. Young, R. P. Infrared spectroscopic studies of adsorption and catalysis. Part 3. Carboxylic acids and their derivatives adsorbed on silica. *Canadian Journal of Chemistry* **47,** 2237–2247 (1969).

32. Zeinalipour-Yazdi, C. D., Willock, D. J., Thomas, L., Wilson, K. and Lee, A. F. CO adsorption over Pd nanoparticles: A general framework for IR simulations on nanoparticles. *Surface Science* **646,** 210–220 (2016).

33. Street, S. C. and Gellman, A. J. FT-IRAS of adsorbed alkoxides: 1-propoxide on Cu(111). *Surface Science* **372,** 223–238 (1997).

34. Nakamoto, K. in *Infrared and Raman Spectra of Inorganic and Coordination Compounds* (John Wiley & Sons, Inc., Hoboken, NJ, USA, 1987).

35. Rachmady, W. and Vannice, M. Acetic Acid Reduction by H_2 on Bimetallic Pt-Fe Catalysts. *Journal of Catalysis* **209,** 87–98 (2002).

36. Tong, S. R., Wu, L. Y., Ge, M. F., Wang, W. G. and Pu, Z. F. Heterogeneous chemistry of monocarboxylic acids on α-Al_2O_3 at different relative humidities. *Atmospheric Chemistry and Physics* **10,** 7561–7574 (2010).

37. Nolin, B. and Norman Jones, R. The infrared absorption spectra of deuterated esters. II. Ethyl acetate. *Can. J. Chem.* **34,** 1392–1404 (1956).

38. Hanspal, S., Young, Z. D., Shou, H. and Davis, R. J. Multiproduct steady-state isotopic transient kinetic analysis of the ethanol coupling reaction over hydroxyapatite and magnesia. *ACS Catalysis* **5,** 1737–1746 (2015).

39. Ballard, C. C., Broge, E. C., Iler, R. K., St. John, D. S. and Mcwhorter, J. R. Esterification of the surface of amorphous silica. *Journal of Physical Chemistry* **65,** 20–25 (1961).

40. Kimura, T., Kuroda, K., Sugahara, Y. and Kuroda, K. Esterification of the Silanol Groups in the Mesoporous Silica Derived from Kanemite. *Journal of Porous Materials* **5,** 127–132 (1998).

41. Brinker, C. Hydrolysis and condensation of silicates: Effects on structure. *Journal of Non-Crystalline Solids* **100,** 31–50 (1988).

42. Der Voort, P. V. and Vansant, E. F. Silylation of the Silica Surface A Review. *Journal of Liquid Chromatography & Related Technologies* **19,** 2723–2752 (1996).

43. Vajo, J., Sun, Y.-K. and Weinberg, W. Acetic acid decomposition on a polycrystalline platinum surface. *Applied Surface Science* **29,** 165–178 (1987).

44. Kim, K. S. and Barteau, M. A. Pathways for carboxylic acid decomposition on TiO_2. *Langmuir* **4,** 945–953 (1988).

45. Bender, B. R., Kubas, G. J., Jones, L. H., Swanson, B. I., Eckert, J., Capps, K. B. and Hoff, C. D. Why does D_2 bind better than H_2? A theoretical and experimental study of the equilibrium isotope effect on H_2 binding in a M(η^2-H_2) complex. Normal coordinate

analysis of $W(CO)_3(PCy_3)_2(\eta^2\text{-}H_2)$. *Journal of the American Chemical Society* **119,** 9179–9190 (1997).

4

Reduction of Carboxylic Acids over Oxide-supported Pd-promoted WO_x and Phosphotungstic Acid Catalysts

Abstract

Silica-, titania-, and zirconia-supported W oxide and phosphotungstic acid (PTA) catalysts were synthesized by wetness impregnation techniques. When promoted with Pd, these catalysts performed the reduction of propionic acid to 1-propanol with a selectivity of up to 92% at 13.5% conversion in atmospheric pressures of H_2. While phosphotungstic acid catalysts had higher reduction rates, they were less selective to oxygenated products. Reaction kinetics measurements indicated a 0.2 order in H_2 pressure and a 0.7 order in propionic acid pressure over Pd-promoted WO_x/TiO_2 and PTA/TiO_2. The apparent activation energy for propionic acid reduction over $PdWO_x/TiO_2$ and $PdPTA/TiO_2$ was 54 and 60 kJ mol^{-1}, respectively. X-Ray diffraction and X-ray absorption spectroscopy revealed an increase in disorder of monoclinic WO_3 and a slight reduction of the W from W(VI) to an average oxidation state of between W(VI) and W(IV) on $PdWO_x/SiO_2$ during H_2 treatment above 473 K. Infrared spectroscopy indicates the catalyst surface is covered mostly by propionate species.

4.1 Introduction

World demand for oil-derived products, especially chemicals, is expected to grow rapidly in the coming years, as emerging economies develop an increased desire for plastics.[1] While many current technologies still use fossil resources to produce chemicals, a significant effort is underway to develop cost-effective ways to convert biomass to commodity chemicals. Biomass has a similar effective hydrogen-to-carbon ratio as many value-added chemicals, and offers the potential to produce these chemicals at a lower carbon cost in efficient processes.[2] A study performed by the Department of Energy in 2004 found that many of the top building block chemicals that could

theoretically be produced from biomass are carboxylic acids.[3] A number of these building blocks continue to show promise as potential platform molecules, including short chain carboxylic acids such as lactic acid, succinic acid, 3-hydroxypropionic acid, and levulinic acid, which can be upgraded through reduction of their carboxylic acid functionality.[4] As a result, selective reduction of carboxylic acids to produce aldehydes and alcohols is of significant importance to the development of cost-effective technologies for biomass valorization.

Copper-based oxide spinels (such as copper chromite) are well-known catalysts for the reduction of esters (and carboxylic acids) to their corresponding alcohols,[5] whereby dissociation of the ester into alkoxy and acyl species followed by hydrogenation of the acyl species determined the rate of alcohol formation in this process over copper chromite and supported copper.[6–8] Other works studied metal oxides such as Re,[9,10] Sn,[11] and Mo[12] promoted by platinum group metals and found they are effective catalysts for the direct catalytic reduction of carboxylic acids. A recent review by Pritchard et al. highlights some of the major recent findings concerning heterogeneous reduction of carboxylic acids.[13] An overarching theme in many of these studies is that the combination of a reducible metal and an oxophilic metal results in an active material when the two metals are placed in close proximity to one another on the catalyst support. By doing so, the active site on the metal oxide species gains access to dissociatively adsorbed H, which results in the reduction of the carboxylic to an aldehyde intermediate that is subsequently hydrogenated to form the corresponding alcohol. However, the ability of supported, Pd-promoted tungsten oxides to catalyze selective reduction of carboxylic acids to alcohols has not been very thoroughly assessed.

Tungsten oxide has a variety of uses as a heterogeneous catalyst, and it is well-known

to produce Brønsted acid sites of varying acid strength and site density, depending on the support upon which it is dispersed. Yamaguchi et al. found that WO_x supported on TiO_2, Al_2O_3, and ZrO_2 resulted in the formation of higher densities of acidic sites compared to unsupported WO_x or WO_x supported on SiO_2 and MgO.[14] The resulting acidic sites were catalytically active for 1-butene disproportionation at 373 K. Hino and Arata found that controlled synthesis could produce WO_x/ZrO_2 with superacid properties capable of performing butane isomerization at temperatures as low as 303 K.[15] There is good agreement in the literature that the rate of catalytic isomerization reactions per tungsten atom over WO_x/ZrO_2 is maximized at loadings slightly above the theoretical monolayer coverage of WO_x on the ZrO_2.[16–18] Similar trends in reactivity can be found on supports other than zirconia, and apparently dispersion of the WO_x phase still appears to play a critical role.[19] One explanation for this trend in activity is the formation of reducible polytungstate clusters at "intermediate" WO_x surface loading that could stabilize Brønsted acidic protons.[20] Lower loadings of WO_x resulted in irreducible monotungstate species that were less active for the isomerization reactions, while higher loadings resulted in the formation of inactive WO_3 crystallites. The addition of platinum allowed the slight reduction of WO_x polytungstate clusters to occur at mild temperatures (350 K), and resulted in turnover frequencies on the order of 10^2 s^{-1} for *n*-heptane isomerization at 473 K.[21] However, acid site densities measured by *ex situ* and *in situ* titration with pyridine, ammonia, or sterically hindered pyridine found conflicting trends in Brønsted acid density with relation to activity.[17,18,22] Some studies reported a maximum in Brønsted acidity per W atom at intermediate loadings, while others have found that Brønsted acidity per W atom, as well as Lewis acidity per W atom, decreases continuously with increasing W loading. On the other hand, Zr-stabilized, distorted WO_3 crystallites have

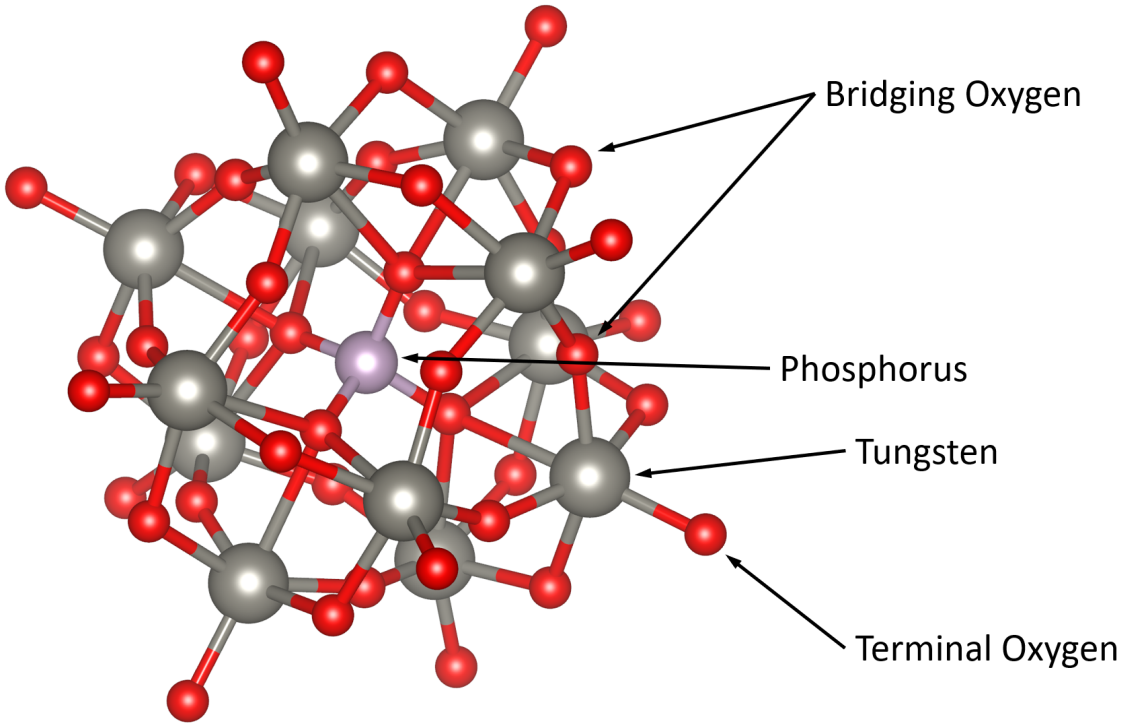

Figure 4.1: The Keggin structure of phosphotungstic acid, consisting of 12 octahedral tungsten (VI) oxide species surrounding a tetrahedrally coordinated phosphorus atom. The central oxygens connect the central phosphorus atom to the surrounding tungsten octahedra, while bridging oxygens are capable of stabilizing Brønsted-acidic protons.[24]

also been suggested to play a key role in catalysis, for example, in the acid-catalyzed dehydration of methanol to dimethyl ether.[23] Evidently, the catalytic activity of supported WO_x catalysts is not completely understood.

Heteropolyanions derived from tungsten such as phosphotungstic acid ($H_3PW_{12}O_{40}$) also have many uses as heterogeneous acid catalysts.[25] Phosphotungstic acid (PTA) consists of a tetrahedrally coordinated phosphorus atom surrounded by 12 tungsten (VI) oxide octahedra, forming a well-defined Keggin unit (Figure 4.1). The resulting compound can stabilize up to three Brønsted acidic protons, which can be used to catalyze alkylation, condensation, and dehydration reactions, among many other acid-catalyzed reactions. More information about the properties and uses of tungsten heteropolyanions can be found in reviews by Kozhevnikov[25] and Misono.[26]

Recent studies have also investigated PTA as a catalyst for conversions of biomass. Examples include the hydrolysis-hydrogenation of cellulose in the presence of Ru/C,[27] and the esterification of triethylene glycol and methacrylic acid.[28]

Few studies have explored tungstates as catalysts for carboxylic acid reduction. In 1989, tungstate species were identified as a key component of the enzymatic reduction of carboxylic acids to aldehydes in *Clostridium thermoaceticum*.[29] Several years later, a patent by Kitson and Williams claimed a mixture of platinum group metals and rhenium, molybdenum, and tungsten for the conversion of carboxylic acids to alcohols and esters, but only gave details of the synthesis of several Pd-alloy-promoted Re catalysts.[30] In 1997, Pestman et al. screened a number of metal oxide catalysts for the reduction of acetic acid and reported that WO_3 produced a small amount (17% selectivity) of acetaldehyde in H_2 at 723 K, while the majority product was acetone.[31] In 2013, a catalyst comprised of tungsten trioxide WO_3, an alkaline earth metal promoter, and a Sn-promoted transition metal component was claimed by Kong et al. for the reduction of carboxylic acids to alcohols.[32] Recent studies by Gosselink and Hollak found that WO_3 and W_2C performed selective hydrodeoxygenation of stearic acid, tristearin, and methyl stearate to C_{17} and C_{18} hydrocarbon products at 523 K.[33,34] Palladium-promoted WO_x/Al_2O_3 also demonstrated activity for the hydrodeoxygenation of guaiacol,[35] and Pt-promoted WO_x/Al_2O_3 and WO_x/ZrO_2 were active in the hydrogenolysis of glycerol to 1,3-propanediol and could be promoted with SiO_2 addition.[36,37] These previous findings suggest that Pd- and Pt-promoted WO_x materials have the potential to catalyze the selective reduction of carboxylic acids.

In this work, we investigated the catalytic activity of SiO_2-, TiO_2-, and ZrO_2-supported Pd-promoted WO_x and phosphotungstic acid (PTA) in the gas-phase reduction of propionic

acid. The adsorption of H_2 and CO was performed to estimate the dispersion of Pd and explore the effect of spillover on H_2 uptake by WO_x. Temperature-programmed reduction, *ex situ* X-ray diffraction, and *in situ* X-ray absorption spectroscopy were used to follow changes in structure of the WO_x before and after treatment of the catalysts in flowing H_2, which were correlated to catalyst activity. *In situ* diffuse reflectance infrared Fourier transform spectroscopy provided insights on the species present on the tungsten oxide and support surfaces.

4.2 Experimental Methods

4.2.1 Catalyst Synthesis

Silica-supported (Fuji Silysia Chemical Ltd, 511 $m^2\ g^{-1}$ 75-150 μm particle size) 8 wt % W (W/SiO_2) and 1 wt % Pd, 8 wt % W (PdW/SiO_2) catalysts were synthesized by the incipient wetness impregnation method. The desired loading of tungsten was added as ammonium metatungstate hydrate (Aldrich, 99.99%) to an aqueous solution equal to the pore volume of the SiO_2. The solution was added to the support until the point of incipient wetness. The mixture was dried at 383 K in ambient air, then heated in flowing air to 773 K over 3 h and held at 773 K for 3 h in flowing air. This process was repeated for the desired loading of Pd (using aqueous tetraaminepalladium(II) nitrate, 10 wt%, Aldrich). Titania- and zirconia- supported 8 wt % W (W/TiO_2, W/ZrO_2) and 1 wt % Pd, 8 wt % W (PdW/TiO_2, PdW/ZrO_2) catalysts were synthesized by first adding 5 g of either TiO_2 (Degussa P25, 47 $m^2\ g^{-1}$) or $ZrO(OH)_2$ (MEL Chemicals, 420 $m^2\ g^{-1}$) to 80 cm^3 of distilled, deionized water (16.8 MΩ), and then dissolving the desired loading of tungsten as ammonium metatungstate hydrate into this suspension. The suspension was dehydrated in a rotary evaporator at 353 K, and then dried at 383 K overnight in ambient air.

The dried material was then heated in flowing air to 773 K over 3 hours, held in flowing air at 773 K for 3 h, cooled, and sized to obtain a particle size of between 55 and 180 μm in diameter. The desired loading of Pd was then added as an aqueous solution of tetraaminepalladium(II) nitrate by the incipient wetness procedure outlined above, subjected to the same 773 K treatment in air, and then re-sized to obtain particles between 55 and 180 μm in diameter. Phosphotungstic acid hydrate (Sigma Aldrich, reagent grade) and Pd-promoted phosphotungstic acid (1 wt % Pd, 8 wt % W) catalysts supported on SiO_2 (PTA/SiO_2 and PdPTA/SiO_2) and TiO_2 (PTA/TiO_2 and PdPTA/TiO_2) were also synthesized using the incipient wetness impregnation method. To avoid decomposition of the phosphotungstic acid (PTA) supported on SiO_2 and TiO_2, Pd was added first by the incipient wetness impregnation procedure for Pd addition described earlier, and then an aqueous solution of PTA was added until the point of incipient wetness to the support. The supported PTA was dried at 383 K in ambient air overnight prior to use.

4.2.2 Catalytic Reactions

The effects of catalyst pretreatment and reaction conditions on the reduction of propionic acid (Sigma Aldrich, 99.5%) in H_2 (Praxair, 5.0) and D_2 (Praxair, 2.7) were studied in the gas phase using a packed-bed downward flow reactor. Propionic acid was supplied from a stainless steel vapor saturator equipped with thermocouple to measure the saturator temperature. The reactor consisted of a stainless-steel tube with inner diameter of 0.46 cm, enclosed in a cylindrical aluminum jacket 3.8 cm in diameter, which was heated externally. The reaction temperature was measured by a thermocouple inserted from the top of the reactor tube into the middle of the catalyst bed, which was supported in the center of the reactor tube on a plug of glass wool. Prior

to catalytic testing, all lines and saturators leading to the reactor were purged with N_2 for at least 10 min. The reduction of 0-0.5 kPa propionic acid was studied between 403 and 433 K, at a total pressure of 0.1 MPa composed of 0-0.1 MPa H_2 in a balance of N_2. The components in the product stream were separated using an on-line SRI 8610C gas chromatograph (GC) equipped with an MXT-WAX (0.53 mm i.d., 1 μm film thickness, 30 m) column and quantified using a flame-ionization detector (FID).

The fractional conversion (f_i) and product selectivity of propionic acid (i) to products (j) were obtained using equations (4.1) and (4.2):

$$f_i = \frac{\sum M_j}{M_i + \sum M_j} \tag{4.1}$$

$$S_j = \frac{M_j}{\sum M_j} \tag{4.2}$$

where M_j is defined as the moles of carbon product j. Hydrocarbon products having carbon numbers below C_6 could not be separated using the MXT-WAX column, and therefore were grouped together as light hydrocarbons, or LHC, for analysis.

4.2.3 Catalyst Characterization

The chemisorption of H_2 (Praxair, 5.0) and CO (Praxair, 3.0) was performed using a Micromeritics ASAP 2020 instrument. Prior to analysis, each sample was heated to 473 K in flowing H_2 at 10 K min^{-1}, then held at 473 K for 1 h under flowing H_2. The samples were sub-

sequently evacuated at 473 K for 3 h, before cooling to 373 K or 308 K to perform the H_2 or CO chemisorption, respectively. Dihydrogen or CO was dosed over the range of 0.13 to 67 kPa. The reported chemisorption values were obtained by extrapolating the probe molecule uptake in the high pressure linear region of the isotherm to zero pressure, which was considered the saturated monolayer coverage.

Powder X-ray diffraction (XRD) patterns for each sample were obtained under ambient conditions using a Malvern Panalytical Empyrean X-ray Diffractometer. The instrument utilized a Cu Kα X-ray radiation source with a wavelength of 1.541 Å. A step size of 0.014° (2θ) at 88 s per step was used to collect each sample. Samples that received pretreatment were loaded into a quartz tube, ramped to the desired temperature in H_2 at a rate of 5 K min^{-1}, then cooled in He (Praxair, 5.0) to room temperature. Samples were then exposed to ambient air during transfer to the diffractometer for analysis.

In situ X-ray absorption spectroscopy (XAS) at the tungsten L_I and L_{III} edges was carried out on beamline 8-ID of the National Synchrotron Light Source II (NSLS-II) at Brookhaven National Laboratory in Brookhaven, New York, operated at 3.0 GeV and with a typical current of *ca.* 325 mA. Further details about the beamline setup have been summarized previously.[38] All experiments were performed using the Si(111) double crystal monochromator with uncoated Si higher harmonic rejection mirrors and a spot size of 0.25 mm. Samples were prepared for analysis by packing the desired loading of catalyst to give an edge jump ($\Delta\mu x$) of around 1 into each stainless-steel tube of the high-throughput *in situ* reactor cell described in Appendix D. Samples were held in place in the stainless-steel tubes by supporting the catalyst bed on either side with a plug of shredded graphite felt (AvCarb Felt G200). Prior to treatment, each of the

individually fed reactor tubes were flushed with He at 20 cm^3 min^{-1} for 10 min to remove any residual O_2 in the tubes. Temperature-programmed reduction was then carried out *in situ* by beginning the flow of H_2 at 20 cm^3 min^{-1}, waiting for 5 min to allow replacement of the He atmosphere with H_2, and then ramping the temperature at 3 K min^{-1} from ambient temperature to 673 K. Samples were then cooled in He to room temperature.

Spectra obtained from X-ray absorption spectroscopy were processed and analyzed using the Demeter software package, written by Bruce Ravel.[39] Prior to analysis, X-ray absorption near-edge structure (XANES) and X-ray absorption fine structure (EXAFS) were background-corrected and normalized uniformly at each edge using Athena, an XAS analysis program that is part of the Demeter software package. The oxidation state of each sample was estimated using the measured position of the L_I and L_{III} edges. The edge position at the tungsten L_I edge was arbitrarily determined at 0.75 times the normalized absorbance height to minimize interference with the presence of the observed pre-edge feature of the W(VI) oxide, while the L_{III}-edge position was arbitrarily determined at a step height of unity in the normalized absorbance spectrum to account for the position of the white line. The local coordination structure and EXAFS were analyzed at the tungsten L_{III} edge. Powders of WO_2 (Alfa Aesar, 99.9%), WO_3 (Aldrich, 99.995%), and ammonium metatungstate hydrate were used as standards at the L_I and L_{III} edges. The WO_3 standard was used as an energy reference. Standards were prepared by grinding each powder thoroughly, mixing with boron nitride (Aldrich, 98%), and then compressing the mixture into a self-supporting wafer using a hydraulic press. The wafers were then affixed to Kapton tape and placed in the beam path for measurement.

In situ infrared spectra of propionic acid adsorbed on PdW/TiO_2 and W/TiO_2 were ob-

tained using diffuse reflectance infrared Fourier transform spectroscopy (DRIFTS). Spectra were recorded using a Bruker Vertex 70 FTIR spectrometer equipped with a liquid-nitrogen-cooled MCT detector and a Harrick Praying Mantis *in situ* reactor cell with 5 mm ZnSe windows. Spectra were collected every 20 min, by averaging 800 scans at a resolution of 2 cm^{-1}. The inlet gases were purified using an OMI purifier (Supelco) upstream of a stainless-steel propionic acid vapor saturator with a bypass line leading to the *in situ* cell. Prior to data collection, samples were ramped to 473 K in flowing H_2, and then cooled to 413 K in H_2 for analysis. Each sample was exposed to 0.3 kPa of propionic acid in 0.1 MPa H_2 flowed at 15 cm^3 min^{-1} until the sample reached a steady state (approximately 120 min). The flow was then switched through the bypass line upstream of the *in situ* cell, so that the cell was purged with pure H_2. Again, spectra were recorded until the sample reached the new steady state under purging conditions. All resulting spectra were normalized to a reference spectrum taken prior to exposure of the sample to propionic acid at 413 K in H_2, and converted to Kubelka-Munk units using the Kubelka-Munk equation.[40]

4.3 Results

4.3.1 Influence of Catalyst Composition and Pretreatment on Propionic Acid Reduction

The catalytic reduction of 0.5 kPa propionic acid in 0.1 MPa H_2 at 433 K was studied over Pd-promoted tungsten oxide and phosphotungstic acid supported on SiO_2, TiO_2, and ZrO_2. The steady state rate and product distribution of propionic acid reduction are shown for each catalyst studied (fresh and after pretreatment in H_2 at 673 K) in Figure 4.2. Tungsten oxides and phosphotungstic acid without a Pd promoter were completely inactive for the conversion of

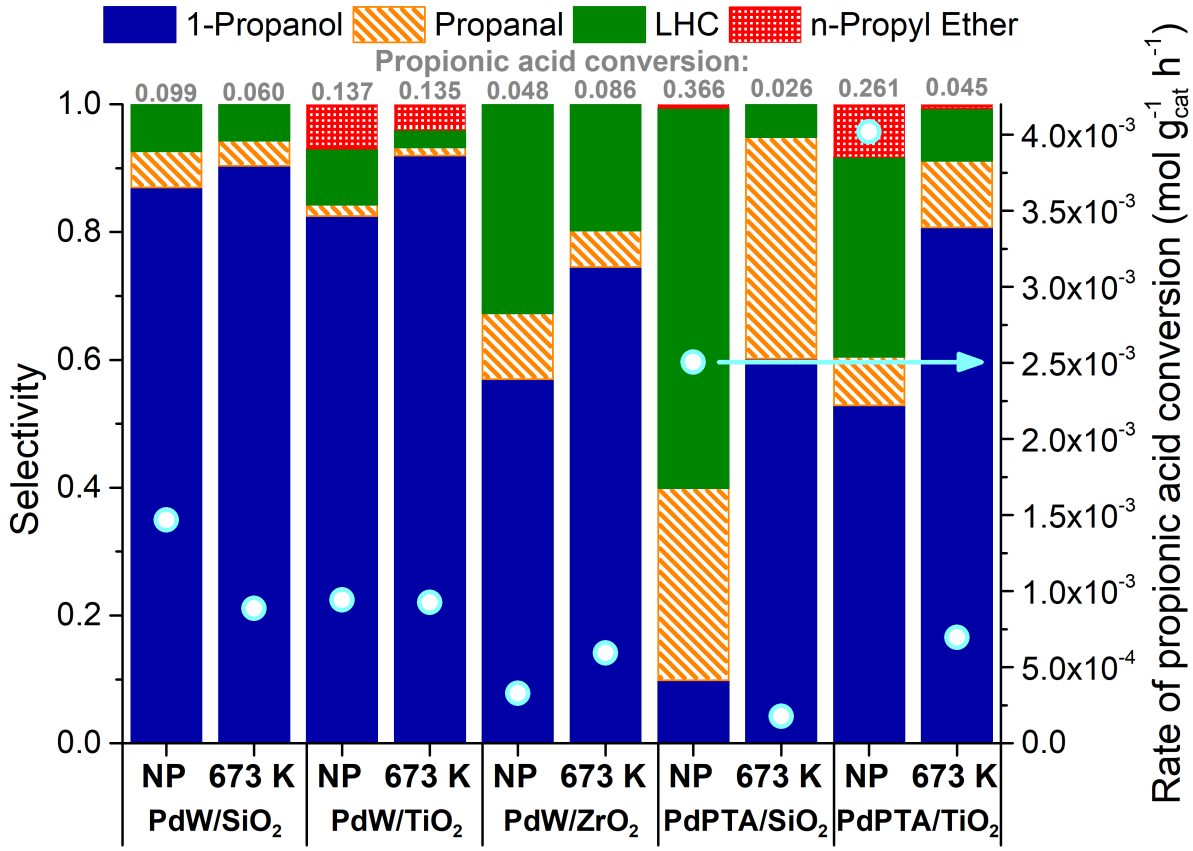

Figure 4.2: Steady-state rate and product distribution of propionic acid (0.5 kPa) reduction over SiO_2-, ZrO_2-, and TiO_2-supported Pd-promoted W-based catalysts in 0.1 MPa H_2 at 433 K. Bars correspond to product selectivity on the left axis, while light blue circles correspond to the rate of propionic acid conversion on the right axis. Values above the bars indicate conversion of acid. NP indicates no *in situ* H_2 pretreatment, while 673 K indicates a 1 h pretreatment *in situ* in flowing H_2 at 673 K prior to reaction.

propionic acid under the conditions studied. Whereas fresh PdW supported on ZrO_2 was active for propionic acid conversion, pretreatment of the catalyst for 1 h in H_2 at 673 K doubled the observed the rate of propionic acid conversion and increased the selectivity towards oxygenated products (propanal and 1-propanol). Fresh PdW/TiO_2 was more active than PdW/ZrO_2, and more selective to oxygenated products, although a small amount of *n*-propyl ether was also formed as a product. Pretreatment of the PdW/TiO_2 in H_2 at 673 K did not have any significant effect on the rate of propionic acid conversion, but selectivity to light hydrocarbons was reduced by the treatment, leading to a 1-propanol selectivity of 92% at 13.5% conversion of the acid. Fresh SiO_2-supported PdW demonstrated the highest rate of propionic acid reduction of the supported WO_x catalysts under the conditions studied, and was 87% selective to 1-propanol at 9.9% acid conversion. Pretreatment of the PdW/SiO_2 catalyst in H_2 at 673 K resulted in a loss of nearly half of the activity of the fresh catalyst.

Although fresh catalysts prepared with phosphotungstic acid were the most active for propionic acid conversion, they were significantly less selective to 1-propanol (at conversions of 26 to 36%), favoring light hydrocarbon products. At the conversion levels reported in Figure 4.2, PdPTA/TiO_2 had 5 times higher selectivity to alcohols than the PdPTA/SiO_2, while retaining the improved activity of the PTA. On TiO_2-supported catalysts, the formation of *n*-propyl ether was also observed. Formation of ethers has been previously observed using TiO_2-supported tungsten oxide and phosphotungstic acid catalysts.[41,42] As treatment at 673 K is known to decompose PTA,[43] the loss of activity in the PTA catalysts after 673 K treatment in flowing H_2 is not surprising.

4.3.2 Influence of Reaction Conditions

The rate of reduction of carboxylic acids over fresh PdW/TiO_2 and $PdPTA/TiO_2$ slowly decreased over time, with $PdPTA/TiO_2$ deactivating faster than PdW/TiO_2. The PdW/TiO_2 lost 18% of its activity over 15.75 h time on stream, while the $PdPTA/TiO_2$ lost 40% of its activity over 21.5 h on stream.

The rate of propionic acid reduction versus inverse flowrate is plotted in Figure 4.3(a). Differential conversion was not achieved until conversion was below 5% over $PdPTA/TiO_2$, and 3% over PdW/TiO_2. The selectivity of propionic acid conversion towards 1-propanol decreased in favor of propanal as conversion was lowered. This influence of conversion on selectivity is plotted in Figure C.1 and is consistent with a two-step alcohol formation reaction proceeding through an aldehyde intermediate, which has been reported previously.[44] Under differential conditions, the influence of temperature on the rate of reaction was measured and is summarized in Figure 4.3(b). The apparent activation energy for propionic acid conversion was 60 kJ mol^{-1} over $PdPTA/TiO_2$ and 54 kJ mol^{-1} over PdW/TiO_2. The orders of reaction with respect to H_2 pressure and propionic acid pressure were 0.2 and 0.7, respectively, as determined from the results reported in Figures 4.3(c) and (d). The influence of H_2 pressure on product selectivity is shown in Figure C.2. While changing the H_2 pressure did not have a strong effect on the rate of propionic acid reduction, lowering the H_2 pressure first leads to an increase in 1-propanol selectivity, followed by decreasing selectivity as the H_2 pressure is lowered further. While the rate of reaction did not appear to depend strongly on H_2 pressure, the rate of propionic acid conversion became immeasurably small when H_2 was completely removed from the reactant stream. An inverse kinetic isotope effect of 0.91 was also observed when the H_2 in the reactant stream was replaced by D_2

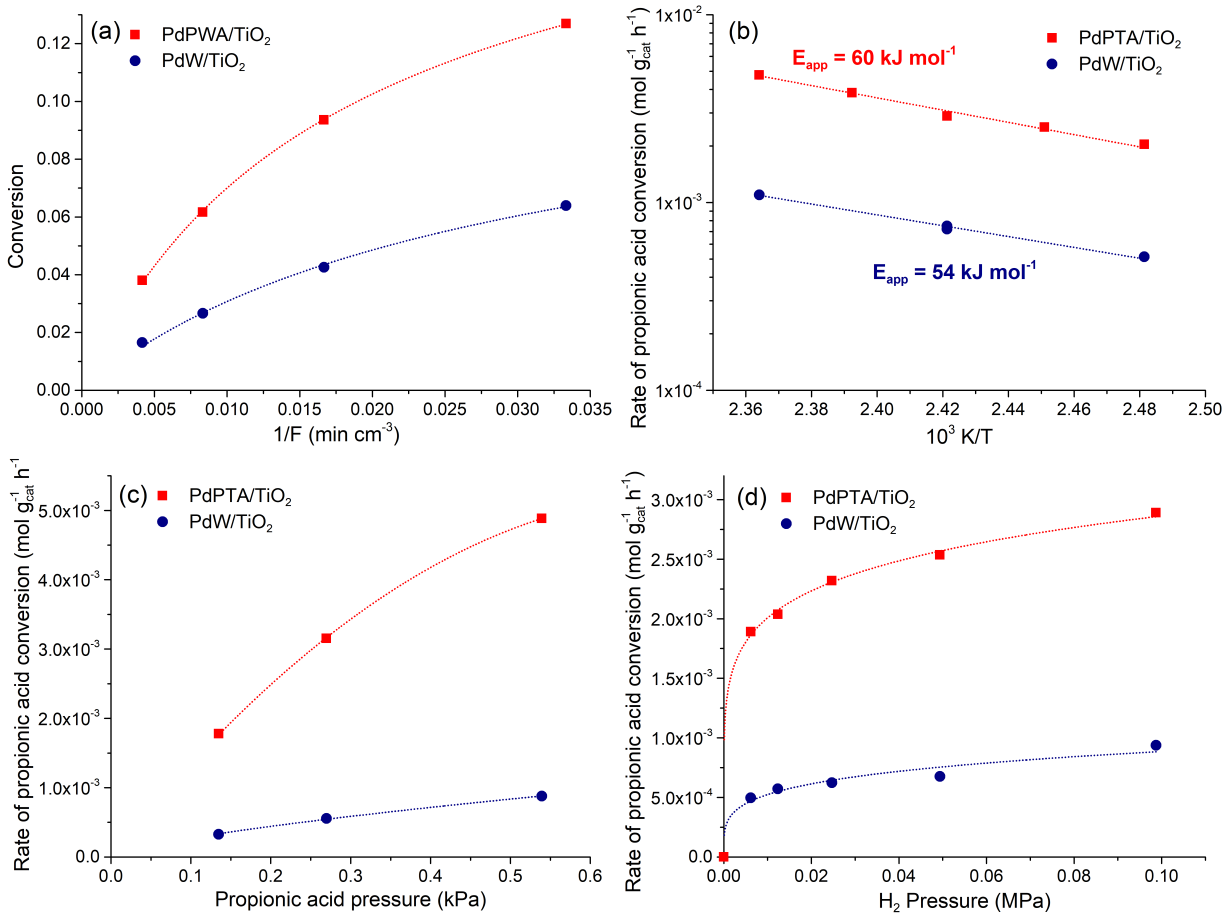

Figure 4.3: Comparison of (a) inverse flowrate versus propionic acid conversion, (b) inverse temperature versus rate of propionic acid conversion, (c) propionic acid pressure versus rate of conversion, and (d) H_2 pressure versus rate of propionic acid conversion between fresh PdW/TiO_2 and $PdPTA/TiO_2$. All reactions were carried out at 413 K in 0.5 kPa propionic acid and 0.1 MPa H_2 unless otherwise specified. Dotted lines have been inserted to highlight observed trends.

(Table C.1) during the reduction of propionic acid by PdW/TiO_2.

4.3.3 Adsorption of H_2 and CO

The adsorption of H_2 and CO on Pd-promoted WO_x and PTA revealed differences in H_2 uptake by the TiO_2 and SiO_2 supported catalysts (Table 4.1). The calculated Pd dispersions of PdW/TiO_2 and $PdPTA/TiO_2$, assuming a ratio of 1.0 H/Pd for TiO_2 supported Pd, were 62% and 58%, respectively. Assuming a ratio of 0.53 CO/Pd,[45] the calculated Pd dispersions of PdW/TiO_2 and $PdPTA/TiO_2$ were 69% and 71%, respectively. In contrast, the calculated Pd dispersions of PdW/SiO_2 and $PdPTA/SiO_2$, assuming a ratio of 1.0 H/Pd for SiO_2 supported Pd, were 36% and 32%, respectively. Assuming a ratio of 0.75 CO/Pd,[46] the calculated Pd dispersions of PdW/SiO_2 and $PdPTA/SiO_2$ were 25% and 40%, respectively. Uptake of CO on TiO_2-supported Pd is expected to be lower than on SiO_2-supported Pd as a result of the strong metal-support interaction. Apparently, the H_2 uptake per Pd on the TiO_2-supported catalysts was approximately twice that of the Pd supported on SiO_2-supported catalysts. Adsorption of H_2 on reducible TiO_2 may be responsible for some increase in the uptake of H_2. However, CO uptake was also higher on the TiO_2 supported catalysts. Interestingly, the uptake of H_2 on the

Table 4.1: Total chemisorption uptake of H_2 and CO on Pd-promoted WO_x catalysts.

	Chemisorption (μmol g_{cat}^{-1})			
Sample	H_2 (373 K)	CO (308 K)	H/Pd[a] (373 K)	CO/Pd[a] (308 K)
PdW/TiO_2	33	39	0.62	0.37
$PdPTA/TiO_2$	31	40	0.58	0.38
PdW/SiO_2	19	20	0.36	0.19
$PdPTA/SiO_2$	17	32	0.32	0.30

(a) Calculated using nominal weight loading of 1 wt % Pd

PdW/SiO_2 was higher than the uptake of CO, which was not observed for any of the other catalysts studied.

4.3.4 X-Ray Diffraction

The W and PdW catalysts supported on SiO_2 and TiO_2 were investigated *ex situ* using XRD to determine whether deactivation of the catalyst was caused by a structural change in the active material. Diffraction patterns of W and PdW supported on SiO_2 and TiO_2 obtained before and after treatment in H_2 at 473 K and 673 K are shown in Figure 4.4. On the TiO_2, the broad feature from 22.5° to 25° is assigned to the convoluted 002, 020, and 200 reflections of monoclinic WO_3, while the feature centered around 34° is assigned to the convoluted 022, $\bar{2}02$, and 202 reflections of monoclinic WO_3 and the PdO 101 reflection.[47] Higher-angle reflections near 50° and 55° observed on SiO_2 are also assigned to WO_3, and a convolution of WO_3 and PdO reflections, respectively.[48,49] The WO_3 features did not change significantly after treating the PdW/TiO_2 in H_2 at 473 K. In contrast, the diffraction peaks from monoclinic WO_3 on the SiO_2-supported PdW became less intense after pretreatment, with higher angle peaks near 50° and 55° becoming indistinguishable from the background, as shown in the inset of Figure 4.4(b). Evidently, treatment of PdW/SiO_2 in H_2 above 473 K resulted in the loss of the monoclinic WO_3 phase. This might be expected as a result of the phase transition from monoclinic to orthorhombic tungsten trioxide that takes place at 600 K, or reduction of the WO_x which will be discussed in the next section.[50] In all cases, treatment in H_2 resulted in reduction of the PdO phase to a metallic Pd phase of a high enough dispersion that the metallic peak could hardly be distinguished from the background. Diffraction patterns obtained of PTA-containing materials without pretreatment

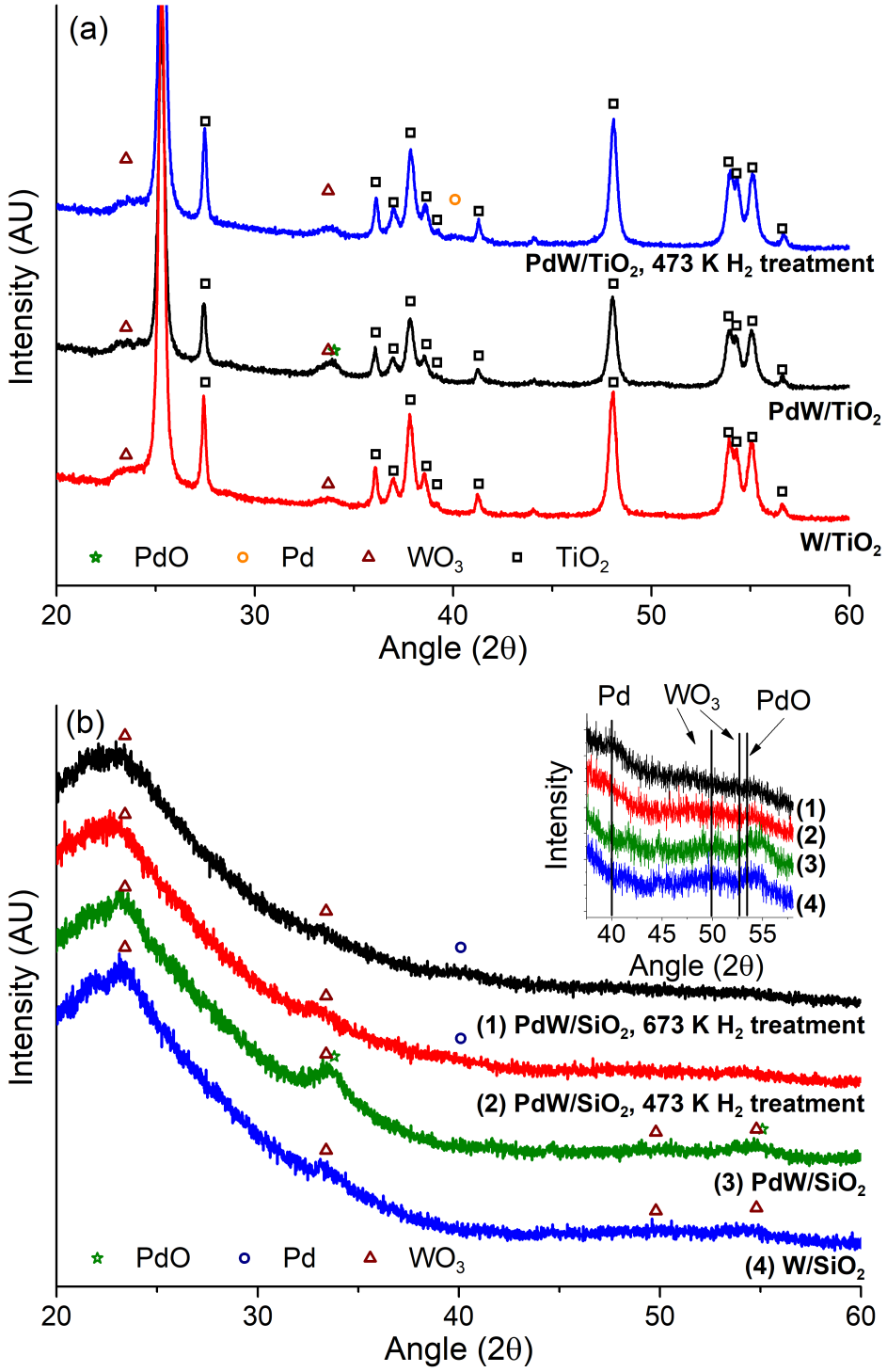

Figure 4.4: X-Ray diffraction patterns obtained from W and PdW supported on (a) TiO_2 before and after treatment in flowing H_2 at 473 K, and (b) SiO_2 before or after treatment at 473 K or 673 K in flowing H_2. Smoothed diffraction patterns from the inset can be found in Figure C.3.

and after pretreatment at 473 K in H_2 did not contain any diffraction peaks associated with the W-containing material.

4.3.5 X-Ray Absorption Spectroscopy

The XANES of PdW/SiO_2 and W/SiO_2 was investigated at the tungsten L_I and L_{III} edges during *in situ* H_2 temperature programmed reduction (TPR) to determine the role of pretreatment on the electronic structure and coordination environment of the W. As reported earlier, the treatment of PdW/SiO_2 at 673 K in H_2 results in a loss of nearly half of its catalytic activity (Figure 3.1). The tungsten L_I-edge energy of the PdW/SiO_2 and W/SiO_2 samples, measured at a step height of 0.75 in the normalized spectrum, was followed as the samples were heated in flowing H_2 up to 673 K (Figure C.4(a)). On exposure of the samples to H_2, the L_I-edge energy of the PdW/SiO_2 and W/SiO_2 energy remained fairly constant until 570 K. Above 570 K, the PdW/SiO_2 and W/SiO_2 L_I-edge energies started to decrease, and continued to steadily decrease until the end of the experiment. As shown in Figure 4.5, the L_I-edge energy of PdW/SiO_2 and W/SiO_2 both decreased by 1.2 eV over the course of the H_2-TPR. The pre-edge features of both catalysts also shifted to slightly lower energy and increased in intensity during the H_2 treatment, which is consistent with an increased distortion of the octahedral W center in WO_x.[51]

The tungsten L_{III}-edge XANES were also investigated during H_2-TPR, and selected spectra of PdW/SiO_2 are shown in Figure 4.6. During the H_2-TPR, the whiteline feature was initially asymmetrical, indicative of a distorted octahedral structure typical of clusters of W(VI), including ammonium metatungstate and bulk WO_3 (standards shown in appendix Figure C.5(a)). However, upon heating to 440 K, the width of the white line decreased, indicating a decrease in the

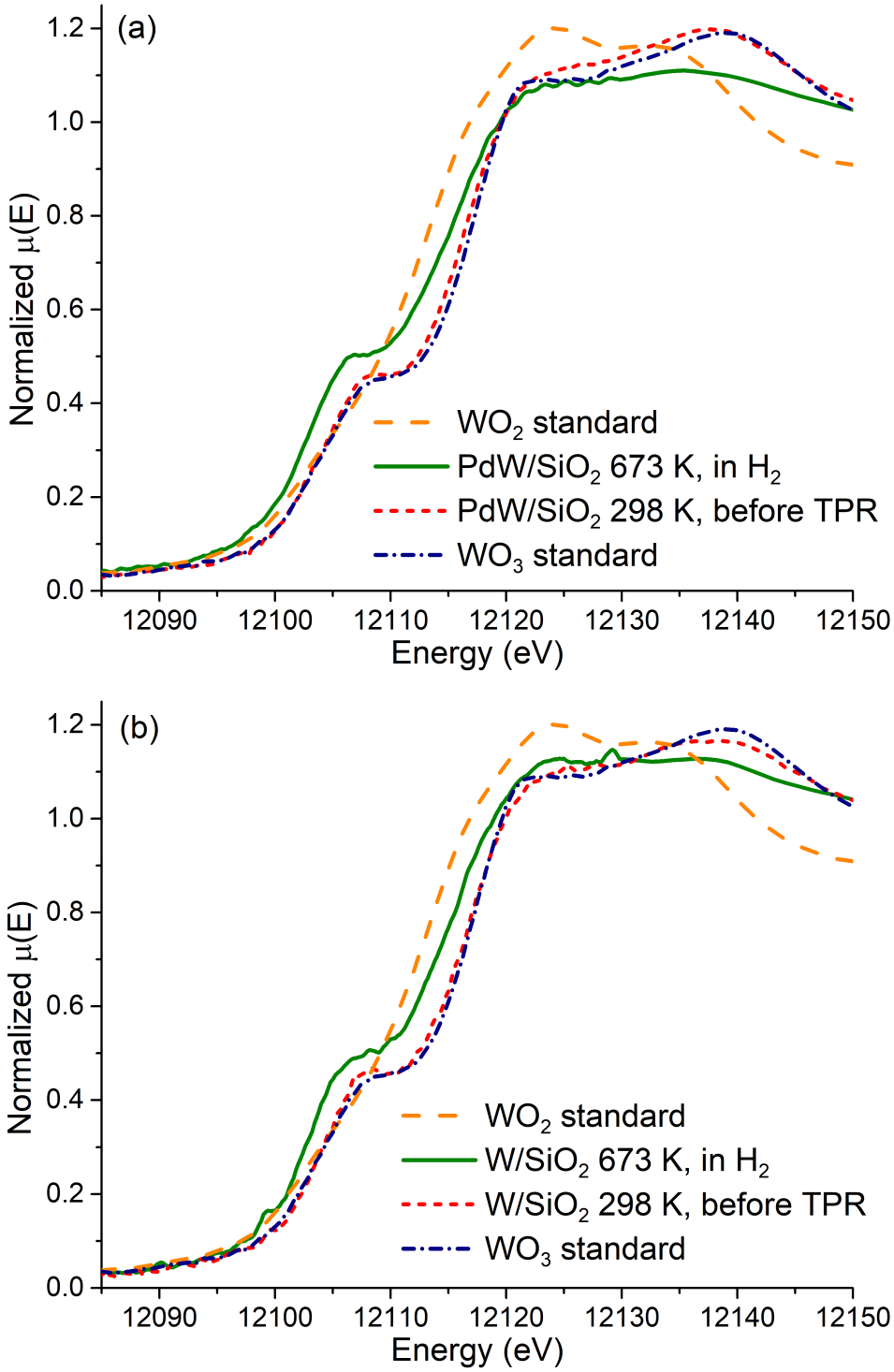

Figure 4.5: (a) The tungsten L_I-edge XANES of PdW/SiO_2 before pretreatment (short dash) and at 673 K in 0.1 MPa flowing H_2 (solid) compared to the WO_2 (long dash) and WO_3 (dash-dot) standard spectra. (b) The tungsten L_I-edge XANES of W/SiO_2 before pretreatment (short dash) and at 673 K in 0.1 MPa flowing H_2 (solid) compared to the WO_2 (long dash) and WO_3 (dash-dot) standard spectra.

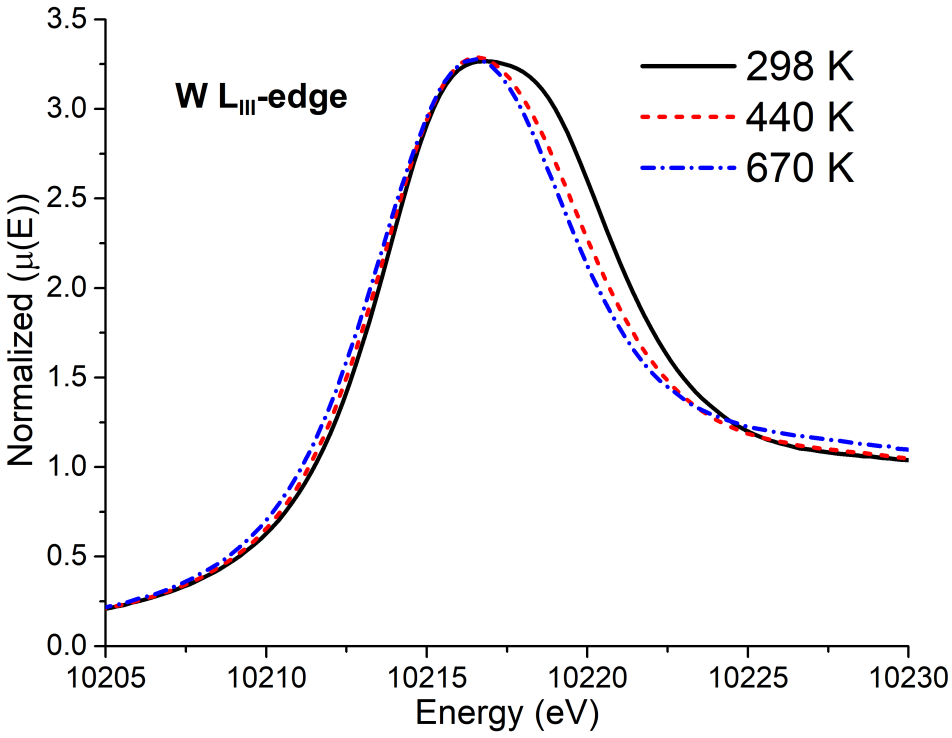

Figure 4.6: The tungsten L_{III}-edge XANES spectra obtained during *in situ* H_2-TPR of PdW/SiO_2 in 6% H_2/He at 298 K, 440 K, and 670 K.

splitting of the W 5-d orbitals.[51] This behavior has been observed previously in W(VI) oxides and heteropolyacids, and is attributed to an increase of the distortion of the octahedral coordination geometry of O surrounding W.[51–53] When the temperature was increased from 440 K to 670 K, the L_{III}-edge position decreased in energy, suggesting that W(VI) was reduced to an average oxidation state between W(IV) and W(VI). Prior to the H_2-TPR, the edge positions of W/SiO_2 and PdW/SiO_2 were both 10205.8 eV. After the TPR, the edge positions shifted to 10205.2 eV (W/SiO_2) and 10204.9 eV (PdW/SiO_2). The edge positions of the WO_3 and WO_2 standards were 10205.7 and 10204.7 eV, respectively, indicating that WO_x in both catalysts had been reduced to an average oxidation state between W(VI) and W(IV). Evidently, the Pd-promoted W/SiO_2 was reduced to a lower average oxidation state than the unpromoted W/SiO_2 after the TPR. This reduction behavior is illustrated in appendix Figure C.5(b), and supports the results

obtained at the tungsten L_I edge. Analysis of the L_{III}-edge EXAFS (k-space oscillations and Fourier-transform magnitudes plotted in appendix Figure C.6) from 298 K to 440 K does not indicate any significant change in the coordination number of the first shell W-O scattering path or the W-O scattering path length (Table C.2, representative fitting shown in Figure C.7). This result indicates minimal reduction of the W (which remained in an oxidation state near W(VI)) in the PdW/SiO_2 under the conditions studied.

4.3.6 Diffuse Reflectance Infrared Fourier Transform Spectroscopy

Diffuse reflectance infrared Fourier transform spectroscopy (DRIFTS) was used to probe the surface species present under reaction conditions on the PdW/TiO_2 and W/TiO_2. When propionic acid in H_2 was introduced to PdW/TiO_2 and W/TiO_2, similar DRIFTS spectra were obtained, which are plotted in Figure 4.7. In the C-H stretching region, three weak peaks were visible at 2985, 2949, and 2892 cm^{-1}. These features are redshifted from the three main visible C-H stretching modes of vapor phase propionic acid at 2993, 2954, and 2900 cm^{-1}, indicating chemisorption of the propionic acid on the PdW/TiO_2 surface. A very weak feature in the PdW/TiO_2 spectrum in the presence of propionic acid was observed at 1965 cm^{-1}, suggesting a small amount of strongly bound CO was present. In the carbonyl stretching region, vibrational modes at 1791, 1772, and 1730 cm^{-1} are consistent with the vapor phase acid monomer and acid dimer vibrations. Strong bands at 1661 and 1663 cm^{-1} cm were observed on PdW/TiO_2 and W/TiO_2 respectively, which were not observed during the adsorption of propionic acid on TiO_2 or Pd/TiO_2. This mode was assigned to an asymmetrical O–C=O vibration characteristic of the binding of propionic acid to the tungsten component of the catalyst. The broad band at

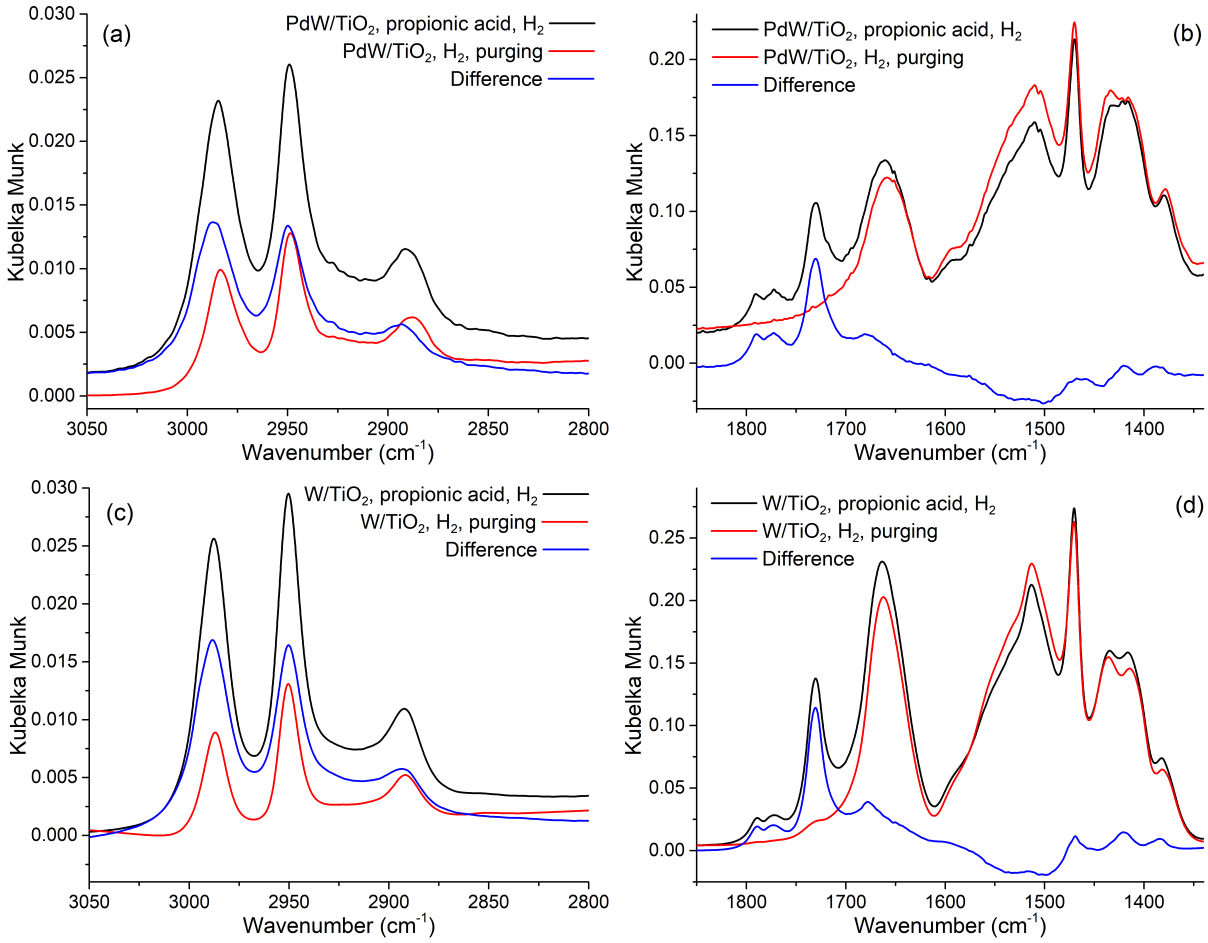

Figure 4.7: Infrared spectra recorded at a sample temperature of 413 K showing PdW/TiO_2 and W/TiO_2 in the (a, c, respectively) C-H stretching region and (b, d, respectively) carbonyl and backbone deformation region during treatment in 0.3 kPa propionic acid in 0.1 MPa H_2 and after treatment in 0.1 MPa H_2 (purging). Difference spectra were obtained by subtracting the spectra taken during H_2 purging from the spectra obtained during propionic acid treatment.

1511 cm^{-1} is assigned to bridging bidentate adsorption of propionic acid on TiO_2, while the sharp feature at 1470 cm^{-1} is assigned to a C-H deformation mode in adsorbed propionic acid. Features at 1435 cm^{-1} and 1418 cm^{-1} are assigned to the symmetrical O–C=O vibrations of bidentate bridging propionate on TiO_2 and adsorption of propionate on W, respectively, and the feature at 1380 cm^{-1} is assigned to a C-H bending mode in adsorbed propionic acid.[54,55] These assignments are summarized in Table 4.2.

When the spectra collected in flowing H_2 after propionic acid treatment are subtracted

Table 4.2: Assignment of vibrational modes observed during reduction of 0.3 kPa propionic acid in 0.1 MPa H_2 at 413 K over PdW/TiO_2 and W/TiO_2.

Adsorbent	Conditions	Vibrational mode	Frequency (cm^{-1})	Assignment
PdW/TiO_2 or W/TiO_2	0.3 kPa propionic acid, 0.1 MPa H_2, 413 K	ν(OH)	3500-3100 broad	Propionic acid, water (physisorbed)
		$\nu_a(CH_3)$	2985	Propionic acid, bidentate[56,57]
		$\nu_a(CH_2)$	2949	Propionic acid, bidentate
		$\nu_s(CH_3)$	2930-2900 w	Propionic acid, bidentate
		$\nu_s(CH_2)$	2892	Propionic acid, bidentate
		ν(C=O)	1791,1772,1732	Propionic acid, (vapor, monomer and dimer)
			1680	Propionyl[56,58,59]
		ν_a(O–C=O)	1661	Propionic acid, WO_x
			1520	Propionic acid, bidentate,[55,57] TiO_2
		δ(C–H)	1470	Propionic acid
		ν_s(O–C=O)	1436, 1418	Propionic acid[55]
		δ(C–H)	1380	Propionic acid

from the spectra obtained in flowing H_2 and propionic acid, the vapor-phase propionic acid features are clearly visible (Figure 4.7(a,c)), as is a carbonyl stretching mode near 1680 cm^{-1} (Figure 4.7(b,d)). Carbonyl stretching modes of similar values have previously been reported during acetaldehyde adsorption on Pd/CeO_2[58] and Pt/SiO_2 promoted by Na,[59] and acetic acid reduction on Pt/TiO_2,[56] and were attributed to the formation of acetyl surface species. The difference spectra also revealed a decrease in the intensity of the C-H stretching modes at higher wavenumber than the species observed on both catalyst surfaces in the *in situ* or H_2 purging spectra, indicating the desorption of more weakly bound propionic acid species during H_2 purging.

4.4 Discussion

4.4.1 Catalytic Activity of Pd-promoted WO_x and PTA

Promotion of SiO_2, TiO_2, and ZrO_2-supported WO_x and PTA with Pd produced active catalysts for the conversion of carboxylic acids that could reduce propionic acid at a higher rate per mass of catalyst than Pd-promoted Re catalysts previously studied under similar conditions.[60] The observed activity depended strongly on both support and pretreatment of the catalyst, and required the presence of a metal promoter that can dissociatively adsorb H_2. Supports such as TiO_2 and ZrO_2, which form Brønsted acid sites when loaded with dispersed WO_x species,[14,17,18] produced catalysts that were not as active for the reduction of propionic acid as SiO_2-supported WO_x. Interestingly, when Pd-promoted PTA was supported on SiO_2 and TiO_2, higher activity for the reduction of propionic acid was observed relative to Pd-promoted WO_x on SiO_2 or TiO_2.

Despite their higher activity, PdPTA catalysts were only half as selective for the formation of oxygenated products, and the observed rate of formation of oxygenated products over PdPTA

was still comparable to the rate of oxygenate formation observed over the PdW catalysts on SiO_2 and TiO_2. In light of this observation, we propose that higher surface densities of Brønsted acid sites lead to less selective reduction of the carboxylic acid functionality, as was observed for PdW supported on ZrO_2 and the supported heteropolyacids. Presumably, Brønsted acid sites catalyze unselective dehydration steps that lead to hydrocarbons and ethers. Yamaguchi et al. found that the isomerization of cyclopropane over similarly made WO_x catalysts found that WO_x/ZrO_2 was more active for the isomerization reaction, while WO_x/TiO_2 was less active and WO_x/SiO_2 demonstrated no activity. This trend followed the reported acid site strength of each catalyst, where WO_x/ZrO_2 and WO_x/TiO_2 had stronger acid sites, and WO_x/SiO_2 had weaker acid sites. However, the trend in reactivity observed here was the opposite. Apparently, supports that are expected to generate weaker acid sites when combined with WO_x can be correlated with higher activity for the reduction of carboxylic acids.

In contrast, strong Lewis acid sites may also catalyze the C-OH bond breaking of weakly adsorbed carboxylic acids. A strong dependence of the rate on the pressure of propionic acid was observed, which contrasted previously studied Re and Pd-promoted Re systems wherein the rate was nearly zero order in acid.[44,60,61] Under similar conditions, Pd-promoted Re was found in an average oxidation state of Re(IV), while the Pd-promoted W studied here was in an average oxidation state between W(IV) and W(VI). A lower density of exposed metallic centers (Lewis acid sites) on W compared to Re might result in fewer adjacent Lewis acidic sites, and weaker interaction between the propionic acid and the catalyst surface in the absence of bidentate binding of propionate to the active site. Furthermore, the weak dependence of the propionic acid reduction rate on H_2 pressure and lack of a strong kinetic isotope effect are consistent with

rate-determining C-OH bond breaking of the weakly adsorbed carboxylic acid species in the absence of high coverage of carboxylate species on the active site. Rate determining dissociative adsorption has been proposed for the reduction of acetate esters and acetic acid over Cu/SiO_2 previously.[8] Evidently, the role of acid site type remains unclear and merits further study.

4.4.2 Characterization of SiO_2- and TiO_2-supported W

Results from XRD and the W L_I-edge and L_{III}-edge XANES suggest that treatment at increased temperature in H_2 results in the disappearance of the monoclinic WO_3 structure of PdW/SiO_2. The slight shift to lower energy and increase in intensity of the pre-edge feature at the L_I edge suggests that octahedral WO_x species are shifting to a more distorted coordination environment during H_2 treatment. Furthermore, W L_I- and L_{III}-edge XANES indicate that WO_3 PdW/SiO_2 and W/SiO_2 is reduced from W(VI) to an average oxidation state of between W(VI) and W(IV) during H_2 treatment at 673 K. Reactivity results suggest, however, that PdW/SiO_2 loses almost half of its activity after pretreatment at 673 K. These results suggest that reduction of WO_3 to a WO_x of $2<x<3$ phase or the disappearance of the monoclinic WO_3 phase warrant further investigation as potential causes of catalyst deactivation.

The most abundant species on the surface of the PdW/TiO_2 and W/TiO_2 under reaction conditions can be identified as propionate bound to the WO_x and TiO_2 surfaces, giving characteristic asymmetrical O–C=O vibrational modes observed using DRIFTS near 1660 cm^{-1} and 1510 cm^{-1}, respectively. The symmetrical O–C=O modes were more similar, at 1430 cm^{-1} and 1418 cm^{-1}. The splitting between the asymmetrical and symmetrical modes can give insight into the type of interaction between the acid and the surface.[57] A splitting of 80 cm^{-1} between the

symmetrical and asymmetrical C–O=O modes is in the range of bidentate and bidentate bridging species. These species have been observed on TiO_2 in the absence of any active metal, and calculated adsorption modes of acetic acid adsorption on TiO_2 suggest that this species is a bidentate bridging species.[62] In contrast, a splitting of 230 cm^{-1} between the two modes observed in the presence of WO_x is closer to the expected values found in unidentate or asymmetrical bidentate carboxylate species, indicative of weaker binding of the propionate species on WO_x.[57]

Upon removal of the carboxylic acid from the gas phase over both catalysts, the difference spectra revealed a peak near 1680 cm^{-1}. Peaks in this location have been observed in the past during acetaldehyde adsorption on Pd/CeO_2,[58] Pt/SiO_2 promoted by Na,[59] and acetic acid reduction over Pt/TiO_2,[56] and were assigned to the formation of acetyl species on the catalyst surface. While this peak is present on both PdW/TiO_2 and W/TiO_2, only PdW/TiO_2 was active for propionic acid conversion. We propose that this species is a propionyl intermediate bound to the WO_x surface. Spontaneous C-O bond breaking on the W surface or Brønsted acid catalyzed C-O bond breaking to form the species while the active surface is saturated with Brønsted acidic H atoms would account for the observed weak dependence on H_2. In the presence of Pt (or Pd), water, and H_2, the transport of reducing H across WO_x to form the H_xWO_3 bronze occurs readily,[63] and is proposed to hydrogenate these propionyl species to propanal which can be subsequently hydrogenated to 1-propanol. In the absence of metal function such as Pd however, it is unlikely that this hydrogenation could occur under such mild conditions, resulting in a catalytic "dead end" for the propionyl surface species.

4.5 Conclusions

Palladium-promoted SiO_2-, TiO_2-, and ZrO_2-supported WO_x and PTA synthesized by wetness impregnation of ammonium metatungstate and phosphotungstic acid performed the catalytic reduction of gas-phase propionic acid in atmospheric pressures of H_2. Major products of the reduction included of 1-propanol, propanal, *n*-propyl ether, and light hydrocarbons. Treatment of these catalysts at 673 K in flowing H_2 resulted in decreases in conversion rates for SiO_2 supported WO_x and SiO_2 or TiO_2 supported PTA, while the rate over W/TiO_2 remained about the same and the rate over W/ZrO_2 nearly doubled. The apparent barriers to propionic acid conversion over PdW/TiO_2 and $PdPTA/TiO_2$ were 54 and 60 kJ mol^{-1}, respectively. Propionic acid reduction over these two catalysts was 0.2 order in H_2, and 0.7 order in propionic acid, and a small inverse kinetic isotope of $rate_H/rate_D$ = 0.91 during reduction of propionic acid with D_2 was observed. Adsorption of H_2 and CO suggested higher dispersion of the Pd on the TiO_2 supported catalysts than on the SiO_2 supported catalysts. X-ray absorption spectra at the W L_I edge indicated that H_2 treatment resulted in the slight reduction of WO_x near reaction temperatures at 440 K and further reduction during 673 K H_2 treatment. X-Ray diffraction patterns indicated that treatment at 473 K and above in flowing H_2 resulted in the disappearance of monoclinic WO_3 in PdW/SiO_2 on the SiO_2 support while 473 K treatment of PdW/TiO_2 did not, and X-ray absorption spectra at the W L_I and L_{III} edges also suggested that distortion of the WO_x octahedra increased. Infrared studies of W/TiO_2 and PdW/TiO_2 indicated that the catalyst surface is highly covered in propionate species, but also contained a small fraction of an unknown carbonyl stretching mode that was assigned to a propionyl species. The findings reported here offer insight into tungsten-oxide-catalyzed reduction of carboxylic acids to primary alcohols, which

has not been reported on previously. Further investigation is needed to determine the effects of acid site type and density on the rate and selectivity of propionic acid reduction using supported WO_x catalysts.

Acknowledgements

Gordon Brezicki is acknowledged for assistance with beamtime acquisition and beamline operations. Naomi Miyake is acknowledged for assistance collecting the X-ray diffraction patterns analyzed here. This work used beamline 8-ID of the National Synchrotron Light Source II, a U.S. Department of Energy (DOE) Office of Science User Facility operated for the DOE Office of Science by Brookhaven National Laboratory under Contract No. DE-SC0012704. This material is based upon work supported by the National Science Foundation (NSF) under Award No. EEC-0813570. Any opinions, findings, and conclusions or recommendations expressed in this material are those of the author(s) and do not necessarily reflect the views of the NSF.

References

1. International Energy Agency. *The Future of Petrochemicals* tech. rep. (International Energy Agency, 2018).

2. Vennestrøm, P. N. R., Osmundsen, C. M., Christensen, C. H. and Taarning, E. Beyond petrochemicals: The renewable chemicals industry. *Angewandte Chemie - International Edition* **50,** 10502–10509 (2011).

3. Werpy, T. and Peterson, G. *Top Value Added Chemicals from Biomass Volume 1 – Results of Screening for Potential Candidates from Sugars and Synthesis Gas* tech. rep. (2004).

4. Bozell, J. J. and Petersen, G. R. Technology development for the production of biobased products from biorefinery carbohydrates – the US Department of Energy's "Top 10" revisited. *Green Chemistry* **12,** 539–554 (2010).

5. Adkins, H. and Connor, R. The catalytic hydrogenation of organic compounds over copper chromite. *Journal of the American Chemical Society* **53,** 1091–1095 (1931).

6. Yan, T. Y., Albright, L. F. and Case, L. C. Hydrogenolysis of esters, particularly perfluorinated esters. *Industrial and Engineering Chemistry Product Research and Development* **4,** 101–107 (1965).

7. Evans, J. W., Wainwright, M. S., Cant, N. W. and Trimm, D. L. Structural and Reactivity Effects in the Copper-Catalyzed Hydrogenolysis of Aliphatic Esters. *Journal of Catalysis* **88,** 203–213 (1984).

8. Santiago, M., Sánchez-Castillo, M., Cortright, R. and Dumesic, J. Catalytic Reduction of Acetic Acid, Methyl Acetate, and Ethyl Acetate over Silica-Supported Copper. *Journal of Catalysis* **193,** 16–28 (2000).

9. Broadbent, H. S. RHENIUM AND ITS COMPOUNDS AS HYDROGENATION CATALYSTS. *Annals of the New York Academy of Sciences* **145,** 58–71 (1967).

10. Trivedi, B., Grote, D. and Mason, T. Hydrogenation of Carboxylic Acids and Synergistic Catalysts. *Journal of the American Oil Chemists' Society* **58,** 17–20 (1981).

11. Tahara, K., Nagahara, E., Itoi, Y., Nishiyama, S., Tsuruya, S. and Masai, M. Liquid phase hydrogenation of carboxylic acid catalyzed by supported bimetallic Ru-Sn/alumina catalyst: effects of tin compounds in impregnation method. *Journal of Molecular Catalysis A: Chemical* **110,** L5–L6 (1996).

12. Chen, L., Zhu, Y., Zheng, H., Zhang, C. and Li, Y. Aqueous-phase hydrodeoxygenation of propanoic acid over the Ru/ZrO_2 and Ru–Mo/ZrO_2 catalysts. *Applied Catalysis A: General* **411-412,** 95–104 (2012).

13. Pritchard, J., Filonenko, G. A., van Putten, R., Hensen, E. J. M. and Pidko, E. A. Heterogeneous and homogeneous catalysis for the hydrogenation of carboxylic acid derivatives: history, advances and future directions. *Chem. Soc. Rev.* **44,** 3808–3833 (2015).

14. Yamaguchi, T., Tanaka, Y. and Tanabe, K. Isomerization and disproportionation of olefins over tungsten oxides supported on various oxides. *Journal of Catalysis* **65,** 442–447 (1980).

15. Hino, M. and Arata, K. Synthesis of Solid Superacid of Molybdenum Oxide Supported on Zirconia and Its Catalytic Action. *Chemistry Letters* **18,** 971–972 (1988).

16. Barton, D. G., Soled, S. L. and Iglesia, E. Solid acid catalysts based on supported tungsten oxides. *Topics in Catalysis* **6,** 87–99 (2006).

17. Baertsch, C. D., Soled, S. L. and Iglesia, E. Isotopic and chemical titration of acid sites in tungsten oxide domains supported on zirconia. *Journal of Physical Chemistry B* **105,** 1320–1330 (2001).

18. Soultanidis, N., Zhou, W., Psarras, A. C., Gonzalez, A. J., Iliopoulou, E. F., Kiely, C. J., Wachs, I. E. and Wong, M. S. Relating *n*-Pentane Isomerization Activity to the Tungsten Surface Density of WO_x/ZrO_2. *Journal of the American Chemical Society* **132,** 13462–13471 (2010).

19. Herrera, J. E., Kwak, J. H., Hu, J. Z., Wang, Y., Peden, C. H., Macht, J. and Iglesia, E. Synthesis, characterization, and catalytic function of novel highly dispersed tungsten oxide catalysts on mesoporous silica. *Journal of Catalysis* **239,** 200–211 (2006).

20. Barton, D. G., Shtein, M., Wilson, R. D., Soled, S. L. and Iglesia, E. Structure and Electronic Properties of Solid Acids Based on Tungsten Oxide Nanostructures. *The Journal of Physical Chemistry B* **103,** 630–640 (1999).

21. Barton, D. G., Soled, S. L., Meitzner, G. D., Fuentes, G. A. and Iglesia, E. Structural and catalytic characterization of solid acids based on zirconia modified by tungsten oxide. *Journal of Catalysis* **181,** 57–72 (1999).

22. Baertsch, C. D., Komala, K. T., Chua, Y. H. and Iglesia, E. Genesis of Brønsted acid sites during dehydration of 2-butanol on tungsten oxide catalysts. *Journal of Catalysis* **205,** 44–57 (2002).

23. Ross-Medgaarden, E. I., Knowles, W. V., Kim, T., Wong, M. S., Zhou, W., Kiely, C. J. and Wachs, I. E. New insights into the nature of the acidic catalytic active sites present in ZrO_2-supported tungsten oxide catalysts. *Journal of Catalysis* **256,** 108–125 (2008).

24. Bardin, B. B. and Davis, R. J. Effect of water on silica-supported phosphotungstic acid catalysts for 1-butene double bond shift and alkane skeletal isomerization. *Applied Catalysis A: General* **200,** 219–231 (2000).

25. Kozhevnikov, I. V. Heteropoly Acids and Related Compounds as Catalysts for Fine Chemical Synthesis. *Catalysis Reviews* **37,** 311–352 (1995).

26. Misono, M. *Heterogeneous Catalysis by Heteropoly Compounds of Molybdenum and Tungsten* **2-3,** 269–321 (1987).

27. Palkovits, R., Tajvidi, K., Ruppert, A. M. and Procelewska, J. Heteropoly acids as efficient acid catalysts in the one-step conversion of cellulose to sugar alcohols. *Chemical Communications* **47,** 576–578 (2011).

28. Shanmugam, S., Viswanathan, B. and Varadarajan, T. K. Esterification by solid acid catalysts - A comparison. *Journal of Molecular Catalysis A: Chemical* **223,** 143–147 (2004).

29. White, H., Strobl, G., Feicht, R. and Simon, H. Carboxylic acid reductase: a new tungsten enzyme catalyses the reduction of non-activated carboxylic acids to aldehydes. *European Journal of Biochemistry* **184,** 89–96 (1989).

30. Kitson, M. and Williams, P. S. *US Patent* 5149680 (1992).

31. Pestman, R., Koster, R., Pieterse, J. and Ponec, V. Reactions of carboxylic acids on oxides: 1. Selective hydrogenation of acetic acid to acetaldehyde. *Journal of Catalysis* **168,** 255–264 (1997).

32. Jevtic, R., Johnston, V., Weiner, H. and Zhou, Z. *US Patent* 8536382 (2013).

33. Gosselink, R. W., Stellwagen, D. R. and Bitter, J. H. Tungsten-based catalysts for selective deoxygenation. *Angewandte Chemie - International Edition* **52,** 5089–5092 (2013).

34. Hollak, S. A. W., Gosselink, R. W., van Es, D. S. and Bitter, J. H. Comparison of Tungsten and Molybdenum Carbide Catalysts for the Hydrodeoxygenation of Oleic Acid. *ACS Catalysis* **3,** 2837–2844 (2013).

35. Hong, U. G., Kim, J. K., Lee, J., Lee, J. K., Song, J. H., Yi, J. and Song, I. K. Hydrogenation of succinic acid to tetrahydrofuran (THF) over ruthenium–carbon composite (Ru–C) catalyst. *Applied Catalysis A: General* **469,** 466–471 (2014).

36. Zhu, S., Gao, X., Zhu, Y. and Li, Y. Promoting effect of WOx on selective hydrogenolysis of glycerol to 1,3-propanediol over bifunctional Pt-WO_x/Al_2O_3 catalysts. *Journal of Molecular Catalysis A: Chemical* (2014).

37. Zhu, S., Gao, X., Zhu, Y., Cui, J., Zheng, H. and Li, Y. SiO_2 promoted Pt/WO_x/ZrO_2 catalysts for the selective hydrogenolysis of glycerol to 1,3-propanediol. *Applied Catalysis B: Environmental* **158-159,** 391–399 (2014).

38. Palomino, R. M., Stavitski, E., Waluyo, I., Chen-Wiegart, Y. c. K., Abeykoon, M., Sadowski, J. T., Rodriguez, J. A., Frenkel, A. I. and Senanayake, S. D. New In-Situ and Operando Facilities for Catalysis Science at NSLS-II: The Deployment of Real-Time, Chemical, and Structure-Sensitive X-ray Probes. *Synchrotron Radiation News* **30,** 30–37 (2017).

39. Ravel, B. and Newville, M. ATHENA, ARTEMIS, HEPHAESTUS: Data analysis for X-ray absorption spectroscopy using IFEFFIT. *Journal of Synchrotron Radiation* **12,** 537–541 (2005).

40. Nobbs, J. H. Kubelka—Munk Theory and the Prediction of Reflectance. *Review of Progress in Coloration and Related Topics* **15,** 66–75 (1985).

41. Yada, A., Murayama, T., Hirata, J., Nakashima, T., Tamura, M., Kon, Y. and Ueda, W. W-Ti-O mixed metal oxide catalyzed dehydrative cross-etherification of alcohols. *Chemistry Letters* **47,** 2017–2019 (2018).

42. Venkateswara Rao, K. T., Rao, P. S., Sai Prasad, P. S. and Lingaiah, N. Cesium exchanged heteropoly tungstate supported on zirconia as an efficient and selective catalyst for the preparation of unsymmetrical ethers. *Catalysis Communications* **10,** 1394–1397 (2009).

43. Tsigdinos, G. A. in *Topics in Current Chemistry* 1–64 (Springer-Verlag, Berlin/Heidelberg, 1978).

44. Rozmysłowicz, B., Kirilin, A., Aho, A., Manyar, H., Hardacre, C., Wärnå, J., Salmi, T. and Murzin, D. Y. Selective hydrogenation of fatty acids to alcohols over highly dispersed ReO_x/TiO_2 catalyst. *Journal of Catalysis* **328,** 197–207 (2015).

45. Tauster, S. J., Fung, S. C. and Garten, R. L. Strong Metal-Support Interactions. Group 8 Noble Metals Supported on TiO_2. *Journal of the American Chemical Society* **100,** 170–175 (1978).

46. Joyal, C. L. M. and Butt, J. B. Chemisorption and disproportionation of carbon monoxide on palladium/silica catalysts of differing percentage metal exposed. *Journal of the Chemical Society, Faraday Transactions 1* **83,** 2757–2764 (1987).

47. Choi, H. G., Jung, Y. H. and Kim, D. K. Solvothermal synthesis of tungsten oxide nanorod /nanowire/nanosheet. *Journal of the American Ceramic Society* **88,** 1684–1686 (2005).

48. Kuzmin, A., Purans, J., Cazzanelli, E., Vinegoni, C. and Mariotto, G. X-ray diffraction, extended x-ray absorption fine structure and Raman spectroscopy studies of WO_3 powders and (1-x)WO_{3-y}·xReO_2 mixtures. *Journal of Applied Physics* **84,** 5515–5524 (1998).

49. Ganji, S., Bukya, P., Vakati, V., Rao, K. S. R. and Burri, D. R. Highly efficient and expeditious PdO/SBA-15 catalysts for allylic oxidation of cyclohexene to cyclohexenone. *Catalysis Science and Technology* **3,** 409–414 (2013).

50. Locherer, K. R., Swainson, I. P. and Salje, E. K. Phase transitions in tungsten trioxide at high temperatures - A new look. *Journal of Physics Condensed Matter* **11,** 6737–6756 (1999).

51. Yamazoe, S., Hitomi, Y., Shishido, T. and Tanaka, T. XAFS study of tungsten L_1- And L_3-edges: structural analysis of WO_3 species loaded on TiO_2 as a catalyst for photo-oxidation of NH_3. *Journal of Physical Chemistry C* **112,** 6869–6879 (2008).

52. Hilbrig, F., Göbel, H. E., Knözinger, H., Schmelz, H. and Lengeler, B. X-ray absorption spectroscopy study of the titania- and alumina-supported tungsten oxide system. *Journal of Physical Chemistry* **95,** 6973–6978 (1991).

53. Horsley, J. A., Wachs, I. E., Brown, J. M., Via, G. H. and Hardcastle, F. D. Structure of surface tungsten oxide species in the tungsten trioxide/alumina supported oxide system from x-ray absorption near-edge spectroscopy and Raman spectroscopy. *The Journal of Physical Chemistry* **91,** 4014–4020 (1987).

54. Young, R. P. Infrared spectroscopic studies of adsorption and catalysis. Part 3. Carboxylic acids and their derivatives adsorbed on silica. *Canadian Journal of Chemistry* **47,** 2237–2247 (1969).

55. Tong, S. R., Wu, L. Y., Ge, M. F., Wang, W. G. and Pu, Z. F. Heterogeneous chemistry of monocarboxylic acids on α-Al_2O_3 at different relative humidities. *Atmospheric Chemistry and Physics* **10,** 7561–7574 (2010).

56. Rachmady, W. and Vannice, M. Acetic Acid Reduction by H_2 over Supported Pt Catalysts: A DRIFTS and TPD/TPR Study. *Journal of Catalysis* **207,** 317–330 (2002).

57. Nakamoto, K. in *Infrared and Raman Spectra of Inorganic and Coordination Compounds* (John Wiley & Sons, Inc., Hoboken, NJ, USA, 1987).

58. Idriss, H., Diagne, C., Hindermann, J., Kiennemann, A. and Barteau, M. Reactions of Acetaldehyde on CeO_2 and CeO_2-Supported Catalysts. *Journal of Catalysis* **155,** 219–237 (1995).

59. Boujana, S., Demri, D., Cressely, J., Kiennemann, A. and Hindermann, J. P. FT-IR and TPD studies on support-metal and promoter-metal interaction. Pt and Pd catalysts. *Catalysis Letters* **7,** 359–366 (1991).

60. Kammert, J. D., Xie, J., Godfrey, I. J., Unocic, R. R., Stavitski, E., Attenkofer, K., Sankar, G. and Davis, R. J. Reduction of Propionic Acid over a Pd-Promoted ReO_x/SiO_2 Catalyst Probed by X-ray Absorption Spectroscopy and Transient Kinetic Analysis. *ACS Sustainable Chemistry & Engineering* **6,** 12353–12366 (2018).

61. Takeda, Y., Tamura, M., Nakagawa, Y., Okumura, K. and Tomishige, K. Characterization of Re-Pd/SiO_2 Catalysts for Hydrogenation of Stearic Acid. *ACS Catalysis* **5,** 7034–7047 (2015).

62. Wang, S. and Iglesia, E. Experimental and theoretical assessment of the mechanism and site requirements for ketonization of carboxylic acids on oxides. *Journal of Catalysis* **345,** 183–206 (2017).

63. Benson, J. E., Kohn, H. W. and Boudart, M. On the reduction of tungsten trioxide accelerated by platinum and water. *Journal of Catalysis* **5,** 307–313 (1966).

5

Conclusions

5.1 Summary of findings

In this work, the catalytic reduction of carboxylic acids using metal oxide supported Re and W catalysts promoted by Pd was investigated. First, a Pd-promoted Re/SiO_2 catalyst and monometallic Pd/SiO_2 and Re/SiO_2 were synthesized by incipient wetness impregnation. A comparison of the reduction of liquid-phase octanoic acid in a decane solvent pressurized with 8 MPa of H_2 and the reduction of gas-phase propionic acid in atmospheric pressures of H_2 revealed very similar behavior of the Pd-promoted Re system under both sets of conditions. Prior to reaction, the as-synthesized Re-containing catalysts consisted of dispersed Re^{7+} species. When

Re/SiO_2 is promoted by Pd, Re^{7+} species are reduced to Re^{4+} species under mild conditions in H_2 as a result of hydrogen spillover from Pd to Re. No evidence of alloying of the Pd and Re components could be detected. As Pd/SiO_2 is not active for the reduction of carboxylic acids to oxygenates under the conditions studied, complete reduction of the Re^{7+} to Re^0 was not required to produce an active catalyst. Transient kinetic analysis revealed that a large quantity of reactive intermediates leading to 1-propanol, equal to about half the number of Re atoms in the active catalyst, covered the catalyst surface under the conditions studied.

As discussed in Chapter 3, Pd-promoted Re/TiO_2 and corresponding monometallic catalysts were synthesized using incipient wetness impregnation and evaluated for their ability to perform the gas-phase reduction of propionic acid. The steady-state kinetics of the Pd-promoted Re/TiO_2 catalyst were very similar to the steady-state kinetics of the Pd-promoted Re/SiO_2 catalyst. The monometallic TiO_2-supported catalysts demonstrated increased rates of conversion of propionic acid compared to their SiO_2-supported counterparts, which was likely the result of using a reducible support. A shift in selectivity toward propanal over 1-propanol using Pd-promoted Re catalysts at low conversion indicated that propanal was an intermediate in the formation of 1-propanol. Over catalysts on both supports, the rate of reduction of propionic acid demonstrated a 0.6 order dependence on H_2 pressure. The apparent barrier for propionic acid conversion was 60-75 kJ mol^{-1} over the supported Re-containing catalysts. Inverse kinetic isotope effects were observed for the reduction of propionic acid and the reduction of 1-propanol over Pd-promoted Re catalysts when D_2 was used as the reactant instead of H_2, while the hydrogenation of propanal demonstrated a normal kinetic isotope effect when studied in the absence of propionic acid at slightly lower temperature. Lack of a normal kinetic isotope effect and

complete conversion of co-fed butanal suggested that hydrogenation of aldehydes under reaction conditions was facile, and reduction of the carboxylic acid to form an aldehyde begins a cascade reaction leading to 1-propanol.

When the amount of water in the reactant stream was changed (or H_2 was replaced with N_2) during steady-state conversion of propionic acid over Pd-promoted Re/SiO_2, a transient response lasting approximately 10 hours was observed. The effects of cofeeding water or switching from H_2 to N_2 on the species present on the catalyst surface at steady state were investigated using DRIFTS. Results from DRIFTS revealed that surface propoxy species built up on the SiO_2 surface during steady state reaction, and were removed by feeding water or propionic acid. This result suggested that propoxy species desorbing from the SiO_2 masked the transient response of 1-propanol formation on the catalytically active metal surface. The Pd-promoted Re/TiO_2 did not accumulate measurable amounts of these species under the same conditions. Analysis of the transient response of propionic acid and butyric acid conversion over the Pd-promoted Re/TiO_2 revealed higher turnover frequencies (on the order of 10^{-2} s^{-1}) and lower surface coverages (less than 2% of the amount of Re) of reactive intermediates leading to oxygenated products than previously observed over the Pd-promoted Re/SiO_2.

As described in Chapter 4, Pd-promoted catalysts consisting of W oxide or phosphotungstic acid (PTA) supported on SiO_2, TiO_2, or ZrO_2 were synthesized by wetness impregnation. These catalysts demonstrated comparable rates of propionic acid reduction to rates observed over Pd-promoted Re catalysts under similar conditions. In the absence of a Pd promoter, supported WO_x catalysts were completely inactive under the conditions studied. Pretreatment of these catalysts in H_2 at 673 K had a mixed effect on the ability of each catalyst to convert

propionic acid. After the treatment, the rate of propionic acid over the SiO_2-supported PdW decreased, while over TiO_2-supported PdW the rate was unchanged, and over ZrO_2-supported PdW the rate increased. The apparent activation energy for the reduction of propionic acid over PdW/TiO_2 or PdPTA/TiO_2 was 54 or 60 kJ mol^{-1}, respectively. The reduction reaction was 0.2 order in H_2 pressure, and in the absence of H_2 the reaction completely ceased. The reduction reaction was 0.7 order in propionic acid pressure. A small inverse isotope effect of 0.91 was observed. Evidently, neither the loss of the monoclinic WO_3 phase nor reduction of the WO_x species observed during the 673 K treatment in H_2 resulted in an increase in activity on the SiO_2-supported PdW catalyst. Pd-promoted W catalysts, which had not been studied previously in the literature for the reduction of carboxylic acids, demonstrated a higher rates of propionic acid reduction than similarly synthesized Pd-promoted Re catalysts, and raise questions about the role of Brønsted and Lewis acid site strengths and densities in the reduction of carboxylic acids.

The structures of Pd-promoted Re/SiO_2 and its components were determined under reaction conditions. The kinetic behavior of SiO_2 and TiO_2 supported Pd-promoted Re catalysts was investigated using steady state and transient kinetic analysis. Using an improved understanding of the mechanism for carboxylic acid reduction by a bifunctional catalyst consisting of a reducible metal and an oxophilic metal, Pd-promoted W oxide catalysts for the selective reduction of propionic acid to 1-propanol were synthesized. These catalysts demonstrated comparable rates of propionic acid reduction to the Pd-promoted Re catalysts when studied in the gas phase under atmospheric pressures of H_2, and some remained selective to the alcohol product.

5.2 Future Work

5.2.1 Synthesis of Controlled Structures of Tungsten Oxide

The surface density of WO_x species and corresponding metal oxide structure of supported tungsten oxide catalysts can have a large effect on the turnover rate of acid-catalyzed reactions. The tungsten loading and oxidation temperature of WO_x supported on SiO_2, TiO_2, and ZrO_2 should be varied and the effects of these treatments on carboxylic acid reduction rates should be determined. Subsequent characterization using X-ray diffraction and X-ray absorption spectroscopy may provide insights into the size and structure of WO_x domains that are formed under these different conditions, and their usefulness for catalysis. These characterization techniques should be supported by the use of UV/visible, Raman, and infrared spectroscopy to determine the types of WO_x species present in mixtures of W oxides in different phases. Furthermore, investigation of synthesis effects using transient kinetic analysis offers the opportunity to count the number of reactive intermediates on the catalyst surface, and directly observe the effects of the WO_x structure on reactive intermediate coverage and turnover frequency.

5.2.2 Brønsted and Lewis Acidity Under Carboxylic Acid Reduction Conditions

The improved activity of propionic acid conversion over tungsten oxides and especially tungsten heteropolyacids, which are well-known for exposing strong Brønsted acid sites, indicates that these acid sites may play a role in the reduction of carboxylic acids. This Brønsted acidity could impact reactivity in the reduction of carboxylic acids over both W-based and Re-based catalysts. Previous work by Chia et al. found that metal-promoted Re clusters could support strong Brønsted acidic protons.[1] Falcone et al. demonstrated that these species were also present

during aqueous-phase hydrogenolysis of glycerol to propanediols. Typical Brønsted acid titration techniques, such as pyridine adsorption using infrared spectroscopy or ammonia temperature programmed desorption (NH_3 TPD), may not be sufficient to probe Brønsted acidity that might form in a dynamic equilibrium with gas-phase hydrogen,[2] as may be the case with spillover from the Pt group metal promoter to the ReO_x and WO_x surfaces.

Previous studies have used a variety of methods to probe acidity under reaction conditions. For example, a reaction such as the dehydration of 2-propanol[3] can be used to probe the *in situ* Brønsted acid site strength and density on a given catalyst surface. Additionally, the titration of active sites with molecules that selectively inhibit Brønsted acidity may provide quantitative information about the number of Brønsted acid sites formed *in situ* relative to the total number of acid sites. Previous studies have used molecules such as 2,6-di-tert-butyl-pyridine to titrate Brønsted acid sites during reaction.[4] However, under hydrogenating conditions, unsaturated rings like pyridine may lead to side reactions in the presence of Pd. Instead, hindered basic probes such as 2,2,6,6-tetramethylpiperidine (that are fully saturated) may be used to titrate Brønsted acid sites *in situ*, while non-hindered basic probes could be used to titrate total Lewis and Brønsted acid sites. The effects of catalyst synthesis, pretreatment, and *in situ* structural changes on the acidity of each catalyst could be measured using this technique. For comparison, the density of Brønsted and Lewis acid sites could also be measured using FT-IR pyridine adsorption to determine the ratios of acid sites and the adsorption of other basic probe molecules (NH_3 TPD, for example) to quantify the total acid sites in the system.

5.2.3 Variation of the Metal Promoter

Finally, the dependence of the rate of propionic acid reduction on the spillover-active promoter needs to be investigated more thoroughly. As mentioned earlier, the inclusion of Pd results in the formation of a small amount of side products including hydrocarbons resulting from decarbonylation of the carboxylic acid. Modification of the supported tungsten catalysts using alternative promoters (e.g. copper) that are able to dissociate H_2 should be investigated. Moreover, the design of an effective hydrogen spillover catalyst that does not produce side products should be attempted. The examination of mixed metal oxide spinels of alternative promoters and W (in the same vein as copper chromite) may yield an improved catalyst for the reduction of carboxylic acids to alcohols. Furthermore, tungsten carbide materials, which can perform selective hydrodeoxygenation that conserves the starting carbon number of the carboxylic acid,[5] should also be investigated. Tungsten carbides previously demonstrated the ability to behave like platinum and dissociate dihydrogen in the presence of water.[6] This ability may result in a catalyst with improved activity over the tungsten-oxide-based catalysts.

References

1. Chia, M., Pagán-Torres, Y. J., Hibbitts, D., Tan, Q., Pham, H. N., Datye, A. K., Neurock, M., Davis, R. J. and Dumesic, J. A. Selective hydrogenolysis of polyols and cyclic ethers over bifunctional surface sites on rhodium-rhenium catalysts. *Journal of the American Chemical Society* **133,** 12675–12689 (2011).

2. Barton, D. G., Soled, S. L., Meitzner, G. D., Fuentes, G. A. and Iglesia, E. Structural and catalytic characterization of solid acids based on zirconia modified by tungsten oxide. *Journal of Catalysis* **181,** 57–72 (1999).

3. Turek, W., Haber, J. and Krowiak, A. Dehydration of isopropyl alcohol used as an indicator of the type and strength of catalyst acid centres. *Applied Surface Science* **252,** 823–827 (2005).

4. Baertsch, C. D., Komala, K. T., Chua, Y. H. and Iglesia, E. Genesis of Brønsted acid sites during dehydration of 2-butanol on tungsten oxide catalysts. *Journal of Catalysis* **205,** 44–57 (2002).

5. Gosselink, R. W., Stellwagen, D. R. and Bitter, J. H. Tungsten-based catalysts for selective deoxygenation. *Angewandte Chemie - International Edition* **52,** 5089–5092 (2013).

6. Levy, R. B. and Boudart, M. Platinum-like behavior of tungsten carbide in surface catalysis. *Science* **181,** 547–549 (1973).

A

Supporting information for Chapter 2

Electron Microscopy

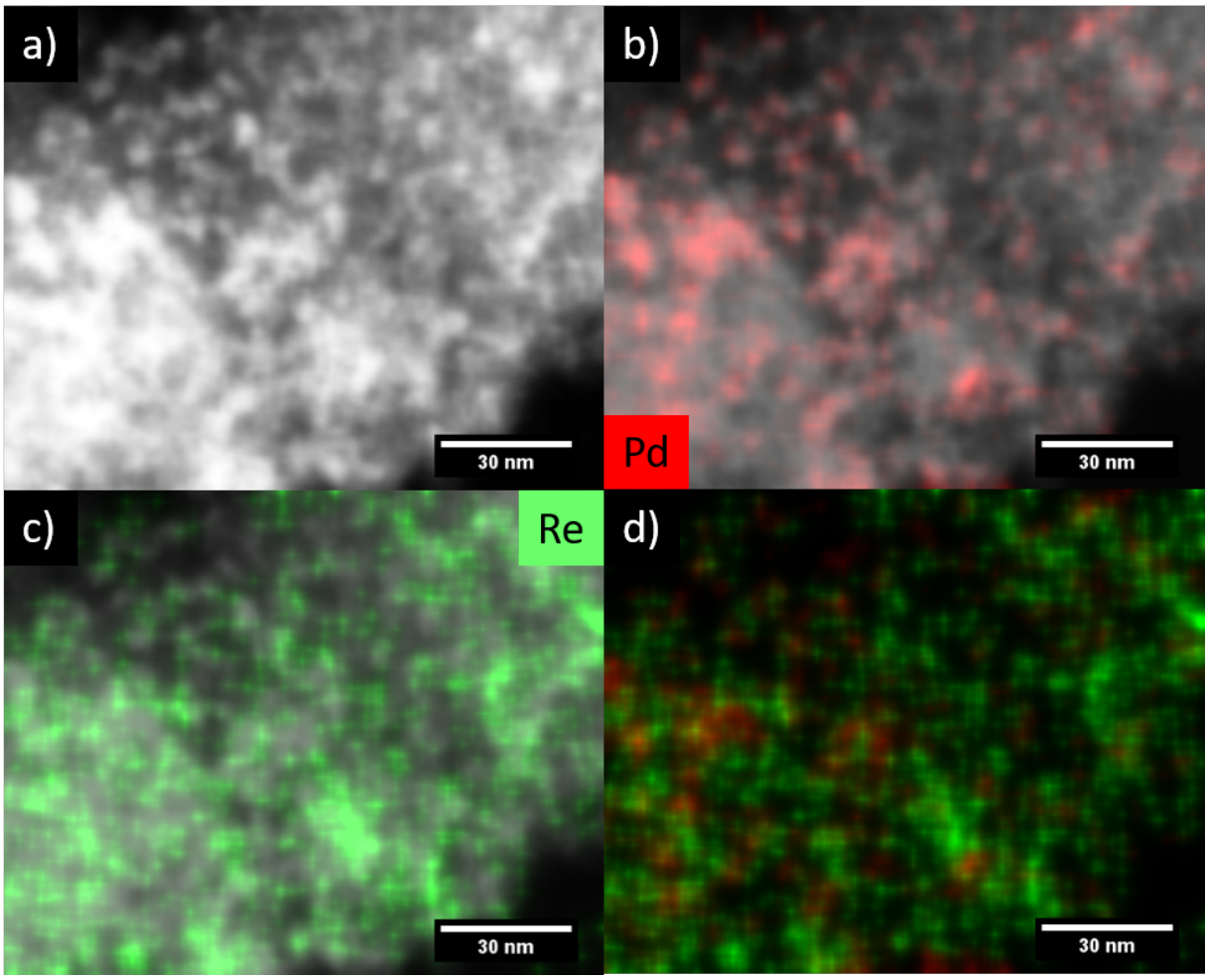

Figure A.1: STEM-EDS mapping of $PdRe/SiO_2$ catalyst before reaction showing (a) STEM image (b) EDS signal corresponding to Pd, which correlates well with visible particles (c) EDS signal corresponding to Re, which is not correlated with visible particles (d) Composite EDS signals corresponding to Pd and Re showing areas of concentrated Re and Pd with little overlap of the two elements.

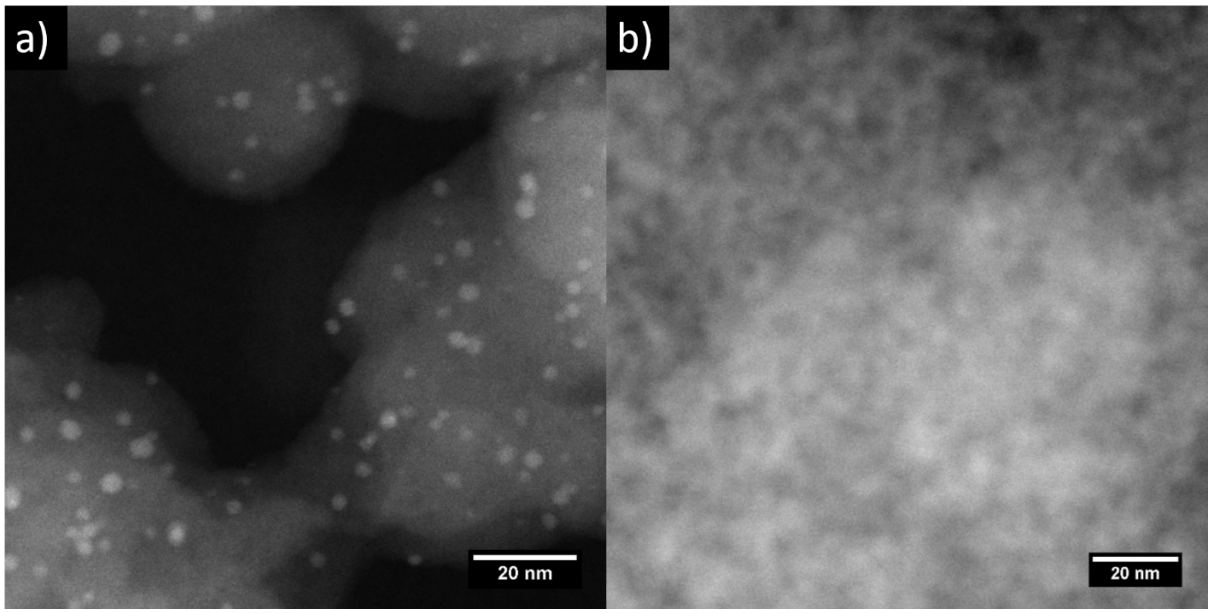

Figure A.2: STEM-HAADF image of fresh Pd/SiO_2 catalyst (b) STEM-HAADF image of fresh Re/SiO_2 catalyst.

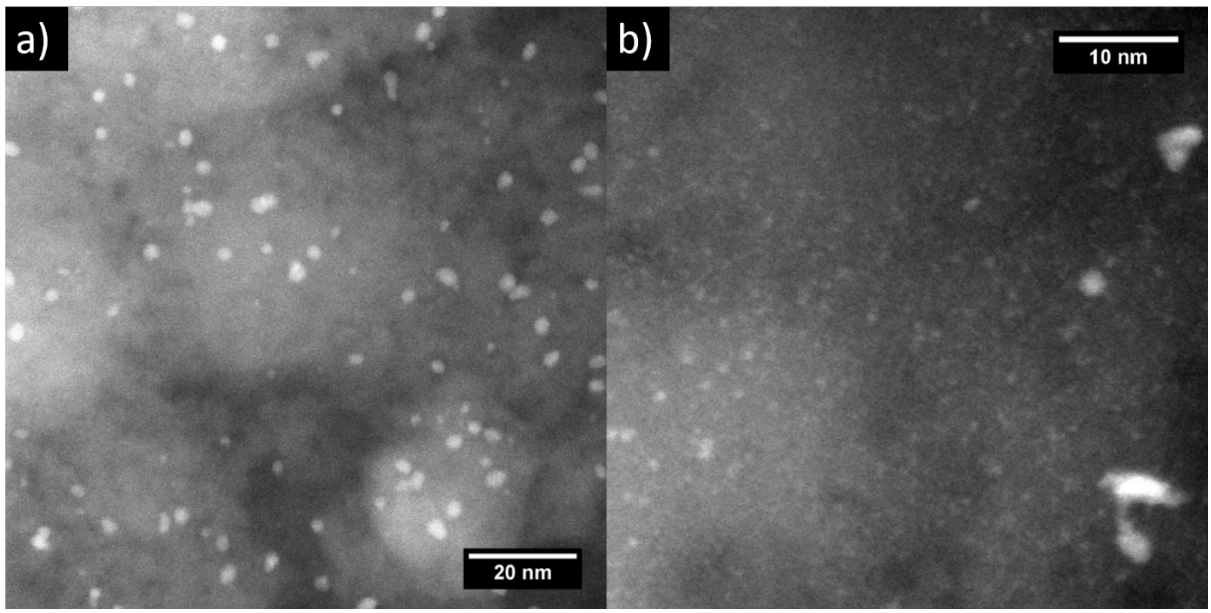

Figure A.3: Pd/SiO_2 and (b) Re/SiO_2 catalysts after exposure to H_2 at 473 K under reaction conditions with appropriate pretreatment.

X-ray Absorption Spectroscopy

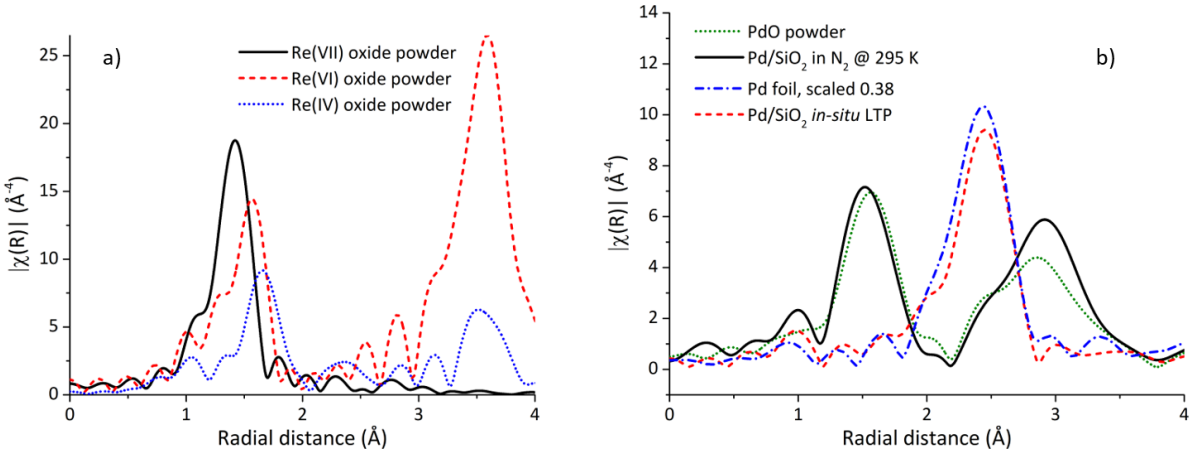

Figure A.4: Magnitude of the Fourier transform (not corrected for phase shift) of (a) the Re L_{III}-edge EXAFS of Re standards and (b) Pd K-edge EXAFS of Pd standards together with Pd/SiO_2 after various pretreatments.

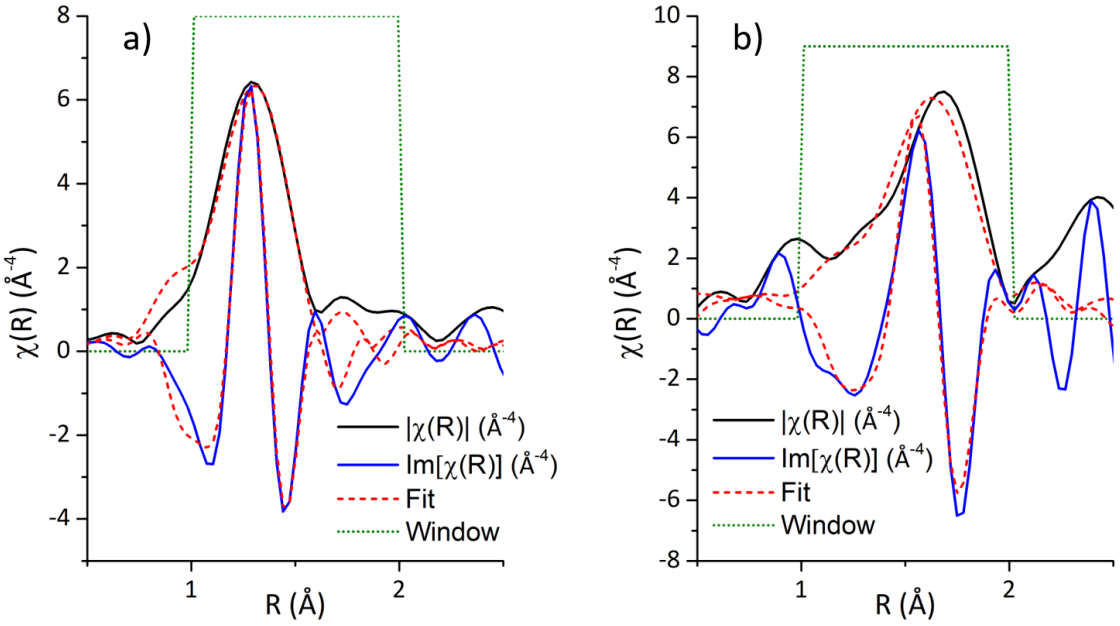

Figure A.5: Representative fitting of EXAFS results for (a) $PdRe/SiO_2$ and (b) Re/SiO_2 after NP at 433 K in 0.1 MPa 4% H_2/N_2 and ambient temperature propionic acid saturator.

Table A.1: EXAFS fitting results for Re and Pd standards using S_0^2 values determined from ReO_3, Re foil, PdO, and Pd foil.

Standard	Shell	*R (Å)*	*N*	σ^2 *(Å^2)*	ΔE_0 *(eV)*	*R-factor*
Re_2O_7	Re-O	1.737 ±0.008	4.1 ±0.5	0.0008 ±0.0008	6.7 ±1.8	0.02
ReO_3	Re-O	1.856 ±0.013	6.0 ±0.7	0.0038 ±0.0013	0.2 ±2.3	0.03
ReO_2	Re-O	2.002 ±0.008	4.2 ±0.5	0.0035 ±0.0014	6.5 ±2.0	0.02
Re	Re-Re	2.753 ±0.001	12. ±0.4	0.0039 ±0.0002	3.4 ±0.3	0.003
PdO	Pd-O	2.024 ±0.007	4.0 ±0.3	0.0011 ±0.0009	-1.9 ±0.9	0.01
	Pd-Pd	3.046 ±0.017	3.3 ±2.1	0.0054 ±0.0042		
	Pd-Pd	3.450 ±0.013	6.5 ±4.3	0.0096 ±0.0060		
Pd	Pd-Pd	2.743 ±0.001	12. ±0.5	0.0054 ±0.0002	-3.6 ±0.3	0.003

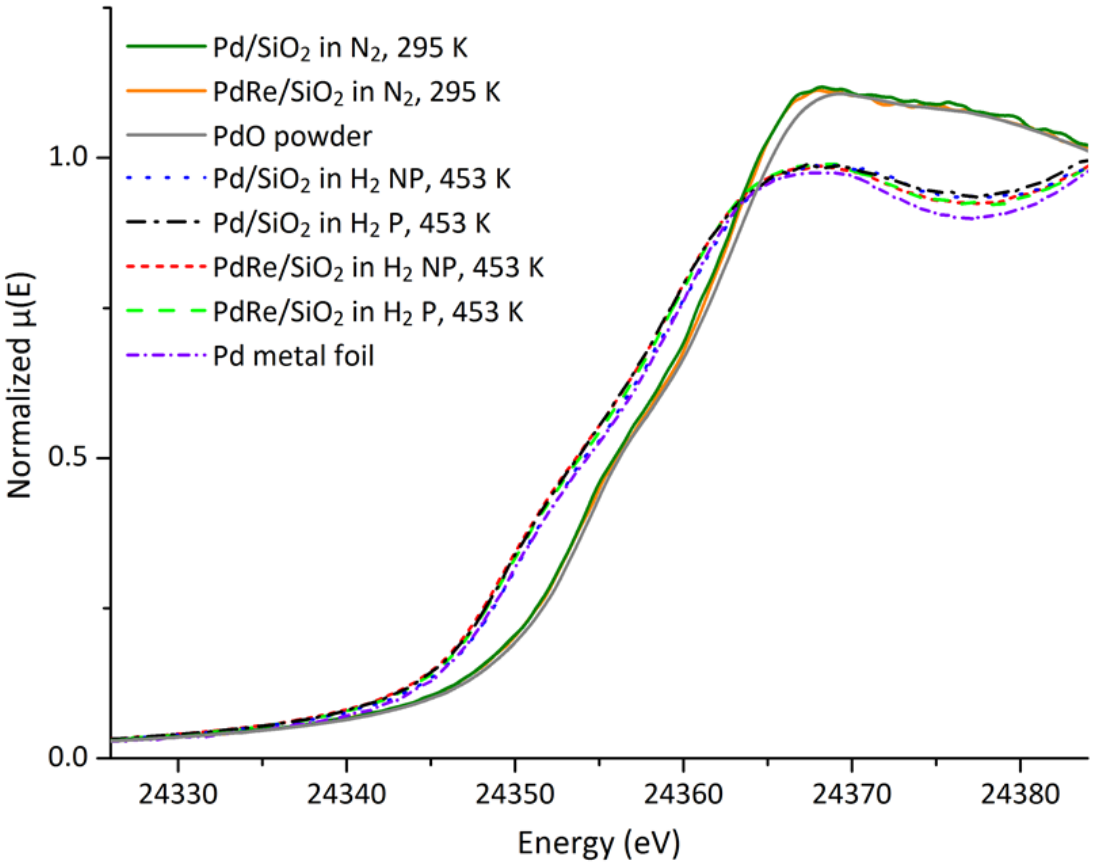

Figure A.6: Pd K-edge XANES. Solid lines represent Pd samples as synthesized, and PdO for comparison. Dashed lines represent Pd samples under reducing conditions, with Pd metal foil for comparison.

Catalytic Reduction of Carboxylic Acids

The reduction of octanoic acid (Acros Organics, 99%) to 1-octanol and octanal was carried out in a stainless steel upward flow reactor with inner diameter 0.46 cm contained within the reactor system depicted in Figure A.7. The catalyst bed consisted of the supported metal catalyst powder (0.015-0.020 g) diluted with 0.285-0.280 g of SiC (Strem Chemicals, 100 mesh) resting between two plugs of glass wool. Temperature measurements were made using a thermocouple inserted from the top of the reactor tube into the top of the catalyst bed. Prior to reaction, the system was purged with flowing N_2 at 30 cm^3 min^{-1} for at least 10 min. After purging with N_2, the reactor was purged with H_2 at 15 cm^3 min^{-1} for 10 min before ramping the temperature to 453 K. Once the temperature was stable, flow of liquid (0.1 cm^3 min^{-1}) from two Teledyne Isco 500D syringe pumps was mixed to form a solution of degassed 0-5 wt % octanoic acid that was fed through a heated static mixing bed packed with inert SiC then into to the catalyst bed. A mass flow controller was used to feed 0-1 standard cm^3 min^{-1} into the static mixing bed to dissolve H_2 into the reactant stream. The reactor was pressurized to 8 MPa with N_2 from the condenser side. After reaching 8 MPa, a steady stream of N_2 at 100 standard cm^3 min^{-1} was used to flush the condenser of residual H_2. The reactor effluent liquids were collected in the pressurized condenser, extracted in aliquots of 0.25 cm^3 using a two-step pressure relief chamber so as not to disturb the flow, and analyzed by liquid injection using an Agilent Technologies 7890A gas chromatograph (GC-FID) equipped with an DB-FFAP column (0.25 mm i.d., 60 m) and a flame-ionization detector (FID) using a split ratio of 30:1.

The conversion of the acid to its corresponding aldehyde, alcohol, and side products was evaluated from the integrated product peak areas. Dodecane was used as the internal standard,

and the major products were 1-octanol (92-85%), octanal (3-9%), octane (3%), and heptane (1-2%), which varied slightly depending on the level of conversion. Small amounts of the ester product, octyl octanoate (2%), were also detected, likely due to coupling of the alcohol product and the acid reactant. Hydrocarbon products were typically produced in very low amounts (5% total selectivity) under the conditions studied here. The fractional conversion (f_i) of acid i to the corresponding products j was calculated using the expression

$$f_i = \frac{\sum M_j}{M_i + \sum M_j} \tag{A.1}$$

where M_j is the molar flow rate of the component j. Similarly, the selectivity of the reaction towards each product j was calculated using the expression

$$S = \frac{M_j}{\sum M_j} \tag{A.2}$$

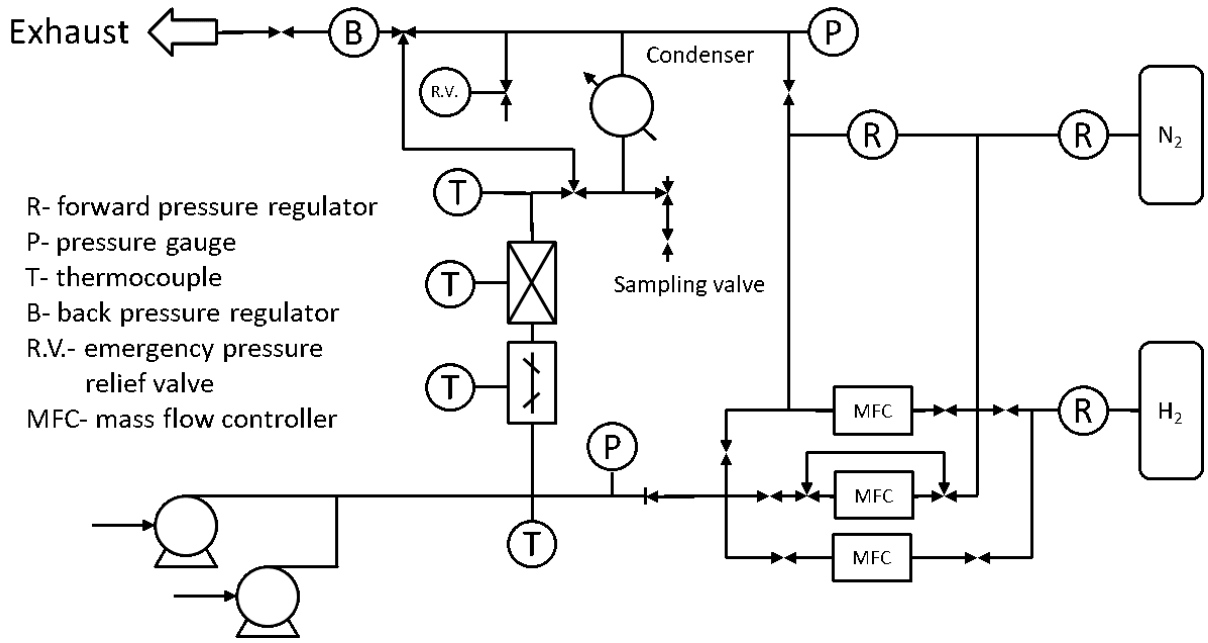

Figure A.7: Schematic representation of the reactor system used to collect steady-state reaction rate of the reduction of octanoic acid under high pressure.

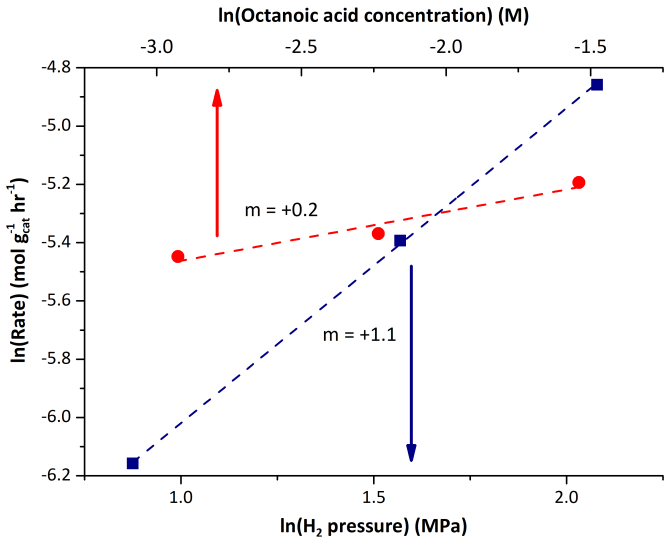

Figure A.8: Influence of reactant partial pressure or concentration on the observed rate of 1-octanol formation over $PdRe/SiO_2$ at 453 K. When H_2 pressure was varied, octanoic acid concentration was held at 0.2 M, and when octanoic acid concentration was varied, H_2 feed was held at 8 MPa.

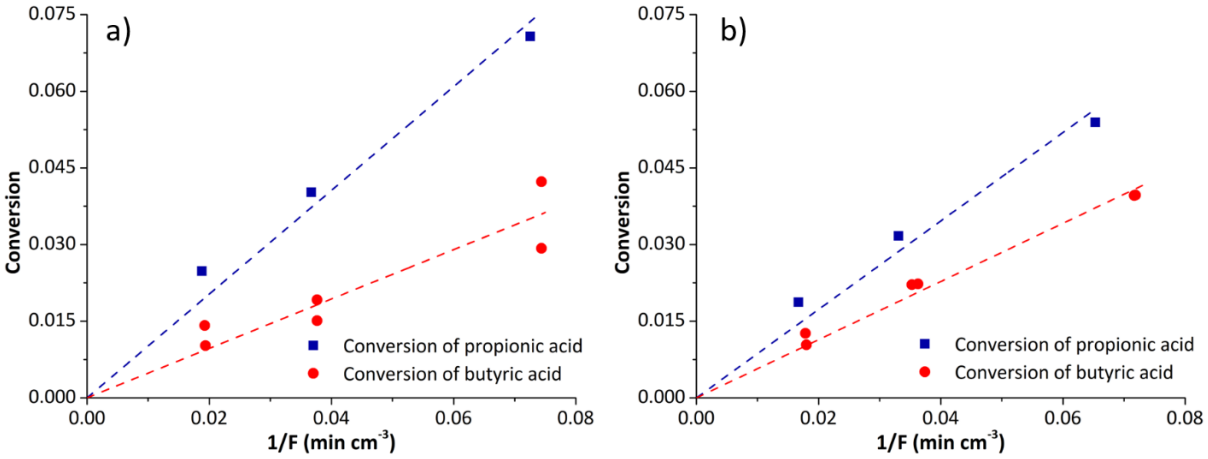

Figure A.9: Evidence for differential conversion over $PdRe/SiO_2$ at 433 K and 1 kPa carboxylic acid at (a) 0.1 MPa H_2. And (b) 0.2 MPa H_2.

Transient Kinetic Analysis

Table A.2: Conditions of transient kinetic experiments and integrated mean surface residence times of intermediates leading to 1-propanol (PrOH) and 1-butanol (BuOH) over $PdRe/SiO_2$.

Catalyst	Flow rate ($cm^3\ min^{-1}$)	Pressure (MPa)	τ_{PrOH} (min)	Flow rate ($cm^3\ min^{-1}$)	Pressure (MPa)	τ_{BuOH} (min)
$PdRe/SiO_2$	13.8	0.109	149.	13.4	0.111	202.
	13.8	0.109	155.	13.4	0.111	196.
	27.2	0.110	132.	26.6	0.113	198.
	27.2	0.110	121.	26.6	0.113	149.
	53.1	0.113	94.0	51.6	0.116	140.
	53.1	0.113	95.4	51.9	0.116	148.
	15.3	0.196	52.9	13.9	0.216	99.8
	15.3	0.196	73.7	14.0	0.215	110.
	30.2	0.199	52.0	27.6	0.218	93.5
	30.2	0.199	68.3	28.4	0.212	106.
	59.8	0.201	47.7	56.0	0.214	92.5
	59.8	0.201	54.2	55.5	0.216	76.9

Table A.3: Conditions of transient kinetic experiments and integrated mean surface residence times of intermediates leading to propionaldehyde (PrO) and butyraldehyde (BuO) over $PdRe/SiO_2$ and Re/SiO_2.

Catalyst	Flow rate ($cm^3\ min^{-1}$)	Pressure (MPa)	τ_{PrOH} (min)	Flow rate ($cm^3\ min^{-1}$)	Pressure (MPa)	τ_{BuOH} (min)
$PdRe/SiO_2$	13.8	0.109	4.32	13.5	0.111	4.00
	13.8	0.109	4.96	13.5	0.111	7.82
	26.7	0.112	2.86	26.4	0.114	2.35
	26.7	0.112	1.43	26.4	0.114	1.39
	50.7	0.118	2.39	51.3	0.117	1.64
	50.7	0.118	1.34	51.3	0.117	2.57
Re/SiO_2	17.8	0.112	3.75	18.1	0.110	3.49
	18.1	0.110	3.33	18.3	0.110	3.83
	26.7	0.112	2.96	26.7	0.112	2.95
	26.6	0.113	4.22	26.7	0.112	4.04
	51.0	0.118	1.90	51.3	0.117	2.01
	51.3	0.117	2.20	51.9	0.116	2.40

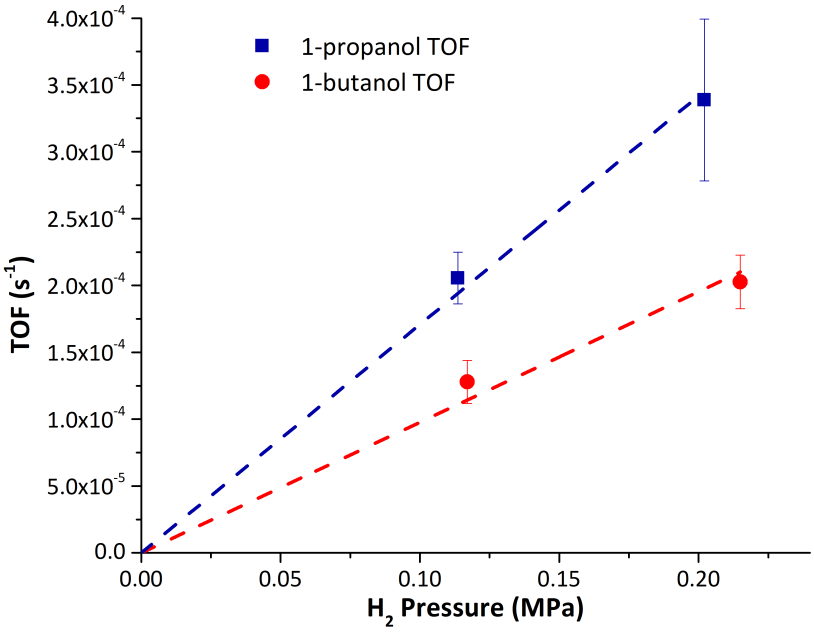

Figure A.10: Effect of varying the H_2 pressure on the intrinsic rates of alcohol formation over $PdRe/SiO_2$ at 433 K.

Table A.4: Kinetic parameters derived from transient kinetic analysis of 1 kPa propionic and butyric acid reduction in 0.2 MPa H_2 at 433 K, including the ratio of reactive intermediates to Re atoms N_i/Re.

Catalyst	Product	Rate of formation[a] (mol g_{cat}^{-1} h^{-1})	τ_0 (min)	TOF[b] (s^{-1})	N_i/Re[c]
$PdRe/SiO_2$	1-propanol	2.5×10^{-4}	49	3.4×10^{-4}	0.54
	1-butanol	1.4×10^{-4}	82	2.1×10^{-4}	0.46

(a) Calculated by extrapolation to infinite flow rate
(b) TOF is calculated as τ_0^{-1}
(c) Ratio of intermediates leading to specified product divided by total Re in sample

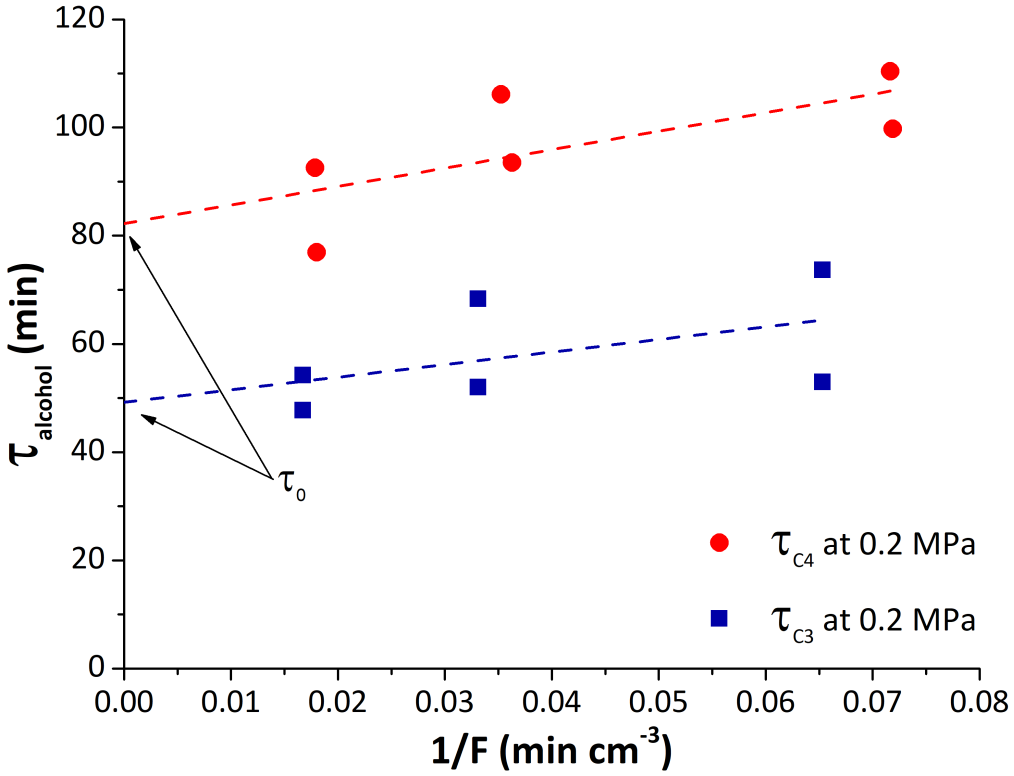

Figure A.11: Mean surface residence times of species leading to alcohols at 433 K extrapolated to infinite flowrate to remove artifacts from product readsorption. Red circles represent the mean surface residence time of intermediates leading to 1-butanol while blue squares represent the mean surface residence time of intermediates leading to 1-propanol.

B

Supporting information for Chapter 3

X-Ray Diffraction

X-Ray diffraction was carried out to determine the dispersion of the Pd in the bimetallic TiO_2-supported catalysts. The XRD patterns of a 1 wt % Pd, 8 wt % Re/TiO_2 (1Pd8Re/TiO_2), 1 wt % Pd, 13 wt % Re/TiO_2 (1Pd13Re/TiO_2), and 0.5 wt % Pd, 8 wt % Re/TiO_2 (0.5Pd8Re/TiO_2) are shown in Figure B.1. The PdO(101) peak was visible in the 1Pd8Re/TiO_2 catalyst, but could not be discerned in either the 0.5Pd8Re/TiO_2 or 1Pd13Re/TiO_2 catalysts. The calculated average crystallite size using the Scherrer equation indicated that the average diameter of the PdO particles in the 1Pd8Re/TiO_2 sample was 9 nm. The PdO peaks in the 1Pd13Re/TiO_2 and 0.5Pd8Re/TiO_2 are expected to contain particles of an equal or smaller diameter. For comparison, the XRD pattern of a 34% disperse Pd/TiO_2 catalyst (determined by H_2 chemisorption) is also shown in Figure B.1.

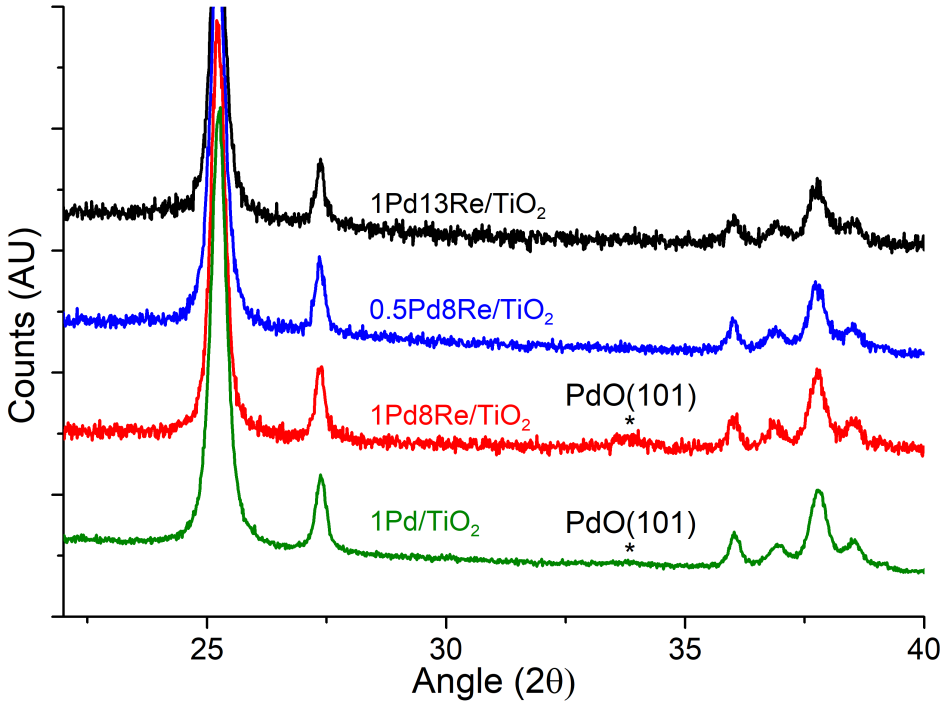

Figure B.1: X-Ray diffraction patterns of 1Pd8Re/TiO_2, 0.5Pd8Re/TiO_2, 1Pd13Re/TiO_2, and 1Pd/TiO_2 indicating an average PdO particle size of 9 nm or less.

Table B.1: Vibrational modes observed after *in situ* exposure of propionic acid and 1-propanol to SiO_2.

Adsorbent	Conditions	Vibrational mode	Frequency (cm^{-1})	Assignment
SiO_2	0.3 kPa propionic acid, 0.1 MPa H_2, 413 K	ν(OH)	3530-3130 broad	Propionic acid, water (physisorbed)
		$\nu_a(CH_3)$	2990	Propionic acid (physisorbed, silyl ester)
		$\nu_a(CH_2)$	2951	Propionic acid (physisorbed, silyl ester)
		$\nu_s(CH_3)$	2931 sh	Propionic acid (physisorbed, silyl ester)
		$\nu_s(CH_2)$	2893	Propionic acid (physisorbed, silyl ester)
		ν(C=O)	1755	Propionic acid, silyl ester
			1740-1730	Propionic acid, physisorbed/dimer
		δ(C–H)	1467	Propionic acid
		ν(C–O)/δ(C–H)	1440, 1428	Propionic acid
		δ/ω(C–H)	1386	Propionic acid
			1370	Propionic acid
	0.1 kPa 1-propanol, 0.1 MPa H_2, 413 K	ν(OH)	3530-3130 broad	1-propanol, water (physisorbed)
		$\nu_a(CH_3)$	2969	Propoxy
		$\nu_a(CH_2)$	2945	Propoxy
		$\nu_s(CH_3)$	2928 sh	Propoxy
		$\nu_s(CH_2)$	2887	Propoxy
		ν(C=O)	1734	Weak propionic acid contamination
		δ(C–H)	1480	Propoxy
			1467	Propoxy
			1458	Propoxy

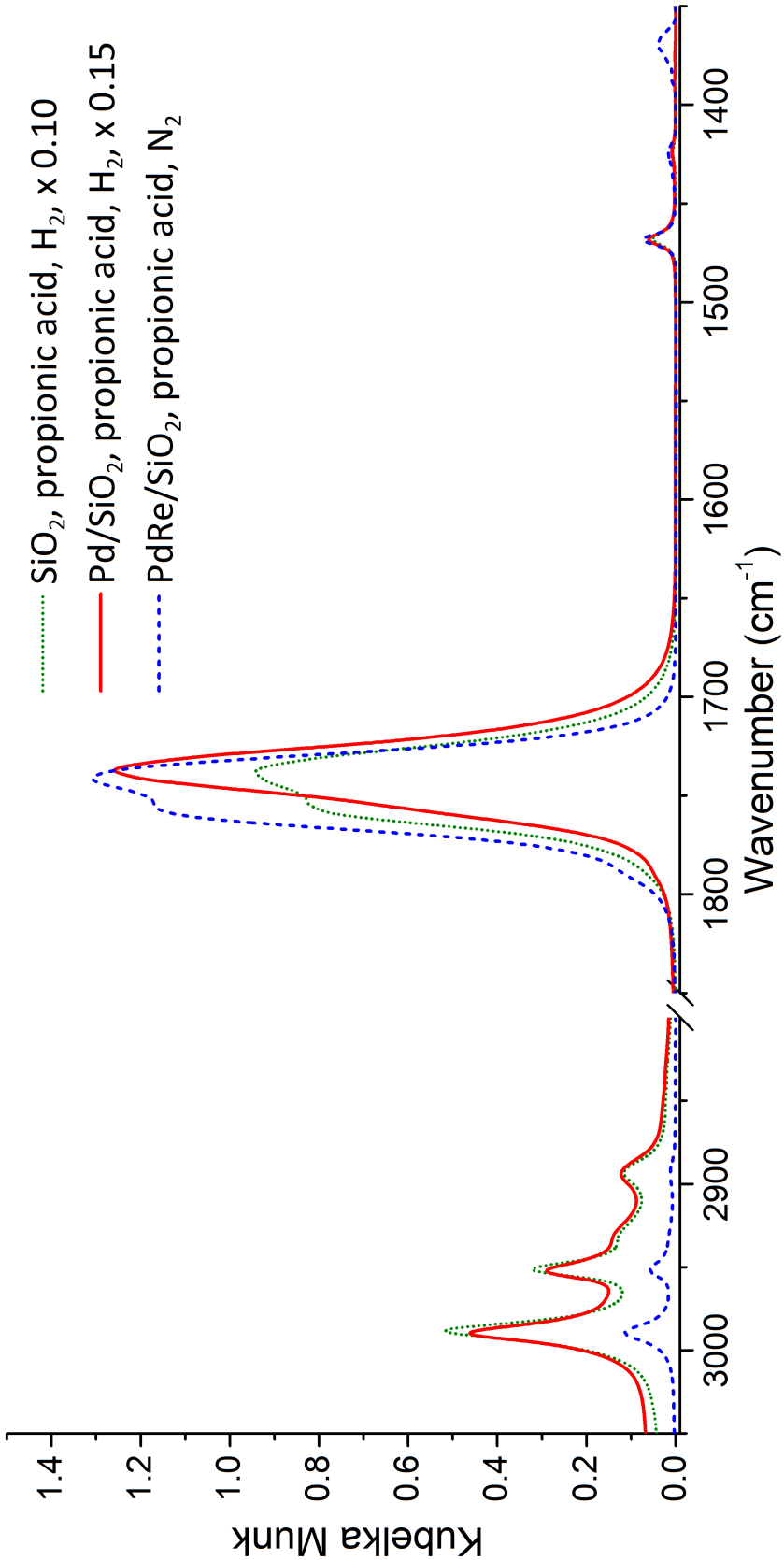

Figure B.2: Diffuse reflectance spectra of SiO_2 and Pd/SiO_2 in 0.3 kPa propionic acid and 0.1 MPa H_2, compared to $PdRe/SiO_2$ in 0.3 kPa propionic acid and 0.1 MPa N_2.

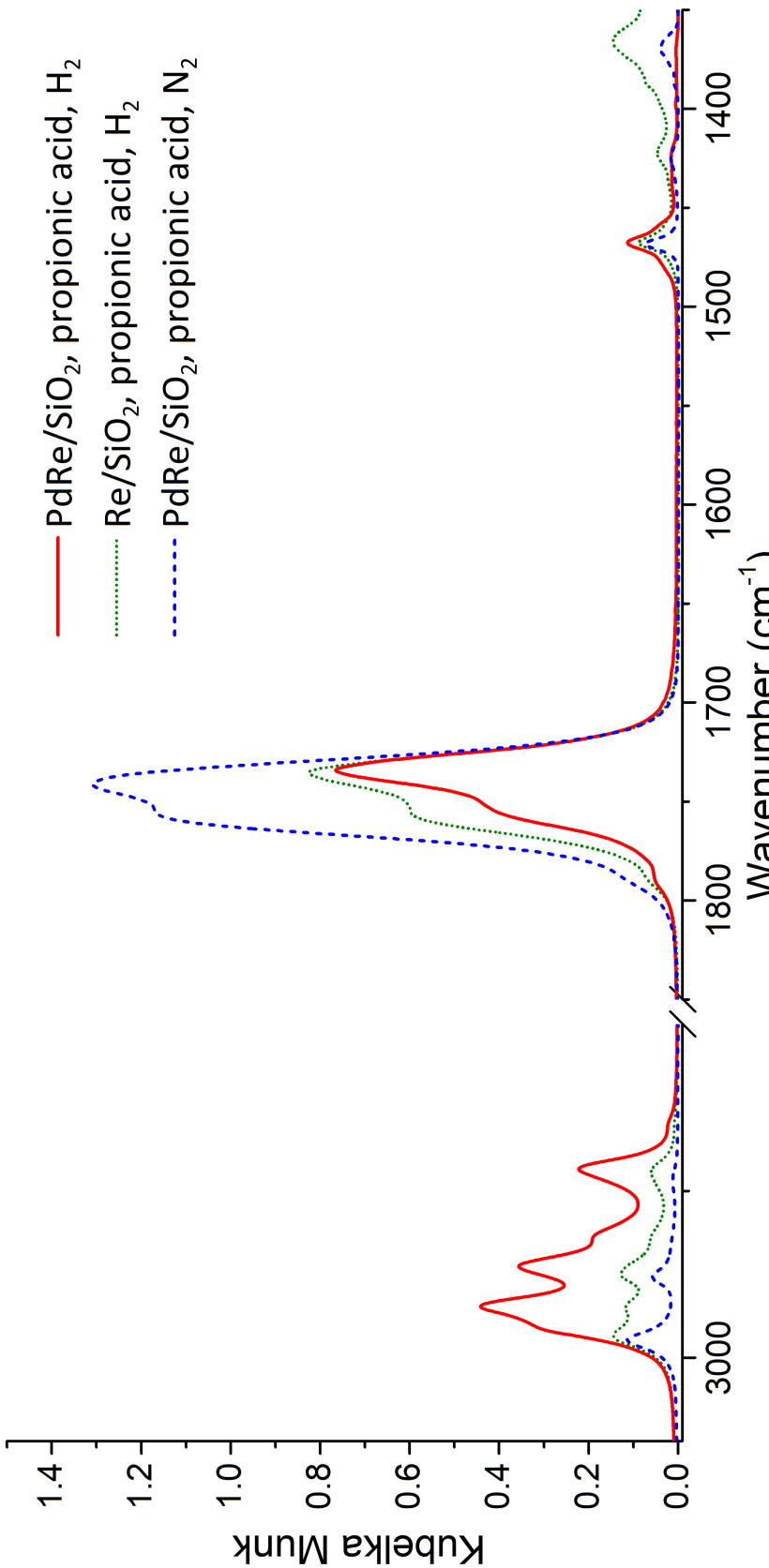

Figure B.3: Diffuse reflectance spectra of PdRe/SiO_2 and Re/SiO_2 in 0.3 kPa propionic acid and 0.1 MPa H_2, compared to PdRe/SiO_2 in 0.3 kPa propionic acid and 0.1 MPa N_2.

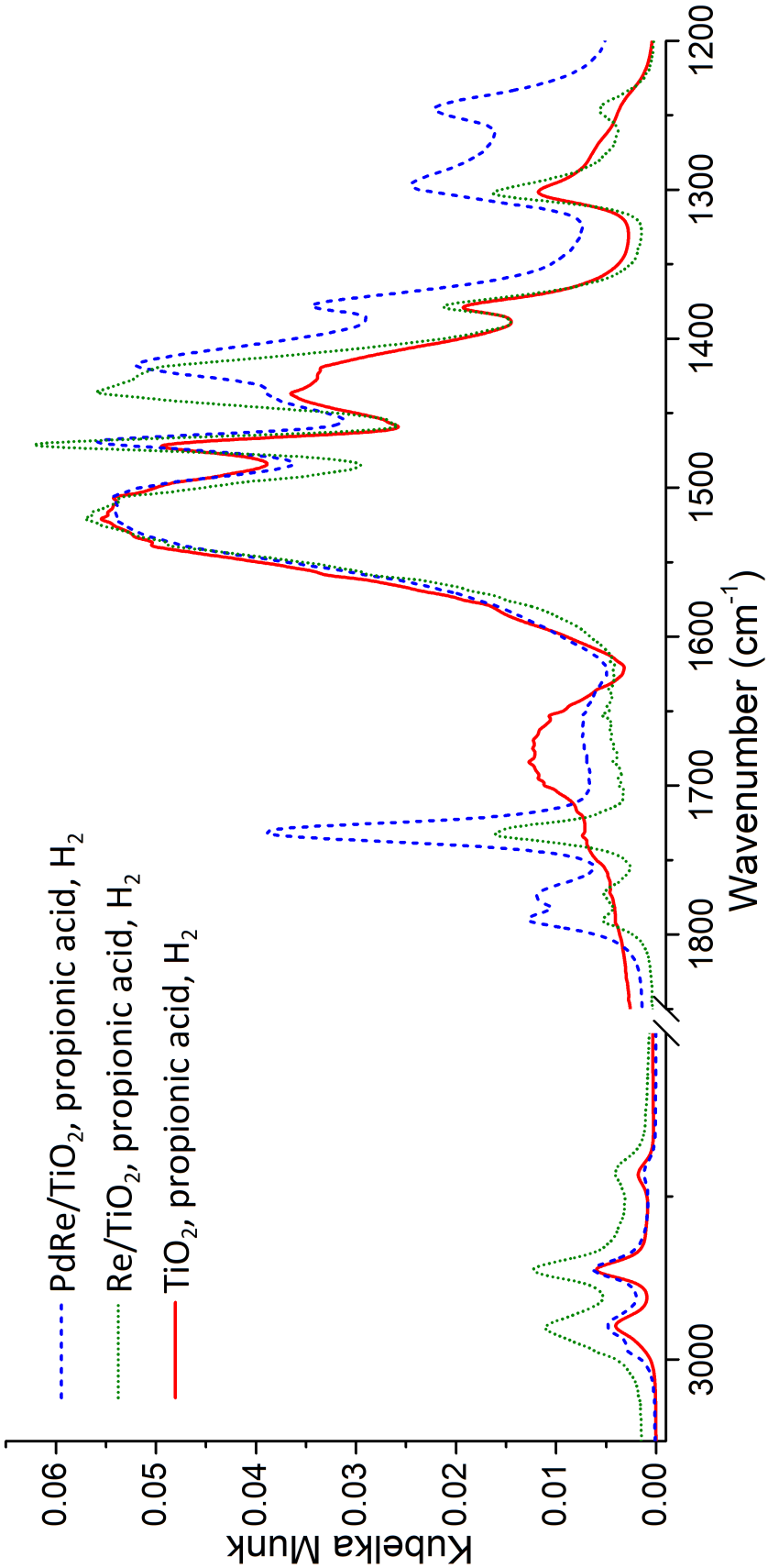

Figure B.4: Diffuse reflectance spectra of $PdRe/TiO_2$ and Re/TiO_2 compared to TiO_2 in 0.3 kPa propionic acid and 0.1 MPa H_2.

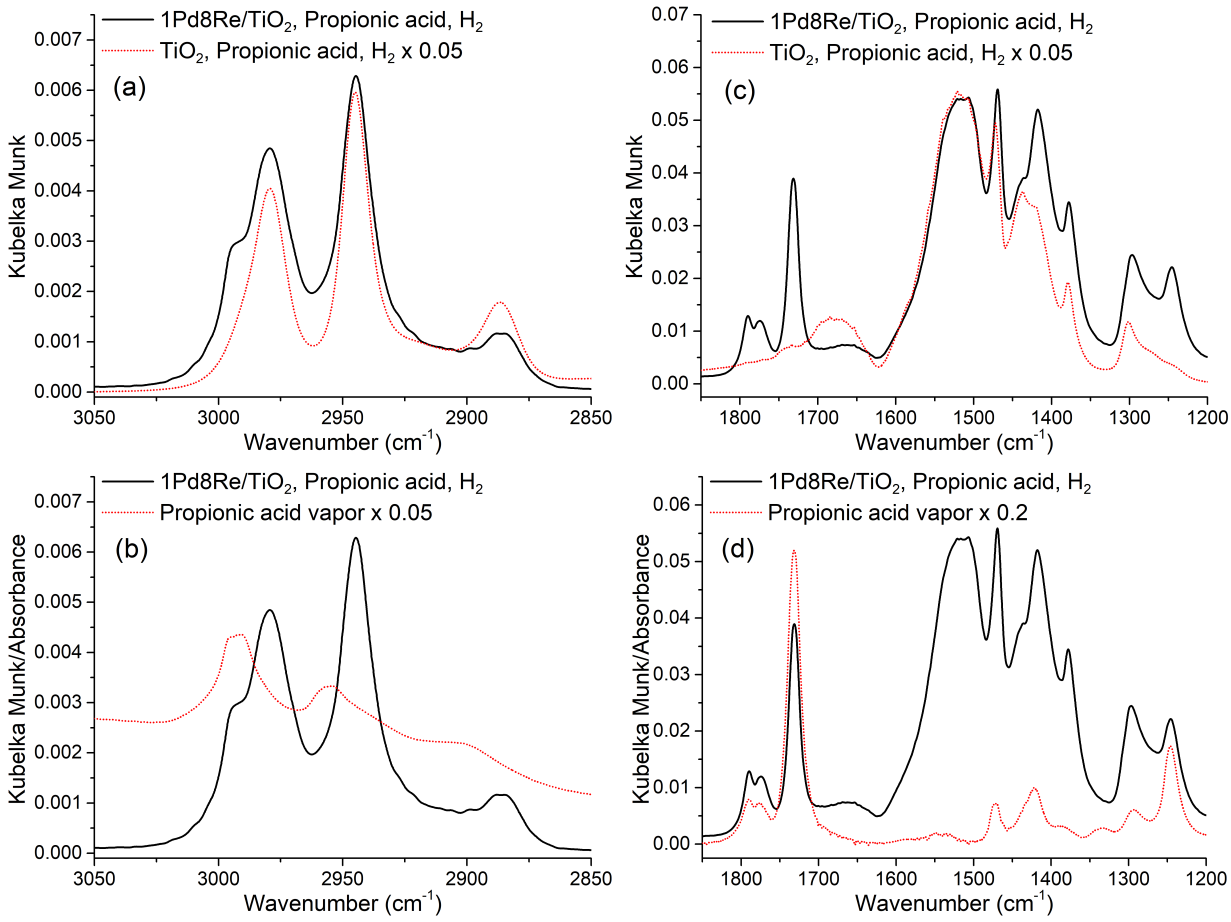

Figure B.5: Spectra obtained during *in situ* DRIFTS over $PdRe/TiO_2$ and TiO_2 or gas phase transmission in 0.3 kPa propionic acid, 0.1 MPa H_2 at 413 K in the (a) C-H stretching region, (b) compared to gas phase propionic acid, (c) carbonyl/backbone vibration region, (d) compared to gas phase propionic acid, collected in transmission mode.

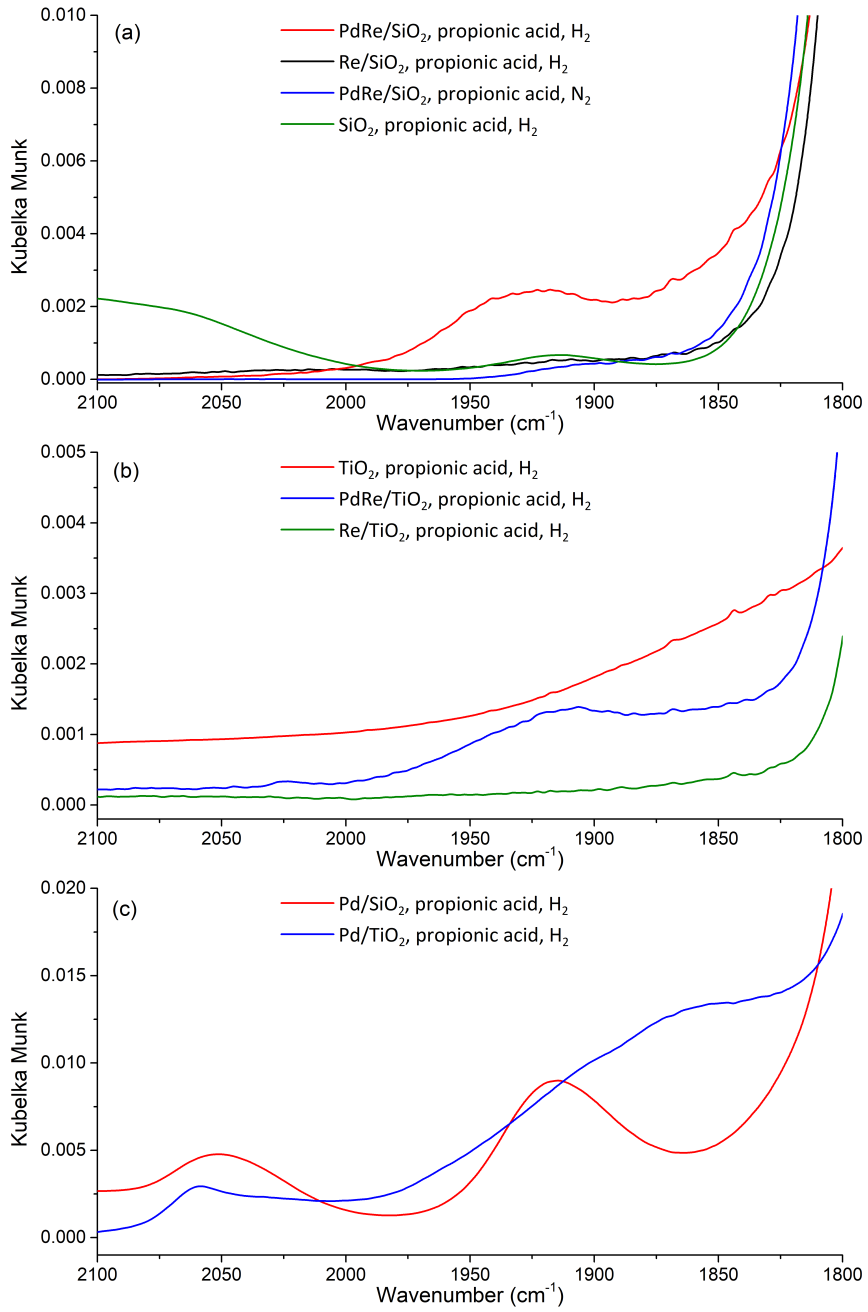

Figure B.6: C≡O stretching region of (a) SiO_2-supported Re catalysts, (b) TiO_2-supported Re catalysts, and (c) supported Pd catalysts, illustrating that the reduction of propionic acid in the presence of Pd leads to the formation of C≡O features, likely associated with CO bound to Pd or Re.

Derivation of the rate laws for rate-determining C-OH or C-OH_2 bond breaking steps in the reduction of carboxylic acids to aldehydes

The adsorption of the carboxylic acid is assumed to occur dissociatively, to form a carboxylate species and surface hydrogen species. The adsorption of H_2 is assumed to dissociatively adsorb on two adjacent surface sites. The elementary steps of the reaction are shown below.

$$\begin{aligned}
H_2 + {}^{**} &\rightleftharpoons 2H^* && (S.1)\\
RCOOH &\rightleftharpoons RCOOH^* && (S.2)\\
RCOOH^* + {}^* &\rightleftharpoons RCOO^* + H^* && (S.3)\\
RCOOH^* &\rightarrow RCO^* + OH^* && (S.4)\\
RCOOH^* + H^* &\rightleftharpoons RCOOH_2{}^* + {}^* && (S.5)\\
RCOOH_2{}^* &\rightarrow RCO^* + H_2O && (S.6)\\
RCO^* + H^* &\rightleftharpoons RCHO + {}^{**} && (S.7)\\
OH^* + H^* &\rightleftharpoons H_2O + {}^{**} && (S.8)
\end{aligned}$$

The reaction scheme results in the following equilibrium relationships:

$$K_1 = \frac{[H*]^2}{[H_2]\,[*]^2} \qquad (E.1)$$

$$K_2 = \frac{[RCOOH*]}{[RCOOH]\,[*]} \qquad (E.2)$$

$$K_3 = \frac{[RCOOH*]\,[*]}{[RCOO*]\,[H*]} \qquad (E.3)$$

$$K_5 = \frac{[RCOOH_2*]\,[*]}{[RCOOH*]\,[H*]} \qquad (E.5)$$

The rate-determining steps, (S.4) and (S.6), are determined by the following expressions:

$$r_4 = k_4[RCOOH*] \qquad (R.4')$$

$$r_6 = k_6[RCOOH_2*] \qquad (R.6')$$

If the most-abundant reactive intermediate on the catalyst surface is assumed to be carboxylate species (as suggested by DRIFTS), then the site balance is given by:

$$[*]_0 = [*] + [RCOO*] \qquad (SB)$$

The equilibrium expressions and site balance can be substituted back into the rate expressions (R.4') and (R.6') to yield:

$$r_4 = \frac{k_4 K_2 [RCOOH]}{1 + \frac{K_2 K_3 [RCOOH]}{K_1^{1/2} [H_2]^{1/2}}} \qquad (R.4)$$

$$r_6 = \frac{k_4 K_1^{1/2} K_2 [RCOOH][H_2]^{1/2}}{1 + \frac{K_2 K_3 [RCOOH]}{K_1^{1/2} [H_2]^{1/2}}} \qquad (R.6)$$

Since the coverage of acid is saturated, the second term in the denominator is expected to outweigh the first, resulting in the effective rate laws:

$$r_4 \approx \frac{k_4 K_1^{1/2} K_2}{K_3} [H_2]^{1/2} \qquad (R_{eff}.4)$$

$$r_6 \approx \frac{k_4 K_1 K_2}{K_3} [H_2] \qquad (R_{eff}.6)$$

C

Supporting information for Chapter 4

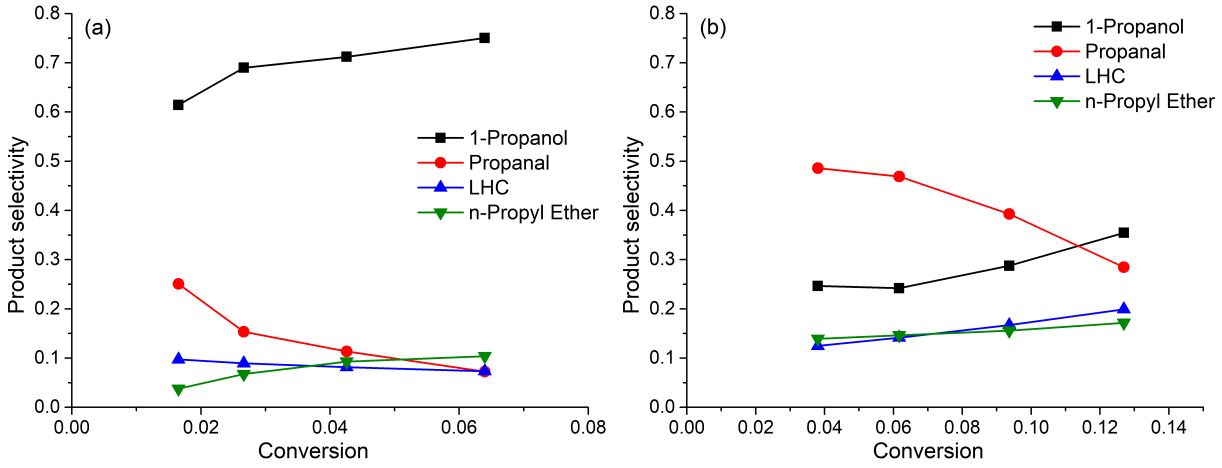

Figure C.1: Selectivity versus conversion for the reduction of propionic acid in 0.5 kPa propionic acid and 0.1 MPa H_2 at 413 K over (a) $PdPTA/TiO_2$ and (b) PdW/TiO_2. Solid lines are linear interpolation between data points.

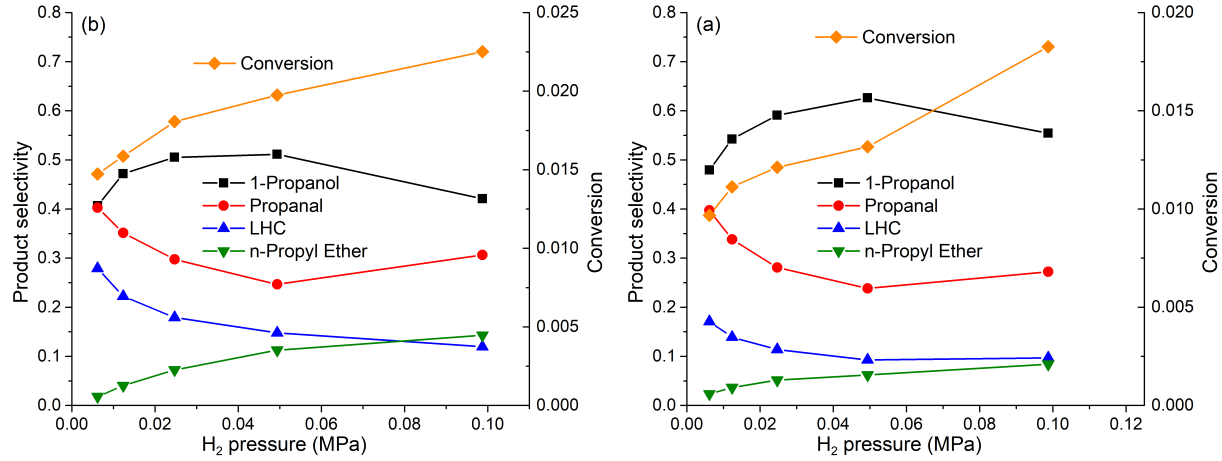

Figure C.2: Selectivity versus H_2 pressure for the conversion of propionic acid in 0.5 kPa propionic acid at 413 K over (a) PdW/TiO_2 and (b) $PdPTA/TiO_2$. Solid lines are linear interpolation between data points.

Table C.1: Comparison of rate of reduction of 0.5 kPa propionic acid in 0.1 MPa H_2 or D_2 at 413 K over PdW/TiO_2.

Catalyst	H_2/D_2	Conversion	Rate of reduction (mol g_{cat}^{-1} h^{-1})	Product selectivity				Overall isotope effect ($rate_H/rate_D$)
				1-Propanol	Propanal	LHC	*n*-Propyl ether	
PdW/TiO_2	H_2	6.7%	4.5×10^{-4}	0.74	0.07	0.07	0.11	**0.91**
	D_2	7.4%	4.9×10^{-4}	0.74	0.06	0.07	0.12	

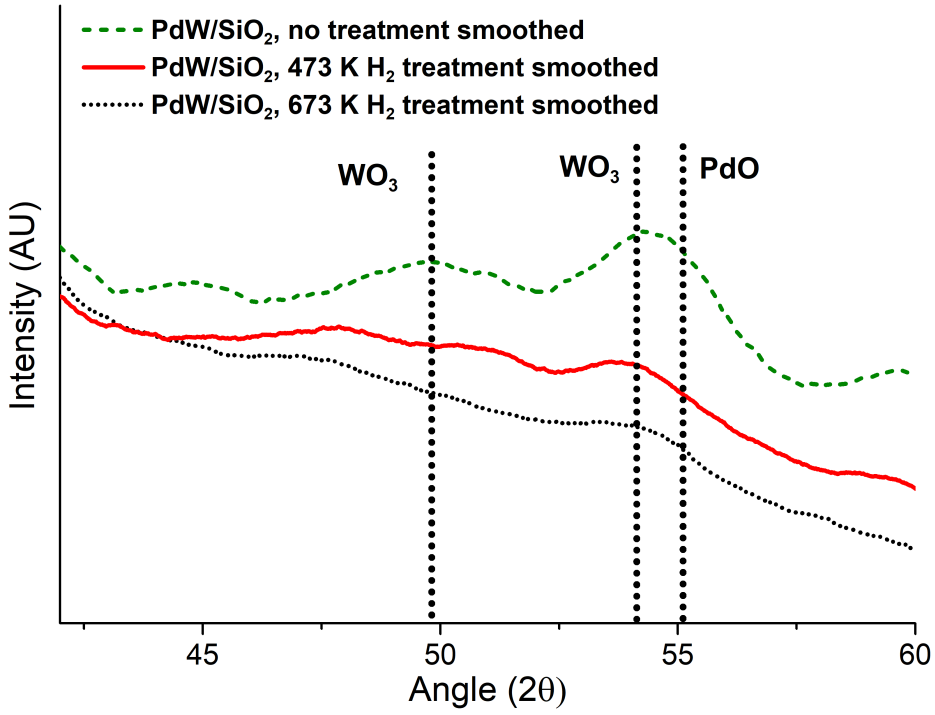

Figure C.3: PdW/SiO_2 before treatment and after treatment at 473 K or 673 K in flowing H_2. Catalysts were heated to the desired temperature at 5 K min^{-1}. Diffraction patterns have been smoothed for clarity.

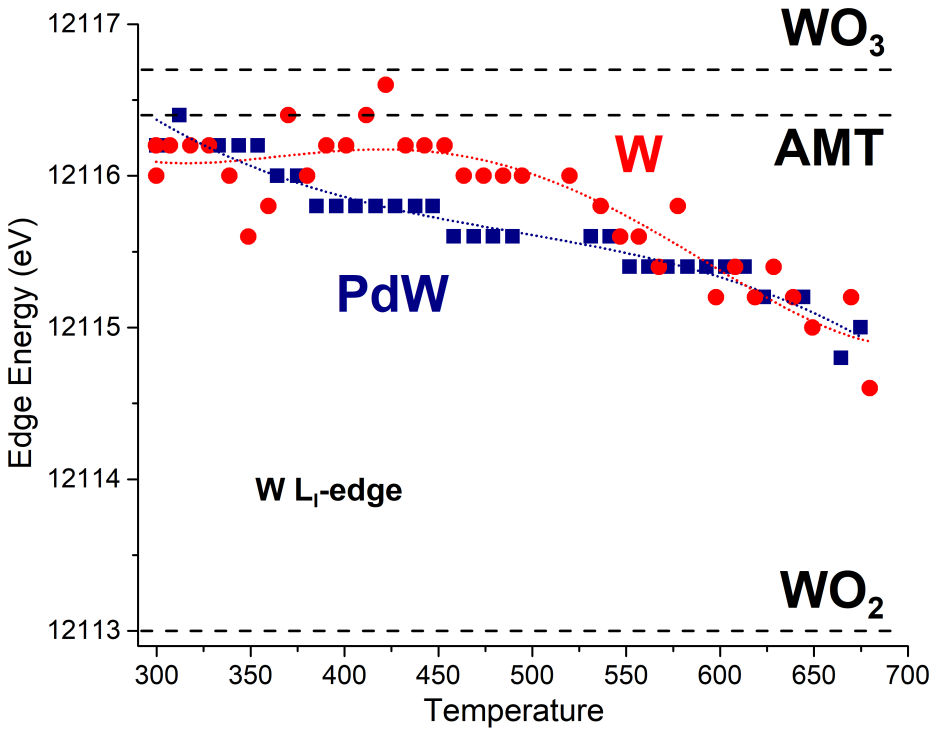

Figure C.4: The tungsten L_I-edge energy measured at 0.75 of the normalized μ(E) as a function of temperature for PdW/SiO_2 and W/SiO_2 during *in situ* TPR in 0.1 MPa flowing H_2. Dashed lines indicate the position of the standards, while dotted lines are present to illustrate the observed trend.

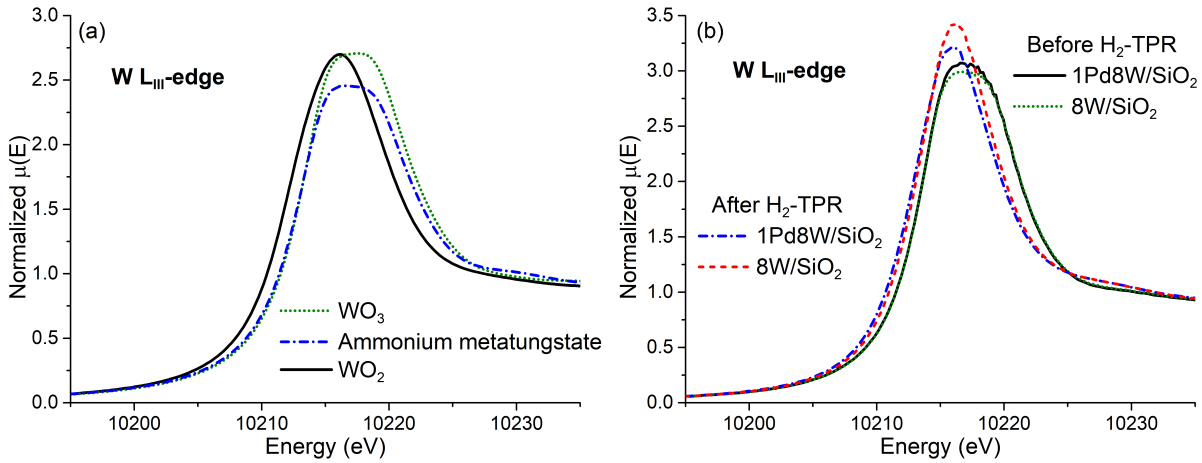

Figure C.5: (a) X-Ray absorption near-edge structure of (a) W oxide standards, and (b) PdW/SiO_2 and W/SiO_2 before and after H_2-TPR in 0.1 MPa H_2 to 673 K, collected at ambient temperature.

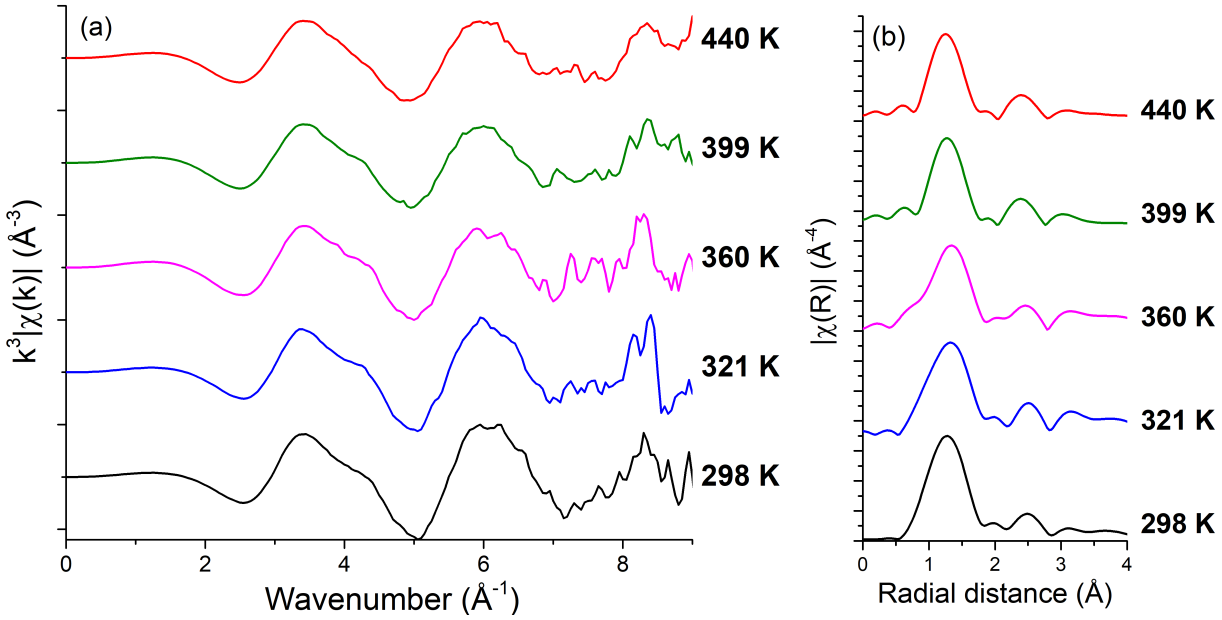

Figure C.6: Tungsten L_{III}-edge EXAFS of PdW/SiO_2 during H_2-TPR in 6% H_2/He showing (a) k^3 weighted oscillations in k-space and (b) magnitude of the Fourier transform (not phase-shift corrected) over the k range of 2.0 to 9.0 $Å^{-1}$.

Table C.2: Tungsten L_{III}-edge EXAFS fitting results for first shell W-O scattering paths in SiO_2-supported PdW during *in situ* temperature-programmed reduction in 6% H_2/He. A S_0^2 value of 0.9 was assumed to calculate the coordination number N.

Temp. (K)	R (Å)	N	σ^2 (Å^2)	ΔE_0 (eV)	R-factor
Ambient	1.83 ±0.02	3.6 ±0.82	0.0097 ±0.0037	-6.5 ±3.2	0.009
321	1.85 ±0.03	3.8 ±0.91	0.0117 ±0.0042	-4.5 ±3.3	0.01
360	1.87 ±0.03	4.3 ±0.88	0.0156 ±0.0039	-2.5 ±2.8	0.008
399	1.86 ±0.03	4.1 ±1.2	0.0157 ±0.0052	-4.3 ±3.8	0.02
440	1.85 ±0.04	4.2 ±1.3	0.0154 ±0.0057	-5.2 ±4.3	0.02

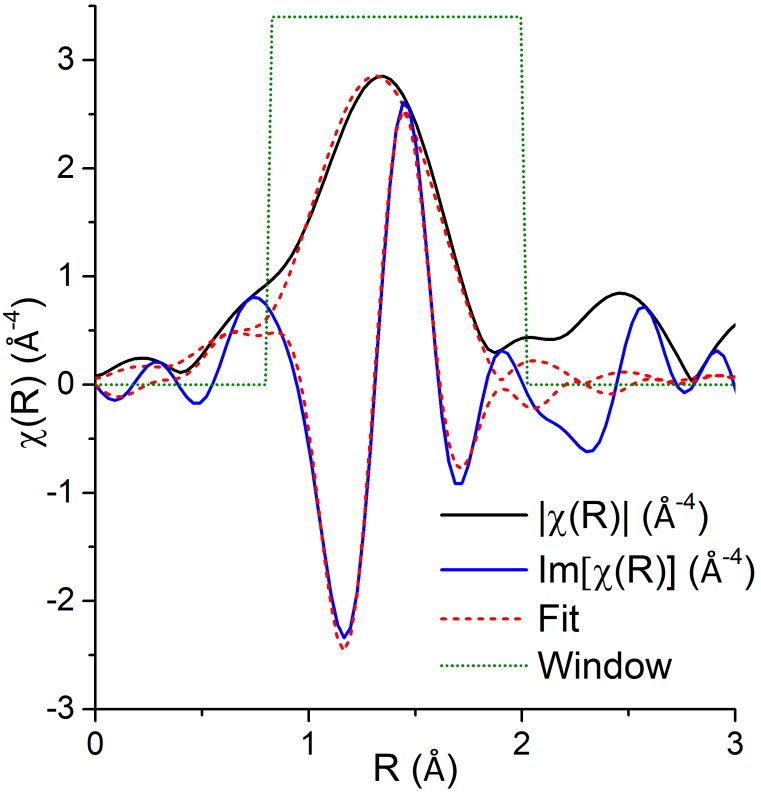

Figure C.7: Representative fitting of EXAFS results for PdW/SiO_2 during temperature-programmed reduction in 6% H_2/He at 360 K.

D

High-Throughput *Operando*-Ready X-Ray Absorption Spectroscopy Flow Reactor Cell for Powder Samples

Abstract

A high-throughput, *operando*-ready X-ray absorption spectroscopy cell consisting of 4 parallel reactors was designed to collect X-ray absorption near edge structure (XANES) and extended fine structure (EXAFS) spectra under reaction conditions. The cell is capable of operating at temperatures from ambient conditions to 773 K and pressures from ambient to 300 psig in a variety of gas environments. The cell design is mechanically simple, and programmable operation at beamline 8-ID (NSLS-II, Brookhaven National Lab) makes it straightforward to use. Reactor tube parts were available as-fabricated from commercial sources, while the heating jacket and cell mounting required custom machining.

D.1 Introduction

X-ray absorption spectroscopy (XAS) is a well-known technique for obtaining structural and electronic information about transition metal compounds. It is among a small but growing number of techniques that offers the opportunity to gain insights into the atomic structure and chemical state of reacting systems under true reaction conditions. The investigation of heterogeneous catalysts under operating conditions, utilizing *in situ* or *operando* techniques, is highly desirable to provide insights into the active chemical state of catalysts,[1] how catalysts evolve with time on stream,[2] and even the structure of single-site catalysts in zeolites.[3] Many more examples can be found in the literature, as the use of *in situ* XAS in the field of heterogeneous catalysis has become a standard practice. Further examples and more information can be found in the recent review by Bordiga et al. detailing the use of *in situ* X-ray techniques.[4]

The latest generation of synchrotron facilities has state-of-the art technology that utilizes

high fluxes of X-rays in monochromatic beams. Advances in the measurement of X-rays have resulted in the production of larger datasets and yielded greater insights than ever before.[5] The scan time required to obtain a single absorption spectrum has been reduced from hours to minutes and even seconds with a standard ion chamber X-ray detector. As a result, the rate-limiting step in data collection is no longer the counting of photons, but the introduction of appropriately prepared samples into the X-ray beam. However, heterogeneous catalysts often consist of loose powders or pellets that must be reshaped into appropriately thin, fragile wafers. These samples are time consuming to produce and are not optimal for *in situ* or *operando* investigation as they may crack due to temperature, pressure, or flow rate changes and compressed pellet geometry results in mass transfer effects on the measured rates of product formation. To investigate the behavior of heterogenous catalyst systems under reaction conditions, a number of design constraints must be considered. Reactions often occur at high temperatures, in pressures ranging from near vacuum to tens of MPa, and frequently take place in chemically-harsh environments. To draw meaningful conclusions about catalyst performance, accurate control of the temperature, pressure, and gas flow rate through each catalyst bed must be achieved. Robust construction materials that can withstand a wide range of temperatures and pressures are required, and the reactor must be made of materials that will not react and degrade under experimental conditions. If *operando* measurements are desired, the cell should allow for optimization of the loading of catalyst for spectroscopic analysis and the amount of product formed. Furthermore, the cell must meet stringent safety requirements demanded by the latest generation of synchrotron user facilities, where user safety is paramount and costly components can result in a high price for a small mistake. Finally, the cell must be compact enough to reside in a small space, frequently less than 1.5 ft in

any direction. Ideally, a packed-bed reactor that would require little modification from an experimental reactor setup could be used as the cell to best approximate the behavior of the catalyst under test reaction conditions in a laboratory.

Past designs for high throughput collection of X-ray absorption spectra include a sample holder capable of holding up to 6 self-supported wafers in flowing gas,[1] or from an 8-well microreactor that could be used to collect spectra *in situ* with control over the common gas flowed through each well.[6] This cell is reportedly able to control the independent flow through each microreactor well and analyze the effluent of each well independently. These cells, like many others in the literature, have unusual reactor configurations or require structural modification of the catalyst powder such as pelletization that would not be compatible with *operando* study. Aside from multiple-sample-holder-setups, multi-channel ionization chambers have been designed.[7] In the example by Ravel et al., a multi-channel detector was used for the simultaneous measurement of Re standards and the temperature programmed reduction of Ni/Al_2O_3 catalysts using H_2, demonstrating the effect of precursor on the Ni reducibility.[8] This type of design offers the possibility of truly simultaneous *operando* measurements, provided the samples can be packed in a small enough space and exposed to the desired reaction conditions.

To meet the need for both a high-throughput and *in situ* or *operando* capable reactor, a cell was designed to perform a wide variety of measurements on up to four samples in quick succession under a flexible range of temperature, pressure, and flowrate conditions. The cell designed herein draws from several past designs that have been used to investigate heterogeneous catalysts in packed bed reactors, including designs by Bare et al.[9,10], Fingland et al.,[11] Shou and Davis,[12] and Hoffman et al.[13] It also takes advantage of the movable reactor stage available at beamline

8-ID, housed in Brookhaven National Laboratory's state-of-the-art NSLS-II. The functionality of the cell has been demonstrated by performing a temperature-programmed reduction (TPR) of various transition-metal-promoted Mo/SiO_2 catalysts using H_2, for comparisons to catalytic activity and hydrogen consumption obtained during H_2-TPR.

D.2 Experimental and Cell Construction

D.2.1 XAS Measurements

The *in situ* reactor cell was operated at beamline 8-ID of the National Synchrotron Light Source II (NSLS-II) at Brookhaven National Lab. The storage ring was operated at 3.0 GeV, and had a beam current of approximately 325 mA. The beamline was equipped with a high-power damping wiggler to deliver a high flux of photons and the beamline monochromator was driven by a direct drive servo motor to allow for continuous scanning, so that scans could be taken on the order of seconds. More details about the beamline can be found in the beamline summary by Palomino et al.[5] *In situ* H_2-TPR probed by X-ray absorption spectroscopy was carried out at the Mo K-edge *ca.* 20 keV. To perform the *in situ* temperature programmed reduction, 60 mg of metal-promoted 4 wt.% Mo (containing M:Mo of 1:4, Pd, Cu, Ag, or Ni) was loaded into each tube in the *in situ* reactor. The catalyst beds were sandwiched between two plugs of graphite wool (AvCarb Felt G200). Before beginning the H_2-TPR, each tube of the reactor cell was flushed with He at 20 cm^3 min^{-1} for 10 min. The gas flow was then switched to 6% H_2/He at 20 cm^3 min^{-1} and the cell temperature was increased linearly from 298 K to 700 K at a rate of 5 K min^{-1}. Scans were taken every 45 s, for a temperature differential between subsequent scans of the same sample of approximately 15 K.

D.2.2 Catalyst Preparation and Characterization

Supported Mo catalysts promoted by Pd, Cu, Ni, and Ag were prepared by a sequential incipient wetness impregnation method. A loading of 4 wt.% Mo (ammonium heptamolybdate tetrahydrate, Strem Chemicals, 99.98%) was added to 5 g of high-surface-area SiO_2 (Fuji Silysia Chemical Ltd., 0.72 $cm^3\ g^{-1}$, 511 $m^2\ g^{-1}$) by impregnating the support to the point of incipient wetness and mixing until the solution was homogeneously distributed throughout the support particles. The mixture was dried overnight at 383 K, before it was heated to 773 K over 3 h in flowing air at 100 $cm^3\ min^{-1}$, treated in flowing air at 773 K for 3 h, then cooled to room temperature (298 K). After Mo was added, a promoter (Pd, Cu, Ni, or Ag) was added using the same procedure (using solutions of tetraaminepalladium(II) nitrate, 10 wt%, Aldrich, copper(II) nitrate trihydrate, Sigma Aldrich, 99-104%, nickel(II) nitrate hexahydrate, Aldrich, 99.999%, or silver nitrate, Sigma Aldrich, $\geq$99.0%, which was added under low-light conditions) in a ratio of 1 promoter atom to every 4 Mo atoms resulting in 1 wt.% Pd or Ag or 0.6 wt.% Cu or Ni promotion. Catalysts were stored under ambient conditions prior to use.

Temperature programmed reduction using 5% H_2 in Ar (Praxair, certified mixture) (H_2-TPR) was carried out using a Micromeritics Autochem II 2920 with thermal conductivity detector (TCD). A mass of 100 mg of each of the as-synthesized samples was supported on a bed of quartz wool in a U-shaped reaction tube, and were ramped at a rate of 10 K min^{-1} in 50 $cm^3\ min^{-1}$ 5% H_2 in Ar over a temperature range from 305 to 1273 K. Effluent gas was flowed through a stainless-steel loop submerged in a dry-ice and 2-propanol cooling bath to trap water before feeding the dried gas to a thermal conductivity detector (TCD). The inverse TCD signal (indicative of H_2 consumption) and temperature were recorded as a function of time.

D.2.3 Reactor tube and window construction

The tubular reactors are designed to be able to retain a bed of catalyst powder in the X-ray beam in the same configuration as a packed-bed reactor. The reactor design is shown in Figure D.1. Here, each reactor is a 6-in. long, 1/4-in. O.D. 316 stainless steel tube (Swagelok SS-T4-S-035-20) but the tube could be made of a variety of materials including stainless steel, graphite, or beryllium if desired. The tubular reactors are attached to three-way tees (Swagelok SS-400-3-4TFT) at the inlet and outlet of each tube as shown in Figure D.1. A 1/4-inch male NPT (MNPT) to VCR fitting (Swagelok SS-4-VCR-1-4) used to fix the windows to the ends of the reactors. The reactor tubes are swaged to the tees opposite the FNPT fittings, and a 1/4-inch reducing port fitting to 1/8-inch tube adapter (Swagelok SS-401-PC-2) was fixed to the perpendicular at the tee. A Swagelok 1/8-inch quick-connect (Swagelok SS-QM2-B-200 or SS-QM2-D-200) was attached to the 1/8-inch tube adapter to allow for easy connection/disconnection of each reactor individually. At each end of the reactor tube, the three-way tee could be inserted into a bracket that held up to four of the tubes in line with the long direction of the reaction cell base plate. A small screw on the top of each bracket was used to hold the tubes in place during use by compressing the 3-way tees at the end of each tube together. This was necessary to avoid rotating the tubes and moving the sample while the beamline's moving stage was in use. The base of the bracket was mounted to a 1/2-inch thick aluminum baseplate, where it sat in two machined grooves that allowed the brackets to slide to or from the center of the baseplate, to facilitate mounting the four tubes in the center of the heating block. Reactant gases were supplied to each tube independently via an array of 4 MKS mass flow controllers. Flexible copper tubing leading from the flow controllers to the reactor cell allowed for unimpeded vertical motion of the

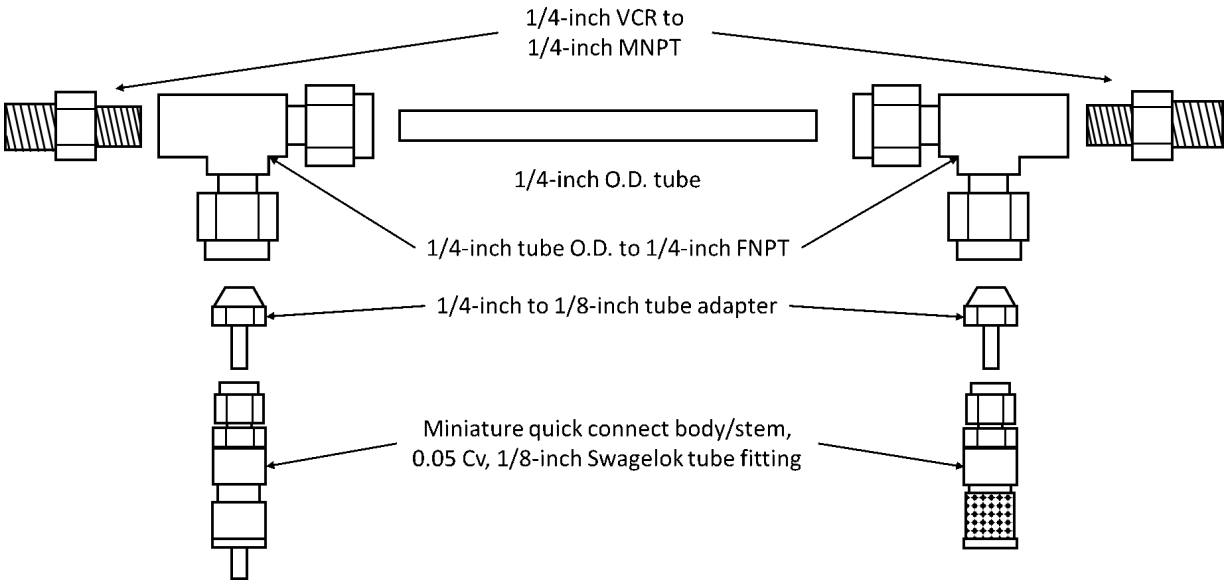

Figure D.1: Design of the reactor tube used for the *in situ* collection of X-ray absorption spectra.

cell to align each set of windows with the X-ray beam path.

The FNPT fittings at the ends of the two reactor three-way tees were used to mount the cell windows, which were attached to the two 1/4-inch MNPT to 1/4-inch VCR adapters. A 1/2-inch diameter hole punch was used to produce 1/2-inch diameter circular pieces of Kapton. Instead of a VCR seal, a 1/2-inch O.D. Viton washer with I.D. 0.17 inches (the inner diameter of the 1/4-inch reactor tube), the Kapton window, and a stainless-steel washer of the same dimensions as the Viton washer were placed inside the VCR nut in the configuration shown in Figure D.2. When the VCR nut was tightened onto the VCR fitting, the stainless-steel washer and Kapton window were compressed against the Viton washer from the outside of the cell, while the VCR fitting sealing surface pressed against the Viton washer from the inside of the cell, creating a gas-tight seal that was capable of withstanding pressures of over 300 psig when 0.02-inch Kapton windows were used. This modular window design was chosen to provide flexibility with regard to the reactor pressure, as changing reactor windows can be done rapidly and all windows

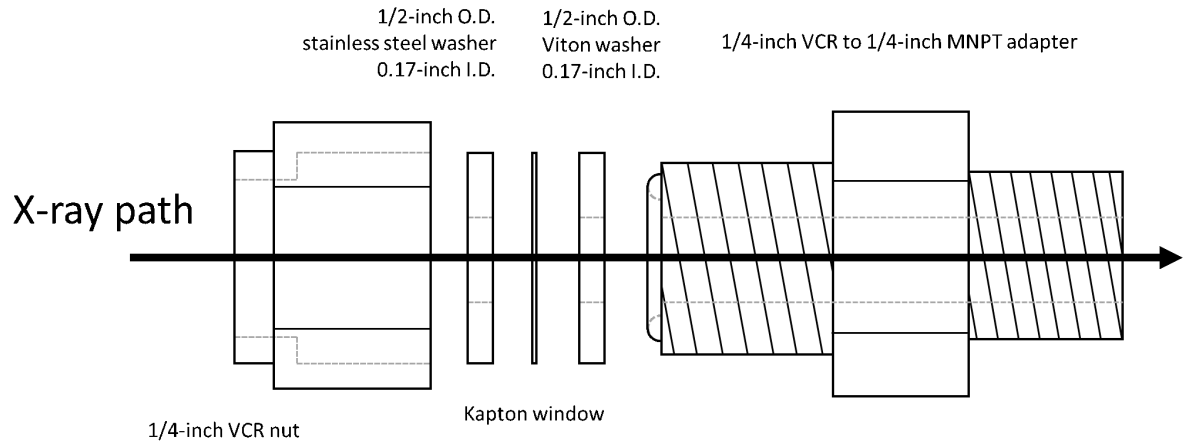

Figure D.2: Design of the modular windows for the reactor tubes used for the *in situ* collection of X-ray absorption spectra.

and sealing materials used can be re-used. The window design is shown in Figure D.2.

D.2.4 Heating block design

An aluminum block 3 inches by 4 inches by 1.5 inches was machined to the specifications in Figure D.3 for use as a heating jacket for the reactor tubes. Four 3/8-inch diameter holes were drilled through the block along the centerline of the 1.5-inch-wide face of the block to allow the reactor tubes to sit inside the aluminum block as shown in Figure D.5(top and middle). The block was then cut in half vertically, splitting the reactor through-holes into two halves, designated (1) and (2) in Figure D.3. A total of 10 holes were drilled on the 1.5-inch wide side, 2.5 inches deep, to allow for the 10 1/4 inch OD cartridge heaters to be inserted into the aluminum block. On the 3-inch by 4-inch faces, 4 holes were drilled through to allow for a 1/16-inch thermocouple to be inserted into the center of each of the reactor channels to measure the temperature on the external surface of each reactor tube. At the top and bottom of this face, a fitting was made for a 1/4-20 bolt to hold the two halves of the heating block together. Steel helicoil inserts in these two fittings were added to prevent the malleable aluminum fittings from being stripped during

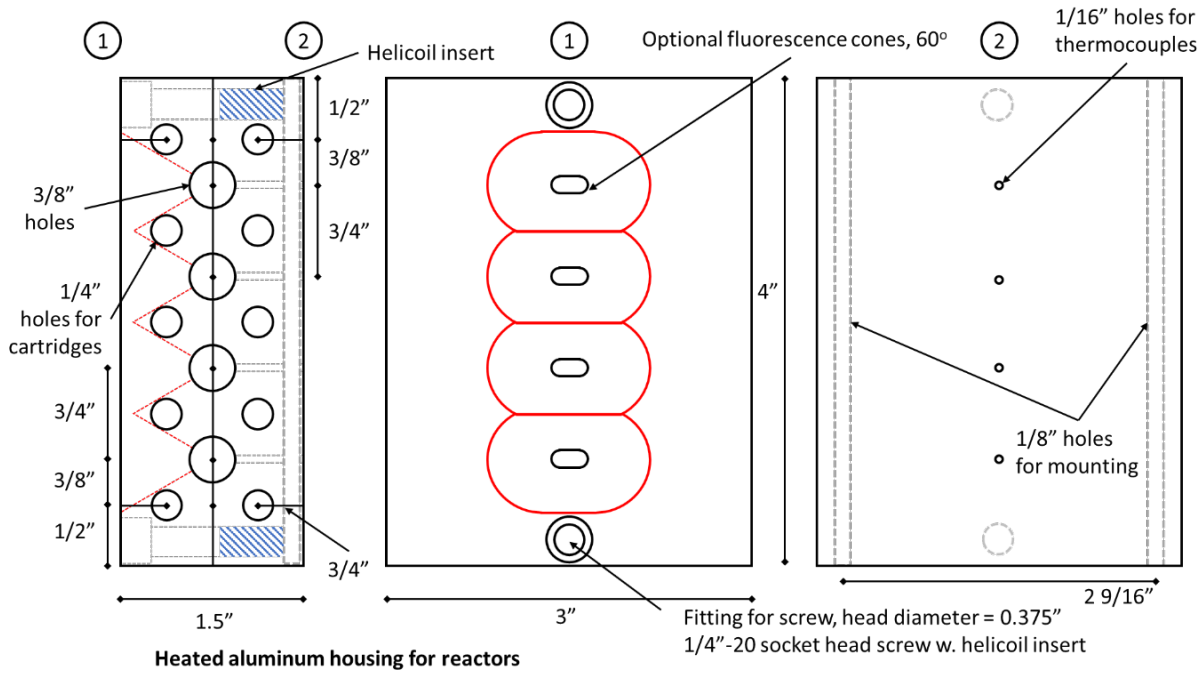

Figure D.3: Design of the aluminum reactor cell heating block, shown with optional drilled fluorescence cones.

repeated use. Vertical 1/8-inch holes were drilled through the block to hold the heating block in place around the reactor tubes as shown in Figure D.3 and Figure D.5 (complete assembled cell). The heating block was also insulated with 0.5-inch-thick calcium silicate insulation, machined to fit flush around the through-block fittings. The heating block sat on a piece of calcium silicate insulation that was supported by 4 stainless steel legs attached to the baseplate. On side (2) (see Figure D.3), two 1/8 inch threaded rods were inserted through the entire heating block, insulation layer, and mounting legs through the 1/8 inch mounting holes, which held the heating block in place vertically.

The 10 cartridge heaters were inserted into the aluminum block in the 10 cartridge holes discussed earlier. The electrical leads for each cartridge were attached in parallel to a terminal block mounted on the cell baseplate and covered by a rubber flap to prevent accidental contact

with the terminal block during operation of the cell. Power was supplied through a connection from the terminal block to a grounded NEMA 5-15P connector. The ground wire of the NEMA 5-15P connector was attached to the cell baseplate. The temperature was controlled using an Omega CN7800-series PID controller equipped with a solid-state relay to supply heating power from a 120 V source.

Optionally, conical slits could be drilled into the heating block on one side as shown in Figure D.3, allowing for the use of an X-ray transparent tube (e.g. graphite, beryllium) to collect fluorescence spectra of the catalyst bed. The vertical vertex angle of each cone was 60 degrees measured from the center of the reactor channel in the heating block, to avoid intersecting the channels containing the heating cartridges. In theory, the reactor tubes can be heated in whatever way is most convenient for a user based on needs, provided even heating is achieved throughout the sample area, as only the geometry of the reactor tubes is relevant to spectral collection.

Performance of the heating block was validated by varying the temperature measured at the outside of the reactor tube using the drilled channel in the heating block. The temperature inside the reactor tubes was measured with 25 cm^3 min^{-1} of He flowing through each tube by removing the Kapton window from the downstream end of each reactor tube and inserting a 1/16 inch thermocouple into the cell. A 1/16-inch ferrule swaged to the thermocouple to prevent the thermocouple tip from contacting the reactor walls. The results of the validation are shown in Figure D.4(a), with He flowing from high thermocouple distances to low thermocouple distances (right to left, as shown). Thermocouple distances from 11 cm to 19 cm fall within the insulated block, with a thermocouple distance of 15 cm corresponding to the center of the block. The central point was measured to be the hottest point in the block, with some asymmetry on either

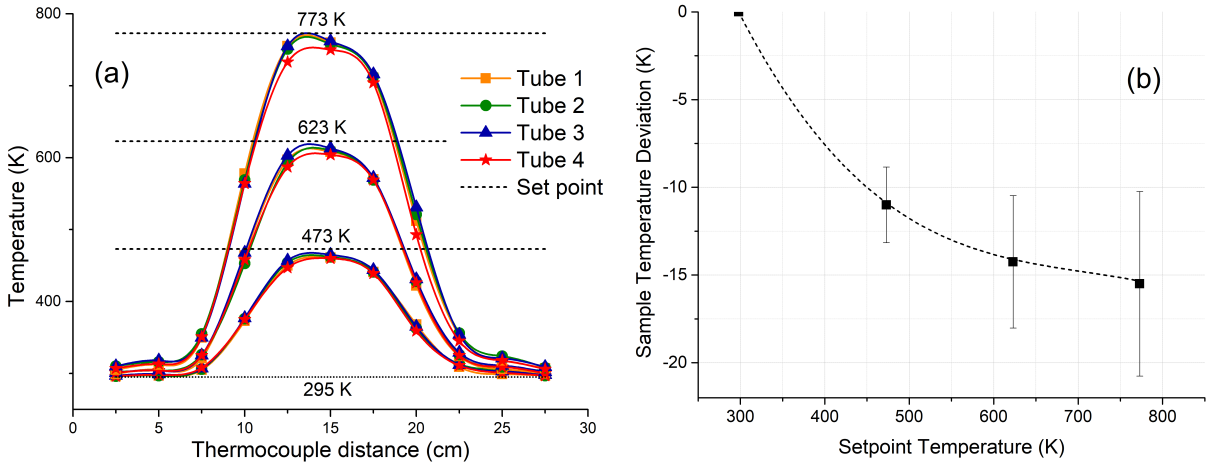

Figure D.4: (a) Validation of the performance of the heating block for the *in situ* cell, showing the temperature measured in the center of each reactor tube at positions along the length of the reactor as the setpoint was varied and He was flowed through each tube from right to left (high to low thermocouple distance). (b) Deviation of the hot zone temperature from the set point temperature, with dashed line to indicate the trend.

side likely due to heat transport by convection through the flowing gas. This hottest point was from 8-23 K below the setpoint temperature depending on the setpoint. A correction based on measured temperature can be found in Figure D.4(b). The points at 12.5 and 17.5 cm fell within the insulation on either end of the block, indicating only slight temperature decrease within the heating block. Outside the insulated section of the block at 10 cm and 20 cm, the temperature begins to drop rapidly. Once the windows are reached, the reactor tube temperature remains only 5-10 K higher than the external temperature. The heating block that was tested was constructed out of aluminum, which should not be heated above 773 K during the cell operation as the melting point of aluminum is 933 K. However, replacement of the block with one made from a more temperature-resistant material or ceramic furnace would increase the maximum allowed temperature of the cell.

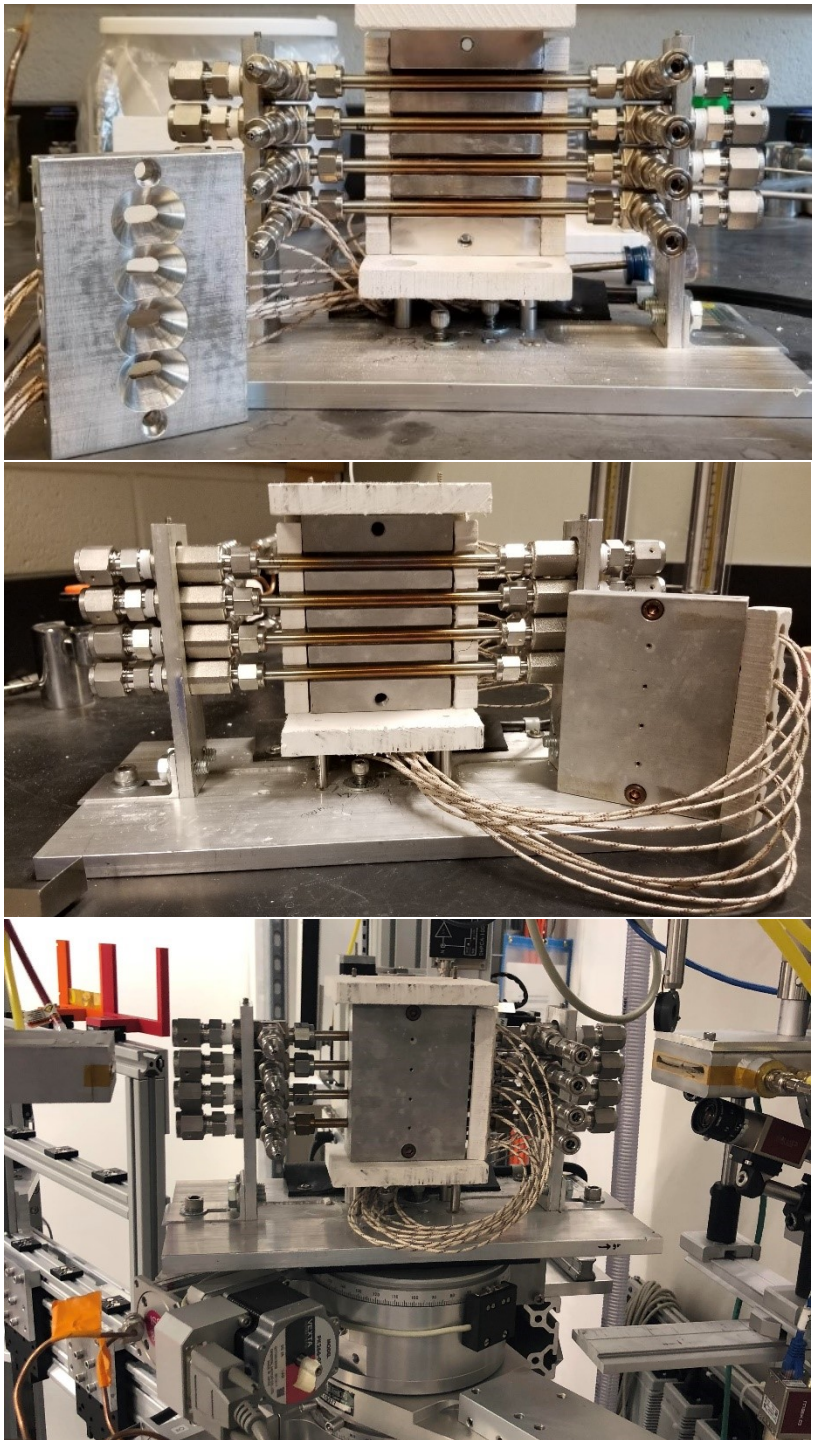

Figure D.5: Top, Middle: Completed reactor cell, with (top) and without (middle) optional fluorescence cones drilled in the heating block. **Bottom:** Reactor cell sitting on the goniometer (rotating stage) in the hutch at 8-ID, after alignment of the tubes with the X-ray beam. Some of the insulation has been removed to display the aluminum transmission heating block with 1/16-inch holes for thermocouple insertion.

D.3 Results and Discussion

D.3.1 Temperature-Programmed Reduction

Temperature programmed reduction using a TCD to detect H_2 was carried out to determine if various reducible metal promoters resulted in differing oxidation states of Mo. The H_2-TPR results are summarized in Figure D.6, where it is evident that H_2 consumption alone is not enough information to determine the Mo oxidation state directly. The H_2-TPR study revealed that there are a number of H_2 consumption peaks in each of the M-promoted Mo catalysts, each of which might correspond to the reduction of at least one metal component of each catalyst. The Pd-promoted Mo began to reduce in H_2 at near-ambient conditions, as low as 320 K. This behavior is expected for Pd-containing materials, indicating reduction of PdO in the as-synthesized material. Subsequent H_2 consumption peaks appeared at 490 K, and then as a broad feature from 700 to 1100 K containing at least two distinct reduction features. The Cu-promoted Mo demonstrated reached a maximum H_2 consumption at 520 K indicative of reduction of CuO,[14] followed by continued H_2 consumption over the range of the temperature treatment. The Ag-promoted Mo demonstrated a lower-temperature pair of H_2 consumption peaks around 390 K and 410 K, consistent with reduction of Ag_2O to Ag,[15] followed again by continuous H_2 consumption over the range of the temperature treatment. The Ni-promoted Mo demonstrated no H_2 consumption until 640 K consistent with reduction of NiO,[16] reaching a maximum at 690 K, followed again by sustained H_2 consumption over the range of the experiment in at least two distinct consumption peaks. In each case, it appeared that the promoting metal must be reduced in order to promote any reduction of the Mo component.

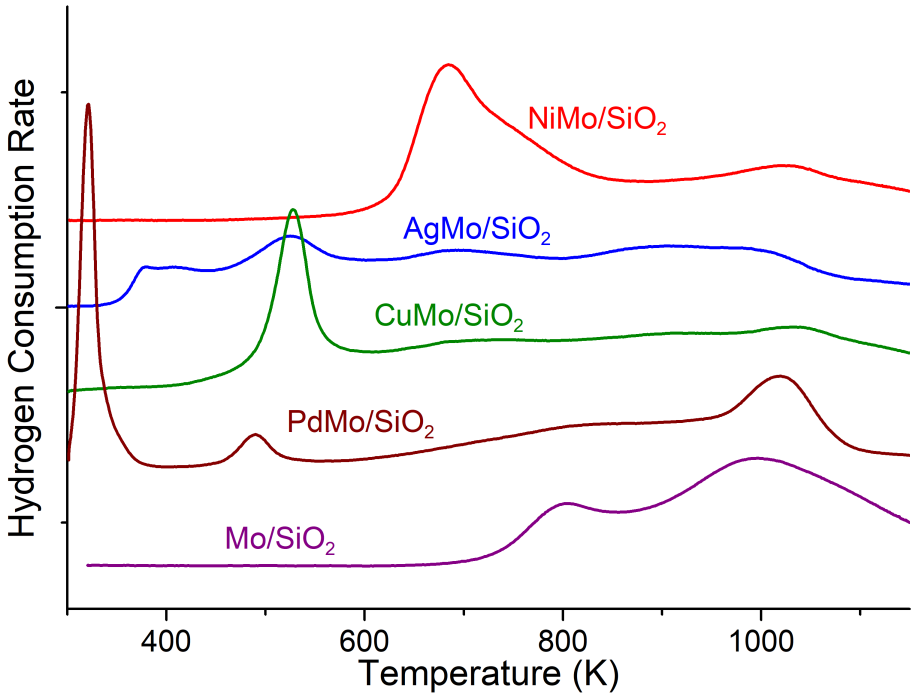

Figure D.6: Temperature programmed reduction of M-promoted MoO_x/SiO_2 catalysts.

D.3.2 *In situ* X-Ray Absorption Spectroscopy

In situ X-ray absorption spectroscopy was used to determine the oxidation state of the Mo in the Pd, Cu, Ag, and Ni-promoted Mo/SiO_2 materials as a function of reduction temperature (FigureD.7). The oxidation state of metal-promoted Mo/SiO_2 during H_2-TPR *in situ* in the constructed high-throughput XAS cell was determined by the position of the Mo K-edge absorption edge energy at a normalized height of 0.5. Based on these results, it is evident that Pd-promoted Mo undergoes low-temperature reduction upon exposure to H_2, followed by a small reduction feature at about 480 K and then sustained reduction above 550 K. Both Cu- and Ag-promoted Mo begin to reduce at above 500 K, with very similar reduction behavior. As suggested by H_2-TPR earlier, Ni-promoted Mo does not undergo reduction until after NiO is expected to be reduced at above 640 K.

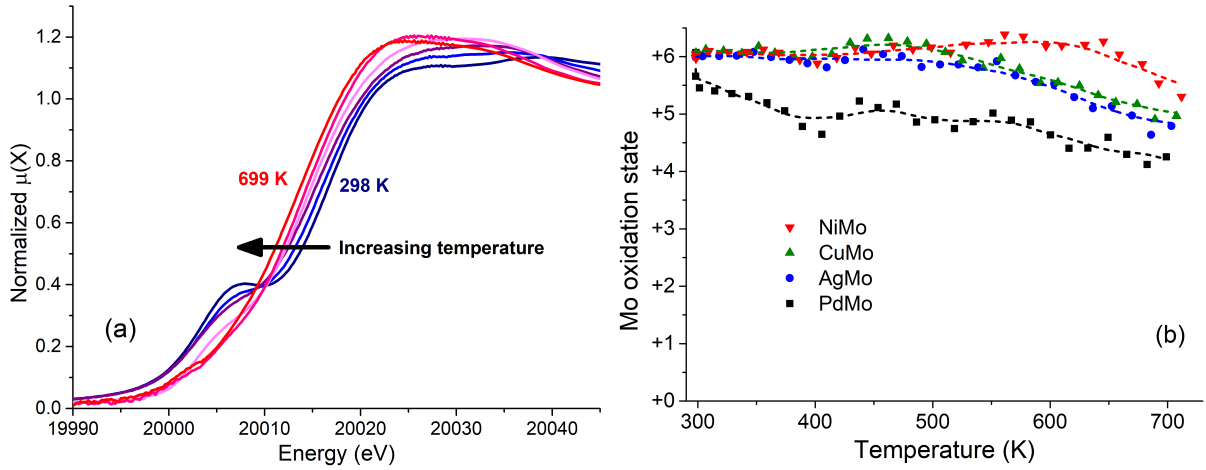

Figure D.7: (a) Mo K-edge XANES of $PdMo/SiO_2$ measured during H_2-TPR using 6% H in He to demonstrate observed change in the Mo K-edge position. (b) Experimentally determined oxidation state of 4% Mo/SiO_2 promoted by Ni, Cu, Ag, and Pd during near-simultaneous temperature programmed reduction in 6% H_2 in He from 298 K to 710 K. Dashed lines are to indicate trends.

The X-ray absorption fine structure spectra that were collected during *in situ* H_2-TPR could also be qualitatively analyzed. Usable EXAFS spectra were obtained for all 4 samples during the H_2 TPR, and approximately 120 total usable spectra were collected over the 2-hour temperature ramping experiment. Qualitative information was obtained from the intensities and peak positions from the Fourier transform of the k-space EXAFS oscillations, take from a k-range of 2.3 to 12 $Å^{-1}$.[17] A subset of the EXAFS spectra and corresponding Fourier transforms collected during *in situ* H_2-TPR of $PdMo/SiO_2$ is plotted in Figure D.8. Results from the XANES indicated that reduction of Mo began immediately after beginning the H_2 feed. Correspondingly, the shortest Mo-O scattering path intensity immediately decreased upon exposure to H_2. Initially, Mo-O and Mo-Mo scattering paths (at 1.2 Å and 3.2 Å, respectively, without phase-shift correction) were present. Upon exposure to H_2, the shorter Mo-O scattering path transformed into at least 2 overlapping Mo-O scattering paths at slightly longer distances and a Mo-Mo scattering path at 3.7 Å. This structure remained fairly constant intensity from 343

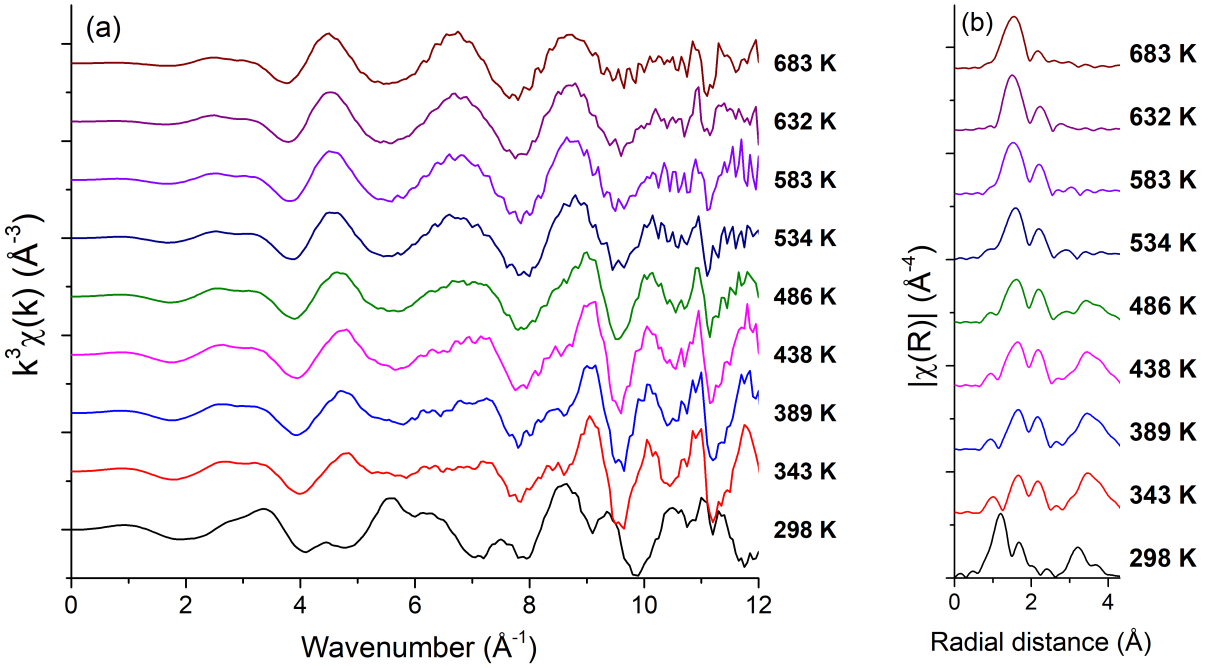

Figure D.8: Extended X-ray absorption fine structure spectra (a) in k-space and (b) the corresponding radial distribution functions (not phase-shift corrected) of $PdMo/SiO_2$ during H_2-TPR.

K to 486 K. Above 486 K, the Mo-Mo scattering path intensity began to decreased, and disappeared by 534 K. This is attributed to the spreading of MoO_x clusters across the surface of SiO_2, which has been observed previously.[18,19] Above 534 K, the Mo-O scattering paths continue to decrease in intensity, and the longer Mo-O multiple scattering path almost completely vanished by 683 K. The two temperature regimes where H_2 consumption occurs according to H_2-TPR results collected using thermal conductivity measurements agrees well with the oxidation states observed in the XANES as well as the qualitative analysis of the EXAFS.

D.3.3 Reactor cell design: advantages and disadvantages

The *in situ* reactor cell designed consists of four 1/4 inch outer-diameter reactor tubes, supported horizontally in an aluminum heating block which was modeled off of designs created by Fingland et al.[11] who designed a cell for simultaneous measurement of X-ray absorption spectra

and *operando* reaction kinetics. The cell was prepared for *operando* use by allowing the catalyst bed to consist of free catalyst powder (particle sizes less than 180 μm preferred), packed between two beds of X-ray transparent material such as small amounts of glass or graphite wool, and transmitting the X-ray beam through both ends of the reactor tube (which includes transmission through the reacting gas). While we have not yet performed any *operando* measurements of catalytic activity using this cell, the design was created with *operando* measurements in mind. Each tube can be supplied independently, and the effluent of each reactor tube can be collected individually. Therefore, this cell may be used at a beamline with infrastructure available for product analysis. Configuration of the reactor cell in this orientation comes with several advantages and disadvantages. One advantage of this design is that brittle or toxic reactor tube materials like graphite, thin quartz, or beryllium are not required to obtain transmission spectra. Using stainless steel tubing for the reactors allows for the potential use of this system under conditions that mimic reaction conditions exactly, including elevated pressures and temperatures. Another advantage of the design is its mechanical simplicity. The stainless-steel reactor tubes can be substituted for any material that is appropriate for the desired study, and the window materials can be easily exchanged to meet the need for various pressure ranges or chemical compatibility with reactants. Reactor tubes can be easily added or removed using the quick-connect fittings. As the reactor tubes are only heated in the reaction zone, the window composition is not strictly limited to materials that are resistant to extreme temperatures.

On the other hand, transmission of the X-ray beam through a long, narrow tube limits the accuracy of temperature measurement by preventing measurements using a thermocouple inserted from one end of the reactor tube into the catalyst bed. Instead, temperature must be

measured externally using a thermocouple in contact with the outside of the reactor tube. Additionally, the tube must be aligned precisely to allow transmission along the path of the reactor tube and window fittings. Using the movable sample stage at beamline 8-ID at NSLS-II, this alignment can be performed easily, but it may present a challenge to align without precise control of the mounting position. Additionally, consideration must be given to the reactant gas mixture. Heavy inert gases such as Ar have a considerable absorption at ambient pressures and at the transmission length of the reactor when using softer X-ray energies. Care should also be taken during packing of the catalyst bed in the reactor cell. If the catalyst bed is not well-packed, or higher flowrates of gas are used, settling of the reactor bed can occur, allowing channeling of the reactants through the top of the reactor bed. While the cost of this cell was approximately $3000 in parts, machine labor and beamline infrastructure to accommodate the cell (including the programmable movable stage, mass flow controllers, temperature controllers, etc.) must also be considered as construction costs.

D.4 Conclusions

An *operando*-ready reactor cell was designed and constructed to be capable of performing XAS measurements using packed beds of sample powders. The reactor cell consists of four parallel tubes with windows at both ends of the tube, allowing for X-ray beam transmission through the catalyst bed. Each of the four tubes in the reactor cell is supplied by its own gas inlet, allowing for the simultaneous performance of up to four independent experiments. Transmission windows can be easily adjusted for chemical compatibility or to perform experiments using reaction pressures of up to 300 psig. An aluminum heating block allows for reaction temperatures

of up to 773 K, but this temperature is only limited by the material of the heating block itself. Performance of the cell in transmission mode was verified by a simple H_2-TPR of Pd, Cu, Ag, and Ni-promoted Mo/SiO_2 catalysts, allowing the oxidation state of the Mo component of each catalyst to be determined as a function of temperature during the TPR using both XANES and qualitative EXAFS analysis.

Acknowledgements

Dr. Eli Stavitski, Dr. Raul Acevedo-Esteves, and Dr. Klaus Attenkofer are acknowledged for their assistance with preparing the beamline to interface with this cell design, including setup of the gas supply system, and for providing technical support during cell testing. Gordon Brezicki is acknowledged for his assistance with testing this cell at the beamline and preparing beam time applications. Ricky Buchanan (UVA Engineering) is acknowledged for his role in the machining and design consultation for the heating block and mounting brackets for the reactor tubes. Helpful conversations with Nicholas Kaylor and Jiahan Xie are also acknowledged. This work received funding from MAXNET Energy and the University of Virginia, and used beamline 8-ID of the National Synchrotron Light Source II, a U.S. Department of Energy (DOE) Office of Science User Facility operated for the DOE Office of Science by Brookhaven National Laboratory under Contract No. DE-SC0012704.

References

1. Jacobs, G., Ji, Y., Davis, B. H., Cronauer, D., Kropf, A. J. and Marshall, C. L. Fischer-Tropsch synthesis: Temperature programmed EXAFS/XANES investigation of the influence of support type, cobalt loading, and noble metal promoter addition to the reduction behavior of cobalt oxide particles. *Applied Catalysis A: General* **333,** 177–191 (2007).

2. Tsakoumis, N. E., Voronov, A., Ronning, M., Beek, W. V., Borg, O., Rytter, E. and Holmen, A. Fischer-Tropsch synthesis: An XAS/XRPD combined in situ study from catalyst activation to deactivation. *Journal of Catalysis* **291,** 138–148 (2012).

3. Alayon, E. M. C., Nachtegaal, M., Kleymenov, E. and Van Bokhoven, J. A. Determination of the electronic and geometric structure of Cu sites during methane conversion over Cu-MOR with X-ray absorption spectroscopy. *Microporous and Mesoporous Materials* **166,** 131–136 (2013).

4. Bordiga, S., Groppo, E., Agostini, G., van Bokhoven, J. A. and Lamberti, C. Reactivity of Surface Species in Heterogeneous Catalysts Probed by In Situ X-ray Absorption Techniques. *Chemical Reviews* **113,** 1736–1850 (2013).

5. Palomino, R. M., Stavitski, E., Waluyo, I., Chen-Wiegart, Y. c. K., Abeykoon, M., Sadowski, J. T., Rodriguez, J. A., Frenkel, A. I. and Senanayake, S. D. New In-Situ and

Operando Facilities for Catalysis Science at NSLS-II: The Deployment of Real-Time, Chemical, and Structure-Sensitive X-ray Probes. *Synchrotron Radiation News* **30,** 30–37 (2017).

6. Tsapatsaris, N., Beesley, A. M., Weiher, N., Tatton, H., Dent, A. J., Mosselmans, F. J., Tromp, M., Russu, S., Evans, J., Harvey, I., Hayama, S. and Schroeder, S. L. High throughput in situ XAFS screening of catalysts. *AIP Conference Proceedings* **882,** 597–599 (2007).

7. Ravel, B., Scorzato, C., Siddons, D. P., Kelly, S. D. and Bare, S. R. Simultaneous XAFS measurements of multiple samples. *Journal of Synchrotron Radiation* **17,** 380–385 (2010).

8. Bare, S. R., Kelly, S. D., Ravel, B., Greenlay, N., King, L. and Mickelson, G. E. Characterizing industrial catalysts using in situ XAFS under identical conditions. *Physical Chemistry Chemical Physics* **12,** 7702 (2010).

9. Bare, S. R., Mickelson, G. E., Modica, F. S., Ringwelski, A. Z. and Yang, N. Simple flow through reaction cells for in situ transmission and fluorescence x-ray-absorption spectroscopy of heterogeneous catalysts. *Review of Scientific Instruments* **77** (2006).

10. Bare, S. R., Yang, N., Kelly, S. D., Mickelson, G. E. and Modica, F. S. Design and operation of a high pressure reaction cell for in situ X-ray absorption spectroscopy. *Catalysis Today* **126,** 18–26 (2007).

11. Fingland, B. R., Ribeiro, F. H. and Miller, J. T. Simultaneous measurement of X-ray absorption spectra and kinetics: A fixed-bed, plug-flow operando reactor. *Catalysis Letters* **131,** 1–6 (2009).

12. Shou, H. and Davis, R. J. Reactivity and in situ X-ray absorption spectroscopy of Rb-promoted Mo_2C/MgO catalysts for higher alcohol synthesis. *Journal of Catalysis* **282,** 83–93 (2011).

13. Hoffman, A. S., Debefve, L. M., Bendjeriou-Sedjerari, A., Ouldchikh, S., Bare, S. R., Basset, J. M. and Gates, B. C. Transmission and fluorescence X-ray absorption spectroscopy cell/flow reactor for powder samples under vacuum or in reactive atmospheres. *Review of Scientific Instruments* **87** (2016).

14. Shimokawabe, M., Takezawa, N. and Kobayashi, H. Characterization of copper-silica catalysts prepared by ion exchange. *Applied Catalysis* **2,** 379–387 (1982).

15. Qu, Z., Huang, W., Cheng, M. and Bao, X. Restructuring and redispersion of silver on SiO_2 under oxidizing/reducing atmospheres and its activity toward CO oxidation. *Journal of Physical Chemistry B* **109,** 15842–15848 (2005).

16. Zhang, L., Lin, J. and Chen, Y. Studies of surface NiO species in NiO/SiO2 catalysts using temperature-programmed reduction and X-ray diffraction. *Journal of the Chemical Society, Faraday Transactions* **88,** 2075–2078 (1992).

17. Kakuta, N., Tohji, K. and Udagawa, Y. Molybdenum oxide structure on silica-supported catalysts studied by Raman spectroscopy and EXAFS. *The Journal of Physical Chemistry* **92,** 2583–2587 (1988).

18. De Boer, M., van Dillen, A. J., Koningsberger, D. C., Geus, J. W., Vuurman, M. A. and Wachs, I. E. Remarkable spreading behavior of molybdena on silica catalysts. An in situ EXAFS-Raman study. *Catalysis Letters* **11,** 227–239 (1991).

19. Braun, S., Appel, L. G., Camorim, V. L. and Schmal, M. Thermal spreading of MoO_3 onto silica supports. *Journal of Physical Chemistry B* **104,** 6584–6590 (2000).

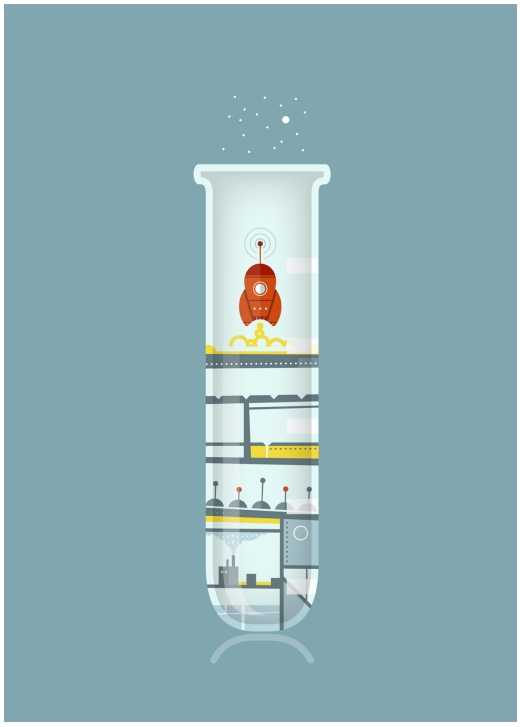

This thesis was typeset using LaTeX, originally developed by Leslie Lamport and based on Donald Knuth's TeX. The body text is set in 12 point Adobe Caslon Pro. This font is an adaptation of a typeface manufactured by the Caslon type foundry, which despite its British origin was used by John Dunlap to typeset the first widely released copy of the Declaration of Independence in 1776, known as the Dunlap Broadside. The above illustration, *Science Experiment 02*, was created by Ben Schlitter and released under CC BY-NC-ND 3.0. A template that can be used to format a PhD dissertation with this look & feel has been released under the permissive AGPL license, and can be found online at github.com/suchow/Dissertate or from its lead author, Jordan Suchow, at suchow@post.harvard.edu.